The Effects of Calcium Channel Blockade and Atrial Natriuretic Peptide Signalling on Proliferation and Differentiation of Cardiac Progenitor Cells

by

Adam G. Hotchkiss

Submitted in partial fulfilment of the requirements
for the degree of Doctor of Philosophy

at

Dalhousie University
Halifax, Nova Scotia
August 2013

Dedicated to my parents, Keith and Mary Ann Hotchkiss

TABLE OF CONTENTS

LIST OF TABLES ix

LIST OF FIGURES x

ABSTRACT xiv

LIST OF ABBREVIATIONS AND SYMBOLS USED xv

ACKNOWLEDGEMENTS xx

CHAPTER 1: INTRODUCTION 1

1.1 Thesis Overview 1

1.2 Cardiovascular Anatomy and Physiology 4

1.2.1 The Cardiovascular System: Form and Function 4

1.2.2 The Cardiac Conduction System 8

1.2.3 The Endocrine Function of the Heart 10

1.2.4 Ultrastructural Features of the Cardiomyocyte 10

1.2.5 Excitation Contraction Coupling 12

1.2.6 The Cardiomyogenic Origin of Working and Conduction System Cardiomyocytes 13

1.3 Cardiogenesis 13

1.3.1 The Cardiogenic Fields and Heart Tube Formation 14

1.3.2 Induction and Differentiation of the Myocardium 16

1.3.3 Cardiac Looping and Formation of the Four Chambered Heart 20

1.3.4 Development of the Cardiac Conduction System 21

1.3.5 Undifferentiated Cardiac Progenitor Cells in the Embryonic Heart Post-Chamber Formation 23

1.4 The Role of Ca^{2+} Signalling in Cardiogenesis 24

1.4.1 Biophysical and Pharmacological Properties of L-type and T-type Ca^{2+} Channels 25

1.4.2 Impaired Cardiogenesis due to Disrupted Intracellular Ca^{2+} Homeostasis 26

1.4.3 Therapeutic Potential of Cardiac Progenitor Cells for Myocardial Repair 28

1.5 The Natriuretic Peptides and their Cell Surface Receptors 30

1.5.1 Section Overview 30

1.5.2 Historical Perspective: Discovery of the 'Atrial Natriuretic Factor' and the Natriuretic Peptide Family 31

1.5.3 Atrial Natriuretic Peptide Gene Expression and Regulation 35

1.5.4 Storage and Secretion of Atrial Natriuretic Peptide 36

1.5.5 Historical Perspective on the Discovery of the Natriuretic Peptide Receptors 41

1.5.6 Natriuretic Peptide Receptor Structure and Functional Activity 42

1.5.7 Physiological Effects of Atrial Natriuretic Peptide 46

1.5.8 Autocrine/Paracrine Regulation of Cell Growth and Proliferation by Atrial Natriuretic Peptide 47

1.5.9 The Potential Role of Atrial Natriuretic Peptide Receptor Signalling in Cardiogenesis 49

CHAPTER 2: MATERIALS AND METHODS 51

2.1 Animal Maintenance and Mouse Strains 51

2.2 Genomic DNA Extraction 52

2.3 Genotyping by Polymerase Chain Reaction (PCR) 53

2.4 Timed Pregnant Female Mice 54

2.5 Embryonic Ventricular Primary Culture and Drug Treatments 54

2.6 Tritiated-Thymidine Labeling 56

2.7 Immune Cytochemistry 56

2.8 Tritiated-Thymidine Autoradiography 59

2.9 Total RNA Extraction from Cells and Tissues 59

2.10 Fluorescence Activated Cell Sorting (FACS) 60

2.11 RNA Quality Control 61

2.12 RT-qPCR 62

2.13 Ca^{2+} Imaging using Fluo-8 64

2.14 Protein Extraction and SDS-*PAGE* Electrophoresis 65

2.15 Western Blot Analysis 66

2.16 Enzyme Linked Immunosorbant Assay (ELISA) 67

2.17 Second Messenger Assays: cGMP and cAMP 68

2.18 Immunohistochemistry 71

2.18.1 Preparation and Processing of Paraffin Embedded Specimens 71

2.18.2 Preparation and Processing of Frozen Specimens 72

2.19 Cell Transplantation and Nifedipine Treatments 73

2.20 Quantification of Graft Sizes 74

2.21 Hematoxylin & Eosin (H&E) Staining on Adult Heart Sections 75

2.22 Electrocardiograms (ECG) 76

2.23 Statistical Analyses 77

CHAPTER 3: THE EFFECTS OF CALCIUM CHANNEL BLOCKADE ON PROLIFERATION AND DIFFERENTIATION OF CARDIAC PROGENITOR CELLS 83

3.1 Background and Hypothesis 83

3.2 Specific Aims 85

3.3 Results 85

3.3.1 Conditional Activation of β-galactosidase in Embryonic Cardiac Cells using Nkx2.5-Cre and Rosa LacZ Double Transgenic Mouse Model 85

3.3.2 Voltage Sensitive L-type and T-type Ca^{2+} Channels are Expressed in the Embryonic Ventricles 86

3.3.3 Characterization of Ca^{2+} Influx in Isoproterenol Stimulated Cells Treated with Nifedipine 88

3.3.4 Nifedipine Causes a Decrease in DNA Synthesis in Cardiac Progenitor Cells and Cardiomyocyte Populations 90

3.3.5 Ca^{2+} Channel Blockade with Nifedipine is Associated with Gene Expression Changes in Cell Cycle Regulating Genes 92

3.3.6 Ca^{2+} Channel Blockade is Associated with High Levels of Sarcomeric Disorganization in Embryonic Cardiomyocytes 93

3.3.7 Nifedipine has Detrimental Effects on Graft Size Formation Following Injection of E11.5 Ventricular Cells into Recipient Hearts 95

CHAPTER 4: CHARACTERIZATION OF THE EFFECTS OF NATRIURETIC PEPTIDE SIGNALLING SYSTEMS ON PROLIFERATION OF CARDIAC PROGENITOR CELLS 119

4.1 Background and Hypothesis 119

4.2 Specific Aims 120

4.3 Results 120

4.3.1 ANP mRNA and Immunoreactive Protein are Expressed in the Ventricles at E11.5 120

4.3.2 Spatial Expression Pattern of Immunoreactive ANP in the Embryonic Heart at E11.5 and E14.5 121

4.3.3 Determination of ANP Secretion from Cultured E11.5 Ventricular Cells 122

4.3.4 Natriuretic Peptide Receptor (NPR) Expression Patterns in the Embryonic Heart 123

4.3.5 Determination of the Effects of ANP on cGMP Production in E11.5 Ventricular Cells 125

4.3.6 Determination of the Effects of ANP on cAMP Production in E11.5 Ventricular Cells 126

4.3.7 ANP High Expression Zones are Associated with a Low Mitotic Index in the E11.5 Ventricles 128

4.3.8 Effects of Exogenous ANP on Proliferation of E11.5 Cardiac Progenitor Cells and Cardiomyocytes 129

CHAPTER 5: INVESTIGATION OF ANP/NPRA SIGNALLING IN DEVELOPMENT OF THE VENTRICULAR CONDUCTION SYSTEM 152

5.1 Background and Hypothesis 152

5.2 Specific Aims 153

5.3 Results 153

5.3.1 Fluorescence Visualization of ANP Positive Cells by Monitoring β-Galactosidase Activity Controlled by ANP Promoter 153

5.3.2 Determination of Conduction System Marker Gene Expression in the ANP Expressing Cell Population 154

5.3.3 Effects of Exogenous ANP Treatment on Conduction System Marker Gene Expression 156

5.3.4 Expression of Proliferation and Conduction System Marker Genes in Ventricles of E14.5 Embryos Lacking NPRA 156

5.3.5 Visualization of Ventricular Conduction System Development using the $Cx40^{egfp}$ Knockin Mouse Model 158

5.3.6 Using the $Cx40^{egfp}$ Model to Characterize Ventricular Cardiac Conduction System Development in Mice Lacking NPRA 159

5.3.7 Electrocardiogram (ECG) Analyses of Mice Lacking NPRA 161

CHAPTER 6: DISCUSSION 180

6.1 Summary of Results 180

6.2 The Effects of Ca^{2+} Channel Blockade on Proliferation and Differentiation of Cardiac Progenitor Cells 181

6.2.1 Context 181

6.2.2 Embryonic and Post-Natal Cardiac Progenitor Cells 182

6.2.3 Intracellular Ca^{2+} Homeostasis and Cell Proliferation 185

6.2.4 Potential Mechanisms of L-Type versus T-type Ca^{2+} Channels in Regulating Proliferation 187

6.2.5 The Effects of Nifedipine on the Assembly of the Contractile Apparatus 189

6.2.6 The Effects of Systemic Administration of Nifedipine on Cell Transplantation 192

6.3 Characterization of ANP Receptor Signalling Systems in the Ventricles at E11.5 stage 196

6.3.1 Context 196

6.3.2 Components of ANP Mediated Signalling Systems are Present in the Embryonic Ventricles at E11.5 Stage 198

6.3.3 Biological Activity of Natriuretic Peptide Receptors in E11.5 Ventricular Cells 200

6.3.4 Effects of Exogenous ANP on Proliferation of Cardiac Progenitor Cells 202

6.4 Investigation into the Potential Role of ANP Signalling in the Development of the Ventricular Cardiac Conduction System 204

6.4.1 Context 204

6.4.2 Investigation into the Direct Inductive Effect of ANP on Expression of Ventricular Conduction System Markers 206

6.4.3 Characterization of Ventricular Conduction System Development in $NPRA^{-/-}$ Mice using the $Cx40^{egfp}$ Mouse Model 208

6.4.4 Proposed Model for the Involvement of ANP/NPRA Signalling Axis in Ventricular Conduction System Development 211

6.5 Significance and Future Directions 213

6.5.1 The Effects of Ca^{2+} Channel Blockade and ANP Signalling on Cell Transplantation 213

6.5.2 The Effects of Ca^{2+} Channel Blockade and ANP Signalling on Cardiac Development 218

REFERENCES 222

LIST OF TABLES

Table 2.3.1: List of primers used for genotyping and expected band sizes……..…...78

Table 2.12.1: List of primers used for real time quantitative PCR and expected amplicon sizes……80

Table 3.3.1: Summary of the effects of Ca^{2+} channel blockade on expression of cell cycle regulating genes……....……108

LIST OF FIGURES

Figure 1.2.1: Schematic model of the external structures of the heart……..6

Figure 1.2.2: Schematic model of the inner structures of the heart…….……..7

Figure 1.2.3: Schematic model of the cardiac conduction system……...……..9

Figure 1.3.1: Schematic diagram of the localization of cardiogenic cells in the epiblast and the formation primitive heart tube……..……...……15

Figure 1.3.2: Induction and differentiation of the cardiomyogenic lineage……...….18

Figure 1.5.1: Structures of the natriuretic peptides and processing of atrial natriuretic peptide ……...……..34

Figure 1.5.2: Alignment of the atrial natriuretic peptide predicted protein sequence from humans and several commonly used experimental species……...39

Figure 1.5.3: Natriuretic peptide receptor structures and ligand preferences…….….45

Figure 2.3.1: Expected band sizes from genotyping of various mouse strains……79

Figure 3.3.1: Conditional activation of the *LacZ* reporter gene genetically labels the Nkx2.5^{+} cell lineage……..…….……..97

Figure 3.3.2: Validation of GAPDH as internal control gene…….……98

Figure 3.3.3: L-type and T-type Ca^{2+} channel expression in E11.5 ventricles……99

Figure 3.3.4: Developmental profiles of L-type and T-type Ca^{2+} channel isoforms……....100

Figure 3.3.5: The effects of Ca^{2+} channel blockade on isoproterenol induced fluctuations in intracellular Ca^{2+}…….……..102

Figure 3.3.6: Identification of E11.5 cardiac progenitor cells and cardiomyocytes in culture……..…….104

Figure 3.3.7: Visualization of cells in the S-phase of the cell cycle using a tritiated [^{3}H] - thymidine incorporation assay……...……105

Figure 3.3.8: The effects of Ca^{2+} channel blockade on proliferation of E11.5 cardiac cell populations……...…….106

Figure 3.3.9: Immunolabelling of $Ca_v1.2$ L-type Ca^{2+} channels in E11.5 cardiac progenitor cells and cardiomyocytes……..…….107

Figure 3.3.10: Graphical summary of the effects of Ca^{2+} channel blockade on expression of cell cycle regulating genes……..….109

Figure 3.3.11: The effects of Ca^{2+} channel blockade on sarcomeric organization of E11.5 cardiomyocytes……..……..111

Figure 3.3.12: The effects of Ca^{2+} channel blockade on the relative distribution of E11.5 cardiac cell populations……..…..112

Figure 3.3.13: Graphical summary of the effects of Ca^{2+} channel blockade on expression of differentiation marker genes……..……..113

Figure 3.3.14: Subcellular localization of MEF2c in response to Ca^{2+} channel blockade…….……114

Figure 3.3.15: Effects of Ca^{2+} channel blockade on expression of atrial natriuretic peptide……..……..116

Figure 3.3.16: The effects of nifedipine on graft size formation following injection of E11.5 ventricular cells into recipient hearts……..……117

Figure 4.3.1: Developmental profile of ANP mRNA expression……..131

Figure 4.3.2: Quantification of ANP protein in E11.5 and neonatal ventricles…….…132

Figure 4.3.3: Spatial expression pattern of immunoreactive ANP in the embryonic heart at E11.5……..…..133

Figure 4.3.4: Spatial expression pattern of immunoreactive ANP in the left ventricle of the E14.5 heart….…….……135

Figure 4.3.5: Detection of ANP in conditioned media samples from E11.5 ventricular cell cultures by Western blot analysis……..……..137

Figure 4.3.6: Developmental gene expression profiles of the ANP high affinity receptors NPRA and NPRC……...……..138

Figure 4.3.7: Direct comparison of NPRA versus NPRC gene expression in the ventricles throughout cardiac development……..……139

Figure 4.3.8: Western blot analyses of ventricular NPRA and NPRC protein at developmental and post-natal stages……..……..140

Figure 4.3.9: Spatial expression pattern of immunoreactive NPRA and NPRC in the embryonic heart at E11.5……..…….……141

Figure 4.3.10: Schematic illustration of the principle of second messenger competitive immunoassays…...……..……143

Figure 4.3.11: Generation of the cGMP standard curve…….…..144

Figure 4.3.12: Cell density optimization for cGMP competitive immunoassays……...…145

Figure 4.3.13: The effects of exogenous ANP on cGMP production in E11.5 ventricular cells…….……..146

Figure 4.3.14: Generation of the cAMP standard curve……..……...……..147

Figure 4.3.15: Cell density optimization for cAMP competitive immunoassays……...148

Figure 4.3.16: The effects of exogenous ANP on cAMP production in E11.5 ventricular cells……..149

Figure 4.3.17: Determination of the mitotic index in regions of high and low immunoreactive ANP..…….……...…….150

Figure 4.3.18: Effects of exogenous ANP on proliferation of E11.5 cardiac progenitor cells and cardiomyocytes……...……...……151

Figure 5.3.1: Visualization of ANP-LacZ expression by fluorescent β-galactosidase substrate fluorescein di β-D- galactopyranoside (FDG)……..163

Figure 5.3.2: Representative Fluorescence Activated Cell Sorting (FACS) experiment using E11.5 ventricular cells from ANP-LacZ^{+} embryos.....164

Figure 5.3.3: Gene expression analysis of ANP^{+} and ANP^{-} cell populations obtained from fluorescence activated cell sorting (FACS) of E11.5 ventricular cells…….……...…….……..165

Figure 5.3.4: Expression of Cx40 protein in E11.5 ANP-LacZ^{+} cells……..……...…166

Figure 5.3.5: Effects of exogenous ANP on expression of conduction system marker genes Cx40 and HCN4.....…...167

Figure 5.3.6: Genotype distribution resulting from NPRA$^{+/-}$ crosses at three weeks of age and E14.5……...…168

Figure 5.3.7: Graphical summary of the effects of NPRA ablation on expression levels of cell cycle regulating genes in E14.5 ventricles…….……..…169

Figure 5.3.8: Expression of conduction system marker genes Cx40 and HCN4 in ventricles of E14.5 embryos lacking NPRA…….……..….170

Figure 5.3.9: Expression of ANP in ventricles of E14.5 embryos lacking NPRA…...171

Figure 5.3.10: Visualization of ventricular conduction system development using the $Cx40^{egfp}$ Knockin mouse model……...……....……172

Figure 5.3.11: Morphological characterization of conduction system development in mice lacking NPRA using the $Cx40^{egfp}$ model……..…….....174

Figure 5.3.12: Electrocardiographic analyses of mice lacking NPRA……..……176

Figure 5.3.13: Electrocardiographic analyses of mice lacking NPRA following administration of dobutamine……..…….…….178

Figure 5.3.14: Evidence of irregular electrical activity triggered by sympathetic activation in mice lacking NPRA……...……...……...……..179

ABSTRACT

Cardiac progenitor cells (CPCs) are abundant in the embryonic heart and have hallmark features which include a rapid rate of cell division and the ability to differentiate into mature heart muscle cells (cardiomyocytes). Based on these features, CPCs are considered an attractive candidate cell type for transplantation therapies which aim to replenish the diseased heart muscle tissue (myocardium) with new muscle forming cells. A better understanding of how pharmacological drugs and endogenous hormones/signalling molecules modulate the balance between proliferation and differentiation of CPCs could be used to develop more effective cell based therapies for myocardial repair. Furthermore, this information could provide valuable new insight into molecular mechanisms regulating normal cardiogenesis during the embryonic period. The specific aims of the present study were to characterize the effects of the Ca^{2+} channel blocking drug nifedipine and the endogenous hormone/paracrine factor atrial natriuretic peptide (ANP) on CPC proliferation and differentiation. Results showed that primary cultured CPCs, isolated from the ventricles of embryonic day (E) 11.5 mouse embryos, underwent a reduction in cell cycle activity following exposure to nifedipine. Furthermore, systemic administration of nifedipine to adult mice receiving transplanted E11.5 ventricular cells (containing CPCs) was associated with smaller graft sizes compared to control animals that did not receive the drug. Results from the present study also demonstrated that ANP receptor mediated signalling systems are biologically active in E11.5 ventricular cells and have an antiproliferative effect on cultured E11.5 CPCs. Moreover, preliminary data provided evidence that genetic ablation of the ANP high affinity receptor (NPRA) may be associated with impaired development of the ventricular cardiac conduction system. Collectively, work from this thesis provides evidence that interactions between transplanted cells and pharmacological drugs could have a significant impact on the effectiveness of cell based therapies and that ANP signalling systems may play a critical role in cardiac ontogeny by regulating the balance between CPC proliferation and differentiation.

LIST OF ABBREVIATIONS AND SYMBOLS USED

%	Percent
Δ	Change
~	Approximately
#	Number
β	Beta
°	Degree
µl	Microliter
µm	Micrometer
µM	Micromolar
1°	Primary
2°	Secondary
$[^3H]$	Tritium
$[Ca^{2+}]_i$	Intracellular Ca^{2+}
H_2O	Water
Ca^{2+}	Calcium
Cl^-	Chloride
K^+	Potassium
Na^+	Sodium
AB/AM	Antibiotic Antimycotic
AC	Adenylyl Cyclase
AM	Acetoxymethyl Ester
AngII	Angiotensin II
ANOVA	Analysis of Variance
ANP	Atrial Natriuretic Peptide
AP	Action Potential
APS	Ammonium Persulphate
ATP	Adenosine Triphosphate
AVB	Atrioventricular Bundle
AV	Atrioventricular

BAPTA	1,2-Bis(o-Aminophenoxy)Ethane-N,N,N',N'-Tetraacetic Acid
BMP	Bone Morphogenetic Protein
BPM	Beats per Minute
BSA	Bovine Serum Albumin
C	Celsius
cc	Cubic Centimeter
Ci	Curie
C_T	Threshold Cycle
CaM	Calmodulin
CaMKII	Ca^{2+}-Calmodulin Kinase II
cAMP	Cyclic Adenosine Monophosphate
CaN	Calcineurin
CCS	Cardiac Conduction System
CDK	Cyclin Dependent Kinase
cDNA	Complementary DNA
cGMP	Cyclic Guanosine Monophosphate
CHD	Congenital Heart Defect
CPC	Cardiac Progenitor Cell
Cx	Connexin
DAB	3, 3' Diaminobenzidine
dd	Double Distilled
DHP	Dihydropyridine
DMEM	Dulbecco's Modified Eagle Media
DMF	Dimethyl Formamide
DMSO	Dimethyl Sulfoxide
DNA	Deoxyribonucleic Acid
dNTP	Deoxynucleoside Tri Phosphate
dRN	Threshold Fluorescence
E	Embryonic Day
EC	Excitation-Contraction
ECG	Electrocardiogram

ECL	Enhanced Chemiluminescence
EGFP	Enhanced Green Fluorescent Protein
EGTA	Ethylene Glycol Tetraacetic Acid
ELISA	Enzyme Linked Immunosorbant Assay
ERK	Extracellular Signal-Regulated Kinase
ES	Embryonic Stem
ET-1	Endothelin-1
FACS	Fluorescence Activated Cell Sorting
FBS	Fetal Bovine Serum
FDG	Fluorescein di β-D- Galactopyranoside
FGF	Fibroblast Growth Factor
FMG	Fluorescein Monogalactosidase
g	Gram
G_i	Inhibitory Heterotrimeric G-Protein
GAPDH	Glyceraldehyde 3-Phosphate Dehydrogenase
GC	Guanylyl Cyclase
HCl	Hydrochloric Acid
HCN4	Hyperpolarization-Activated Cyclic Nucleotide-Gated Channel 4
H&E	Hematoxylin & Eosin
HEPES	4-(2-Hydroxyethyl)-1-Piperazineethanesulfonic Acid
HTRF	Homogeneous Time Resolved Fluorescence
Hz	Hertz
IBMX	3-Isobutyl-1-Methylxanthine
IC_{50}	Half Maximal Inhibitory Concentration
IP	Intraperitoneal
iPS	Induced Pluripotent Stem
IRES	Internal Ribosomal Entry Sequence
ISO	Isoproterenol
k	Kilo
kb	Kilo Bases
K_d	Dissociation Constant

kDa	Kilo Dalton
M	Molar
mAb	Monoclonal Antibodies
MF20	Antibodies against Sarcomeric Myosin
mg	Milligram
MI	Myocardial Infarction
ml	Milliliter
$MLC2_v$	Ventricular Myosin Light Chain 2
MLCK	Myosin Light Chain Kinase
mm	Millimeter
mRNA	messenger Ribonucleic Acid
MSC	Mesenchymal Stem Cell
N	Number
NaCl	Sodium Chloride
NBF	Neutral Buffered Formalin
NCRL	Double Transgenic Nkx2.5-Cre/Rosa-LacZ
ng	Nanogram
NKE	Nkx-Response Element
nm	Nanometer
nM	Nanomolar
NP40	Nonidet 40
NPR	Natriuretic Peptide Receptor
NRG-1	Neuregulin-1
NW	No Wash
OCT	Optimal Cutting Temperature
PBS	Phosphate Buffered Saline
PBST	PBS-Tween
PCR	Polymerase Chain Reaction
PKA	cAMP-Dependent Protein Kinase
PKG	cGMP-Dependent Protein Kinase
PMSF	Phenylmethylsulphonyl Fluoride

qPCR	Real Time Quantitative Polymerase Chain Reaction
RGS2	Regulator of G-protein Signalling 2
RNA	Ribonucleic Acid
RPM	Revolutions per Minute
RT	Reverse Transcription
RyR	Ryanodine Receptor
SA	Sinoatrial
SC	Subcutaneous
SDS	Sodium Dodecyl Sulfate
SEM	Standard Error of Mean
SR	Sarcoplasmic Reticulum
SRE	Serum Response Element
TBE	Tbx-Response Element
Tbx5	T-box 5
TEMED	Tetramethylethylenediamine
TGF-β	Transforming Growth Factor Beta
t-tubule	Transverse Tubule
U	Units
USA	United States of America
v/v	Volume per Volume
w/v	Weight per Volume
X	Times
X-GAL	5-Bromo-4-Chloro-3-Indlyl-β-D-Galactopyranoside

ACKNOWLEDGEMENTS

First and foremost I would like to thank my Supervisor Dr. Kishore Pasumarthi for his exceptional guidance throughout my doctoral studies. His passion for research and dedication to my success as a graduate student were both inspirational and motivational. I will forever be thankful for all of his advice and encouragement.

I would like to extend thanks to all the members of the Pasumarthi lab, past and present, for their friendship, insight and assistance. Special thanks to Dr. Feixiong Zhang for his help in getting me started in the lab. Also, special thanks to Tiam Feridooni for the countless hours of scientific conversation and insight into all aspects of my research.

I would like to thank the members of my advisory committee, Dr. Denis Dupré and Dr. Jana Sawynok as well as our graduate coordinator Dr. Eileen Denovan- Wright for their valuable advice and support during my years of study. I would also like to express my gratitude to the administrative staff in the Department of Pharmacology, Luisa Vaughan, Sandi Leaf, Janet Murphy and Cheryl Bailey for all of their assistance.

I would like to express my sincere appreciation to my thesis examining committee, Dr. Susan Howlett, Dr. Robert Rose and Dr. Mona Nemer for reviewing my thesis work.

I would like to thank my family and friends for their constant encouragement and moral support. Finally, I would like to extend my deepest thanks to my fiancée Nicole for her patience and unwavering support throughout my doctoral studies.

CHAPTER 1: INTRODUCTION

1.1 Thesis Overview

Heart disease continues to be a leading cause of death around the world. Myocardial infarction and other forms of ischemic heart disease result in large scale death of viable cardiomyocytes. The ability of the heart to replace lost cells is severely limited by the inability of mature cardiomyocytes to divide. Instead, the damaged area is replaced by non-contractile scar tissue, which compromises cardiac performance. This in turn leads to a gradual decline in heart function which can culminate in heart failure and ultimately death. A spectrum of pharmacological drugs can slow down the decline in heart function, but cannot stimulate regeneration of lost tissue. As a result, cell transplantation therapies are being developed with the aim of restoring heart function by replenishing the damaged area with new cardiomyocytes.

While there is no consensus on the most suitable cell type, undifferentiated embryonic cardiac progenitor cells (CPCs), which are abundant in the developing heart; have attractive features including high rates of proliferation and the ability to differentiate into mature cardiomyocyte lineages. Moreover, transplantation studies in animals have provided substantial evidence that embryonic cardiomyocytes can functionally integrate with host cardiomyocytes and improve host heart function. **One area which has thus far been largely overlooked is the impact of pharmacological compounds on proliferation and differentiation of embryonic heart cells post-transplantation.** It is important to understand interactions between transplanted cells and commonly used drugs since the majority of candidates that could benefit from transplantation therapy

would have an ongoing drug treatment regimen. It has been reported that nifedipine, a member of the dihydropyridine (DHP) class of Ca^{2+} channel antagonists, impairs proper formation of the embryonic heart. However, the consequences of Ca^{2+} channel blockade on CPC proliferation and differentiation remains incompletely understood.

Impaired cardiac function can also result from malformation of the heart during embryonic development. Congenital defects are more prevalent in the heart than any other organ system. Owing to the limited ability of post-natal cardiomyocytes to divide, disturbances of proliferation and/or differentiation kinetics during development can have life-long deleterious effects after birth. In particular, several forms of congenital heart disease are the result of improper formation or function of the heart's pacemaker/conduction system which is responsible for initiating and propagating the electrical impulses required for each beat. During the normal course of cardiac development, CPCs proliferate rapidly and upon receiving appropriate molecular cues, differentiate into distinct myocardial cell lineages. The highly ordered program of lineage specification and subsequent functional maturation is driven by numerous signalling molecules, many of which are secreted factors from diverse cell types present in the embryonic heart. **Atrial natriuretic peptide (ANP) is a hormone expressed in the embryonic heart, but does not have a clearly defined role in the regulation of cardiac cell proliferation and differentiation during cardiac ontogeny.** In particular, its expression pattern in the developing ventricular chambers is suggestive of a role in specification and/or function of the developing ventricular conduction system. However, a role for ANP in lineage specification of CPCs/immature embryonic cardiomyocytes has not yet been described.

Thus, the first of two hypotheses addressed in my doctoral work was that cardiac defects observed in embryos exposed to the DHP Ca^{2+} channel blocker nifedipine were a result of altered proliferation kinetics and/or impaired differentiation of CPCs and embryonic cardiomyocytes. Towards this, the objectives were (i) to quantify the effects of nifedipine on proliferation and differentiation of CPCs and embryonic cardiomyocytes *in vitro* and (ii) determine the effect of systemic administration of nifedipine on graft size formation following transplantation of embryonic cardiac cells (mixed population of CPCs and cardiomyocytes). **The second hypothesis was that the hormone ANP is an important regulator of CPC proliferation and/or lineage specification during the embryonic period.** To address this hypothesis, my objectives were (i) to determine whether ANP cognate receptors (known as natriuretic peptide receptors) are present and biologically active in the embryonic heart (ii) determine whether ANP has an effect on CPC and/or cardiomyocyte proliferation and lineage specification, and (iii) determine the *in vivo* consequences of disruption of natriuretic peptide receptor signalling systems on molecular and functional aspects of cardiac development.

The outcome of this research work should be informative with regards to (i) providing further insight into the molecular mechanisms of Ca^{2+} mediated regulation of CPC and cardiomyocyte proliferation and differentiation *in vitro* (ii) determining whether interactions between transplanted cells and pharmacological agents occur and (iii) defining the role of ANP on proliferation and differentiation in the embryonic heart.

1.2 Cardiovascular Anatomy and Physiology

The mammalian heart is a sophisticated four-chambered muscular pump that is situated at the center of the cardiovascular system. The primary function of the heart is to circulate blood through an extensive network of blood vessels which comprise the vascular system. Together the heart, the vasculature and the blood comprise the cardiovascular system which delivers oxygen and nutrients to all the body's tissues and also carries metabolic waste products away from these tissues to the lungs and other excretory organs for removal from the body. An understanding of the anatomy and physiology of the cardiovascular system is useful as a point of reference for comparisons to the diseased state and also for developmental studies aimed at clarifying the ontological origins of individual components of the cardiovascular system.

1.2.1 The Cardiovascular System: Form and Function

Schematic diagrams showing the heart and its connections to the major vessels from an exterior view (Figure 1.2.1) as well as from a longitudinal section view (Figure 1.2.2) demonstrate the salient structural features of the mature heart. The heart consists of two upper atrial chambers and two lower ventricular chambers which are physically partitioned by septa to ensure complete separation of oxygen rich and oxygen poor blood. Within the heart, atrioventricular valves prevent the backflow of blood from the ventricles into the atria. Similarly, semilunar vales separate each ventricle from its great artery.

The mammalian heart can be viewed as two separate pumps running in parallel to generate the pulmonary and systemic circulatory systems (Katz, 2011). If the right

atrium is considered as a starting point, de-oxygenated blood enters the right atrium via the superior and inferior vena cava veins and passes through the tricuspid valve into the right ventricle. Blood from the right ventricle is then pumped through the pulmonary artery and into the lungs where it is re-oxygenated. This component of the cardiovascular system is known as the pulmonary circulation. Oxygenated blood from the lungs then passes through the pulmonary vein and enters the left atrium. After being pumped through the mitral valve into the left ventricle, the blood is then propelled via the aorta into the body through the arterial system. This component of the cardiovascular system is known as the systemic circulation.

Each heartbeat results from the cooperative actions of two types of cardiomyocytes, namely (i) working cardiomyocytes and (ii) cardiac pacemaker/conductive cardiomyocytes. The pacemaking and conductive cardiomyocytes are responsible for initiating and propagating electrical impulses of the heart, which are received by working cardiomyocytes and coupled into mechanical contraction of the muscle tissue (myocardium) that generates the force required to efficiently pump blood out of the chambers.

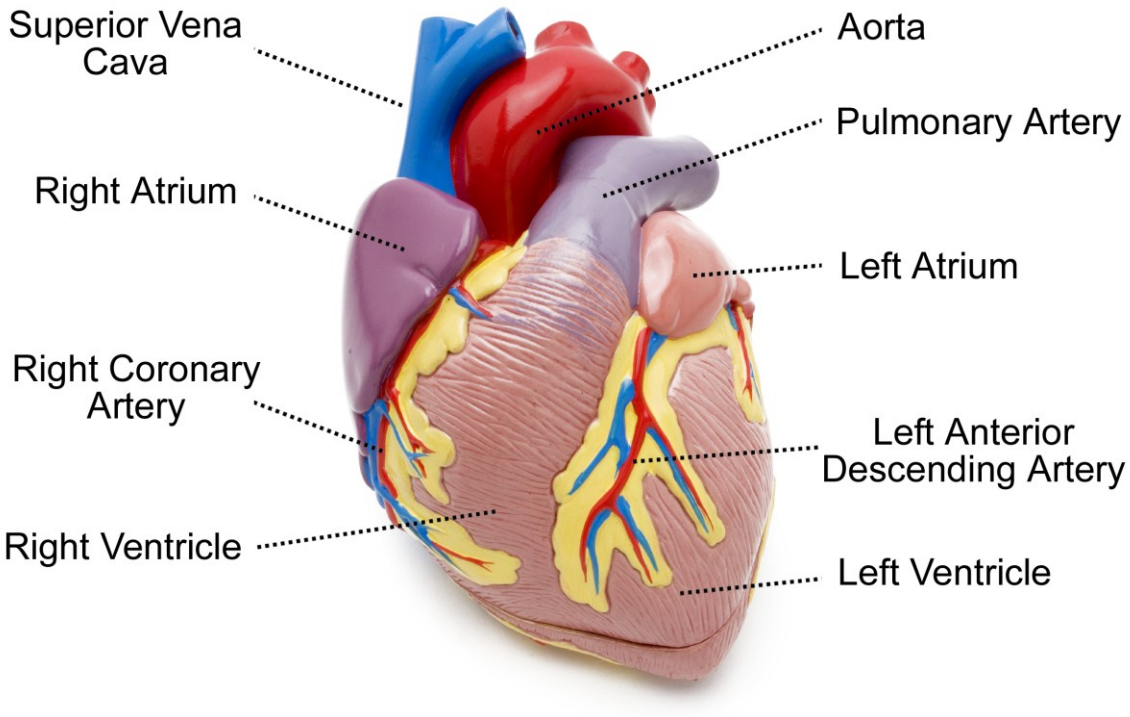

Figure 1.2.1: Schematic model of the external structures of the heart.
The mammalian heart consists of two upper atrial chambers and two lower ventricular chambers. The veins return blood to the heart (i.e. the vena cavae), while the arteries (i.e. aorta) carry blood away from the heart. The pulmonary veins (not shown) carry oxygenated blood to the heart, while pulmonary arteries carry deoxygenated blood to the lungs. The coronary arteries (e.g. left anterior descending artery) deliver oxygen rich blood to the myocardium. (Photo credit, iStockPhoto # 1907828, modified).

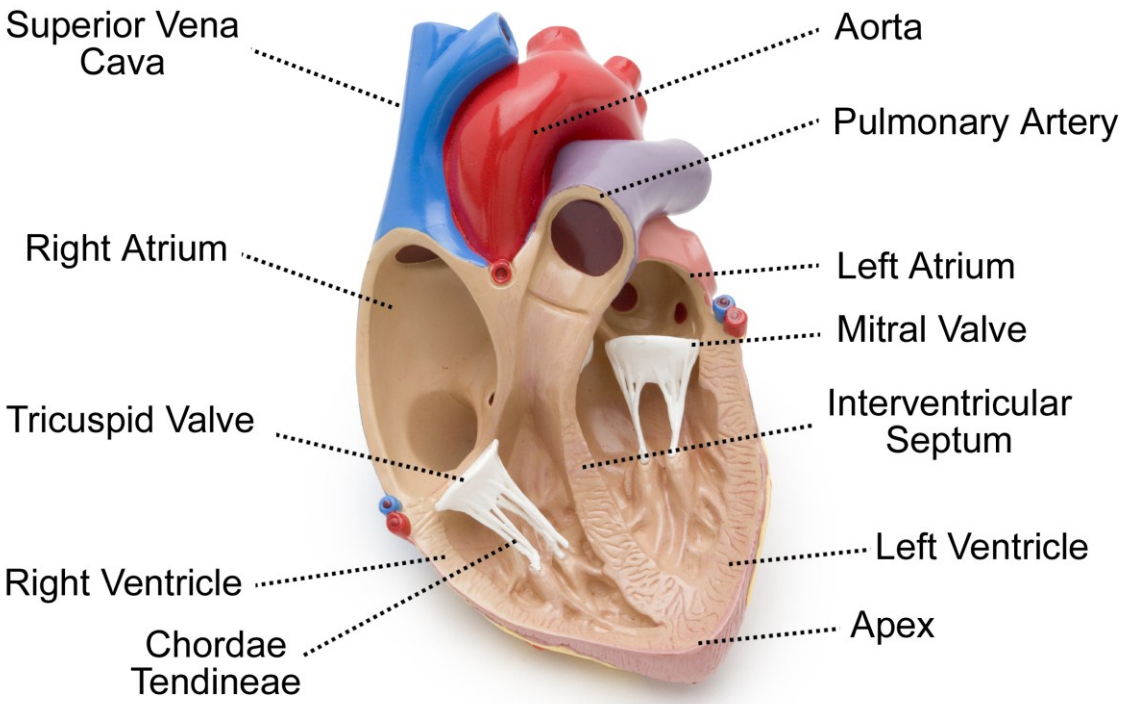

Figure 1.2.2: Schematic model of the inner structures of the heart. The four chambers of the heart are physically partitioned by septa to ensure complete separation of oxygen rich and oxygen poor blood. De-oxygenated blood enters the right atrium via the superior and inferior vena cavae and passes through the tricuspid valve into the right ventricle. Blood from the right ventricle is then pumped through the pulmonary artery and into the lungs where it is re-oxygenated. Oxygenated blood from the lungs then passes through the pulmonary vein and enters the left atrium. After being pumped through the mitral valve into the left ventricle, the blood is then propelled via the aorta into the body through the arterial system. (Photo credit, iStockPhoto # 1907817, modified).

1.2.2 The Cardiac Conduction System

The cardiac conduction system (CCS) is subdivided into distinct functional components which includes the sinoatrial (SA) node, the atrioventricular (AV) node, the bundle of His/atrioventricular bundle (AVB), bundle branches and terminal Purkinje fibers (Figure 1.2.3) (Mikawa and Hurtado, 2007). Each heartbeat is normally initiated in the SA node which serves as the intrinsic pacemaker of the heart and is located between the superior vena cava and the right atrium. Each electrical impulse generated in the SA node then spreads as a wave of depolarization through the right and left atrial myocardium before converging at the AV node located at the base of the right atrium. At the AV node, the electrical impulse is delayed to allow complete ventricular filling prior to ventricular contraction. From the AV node the impulse is carried into the ventricles by a specialized strand of cardiac muscle that comprises the AVB. Because the atrial and ventricular chambers are electrically insulated from each other by fibrous tissue, the AVB serves as the only conduction pathway between the atrial and ventricular chambers. From the AVB, the impulse is transmitted to the bifurcating left and right bundle branches which then arborize extensively to form the Purkinje fiber network which rapidly distributes the electrical impulse to the ventricular myocardium to elicit coordinated contractions of the ventricular chambers and achieve the proper apex to base mode of contraction.

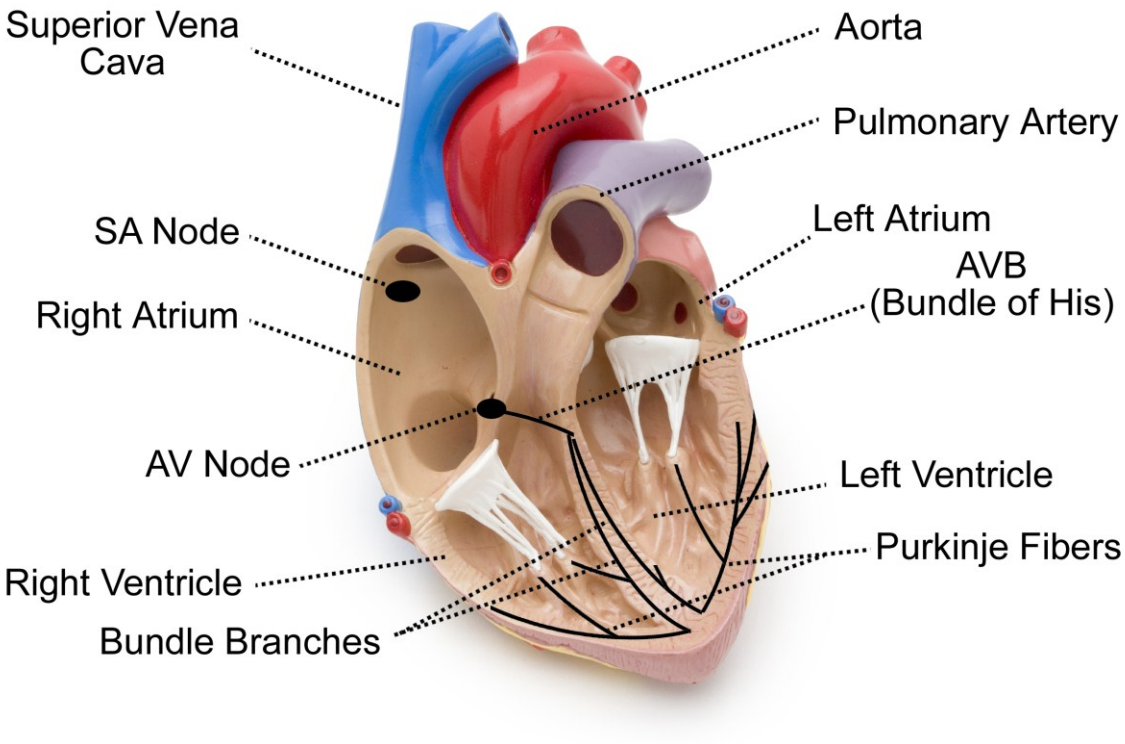

Figure 1.2.3: Schematic model of the cardiac conduction system. Each heartbeat is initiated in the sinoatrial (SA) node which serves as the intrinsic pacemaker of the heart. The electrical impulse then spreads as a wave of depolarization through the right and left atrial myocardium before converging at the atrioventricular (AV) node located near the base of the right atrium. From the AV node, the impulse is carried into the ventricles by atrioventricular bundle (AVB/Bundle of His). From the AVB, the impulse is transmitted to the bifurcating left and right bundle branches which then arborize extensively to form the Purkinje fiber network which rapidly distributes the electrical impulse to the ventricular myocardium. (Photo credit, iStockPhoto # 1907817, modified).

1.2.3 The Endocrine Function of the Heart

While the main function of the adult heart is to serve as a mechanical pump, it also plays an important endocrine role in the regulation of cardiovascular homeostasis by controlling electrolyte and fluid balance in the body (de Bold et al., 1981). Atrial natriuretic peptide (ANP) is a 28 amino acid hormone produced and stored in large quantities in the atrial chambers of the heart. In response to mechanical stretching of the atrial wall due to increased intravascular volume (Lang et al., 1985), ANP is released into the circulation where it then acts on cell surface receptors known as natriuretic peptide receptors (NPRs) in various organs of the body (Potter et al., 2006). Most notably, it stimulates receptors in (i) the kidneys which account for its diuretic and natriuretic effects (ii) in the vasculature to induce smooth muscle relaxation and (iii) on endothelial cells to increase vessel permeability and allow extravasation of fluid (McGrath et al., 2005; Potter et al., 2006). Overall, the net effect of these integrated functions enables the heart to contribute significantly to the regulation of blood volume and blood pressure.

1.2.4 Ultrastructural Features of the Cardiomyocyte

The cardiomyocyte is the fundamental work unit of the heart (Evans et al., 2010). Each cardiomyocyte consists of a bundle of myofibrils that are each composed of smaller contractile units known as sarcomeres. Each sarcomere consists of the contractile proteins myosin (thick filaments) and actin (thin filaments) which are highly organized into a regular array of myofilaments by an elaborate protein scaffold to form the contractile apparatus (Squire, 1997; Katz, 2011).

The plasma membranes of cardiomyocytes contain a variety of ion channels, exchangers and pumps that collectively serve to regulate the composition of the intracellular and extracellular environments (Katz, 2011). Moreover, the plasma membrane contains numerous cell surface receptors and enzymes that participate in diverse cell signalling processes. Extensions of the plasma membrane that penetrate deep into the cell, referred to as transverse tubules (*t*-tubules)(Fawcett and McNutt, 1969), increase the cell membrane surface area and also play a critical role in coupling electrical excitation to mechanical contraction (excitation-contraction; EC coupling)(Bers, 2002).

The intracellular compartment of each cardiomyocyte contains membrane bound organelles including the nucleus, the mitochondria and the sarcoplasmic reticulum (SR)(Katz, 2011). The SR serves as the main storage compartment of intracellular Ca^{2+} and thus plays a critical role in EC coupling by mobilizing these Ca^{2+} stores during muscle contraction. The myocardium forms a functional syncytium by virtue of specialized cell-to-cell junctions, known as intercalated discs, which form the mechanical and electrical connections between individual cardiomyocytes (Perriard et al., 2003). Adherence junctions and desmosomes are mainly involved in maintaining the structural integrity the connections, while gap junction proteins enable electrical coupling of adjacent cells through connexons, which are non-selective ion channels formed by members of the connexin family of proteins (Perriard et al., 2003; Nielsen et al., 2012). By providing low-resistance connections between cells, gap junction channels allow electrical impulses to be conducted rapidly throughout the myocardium. Importantly, connexin isoforms with distinct conductive properties are differentially expressed by

working and conduction system cardiomyocytes which is critical for achieving the coordinated contractions of the heart's four chambers and thus for efficient cardiac function.

1.2.5 Excitation Contraction Coupling

The myocardium is an electrically excitable tissue in that the plasma membranes of individual cardiomyocytes are rhythmically depolarized (Kirby, 2007). Action potentials (AP), which are time-dependent changes in the electrical potential of the membrane surface, occur due to the orchestrated opening and closing of transmembrane ions channels which enables the movement of specific mono and divalent ions into and out of the cell (i.e. Na^+, Ca^{2+}, K^+ and Cl^-) (Katz, 2011). Each AP consists of the following phases: Phase 0 is the upstroke which corresponds to cell depolarization. This is followed by early repolarization (Phase 1), the plateau (Phase 2), repolarization (Phase 3) and resting (Phase 4). Differences in AP shape exhibited by working or CCS cardiomyocytes located in different compartments of the heart are mainly due to the specific complements of ion channels as well as exchangers (e.g. Na^+/Ca^{2+} exchanger) and ATPase pumps (K^+- ATPase) that are expressed by each cell type.

During the cardiac action potential, Ca^{2+} enters the cell via voltage sensitive L-type Ca^{2+} channels located within the *t*-tubules. This influx of Ca^{2+} triggers the release of a larger amount of Ca^{2+} from intracellular Ca^{2+} stores by binding to specialized Ca^{2+} release channels in the SR membrane known as ryanodine receptors (RyR)(Fabiato, 1983). The resulting rise in intracellular Ca^{2+} concentration can in turn activate the contractile apparatus of the cell via interactions of Ca^{2+} ions with myofilament proteins.

1.2.6 The Cardiomyogenic Origin of Working and Conduction System Cardiomyocytes

Working cardiomyocytes and cardiac conduction system cardiomyocytes are derived from a common pool of cardiomyogenic progenitor cells during cardiac ontogeny (Gourdie et al., 1995; Cheng et al., 1999; McMullen et al., 2009) and thus it is not surprising that they share many of the same structural and functional features. However, notable differences also exist between these two cell types which are important determinants of their specialized functions. For example, conduction system cardiomyocytes, which do not contribute significantly to cardiac contraction, have less developed *t*-tubule system, less extensive SR network and considerably lower levels/different compositions of contractile proteins (Lyons, 1994; Kirby, 2007; Moskowitz et al., 2007). Deciphering the precise molecular mechanisms involved in guiding undifferentiated embryonic cardiac progenitor cells towards each cardiomyocyte lineage would be a significant step towards achieving the ability to enrich specific cell types *in vitro* for use in regenerative therapies. Moreover, this information would undoubtedly also contribute to a better understanding of the etiology of congenital heart diseases that involve improper formation and/or function of the heart.

1.3 Cardiogenesis

At its earliest functional stages, the embryonic heart resembles a simple tubular structure consisting of an outer layer of myocardium and an inner layer of endothelial cells. During the remarkable process of cardiogenesis, the early heart tube undergoes major morphological changes to transform into a four chambered pump while continuously maintaining its function to meet the increasing metabolic demands of the

growing embryo. Undifferentiated cardiac progenitor cells (CPCs) play a central role in the cardiogenic process. Due to their high proliferative capacity and cardiomyogenic ability, CPCs are also considered to be an attractive candidate cell type to be used in cell based therapies for myocardial repair (Zhang and Pasumarthi, 2008).

1.3.1 The Cardiogenic Fields and Heart Tube Formation

The earliest heart precursor cells are located on both sides of the midline in the epiblast at the early gastrulation stage (Figure 1.3.1A), which in mouse corresponds to embryonic day (E6.5) (Tam et al., 1997; Kirby, 2007). Epiblast cells then ingress through the primitive streak to form the mesodermal germ layer (Tam et al., 1997). Mesodermal cardiac precursor cells migrate laterally and cranially from the primitive streak which results in the establishment of bi-lateral cardiogenic fields in the regions of the anterior lateral plate mesoderm (Figure 1.3.1B) (Kirby, 2007). Owing to continuous migration of cells from the primitive streak to the lateral plate and to the midline, the bilateral fields merge cranially to form what is referred to as the cardiac crescent (Figure 1.3.1C). Around E7.5-8.0, the lateral wings of the cardiogenic fields move toward the ventral midline where they fuse to form the linear heart tube which consists of an outer layer of myocardium and an inner layer of endothelial cells (Figure 1.3.1D).

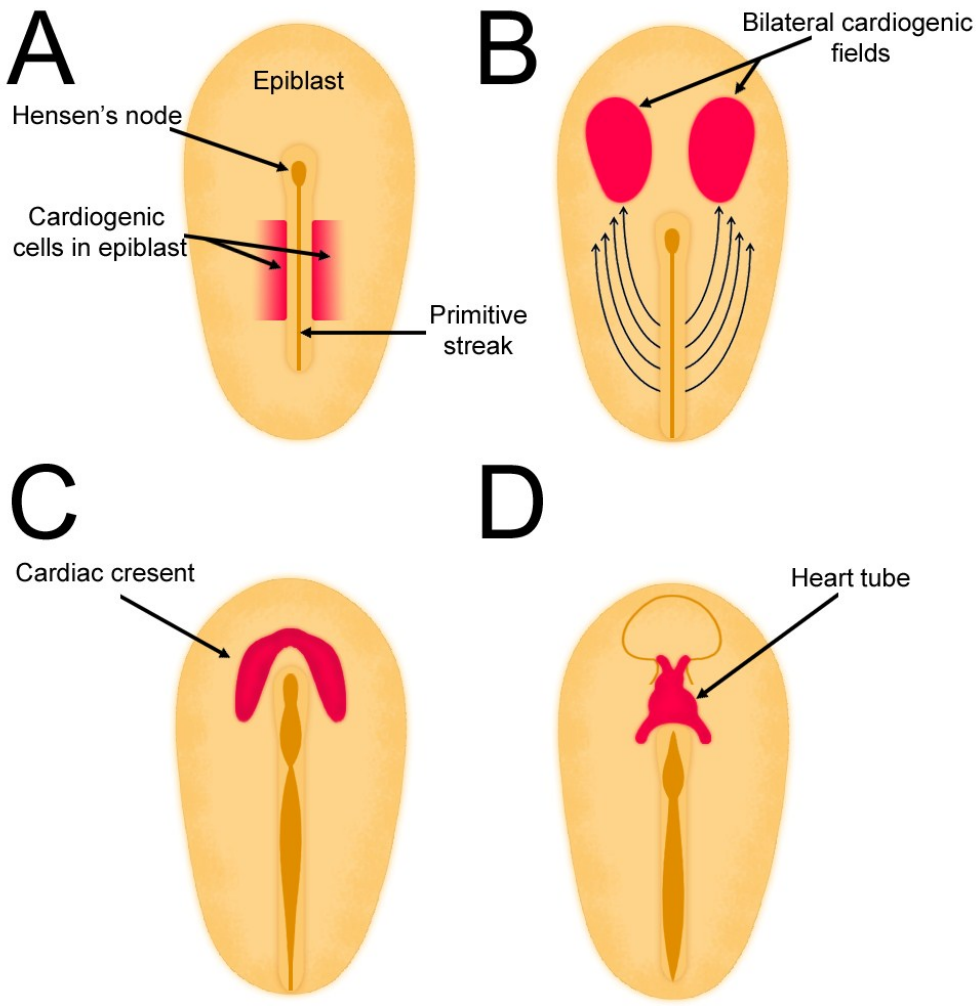

Figure 1.3.1: Schematic diagram of the localization of cardiogenic cells in the epiblast and the formation of the primitive heart tube. A) The earliest cardiogenic precursor cells are located on both sides of the midline in the epiblast at the early gastrulation stage. **B)** Epiblast cells then ingress through the primitive streak to form the mesodermal germ layer. Mesodermal cardiac precursor cells migrate laterally and cranially from the primitive streak which results in the establishment of bi-lateral cardiogenic fields in the regions of the anterior lateral plate mesoderm. **C)** Continuous migration of cells from the primitive streak to the lateral plate and to the midline results in formation of the cardiac crescent. **D)** The lateral wings of the cardiogenic fields move toward the ventral midline where they fuse to form the linear heart tube which consists of an outer layer of myocardium and an inner layer of endothelial cells. Figure re-drawn and modified from Kirby (2007) and Fishman and Chien (1997).

1.3.2 Induction and Differentiation of the Myocardium

Induction refers specifically to the process whereby a particular tissue emits signals in the form of growth factors or morphogens that are able to induce a specific response in a target cell type (Kirby, 2007). In the context of cardiogenesis, induction of the cardiomyogenic lineage from mesodermal cells ingressing through the primitive streak occurs in response to specific protein factors secreted from the underlying tissue layer referred to as the hypoblast in chick or anterior visceral endoderm in mouse (Figure 1.3.2A) (Chapman et al., 2003). These secreted factors, which include members of the transforming growth factor (TGF)β family initiate expression of specific cardiogenic transcription factors such as Nkx2.5 which is considered to be among the earliest markers of the cardiomyogenic lineage (Komuro and Izumo, 1993; Harvey, 1996).

Differentiation, which follows the initial induction step, refers to the morphological appearance of cell specializations that are characteristic of a particular cell lineage (Kirby, 2007). For cardiomyocytes, specializations include the appearance of contractile proteins, specific transmembrane ion channels and gap junction proteins. Interestingly, even prior to formation of the heart tube at the ventral midline, contractile cardiomyocytes expressing isoforms of the muscle proteins actin and myosin can be detected in the bi-lateral cardiogenic fields as early as E7.5-8.0 (Sassoon et al., 1988; Lyons et al., 1990). This early differentiation process occurs in response to secreted factors from the underlying endoderm in a process analogous to the initial induction of the cardiomyogenic lineage (Figure 1.3.2B). These factors, which include members of the bone morphogenetic protein (BMP) and fibroblast growth factor (FGF) families (Srivastava and Olson, 2000; Alsan and Schultheiss, 2002) promote expression of Nkx2.5

as well as several other key cardiac transcription factors from the GATA, MEF2 ,T-box (Tbx), Iroquois (Irx) and Hand families that act in a combinatorial manner to promote cardiomyocyte differentiation by turning on a cardiac specific program of gene expression (Durocher and Nemer, 1998; Srivastava and Olson, 2000). Importantly, inhibitory factors such as canonical Wnt signals secreted from ectodermal tissue and Noggin expressed in the notochord ensure that inappropriate expansion of the myocardium does not occur outside of the defined cardiogenic field (Figure 1.3.2B) (Kirby, 2007). In summary, a combination of positive and negative cardiogenic factors spatially defines the bilateral cardiogenic fields which are comprised of a mixed population of undifferentiated CPCs as well as contractile cardiomyocytes. After fusion of the cardiogenic fields at the ventral midline, a highly ordered program of cardiac cell migration, proliferation and differentiation occurs to transform the primitive heart tube into a complex four chambered pump.

Figure 1.3.2: Induction and differentiation of the cardiomyogenic lineage. A) Induction of the cardiomyogenic lineage from mesodermal cells ingressing through the primitive streak occurs in response to specific protein factors secreted from underlying hypoblast (anterior visceral endoderm in mouse) such as TGF-β (represented by white arrows). **B)** Cardiac progenitor cells within the bi-lateral cardiogenic fields (dark red) differentiate into mature cardiomyocyte lineages in response to secreted factors such as Bone Morphogenetic Protein (BMP) and Fibroblast Growth Factor (FGF) which are secreted from the underlying endoderm (represented by blue arrows). These factors promote expression of Nkx2.5 as well as several other key cardiac transcription factors from the GATA, MEF2, T-box (Tbx), Iroquois (Irx) and Hand families that act in a combinatorial manner to promote cardiomyocyte differentiation by turning on a cardiac specific program of gene expression. Inhibitory factors such as canonical Wnt signals secreted from ectodermal tissue and Noggin expressed in the notochord ensure that inappropriate expansion of the myocardium does not occur outside of the defined cardiogenic field. Figure re-drawn and modified from Kirby (2007).

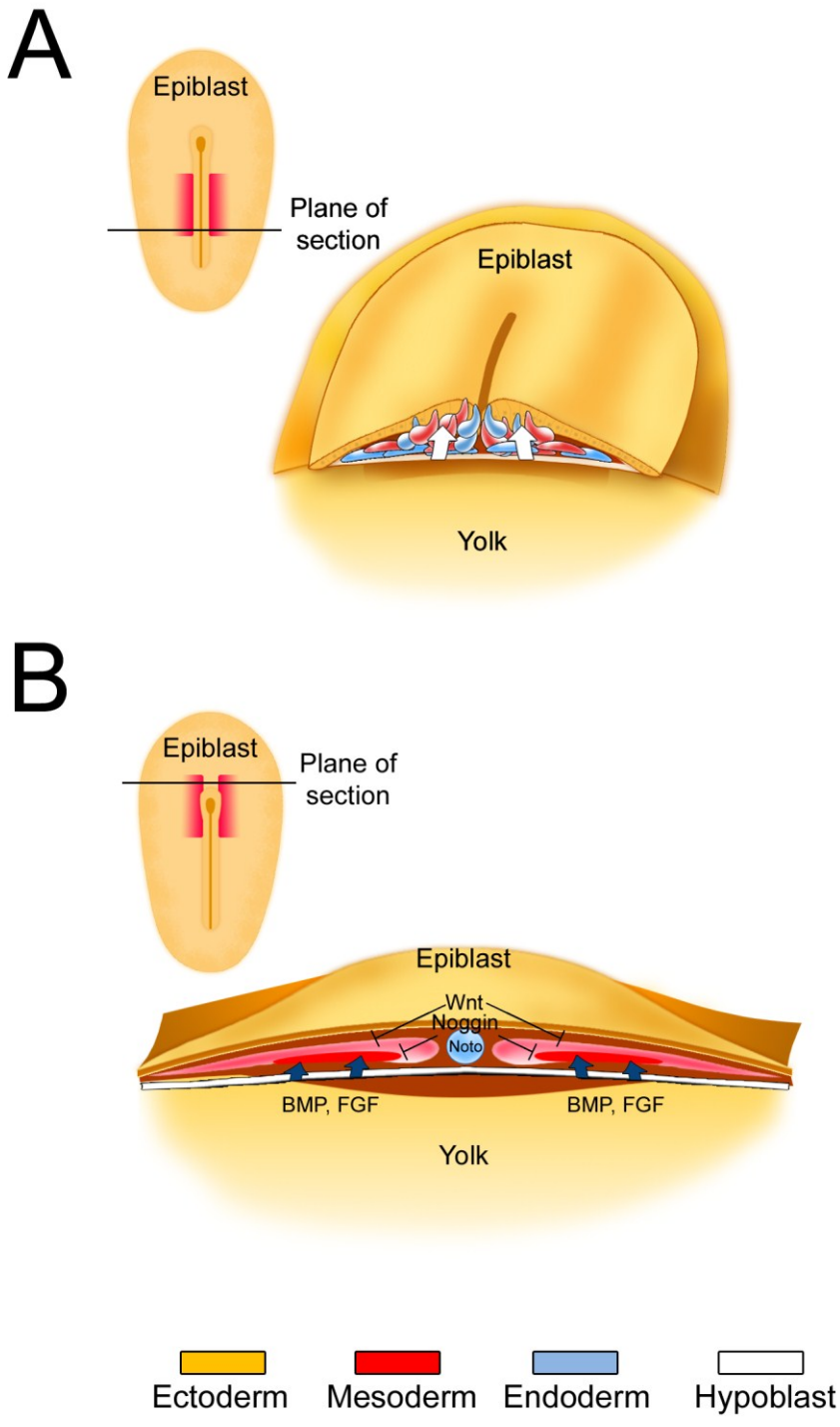
A
Epiblast
Plane of section
Epiblast
Yolk
B
Epiblast
Plane of section
Epiblast
Wnt
Noggin
Noto
BMP, FGF
BMP, FGF
Yolk
Ectoderm
Mesoderm
Endoderm
Hypoblast

1.3.3 Cardiac Looping and Formation of the Four Chambered Heart

The heart tube, which lies in the midline of the embryo, is segmentally patterned along the cranio-caudal axis (Kirby, 2007). Blood enters at venous (inflow) pole located at the caudal end of the heart tube which represents the site of the future atrial chambers. Blood is then moved in a unidirectional manner through the heart tube and exits at the arterial (outflow) pole which is located cranially. At approximately E9 in mouse, the heart tube undergoes rightward looping to form a C-shaped structure which results in the formation of a broad outer curvature and a more narrow inner curvature (Olson and Srivastava, 1996; Christoffels et al., 2000). During the looping process, the future ventricles become visible as they balloon outwards from the outer curvature (Harvey, 2002). Furthermore, the atrial region is forced dorsally and cranially to bring the inflow and outflow regions in close proximity and into their anatomically correct mature positions (Kirby, 2007).

At approximately E9, the internal structures of the heart also become more complex as the primordia of the valves and septa begin to form. In addition, the trabeculae, which are spongiform layers of myocardium that project into the lumen, are also formed along the inner surface of the ventricles and the forming interventricular septum (Harvey, 2002). Formation of the definitive four-chambered heart occurs at approximately E10.5, and is followed by complete septation and valve formation (Buckingham et al., 2005).

Simultaneous with the morphological transformation of the heart tube into a four chambered structure, CPCs enter differentiation pathways toward the mature cardiomyocyte lineages (e.g. atrial, ventricular and conduction system). The specific

contractile, electrophysiological and molecular specializations adopted by each cell type are specified by a highly ordered network of transcriptional regulators that are required for proper cardiogenesis (Barnett et al., 2012; Rana et al., 2013).

1.3.4 Development of the Cardiac Conduction System

In the early heart tube, leading pacemaker activity at the venous pole of the heart can be detected even before the morphological appearance of the distinct components of the cardiac conduction system (Kamino et al., 1981). The resulting impulse then travels relatively slowly toward the arterial pole to initiate a unidirectional, peristaltic mode of contraction (Patten, 1949). This slow conducting myocardium in the early heart tube has been dubbed the "primary myocardium" to distinguish it from more developed working atrial and ventricular chamber myocardium (Moorman and Lamers, 1994).

A prominent feature of the primary myocardium is the presence of action potentials which display slow depolarizations that resemble those of mature SA nodal cells (Sperelakis and Pappano, 1983). The ionic basis for this resemblance comes from the fact that the rising phase of the action potential in early cardiomyocytes is dependent on activity of voltage gated L-type and T-type Ca^{2+} channels rather than fast activating Na^{+} channels (Kirby, 2007). As development proceeds, the mature electrical activation pattern of the four chambered heart is achieved by the differentiation and patterning of the discreet components of the cardiac conduction system.

Of particular interest in our laboratory, is the development of the fast-conducting component of the ventricular conduction system, particularly the Purkinje fiber network. Functional and molecular correlates have indicated that the trabecular myocardium serves

as the preferential route for the conduction of electrical impulses prior to the establishment of the mature ventricular conduction system components (Rentschler et al., 2001; Sankova et al., 2012). Furthermore, the trabecular myocardium has been shown to house the myogenic precursors of the mature Purkinje fiber network (Christoffels and Moorman, 2009). While the precise factors which guide lineage fate decisions in the embryonic heart are still not fully understood, there is evidence that paracrine factors secreted from the adjacent endocardium such as endothelin-1 (ET-1) and neuregulin-1 (NRG-1) provide instructive cues to guide undifferentiated cardiac precursors toward the conduction system cell fate (Gourdie et al., 1998; Rentschler et al., 2002)

Efforts to study the development of the conduction system have benefited from the generation of mouse models which enable direct visualization of either the entire conduction system or specific components therein (Kupershmidt et al., 1999; Davis et al., 2001; Rentschler et al., 2001). The gap junction protein Cx40 generates channels with high conductance (Beblo and Veenstra, 1997) and is expressed in the fast conducting Purkinje fibers of the mature ventricular conduction system (Gourdie et al., 1993; Myers and Fishman, 2003). Moreover, during development, Cx40 is expressed in the fast conducting trabecular myocardium which will form the mature conduction system (Delorme et al., 1995; Sankova et al., 2012). Thus, the $Cx40^{egfp}$ mouse model, in which the vital enhanced green fluorescent protein (EGFP) is expressed under the control of the Cx40 gene (Miquerol et al., 2004), is particularly useful for studying the morphological development of the ventricular conduction system.

1.3.5 Undifferentiated Cardiac Progenitor Cells in the Embryonic Heart Post-Chamber Formation

Owing to the small size of the primitive heart tube at early embryonic stages, a technical limitation associated with investigations into the development of CPCs has been the inability to acquire sufficient cell numbers for experimental purposes. However, the discovery of rare populations of CPCs in the adult myocardium (Hierlihy et al., 2002; Beltrami et al., 2003; Oh et al., 2003) pointed to the possibility that some cardiomyogenic mesodermal precursor cells may remain undifferentiated throughout the entire developmental period and into postnatal life. Thus, we reasoned that if a significant population of undifferentiated CPCs were present at later developmental stages (i.e. post-chamber formation); technical limitations associated with small yields from the heart tube could be overcome. To address this issue, our group used transmission electron microscopy to assess the ultrastructural characteristics of mouse ventricular cells at the post-chamber stage of E11.5 and discovered that at this stage the ventricles contained a significant population of undifferentiated $Nkx2.5^{+}$ CPCs as well as cardiomyocytes with varying degrees of sarcomeric organization (Zhang and Pasumarthi, 2007). Subsequently, we also demonstrated that $Nkx2.5^{+}$ cells isolated from the E11.5 ventricles could differentiate over time into cardiomyocytes *in vitro* (McMullen et al., 2009).

Based on the evidence that a significant number of undifferentiated CPCs exist in the ventricles at E11.5, we concluded that this was an appropriate stage to study CPC development. Accordingly, experiments in this thesis which aimed to clarify the effects of either Ca^{2+} channel blockade or ANP signalling on CPC proliferation and differentiation were routinely carried out using E11.5 ventricular cell populations. The

following section (Section 1.4) is meant to provide an overview of the role of Ca^{2+} signalling in cardiogenesis and provide a context for our investigations into the effects of Ca^{2+} channel blockade on CPC proliferation and differentiation. Similarly, Section 1.5 which follows is meant to provide an overview of atrial natriuretic peptide mediated signalling systems and provide the rationale for our interest in studying the role of this system in regulating cardiac development.

1.4 The Role of Ca^{2+} Signalling in Cardiogenesis

In the mature cardiomyocytes of the adult heart, Ca^{2+} is most recognized for its central role in EC coupling (Bers, 2002). In this process, the influx of Ca^{2+} through voltage gated L-Type Ca^{2+} channels located within the *t*-tubule network induces the release of a much greater amount of Ca^{2+} from the SR through ryanodine receptors in a process referred to as Ca^{2+} induced Ca^{2+} release (CICR) (Fabiato, 1983). This transient rise in intracellular Ca^{2+} in turn facilitates actin and myosin interactions which results in cardiomyocyte contraction. In contrast to adult cardiomyocytes, embryonic cardiomyocytes lack *t*-tubules and have a poorly developed SR (Cohen and Lederer, 1988; Klitzner and Friedman, 1989; Qu and Boutjdir, 2001; Liu et al., 2002; Kirby, 2007). Consequently, most of the Ca^{2+} required for contraction of embryonic cardiomyocytes comes from the extracellular space via sarcolemmal Ca^{2+} channels including L-type as well as T-type voltage gated Ca^{2+} channels. Additionally, Ca^{2+} influx via L-type and T-type Ca^{2+} channels has been implicated in critical aspects of cardiogenesis including lineage specification, gene expression, proliferation and myofibrillogenesis (Li et al., 2005; Puceat and Jaconi, 2005; Nguemo et al., 2013).

1.4.1 Biophysical and Pharmacological Properties of L-type and T-type Ca^{2+} Channels

The L-type and T-type Ca^{2+} channels are two distinct families of voltage gated Ca^{2+} channels, which have integral roles in various aspects of cardiomyocyte physiology. The family of L-type Ca^{2+} channels is comprised of four genetically distinct members referred to as ($Ca_v1.1$-$Ca_v1.4$), while the family of T-type Ca^{2+} channels consists of three members ($Ca_v3.1$-$Ca_v3.3$) (Ertel et al., 2000). The L-type Ca^{2+} channels are oligomeric complexes composed of a relatively large pore forming α1 subunit and smaller auxiliary, β, γ and di-sulfide linked α2/δ subunits which regulate channel function (Katzung, 2009). These channels are characterized by long-lasting, high voltage activated currents (Lipscombe et al., 2004). By contrast, T-type Ca^{2+} channels are monomeric structures which consist of only a α1 subunit (Katzung, 2009), and are characterized by transient currents which are activated at lower voltages (Perez-Reyes, 2003).

The α1 subunit of L- and T-type Ca^{2+} channels contains the known sites of channel regulation by second messengers and pharmacological drugs. The L-type Ca^{2+} channels are also referred to as dihydropyridine (DHP) receptors/channels because they bind with high affinity to this class of Ca^{2+} channel blocking drugs (e.g. nifedipine, isradipine, nisoldipine) (Katzung, 2009). While T-type Ca^{2+} channels were initially described as insensitive to DHPs, there is now substantial evidence that certain DHPs can also inhibit T-type Ca^{2+} channels with relatively low potency (IC_{50} values between ~10-100μM) (Kumar et al., 2002; Shcheglovitov et al., 2005; Perez-Reyes et al., 2009). A limitation to studying T-type Ca^{2+} currents has been the lack of specific pharmacological inhibitors. For instance, while mibefradil was initially presented as a selective T-type

Ca^{2+} channel blocker (Clozel et al., 1997), it was subsequently shown that this molecule also inhibits several other channels (Viana et al., 1997; Gomora et al., 1999).

1.4.2 Impaired Cardiogenesis due to Disrupted Intracellular Ca^{2+} Homeostasis

The cardiogenic process relies on a highly orchestrated balance between proliferation and differentiation of CPCs and cardiomyocytes (Goetz and Conlon, 2007). Research dedicated to understanding the molecular mechanisms governing this balance is driven by the high incidence of congenital heart defects in the human population (Hoffman, 1995) and the potential utility of undifferentiated CPC/cardiomyocytes in the field of regenerative medicine (McMullen and Pasumarthi, 2007). In addition to its role in generating action potentials, Ca^{2+} activates signalling cascades which involve several kinases and phosphatases (Crabtree, 2001; Kahl and Means, 2003; Colomer et al., 2004). These intermediary enzymes can in turn alter the phosphorylation status, and thus the transcriptional activity, of key cardiac transcription factors such as GATA4 and MEF2c which ultimately controls the balance between cardiac cell proliferation and differentiation (McKinsey et al., 2002; Pikkarainen et al., 2004).

In a study carried out by Porter and colleagues (2003), it was reported that whole embryos (E7.5-E8.5) cultured in the presence of the DHP Ca^{2+} channel blocker nifedipine displayed cardiac morphological defects as well as reduced expression of the transcription factor GATA4 and the sarcomeric protein ventricular myosin light chain 2v (MLC2v). Moreover, it was shown that in ES cell derived cardiomyocytes, disruption of intracellular Ca^{2+} homeostasis using the Ca^{2+} chelator BAPTA was associated with impaired myofibrillogenesis and that this effect could be reversed by restoring

intracellular Ca^{2+} by treatment with ionomycin (Li et al., 2002). Taken together, these results provided evidence that intracellular Ca^{2+} signalling pathways are critically involved in the cardiomyogenic process by regulating cardiomyocyte differentiation/maturation.

The T-type Ca^{2+} channels are widely expressed in a variety of cell types during the developmental period, while in post-natal life their expression is restricted to a few specialized cell types including excitable pacemaker cells within the cardiac conduction system (Hirano et al., 1989; Lory et al., 2006; Ono and Iijima, 2010). Accordingly, T-type Ca^{2+} channels have been implicated in cell growth and proliferation during the embryonic period. Consistent with this view, prominent T-type Ca^{2+} currents have been recorded in embryonic/fetal as well as neonatal cardiomyocytes in rodents but were absent at adult stages (Cribbs et al., 2001; Ferron et al., 2002; Niwa et al., 2004). Moreover, pharmacological inhibition of T-type Ca^{2+} channels was shown to reduce glucose stimulated proliferation in neonatal rat ventricular cardiomyocytes (Li et al., 2005), thus providing evidence for a direct link between the T-type Ca^{2+} current and signalling cascades which regulate the cell cycle machinery.

More recently, it was demonstrated that treatment of ES cells with nifedipine was associated with impaired ability of these cells to differentiate into cardiomyocytes, (Nguemo et al., 2013), thus providing indirect evidence that voltage gated Ca^{2+} channels are expressed by CPCs and are critically involved in the earliest stages of cardiomyogenic lineage commitment. Currently, it remains unknown whether influx of extracellular Ca^{2+} via voltage gated Ca^{2+} channels plays a role in regulating proliferation of CPCs derived from the post-chamber formation stage of the embryonic heart.

1.4.3 Therapeutic Potential of Cardiac Progenitor Cells for Myocardial Repair

Shortly after birth, cardiomyocytes lose their capacity to divide (Pasumarthi and Field, 2002). Therefore, cardiomyocytes lost to disease or injury are replaced by fibrotic scar tissue rather than new muscle tissue. Currently, a host of cardiovascular drugs and surgical interventions are used to slow the progression of heart disease (Salters et al., 2010), but neither approach can replace the damaged myocardium. Accordingly, donor cell transplantation has emerged as a promising strategy for myocardial repair (Laflamme and Murry, 2005; McMullen and Pasumarthi, 2007).

The first derivation of embryonic stem (ES) cells from the inner cell mass of the pre-implantation stage mouse (Evans and Kaufman, 1981; Martin, 1981) and subsequently human (Thomson et al., 1998) embryos were major milestones in the field of regenerative medicine. ES cells, which are capable of unlimited undifferentiated proliferation *in vitro*, are capable of forming all of the hundreds of cell types in the human body and thus hold the ultimate regenerative potential (Murry and Keller, 2008). Unfortunately, however, adult myocardium apparently lacks the molecular cues required to guide undifferentiated ES cells toward the appropriate cardiac cell lineages following transplantation. For example, undifferentiated mouse ES cells were shown to form teratomas consisting of cell types from endodermal, ectodermal and mesodermal germ layers following intra-cardiac transplantation into either the uninjured or infracted adult mouse heart (Nussbaum et al., 2007).

Transplantation of committed cell types into the adult myocardium could in principle circumvent problems associated with teratoma formation seen with undifferentiated ES cells (Thomson et al., 1998; Nussbaum et al., 2007). To this end, cell

transplantation of various committed cell types including skeletal myoblasts were investigated for their potential in myocardial repair (McMullen and Pasumarthi, 2007). In experimental models, substantial evidence for engraftment of skeletal myoblasts into host myocardium and improvement in post-infarction cardiac function was reported (Chiu et al., 1995; Murry et al., 1996; Taylor et al., 1998). Similarly, improvements in ejection fraction and improved systolic thickening were reported in the first human clinical trial in which skeletal myoblasts were transplanted into patients with severe ischemic cardiomyopathy (Menasche et al., 2003). It is generally accepted, however, that these functional improvements observed in both experimental and clinical settings were due to the effects of secreted paracrine factors, enhanced angiogenesis and/or favorable scar remodeling rather than transdifferentiation of skeletal myoblasts into cardiomyocytes. Moreover, arrhythmias were prevalent among patients following skeletal myoblast transplantation (Menasche et al., 2003) and were likely due to the inability of these cells to form electrical connections with the host myocardium. By contrast, transplantated fetal cardiomyocytes have been shown to integrate functionally with host myocardium (Rubart et al., 2003) and suppress the induction of ventricular tachycardia in experimental models of cardiac injury (Roell et al., 2007).

While it is neither practical nor ethical to consider the large scale production of fetal cardiomyocytes for human clinical trials, ES cells or autologous induced pluripotent cells (iPS), which can be guided toward the cardiomyogenic lineage (Klug et al., 1996; Zwi-Dantsis and Gepstein, 2012), represent a potentially unlimited source of cardiomyocytes that could be used for cell transplantation therapies. Indeed, ES-cell derived cardiomyocytes have recently been shown to form true gap junctions, couple

electrically with the host myocardium and improve cardiac function in an experimental animal model of cardiac injury (Shiba et al., 2012).

A long standing hurdle in the cardiac transplantation field is the long term engraftment and expansion of the donor cells in the engrafted myocardium (Reinecke and Murry, 2002). To address this issue, it has been suggested that maneuvers to increase cell proliferation of transplanted cells could significantly improve the ability to replenish damaged myocardial tissue (Laflamme and Murry, 2005). In this regard, we believe that CPCs, which have the hallmark feature of high rates of proliferation, represent a promising candidate cell type. Furthermore, CPCs are capable of differentiating into mature cardiomyocyte lineages (i.e. atrial, ventricular and conduction system) (Martin-Puig et al., 2008) and therefore hold the potential to couple functionally with host myocardium. Deciphering the molecular mechanisms underlying differentiation of CPCs toward committed cardiomyocyte lineages and also the potential interactions of CPCs with commonly used cardiovascular drugs would be significant steps toward the development of more effective cell based therapies for myocardial repair.

1.5 The Natriuretic Peptides and their Cell Surface Receptors

1.5.1 Section Overview

Atrial natriuretic peptide (ANP) is part of a family of hormone/paracrine factors known as natriuretic peptides which are involved in regulating cardiovascular homeostasis (McGrath et al., 2005). Natriuretic peptides mediate their cellular and biological effects by binding to cell surface receptors known as natriuretic peptide receptors (NPRs). In the mature heart, the primary site of ANP synthesis and storage is

in the cardiomyocytes of the atrial chambers. While ANP gene expression in the ventricles is normally ~100 fold lower compared to the atria (Nemer et al., 1986), increased expression is associated with pathophysiological situations (Chien et al., 1991). By contrast, in the embryonic heart, ANP mRNA expression in the atria and ventricles is approximately equal (Zeller et al., 1987). At later developmental stages, however, ANP is downregulated in the ventricles, but remains high in the atria into post-natal life. Importantly, immunoreactive ANP persists in a relatively small population of ventricular cardiomyocytes that form the fast conducting Purkinje fibers of the ventricular cardiac conduction system (Toshimori et al., 1987b; Cantin et al., 1989). Moreover, dysregulated expression of ANP in the ventricles during cardiogenesis has been associated with several forms of congenital heart disease which involve abnormal patterning of the heart and conduction system defects (Bruneau, 2011). Despite this knowledge, a specific role for ANP in cardiogenesis remains to be clearly defined. To address this issue, work in this thesis aimed to determine whether ANP mediated signalling systems were biologically intact in the embryonic heart and whether they play any role in regulating cell proliferation and/or differentiation. Accordingly, the following subsections are aimed at providing an overview of the salient structural and physiological features of ANP and its cognate receptors and also provide a rationale for our studies.

1.5.2 Historical Perspective: Discovery of the 'Atrial Natriuretic Factor' and the Natriuretic Peptide Family

Over 50 years ago, it was first speculated that the heart, aside from its vital role as a pump, also served an endocrine function. This speculation was borne from seminal observations of dense granules resembling secretory vesicles in the atrial cardiomyocytes

of several mammalian species (Kisch, 1956; Jamieson and Palade, 1964). The contents and function of these granules, however, remained a mystery for several decades until the land mark study by de Bold and his colleagues showed that injection of atrial extracts could rapidly stimulate natriuresis and diuresis and lower blood volume in rats (de Bold et al., 1981). Because the identity of specific protein (or proteins) responsible for these physiological effects was unknown, the authors assigned it the name atrial natriuretic factor (ANF) (de Bold et al., 1981).

Two years after the discovery of the atrial natriuretic factor, the same group, isolated, purified and sequenced a protein from rat atria capable of inducing an identical diuretic and natriuretic response, and named it cardionatrin I (de Bold and Flynn, 1983; Flynn et al., 1983). The human homolog was sequenced shortly after, and was referred to as human atrial natriuretic polypeptide (Kangawa and Matsuo, 1984). From these studies, it was determined that the biologically active molecule was a 28 amino acid peptide with a looped region formed by a disulfide link between two cysteine residues (Figure 1.5.1). In subsequent years, several other names for this peptide appeared in the literature, but today it is most commonly referred to as atrial natriuretic peptide (ANP).

The discovery of a naturally occurring polypeptide with the ability to lower blood volume and blood pressure was immediately recognized for its clinical potential in treating a range of cardiovascular diseases. This realization served as the driving force behind the ensuing explosion of research aimed at characterizing mechanisms underlying ANP production and storage in atrial granules, its secretion into the circulation and ultimately its actions at target organs throughout the body. These efforts also led to the discovery of the structurally related polypeptides, B-type natriuretic peptide (BNP)

(Sudoh et al., 1988) and C-type natriuretic peptide (CNP) (Sudoh et al., 1990) which, together with ANP, comprise the mammalian natriuretic peptide family (Figure 1.5.1). The natriuretic peptides are genetically distinct and evolutionary studies suggest that all members are derived from gene duplication events of a single natriuretic peptide gene (Rosenzweig and Seidman, 1991; Inoue et al., 2003). All three natriuretic peptides are produced as prepro hormones and processed into smaller, C-terminal, biologically active peptides by specific proteases (Figure 1.5.1). Collectively, natriuretic peptides exert a broad range of physiological functions in cell types from numerous organ system (Potter et al., 2006).

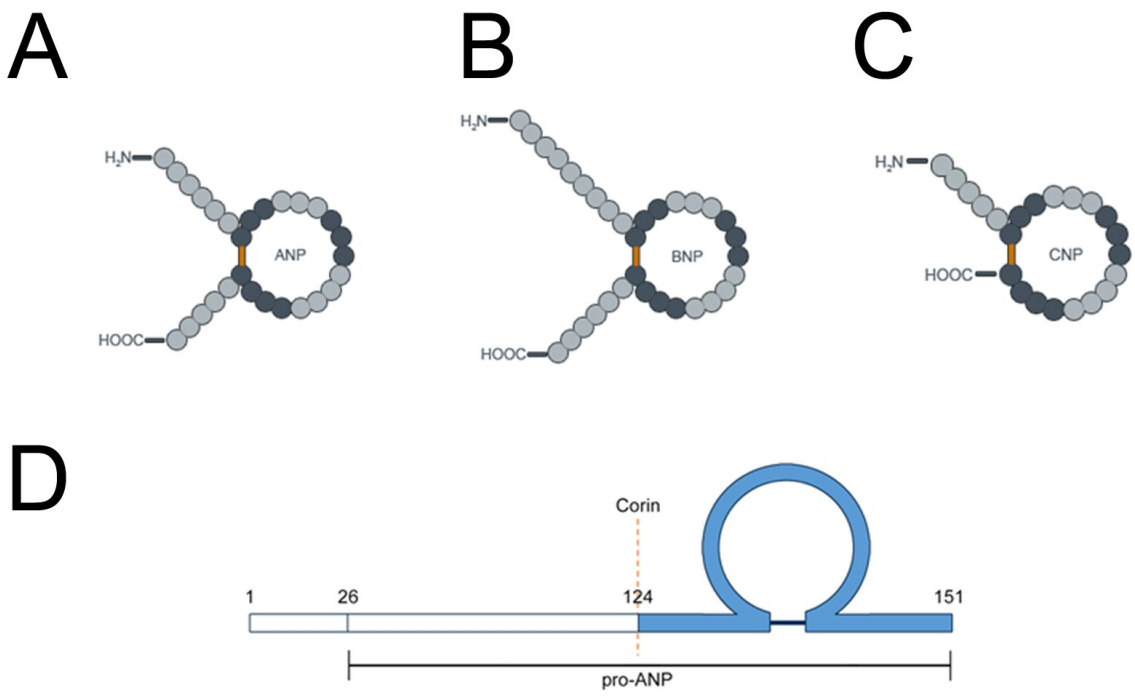

Figure 1.5.1: Structures of the natriuretic peptides and processing of atrial natriuretic peptide. A-C) The mammalian natriuretic peptide family is comprised of three members: atrial natriuretic peptide (ANP), B-type natriuretic peptide (BNP) and C-type natriuretic peptide (CNP). All three natriuretic peptides contain a conserved 17 amino acid disulfide linked ring structure that is required for biological activity. The locations of amino acids that are conserved between all three natriuretic peptides are represented by darker circles. **D)** All three natriuretic peptides are generated as prepro hormones and are proteolytically processed into smaller biologically active peptides. Only the processing steps for ANP are described herein. The signal sequence is cleaved from the N-terminal to form the 126 amino acid proANP molecule (referred to as 1-126). The type II transmembrane protease corin further processes proANP into the 28 amino acid biologically active form (referred to as 99-126).

1.5.3 Atrial Natriuretic Peptide Gene Expression and Regulation

The gene encoding ANP (*Nppa)* contains 3 exons and is located on chromosome 1 in human and chromosome 4 in mouse (Yang-Feng et al., 1985). During mammalian development, expression of ANP mRNA can first be detected in the primitive heart tube (Zeller et al., 1987) and serves as a early marker of the differentiating atrial and ventricular myocardium (Christoffels et al., 2000). In the early four chambered heart, ANP expression persists in the myocardium of both the primitive atrial and ventricular chambers at comparable levels. As development proceeds, high levels of ANP expression persist in the atria, but decline drastically in the ventricles to levels that are ~100 fold lower than those in the atria in the mature heart (Nemer et al., 1986).

Genetic manipulation of the *Nppa* promoter revealed that the *cis*-elements required to achieve the dynamic chamber/developmental stage specific expression pattern of ANP are contained within a ~500 bp upstream sequence and are organized into distinct regulatory modules (Argentin et al., 1994). Each of these modules contains combinations of regulatory elements required for binding of key cardiac transcription factors including Nkx2.5 (NKE), GATA4, Hand, MEF2c ,Tbx5 (TBE), and serum response factor (SRE) which enables differential expression of ANP to occur in a cell-type specific manner at developmental or postnatal stages (Durocher and Nemer, 1998; Belaguli et al., 2000; Morin et al., 2000; Hiroi et al., 2001; Dai et al., 2002; Thattaliyath et al., 2002; Small and Krieg, 2003; Morin et al., 2005). Importantly, mutations in these transcriptional regulators have been shown to be associated with impaired cardiogenesis in experimental animals and human congenital heart diseases and in some cases were shown to be associated with dysregulated expression of ANP (Lin et al., 1997; Molkentin

et al., 1997; Schott et al., 1998; Tanaka et al., 1999; Bruneau et al., 2001; Garg et al., 2003).

In pathological situations associated with prolonged periods of cardiac stress, expression of ANP is re-initiated in the ventricles as part of the "fetal gene expression program" along with a panel of several other metabolic enzymes and contractile proteins normally expressed during the embryonic period (Chien et al., 1991; Schaub et al., 1997). Interestingly, the regulatory sequences that control the expression of ANP during development appear to be distinct from those responsible for reactivation of expression during cardiac disease (Horsthuis et al., 2008), illustrating the complex nature of gene regulation *in vivo*. Overall, the extensively studied ANP promoter provides a valuable tool for delineating the transcriptional control networks involved in regulating both cardiac development and disease.

1.5.4 Storage and Secretion of Atrial Natriuretic Peptide

ANP is synthesized as a prepro peptide of 151 amino acids and subsequently gets cleaved at the amino terminus to yield a 126 amino acid proANP that constitutes the major storage form of ANP in secretory granules (Figure 1.5.1) (Ruskoaho, 1992). Co-incident with its secretion, proANP gets further processed by the type II transmembrane protease corin (Yan et al., 2000) into a 28 amino acid, biologically active peptide (Flynn et al., 1985). Following its release into the circulation, ANP mediates reductions in blood volume and blood pressure via integrated actions on several target organs in an endocrine fashion (Potter et al., 2006). Alternative processing of proANP has also been shown to occur in the kidney to yield a 32 amino acid peptide referred to as urodilatin,

which is thought to play a local role in regulating fluid homeostasis (Forssmann et al., 1998). Like other natriuretic peptides, ANP is characterized by a conserved 17 amino acid disulfide linked ring structure which is required for biological activity (Inagami et al., 1987). Although ANP protein has been well conserved across mammalian species, several differences in amino acid sequences exist between humans and commonly used experimental species including mouse and chicken (Figure 1.5.2).

The main stimulus for ANP release from atrial cardiomyocytes *in vivo* was shown to be mechanical stretch of the atrial myocardial wall which occurs in response to fluid volume expansion (Lang et al., 1985; Edwards et al., 1988). Based on these findings it was hypothesized that mechanosensitive stretch-activated ion channels known to be expressed by cardiomyocytes (Kim, 1992; Kim, 1993) could be involved in coupling the mechanical stimulus into a secretory response. This hypothesis was supported by subsequent experiments which demonstrated that gadolinium, a blocker of stretch activated ion channels, could decrease stretch-induced ANP secretion in the isolated rat atrium (Laine et al., 1994). In addition to mechanical stimuli, several vasoconstrictor peptides including endothelin-1 (ET-1) and angiotensin II (Ang II) have also been shown to stimulate ANP secretion from isolated hearts or cultured cardiomyocytes (Lew and Baertschi, 1989; Sei and Glembotski, 1990; Focaccio et al., 1993; Church et al., 1994a). While the precise molecular mechanisms governing ANP secretion have not been fully resolved, there is substantial evidence that Ca^{2+}, a long recognized regulator of secretion in various excitable and non-excitable cell types (Penner and Neher, 1988), also plays a central role in regulating myocardial ANP secretion (LaPointe et al., 1990; Church et al., 1994b; De Young et al., 1994; McDonough et al., 1994; Rebsamen et al., 1997).

In general, secretion of a protein from any given cell can occur in either a cell-signal dependent (regulated) or constitutive (unregulated) manner (Burgess and Kelly, 1987). Atrial cardiomyocytes of the adult mammalian heart have the hallmark features of a regulated secretory cell type including dense secretory granules, long term storage of granules in the cytoplasm and secretion mechanisms that are coupled to specific extracellular stimuli (Burgess and Kelly, 1987). By contrast, levels of immunoreactive ANP in the adult ventricles are ~1000 fold lower than those seen in the atria and secretory granules are only rarely observed (Nemer et al., 1986). Taken together, these observations suggested that a regulated secretory pathway predominates in the atria, while ANP synthesized in the ventricles is rapidly released as part of a constitutive secretory pathway. Consistent with this view, it was demonstrated that basal secretion of ANP from cultured ventricular cardiomyocytes was inhibited by brefeldin A (inhibits trafficking of newly synthesized proteins but does not affect release of stored proteins), while ANP secretion from atrial cardiomyocytes was enhanced (De Young et al., 1994). Subsequently, however, it was discovered that ET-1 and intracellular Ca^{2+} could stimulate ANP secretion from cultured ventricular cardiomyocytes and from the hypertrophied ventricular myocardium indicating that regulated secretory pathways may also exist in the ventricular compartment (Kinnunen et al., 1991; Irons et al., 1993). Currently, it remains unknown whether ANP is actively secreted by embryonic cardiomyocytes derived from the primitive, four chambered heart at earlier stages of cardiogenesis.

Figure 1.5.2: Alignment of the atrial natriuretic peptide predicted protein sequence from humans and several commonly used experimental species. The shaded boxes correspond to amino acids which are conserved between mouse, rat, sheep (ovine), human and chick. The boxed sequence corresponds to the 28 amino acid, biologically active form of ANP. The amino acid sequence is highly conserved among mammalian species, while the chick has 11 amino acids which differ from mammals.

Formatted Alignments

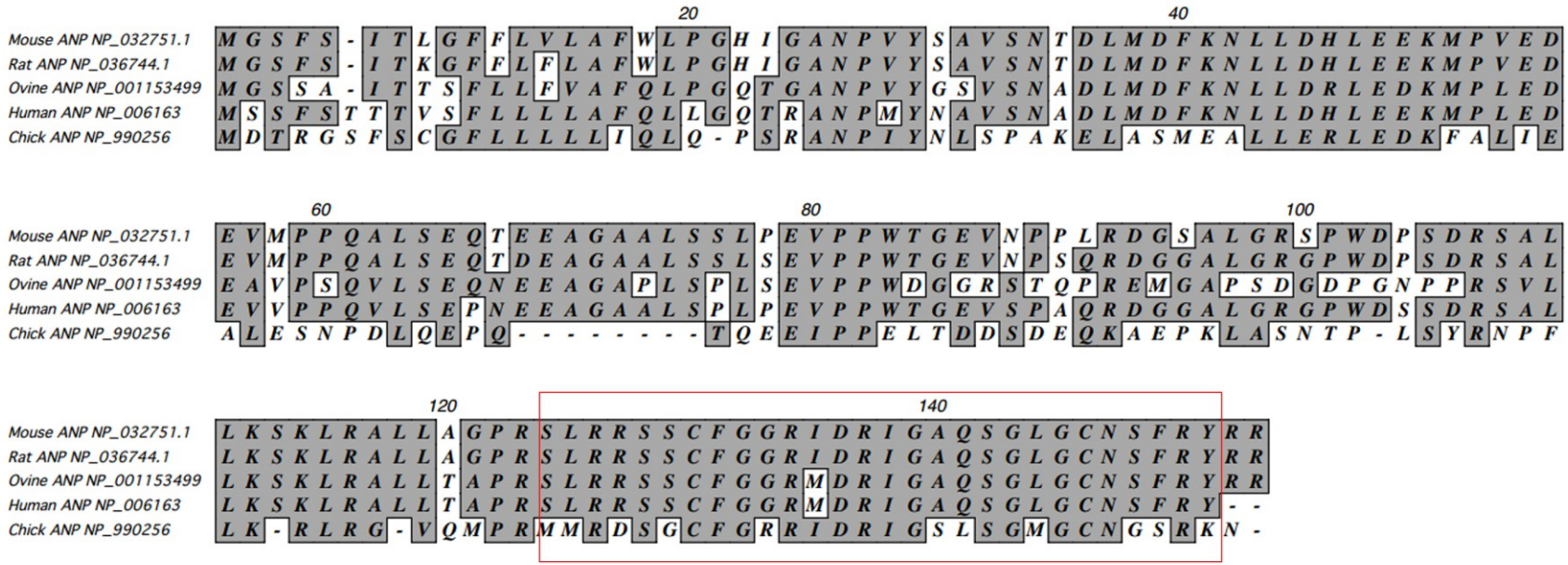

1.5.5 Historical Perspective on the Discovery of the Natriuretic Peptide Receptors

Early observations that ANP could stimulate cGMP production, suggested that the receptors for ANP were closely associated with a guanylyl cyclase enzyme (Hamet et al., 1984; Waldman et al., 1984; Winquist et al., 1984). Interestingly, the guanylyl cyclase enzyme that was isolated and purified was also able bind to ANP, which led to the hypothesis that the same protein was both an ANP receptor and a guanylyl cyclase enzyme (Kuno et al., 1986; Paul et al., 1987). This hypothesis was supported by the amino acid sequence of the ANP receptor which revealed an intracellular domain homologous to the guanylyl cyclase enzyme previously characterized in sea urchin (Singh et al., 1988; Chinkers et al., 1989; Lowe et al., 1989). Furthermore, transfection of the ANP receptor cDNA into heterologous cell systems led to expression of a functional receptor capable of binding ANP and stimulating intracellular production of cGMP (Chinkers et al., 1989; Lowe et al., 1989). This receptor was designated the ANP receptor guanylyl cyclase A (GC-A), also known as natriuretic peptide receptor A (NPRA).

The ANP receptor guanylyl cyclase represented a new paradigm in signal transduction, whereby extracellular ligand binding could allosterically induce second messenger production via intracellular enzyme activity (Lowe et al., 1989). Shortly thereafter, a protein homologous to NPRA, but having distinct pharmacological properties was isolated from human placental cDNA library (Chang et al., 1989). Guanylyl cyclase activity of this receptor was confirmed by expression of its cDNA in a heterologous cell system, and it was designated the natriuretic peptide receptor guanylyl cyclase B (GC-B) or NPRB (Chang et al., 1989). Around the same time, a third

natriuretic peptide receptor was isolated and purified from cultured bovine aortic smooth muscle cells (Schenk et al., 1987). Subsequent cloning of the receptor, designated NPRC, revealed that the intracellular domain, unlike NPRA and NPRB, was relatively small and apparently lacked an intrinsic guanylyl cyclase domain (Fuller et al., 1988). Based on this observation, NPRC was initially classified as a clearance receptor that served to buffer local natriuretic peptide concentrations (Maack et al., 1987). Subsequently, however it was discovered that NPRC could in fact modulate levels of the second messenger cAMP by inhibiting activity of adenylyl cyclase due to the presence of activator sequences for the inhibitory heterotrimeric G protein, (G_i) within the intracellular domain (Murthy and Makhlouf, 1999; Pagano and Anand-Srivastava, 2001).

1.5.6 Natriuretic Peptide Receptor Structure and Functional Activity

The mammalian guanylyl cyclase receptors (NPRA and NPRB) are composed of an extracellular N-terminal ligand binding domain (~450 amino acids), a single hydrophobic transmembrane domain (~20-25 amino acids) and a C-terminal intracellular domain (~570 amino acids) that is further subdivided into kinase homology, dimerization and guanylyl cyclase domains (Figure 1.5.3) (Potter et al., 2006). The gene encoding NPRA (*Npr1)* contains 22 exons and is located on chromosome 1 in human and chromosome 3 in mouse. The gene encoding NPRB (*Npr2*) also contains 22 exons and is located on chromosome 9 in humans and chromosome 4 in mouse. Comparisons between the human NPRA and NPRB DNA sequences revealed that the most highly conserved domain (88% amino acid identity) was found within the 252 residues at the C-terminus corresponding to guanylyl cyclase domain (Chang et al., 1989). Within the

extracellular domains, the overall amino acid sequence was found to be 44% identical, but a highly conserved region consisting of 28 amino acids (79% identity) was observed and was presumed to be important for recognition of natriuretic peptide ligands (Chang et al., 1989).

The rank order of ligand binding for NPRA is ANP > *BNP* >> *CNP* (Schulz et al., 1989; Suga et al., 1992). In the basal state, NPRA exists as a higher ordered oligomer and guanylyl cyclase activity is tightly repressed (Chinkers and Wilson, 1992; Lowe, 1992). Upon ligand binding, a conformational change in the juxtamembrane region is transmitted across the plasma membrane and activates guanylyl cyclase activity and production of cGMP (Ogawa et al., 2004). The principal downstream effectors of cGMP are: 1) cGMP dependent protein kinases (PKG), 2) cGMP-gated ion channels, and 3) cGMP-regulated phosphodiesterases (Lincoln and Cornwell, 1993). The rank order of ligand binding for NPRB is *CNP* >> *ANP* > BNP (Suga et al., 1992) and by mechanisms analogous to those described for NPRA are able to activate guanylyl cyclase activity and production of cGMP (Potter et al., 2006).

The gene encoding NPRC (*Npr3)* contains 8 exons and is located on chromosome 8 in human and chromosome 15 in mouse. The extracellular ligand binding domain of NPRC is similar in topology to the guanylyl cyclase receptors and analysis of the DNA sequence of this domain revealed ~ 30% amino acid identity with NPRA and NPRB (Chang et al., 1989). NPRC has been shown to bind with high affinity to all three natriuretic peptides (Suga et al., 1992). An inter-molecular disulfide bond between cysteine residues in the extracellular domain results in the formation of a covalent dimer and thus NPRC exists as a homodimer (Stults et al., 1994). The intracellular domain of

NPRC, unlike NPRA and NPRB, is relatively small consisting of only 37 amino acids and lacks intrinsic enzymatic activity (Fuller et al., 1988), but can activate Gi proteins to inhibit AC and consequently reduce production of cAMP (Anand-Srivastava et al., 1987). The principle downstream effectors of cAMP include: 1) cAMP dependent protein kinases (PKA), 2) cAMP-gated ion channels, and 3) cAMP-regulated phosphodiesterases (Houslay and Milligan, 1997; Kaupp and Seifert, 2002).

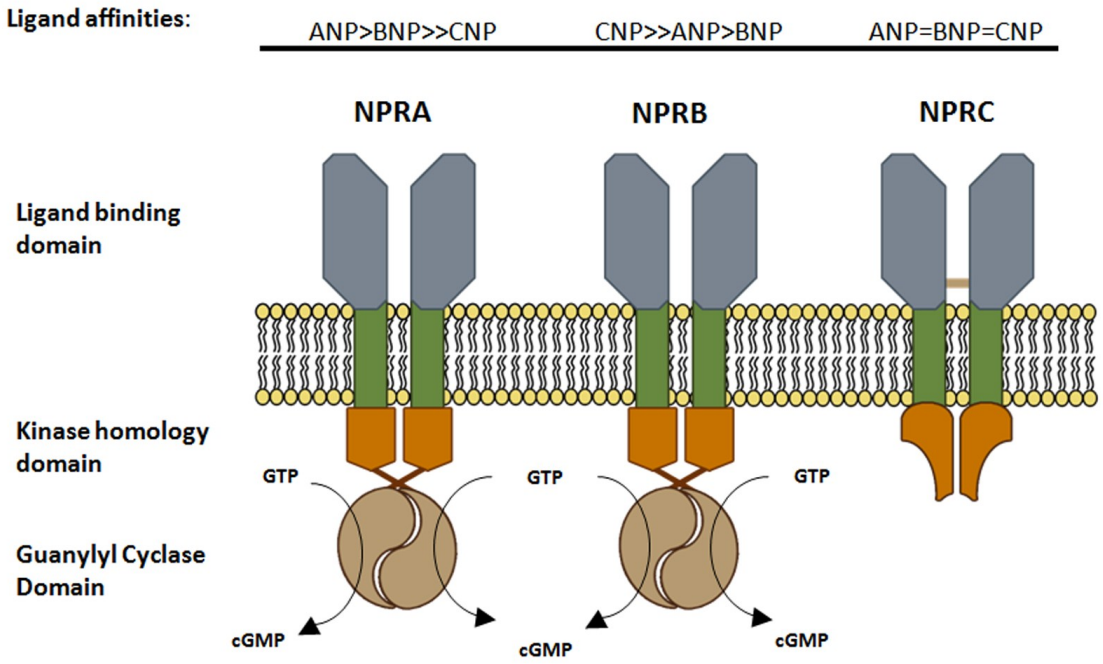

Figure 1.5.3 Natriuretic peptide receptor structures and ligand preferences. Natriuretic peptides bind to three subtypes of natriuretic peptide receptors: NPRA, NPRB and NPRC. Both NPRA and NPRB are guanylyl cyclase receptors which are composed of an extracellular N-terminal ligand binding domain, a single hydrophobic transmembrane domain and a C-terminal intracellular domain that is further subdivided into kinase homology, dimerization and guanylyl cyclase domains. The extracellular ligand binding domain of NPRC is similar in topology to the guanylyl cyclase receptors. An inter-molecular disulfide bond between cysteine residues in the extracellular domain results in the formation of a covalent dimer and thus NPRC exists as a homodimer. The intracellular domain of NPRC lacks intrinsic enzymatic activity, but contains activator sequences for the inhibitory heterotrimeric G protein (G_i) and thus couples to the adenylyl cyclase enzyme.

1.5.7 Physiological Effects of Atrial Natriuretic Peptide

The specific physiological effects of ANP depend upon the tissue distribution of its high affinity receptor subtypes NPRA and NPRC. The ANP/NPRA/cGMP signalling system is considered to be the primary mechanism involved in cardiovascular fluid homeostasis via its actions on target organs that are critically involved in electrolyte and fluid balance including the kidneys, vascular tissues the adrenal gland (Lowe et al., 1989; Nagase et al., 1997; Goy et al., 2001; McGrath et al., 2005; Pandey, 2005). In the kidneys, the natriuretic and diuretic effects of ANP are achieved mainly by stimulating an increase in the glomerular filtration rate and filtration fraction and also by inhibiting sodium reabsorption at the level of the collecting duct (Light et al., 1990; Melo et al., 2000), and inhibiting the release of the renin (Laragh, 1985). In the vascular compartment, ANP decreases vascular smooth muscle tone and thus peripheral resistance and also increases capillary permeability to allow extravasation of fluid and decreased blood volume. The central role of ANP in blood pressure regulation has also been demonstrated by the fact that transgenic mice overexpressing ANP are hypotensive (Steinhelper et al., 1990; Barbee et al., 1994), while ANP-deficient mice are hypertensive (John et al., 1996). Similarly, global disruption of the gene encoding NPRA (*Npr1),* by two independent groups has indicated that null mice also have high blood pressure, cardiac hypertrophy and cardiac fibrosis (Lopez et al., 1995; Oliver et al., 1997).

NPRC is expressed in most tissues of the body including the heart and vasculature (Nagase et al., 1997) and this wide distribution pattern is likely a reflection of its role in buffering local concentrations of natriuretic peptides in various compartments. A clearance role for NPRC specifically in the renal system is supported by observations that

loss of function mutations in mice result in a 2/3 longer half-life of ANP, impaired ability to concentrate urine and moderate hypotension (Matsukawa et al., 1999). Intriguingly, however, it has been demonstrated that CNP, acting via NPRC can markedly inhibit L-Type Ca^{2+} current in isolated sinoatrial node cardiomyocytes (Rose et al., 2004). Furthermore, ANP has been shown to profoundly decrease cAMP production in isolated Purkinje fibers from the adult rabbit heart under basal conditions and in response to adrenergic agonists such as epinephrine, dopamine and isoproterenol (Anand-Srivastava et al., 1989). Together, these studies provide strong evidence for a role of ANP/NPRC/G_i signalling axis in regulating electrophysiological properties of ventricular conduction system cells.

1.5.8 Autocrine/Paracrine Regulation of Cell Growth and Proliferation by Atrial Natriuretic Peptide

Aside from its role in endocrine regulation of fluid homeostasis, ANP has also been shown to function as an important autocrine/paracrine regulator of growth and proliferation of numerous cardiovascular and non-cardiovascular tissues and cell types. For example, ANP has been shown to antagonize cardiomyocyte growth in response to hypertrophic stimuli including AngII, ET-1 and phenylephrine *in vitro* and *in vivo* (Horio et al., 2000; Rosenkranz et al., 2003; Laskowski et al., 2006; Kilic et al., 2007). Similarly, an important role for the ANP/NPRA signalling axis in regulating cardiomyocyte growth *in vivo* has been supported by evidence that genetic ablation of either ANP or NPRA results in marked cardiac hypertrophy (Lopez et al., 1995; John et al., 1996; Oliver et al., 1997). It was not initially clear, however, whether this cardiac

hypertrophy was directly related to a loss of an antihypertrophic effect of ANP or secondary to high blood pressure which is known to occur in these mice. To address this issue, NPRA null mice were treated with anti-hypertensive drugs to normalize blood pressure from an early age and it was shown that, despite being normotensive, hypertrophy and fibrosis persisted (Knowles et al., 2001). Similarly, selective ablation of NPRA specifically in cardiomyocytes was also shown to yield mice that exhibited cardiac hypertrophy while having no effect on blood pressure (Holtwick et al., 2003).

At the cellular level, ANP has also been shown to exert antiproliferative effects on a variety of cardiovascular cell types including cardiac fibroblasts (Cao and Gardner, 1995), vascular smooth muscle cells (Sharma et al., 2002) mesangial cells (Tripathi and Pandey, 2012) and cardiomyocytes (Koide et al., 1996; O'Tierney et al., 2010). Importantly, discrepancies regarding the effects of ANP on proliferation of cardiomyocytes have been reported. Specifically, exogenous addition of human ANP on embryonic chick cardiomyocytes was shown to increase proliferation (Koide et al., 1996), while addition of rat ANP to fetal sheep cardiomyocytes was shown to inhibit Ang II stimulated proliferation (O'Tierney et al., 2010). More recently, it was also demonstrated that ANP was able to cause a reduction in proliferation of CPCs derived from the post-natal heart (Stastna et al., 2010). Collectively, these findings raise the possibility that ANP could also be an important regulator of proliferation of either embryonic CPCs and/or cardiomyocytes derived from the early four chambered heart.

1.5.9 The Potential Role of Atrial Natriuretic Peptide Receptor Signalling in Cardiogenesis

Cardiogenesis relies on a tightly controlled balance between cell proliferation and differentiation. Because cardiomyocytes lose their ability to divide around the time of birth (Pasumarthi and Field, 2002), dysregulated proliferation kinetics during the embryonic period could potentially lead to deleterious effects on cardiac performance in post-natal life. It has been firmly established that both working cardiomyocytes and conduction system myocytes are derived from a common myogenic lineage (Gourdie et al., 1995; Cheng et al., 1999; McMullen et al., 2009) and that secreted paracrine factors from the endothelium/endocardium are capable of guiding undifferentiated cardiac cells toward the conduction system lineage in both the avian and murine ventricles (Gourdie et al., 1998; Takebayashi-Suzuki et al., 2000; Rentschler et al., 2002). The transient expression of ANP in the ventricles during cardiac ontogeny suggests that ANP could also be an important autocrine/paracrine factor involved in regulating aspects of cardiac cell proliferation or differentiation in this compartment. In support of this idea, it has been shown that mice lacking NPRA display reduced survival, cardiac hypertrophy beginning at mid/late gestation and morphological abnormalities including dextrocardia and mesocardia (Lopez et al., 1995; Ellmers et al., 2002; Cameron and Ellmers, 2003; Scott et al., 2009). Currently, however, there is no direct evidence that ANP receptor mediated signalling systems are biologically active in the embryonic heart.

Previously, it was shown by *in situ* hybridization that ANP mRNA transcripts were abundantly expressed in the trabecular myocardium of the early four chambered heart around midgestation (Zeller et al., 1987). A similar pattern of immunoreactive ANP expression in the trabecular myocardium was also documented in the embryonic rat

heart (Toshimori et al., 1987a). Intriguingly, cells within the murine trabecular myocardium have been shown to withdraw from cell cycle at relatively early stages of development and enter into terminal differentiation pathways toward the cardiac conduction system (CCS) lineage (Sedmera et al., 2003). Furthermore, functional and molecular correlates of the CCS have indicated that the trabecular myocardium serves as the preferential route of electrical conduction prior to CCS maturation (Viragh and Challice, 1977; Rentschler et al., 2001; Sedmera et al., 2003; Miquerol et al., 2004; Sankova et al., 2012). Despite this knowledge, it remains unknown whether ANP receptor mediated signalling plays any role in regulating either proliferation or lineage specification of undifferentiated embryonic CPCs or cardiomyocytes during the developmental period.

CHAPTER 2: MATERIALS AND METHODS

2.1 Animal Maintenance and Mouse Strains

All experimental protocols involving the use of animals were approved by the Dalhousie University Committee on Laboratory Animals and were performed in accordance with the Canadian Council on Animal Care Guide to Care and Use of Experimental Animals (CCAC, Ottawa, ON: Vol1.1, 2nd edition, 1993; Vol 2, 1984). All animals were housed in the Carleton Animal Care Facility at Dalhousie University and maintained on a 12 hour light/dark cycle.

CD1 and **C57Bl/6** mouse strains were obtained from Charles River Laboratories (Montreal, Québec, Canada). The **Nkx2.5-Cre** mouse strain (designated as NC), which was originally generated and characterized by Stanley et al. (2002), was obtained from Dr. Richard Harvey (Victor Chang Cardiac Research Institute, University of South Wales, Australia). These mice were engineered to have an internal ribosomal entry sequence (IRES) and a Cre- recombinase (Cre) coding sequence inserted into the 3' untranslated region of the Nkx2.5 gene. The **R26R** reporter strain (designated as Rosa *LacZ* and abbreviated as RL), was obtained from the Jackson Laboratories, (Bar Harbor, Maine, USA). ***Npr1-/-*** mouse strain, originally generated and characterized by Oliver et al. (1997), was received from Dr. Nobuyo Maeda (University of North Carolina, USA). In *Npr1-/-* mice, exon 1 and intron 1 of the *Npr1* gene which encodes the natriuretic peptide receptor A (NPRA) was replaced with a neomycin resistance cassette. The **Cx40$^{egfp/+}$** mouse strain, originally generated and characterized by Miquerol et al. (2004),

was received from Dr. Robert Rose (Dalhousie University, Canada). In the $Cx40^{egfp/+}$ mouse strain, enhanced green fluorescent protein (EGFP) coding sequence followed by pgk-neo cassette was inserted in frame at the Cx40 start codon. The ANF-LacZ mouse strain, originally generated by Habets et al. (2002), was received from Dr. Vincent Christoffels, University of Amsterdam, The Netherlands. These mice were engineered to harbor the ANF regulatory region (+638/+70) coupled to the *nLacZ* reporter gene. All transgenic mouse lines were maintained in C57Bl/6 background. Unless otherwise stated, CD1 mice were used for all experimental procedures.

2.2 Genomic DNA Extraction

Ear punch biopsies were used for routine genotyping of all transgenic mouse strains. Genomic DNA was extracted from ear punch biopsy samples using the Sigma REDExtract-N-AMP tissue PCR kit (Sigma, Oakville, Ontario, Canada), according to the manufacturer's instructions. Each tissue sample was placed in 50µl of DNA extraction solution (40µl Extraction Solution: 10µl Tissue Preparation Solution) and ground manually using a sterile pipette tip. After a10 minute incubation at room temperature, samples were heated to 95ºC in a blocker heater. Next, 10µl of Neutralization Buffer was added to each sample and mixed briefly by vortexing. Samples were then centrifuged to pellet undigested tissue and the supernatant was used directly as a template for polymerase chain reaction (PCR).

2.3 Genotyping by Polymerase Chain Reaction (PCR)

PCR was performed using REDExtract N-AMP kit (Sigma) with a total reaction volume of 10µl. All primers were obtained from Invitrogen (Burlington, Ontario, Canada) and sequences are listed in Table 2.3.1. Each PCR reaction mixture contained 5µl REDExtract-N-AMP PCR mix, 0.5µl of each primer (50ng each) and 2µl of tissue extract. A final volume of 10µl was achieved by adding the required volume of water. For **Nkx2.5-Cre genotyping** PCR reactions were performed for 30 cycles: 30 sec at 94ºC, 20 sec at 60ºC and 60 sec at 72ºC. Expected PCR products were 583 bp for the transgenic allele and 264 bp for the wildtype allele (Figure 2.3.1A). For **Rosa-*LacZ* genotyping** PCR reactions were performed for 30 cycles: 30 sec at 94ºC, 30 sec at 60ºC and 60 sec at 72ºC. Expected PCR product sizes were 650 bp for the wildtype and 320 bp for the transgenic allele (Figure 2.3.1B). For ***Npr1*-/- genotyping** PCR reactions were performed for 34 cycles: 30 sec at 94ºC, 60 sec at 55ºC and 60 sec at 72ºC. Expected PCR product sizes were 339 bp for the wildtype and 500 bp for the transgenic allele (Figure 2.3.1C). For **Cx40$^{egfp/+}$** genotyping PCR reactions were performed for 34 cycles: 30 sec at 94ºC, 60 sec at 55ºC and 60 sec at 72ºC. Expected PCR product sizes were 380 bp for the wildtype and 450 bp for the transgenic allele (Figure 2.3.1D). For **ANF-LacZ** genotyping, PCR reactions were performed for 34 cycles: 30 sec at 94ºC, 60 sec at 55ºC and 60 sec at 72ºC. Expected PCR product size of the ANF-LacZ transgenic allele was 310bp (Figure 2.3.1E). PCR reactions were routinely performed using no template controls to rule out false positive results.

2.4 Timed Pregnant Female Mice

Breeding pairs were placed in the same cage overnight, and the following morning, females were examined for the presence of a vaginal plug. Male ejaculate formed a white/yellow fibrous plug in the female vagina and the presence of a vaginal plug was considered to be indicative of successful copulation. The morning when the vaginal plug was detected was considered to be embryonic day (E) 0.5. Timed pregnant females were anesthetized via inhalation of 4% isoflurane and sacrificed by cervical dislocation. Embryos from various developmental stages (E11.5, E14.5 and E16.5) were isolated from the uterine horns using a Leica MZ16SF stereomicroscope (Leica Microsystems, Richmond Hills, Ontario, Canada).

2.5 Embryonic Ventricular Primary Culture and Drug Treatments

E11.5 embryos were removed from the uterus, the placenta was removed and the embryo was placed in a dish containing warmed PBS supplemented with 1X antibiotic/antimicotic (Gibco, Burlington, Ontario, Canada). Whole hearts were dissected out of the embryos and the atria and outflow tracts were removed. Right and left ventricles from each embryo were then placed into 0.2% v/v type I Collagenase (Worthington Biochemical Corp., Lakewood, New Jersey, USA) in PBS (PBS: 0.138 M NaCl, 0.0027 M KCl, pH 7.4), and rocked for 30 minutes at 37ºC to digest ventricular tissue. Following the 30 minute incubation period, tissue was triturated using a 200µl pipette tip to mechanically dissociate cells from remaining tissue pieces. Cells were then centrifuged at 4,000 rpm for 4 minutes, collagenase was removed, and the pellet was neutralized with two washes of 10% DMEM [(Dulbecco's Modified Eagles Medium;

Wisent, Saint Bruno, Québec, Canada) containing 10% fetal bovine serum (FBS; Wisent) Cell number was then determined using a hemocytometer and cells were re-suspended in 10% DMEM to achieve required cell numbers. Cells were plated at various cell densities on either fibronectin (Sigma) coated 2 or 4-well chamber slides (Nunc, Rochester, New York, USA), 35mm dishes (Corning, Corning, New York, USA), or black-walled clear bottom 96-well plates (Greiner Bio-One, Monroe, North Carolina, USA, Catalogue # 655809).

Nifedipine (Sigma) stock solution was prepared by dissolving 50mg of nifedipine in 1ml of DMSO (Thermo Fisher Scientific, Nepean, Ontario, Canada). From this stock, working solutions of 150mM, 15mM and 1.5mM were prepared, aliquoted and stored at -20°C protected from light. For ventricular cell cultures receiving 100µM nifedipine treatment, 1µl of 150mM nifedipine stock solution was added per 1.5ml culture medium. Similarly, either 1µl of 15mM or 1.5mM nifedipine was added per 1.5ml culture medium in order to achieve a final concentration of 10µM or 1µM respectively. Thus, the final concentration of DMSO in culture medium was maintained at 0.07% in different nifedipine treatments or control. ANP (Bachem, King of Prussia, Pennsylvania, USA Catalogue #H-2100.0500) stock solution was prepared by dissolving 0.5mg of ANP in 0.5ml sterile H_2O (Ambion, USA), which was aliquoted and stored at -80°C. From this stock solution, working solutions of 100ng/µl, 10ng/µl and 1ng/µl were prepared by serial dilution in sterile H_2O (Ambion) immediately prior to use on the day of an experiment. For ventricular cell cultures receiving 100ng/ml treatment, 1µl of 100ng/µl ANP was added per 1ml culture medium. Similarly, either 1µl of 10ng/µl or 1ng/µl ANP solution was added per 1ml culture medium to achieve a final concentration of 10ng/ml

or 1ng/ml respectively. Stock solution of NPRA/NPRB antagonist A71915 (Bachem, Catalogue # H-3048.0500) was prepared by dissolving 0.5mg A71915 in 0.5ml H_20 (Ambion), which was aliquoted and stored at -20°C. For ventricular cell cultures receiving A71915 treatment, a final concentration of 1µM was achieved by adding 2.42µl of A71915 stock per 1ml culture medium.

2.6 Tritiated-Thymidine Labeling

Following the drug treatment period, medium was aspirated and new medium supplemented with tritiated [^{3}H]-thymidine (GE Healthcare Life Sciences, New Jersey, USA) was added to each well at a concentration of 1.0 µCi per 1ml of medium for six hours at 37˚C. After six hours, media containing [^{3}H]-thymidine was removed and cells were rinsed with three washes of PBS and then fixed with ice cold methanol for 15 minutes at 4°C. Following fixation, cells were rinsed with three additional washes of PBS and then processed for immunofluorescence.

2.7 Immune Cytochemistry

After methanol fixation (15 minutes at 4°C), primary NCRL cultures used for thymidine incorporation assays were permeabilized in 0.1% v/v Triton X-100 (Sigma) for 5 minutes. Walls of the chamber slides were then removed and each slide was placed in a humid chamber and covered in blocking buffer solution [10% v/v goat serum (Gibco) 1% w/v bovine serum albumin (BSA; Thermo Fisher Scientific) in PBS] for one hour. After 1 hour, blocking buffer was tipped off and primary antibodies diluted in blocking buffer

were added at the following concentrations: rabbit polyclonal anti-β-galactosidase (1:50) (Research Gift from Cappel, USA) and mouse monoclonal anti-sarcomeric myosin (1:50) (Developmental Studies Hybridoma Bank, University of Iowa, USA, Catalogue # MF20) for 1 hour at room temperature in a humid chamber. Slides were then rinsed three times for five minutes each with PBS and incubated with secondary goat anti-mouse antibodies, conjugated to Alexa Fluor 488 (1:200) (Invitrogen) and goat anti-rabbit antibodies conjugated to Alexa Fluor 555 dye (1:200) (Invitrogen) for one hour. After three washes with PBS (5 minutes each), cell nuclei were counterstained by immersion in a solution of 1μg/ml Hoechst 33258 (Sigma) in PBS, air-dried and then processed for autoradiography described in the following section (Section 2.8).

For experiments where primary cultured E11.5 NCRL or ANF-LacZ cells were stained with X-gal (Goldbio, Missouri, USA) and processed for antibody immunolabelling, cells in 2 or 4 well chamber slides were fixed with Flow Fix (2.7% w/v cacodylic acid, 2.5% w/v paraformaldehyde, 1.66% w/v NaCl and ddH_20, pH 7.4) for 30 minutes at room temperature. Walls of the chamber slides were then removed and each slide was placed in X-gal solution and incubated overnight at 37°C. X-gal solution was prepared as follows: 0.01g of X-gal powder was added to 2.5 ml of N, N-Dimethyl Formamide (DMF, Sigma) to prepare the primary X-gal solution. Once dissolved, the primary X-gal solution was added dropwise to an 80 ml PBS solution containing 200μl of 1M $MgCl_2$, 0.164 g potassium ferricyanide, and 0.212 g potassium ferrocyanide. The following day, slides were rinsed in PBS and then subjected to the immunolabelling protocol exactly as described above. Primary antibodies used for these experiments were diluted in blocking buffer at the following concentrations: rabbit polyclonal anti- $Ca_v1.2$

L-type Ca^{2+} channel (1:50)(Santa Cruz Biotechnology Inc., Santa Cruz, California, Catalogue # sc-25686), rabbit polyclonal Connexin40 (1:50) (Alpha Diagnostics, San Antonio, USA, Catalogue # Cx40-A) and mouse monoclonal MF20 (1:50)(DSHB). In some experiments, primary cultured E11.5 CD1 ventricular cells were grown on 4-well chamber slides cells and fixed with 4%w/v paraformaldehyde for 15 minutes at room temperature. After permeabilization with Triton X-100 (Sigma), cells were incubated at room temperature for 1 hour with blocking buffer supplemented with 0.3M glycine (Sigma). Glycine reduced non-specific fluorescence by binding to free aldehyde groups, which would have otherwise been bound to primary and secondary antibodies and resulted in high background fluorescence. Primary antibodies diluted in blocking buffer (10% goat serum, 1% BSA + 0.3M glycine) were added at the following concentrations: rabbit monoclonal MEF2c (1:400)(Cell Signaling Technology, Danvers Massachusetts USA, Catalogue # 5030) and mouse monoclonal anti mouse MF20 (1:50)(DSHB) overnight at 4ºC in a humid box. Slides were then rinsed three times for five minutes each with PBS, labeled with secondary antibodies and nuclei were counterstained with Hoechst (1µg/ml) as described above.

In the final processing step for all experiments, slides were rinsed extensively with PBS and mounted with 0.1% propyl gallate (Sigma) solution [(0.1% w/v propyl gallate, 50% v/v glycerol (Thermo Fisher Scientific), 50% v/v PBS]. Cells were examined using a Leica DM2500 fluorescence microscope and images were captured using a Leica DFC 500 digital acquisition system.

2.8 Tritiated-Thymidine Autoradiography

In some experiments, following the immunofluorescence labeling protocol, slides were brought to a dark-room where they were coated with Kodak autoradiography emulsion type NTB (MarketLINK Scientific, Burlington, Ontario, Canada) and placed in a light-tight box at 4°C for 3 days. After 3 days, slides were developed in a dark room by placing them in Kodak D-19 developer (Sigma) for four minutes, rinsing them in ddH_2O, and then placing them in Ilford rapid fixer (Polysciences, Pennsylvania, USA) for 4 minutes. Slides were then rinsed with warmed ddH_2O and mounted using 0.1% propyl-gallate solution. Thymidine incorporation into the nuclei of cells in the S-phase of the cell cycle was identified by the presence silver grains in the nucleus. Cells containing more than fifteen silver nuclear grains were considered to be undergoing DNA synthesis.

2.9 Total RNA Extraction from Cells and Tissues

Approximately 20 ventricles (left and right) from E11.5 embryos were collected and pooled from multiple timed-pregnant females to obtain 50-100mg of tissue and then subjected to RNA extraction using the TRIzol (Invitrogen) method. Ventricles obtained from embryos at later developmental (E14.5 and E16.5) or post-natal stages (neonatal and adult) were minced into smaller pieces and then the same amount of tissue (50-100mg) was collected and used for RNA extraction using TRIzol method. Tissue samples were homogenized in 1ml TRIzol for approximately 1 minute using a power homogenizer. For E11.5 ventricular cell cultures, cells were lysed directly in 35mm culture dishes by adding 1mL TRIzol reagent to the dish and passing the cell lysates through a pipette tip.

E11.5 cells collected after FACS were lysed by adding 0.5ml TRIzol to collection tubes and trituration using a pipette tip.

After homogenization/lysis of tissues or cells, all samples were incubated at room temperature for 5 minutes to allow complete dissociation of nucleoprotein complexes. Following incubation, 0.2ml chloroform was added to each sample and shaken vigorously by hand for 15 seconds. After incubation at room temperature for 3 minutes, samples were centrifuged at 13,300 rpm for 15 minutes at 4ºC. Following centrifugation, the colorless aqueous phase containing RNA was carefully removed and transferred to a fresh tube. RNA was precipitated by adding 0.5ml isopropyl alcohol and samples were incubated for 10 minutes at room temperature. Samples were then centrifuged at 13,300 rpm for 10 minutes at 4ºC. The resulting pellet was washed with 75% ethanol in nuclease free H_2O (Ambion), air dried and then solubilized in nuclease free H_2O (Ambion). RNA content was quantified by measuring absorbance at 260nm and 280nm using a spectrometer (SmartSpec^{TM} Plus, Bio-Rad, Mississauga, Ontario, Canada).

2.10 Fluorescence Activated Cell Sorting (FACS)

Ventricles from E11.5 ANF-LacZ embryos were isolated, pooled and digested in 0.2% Type I collagenase (Worthington) for 30 minutes at 37ºC. Cell pellets were then obtained by centrifugation and neutralized with 10% DMEM as described earlier (Section 2.5). To ensure that a single-cell suspension that was devoid of any undigested tissue was achieved; cell preparations were passed through a 40µm mesh filter. Cells were then pelleted once more by centrifugation at 4,000 rpm for four minutes and prepared for FACS analysis by following the instructions of the *FluoReporter* LacZ Flow Cytometry

Kit (Invitrogen, Catalogue # F-1930) which was designed for detection of β-galactosidase activity in single cells. First, cells were resuspended in staining medium (PBS, 4% v/v FBS, 10mM HEPES, pH 7.2) at a concentration of 10^7 cells/ml and 100µl of the cell suspension was transferred to a borosilicate glass flow cytometer tube (Thermo Fisher Scientific). The β-galactosidase substrate fluorescein di β-D-galactopyranoside (FDG) was then loaded into the cells by hypotonic shock for one minute at 37ºC in a water bath. At the end of one minute, FDG loading was stopped by the addition of 1.8ml ice-cold staining medium containing 1.5µM propidium iodide. Ice-cold pipettes, pre-chilled at -20ºC for 30minutes were used to transfer staining medium to the loaded cells. Cells were then placed on ice and promptly used for flow cytometry analysis. The flow cytometer (FACSAria, BD Biosciences, Franklin Lakes, New Jersey, USA), was calibrated to detect fluorescein, propidium iodide and forward scatter according to standard procedures. Unstained ANF-LacZ cells were used to set the background autofluorescence as recommended by the manufacturer. Sorted cells were pelleted by centrifugation at 4,000 rpm for four minutes and cell pellets were processed for RNA extraction using the TRIzol method described earlier (Section 2.9).

2.11 RNA Quality Control

To ensure a high level of RNA purity, only samples with 260:280 ratio >1.6 were used in subsequent gene expression experiments. Additionally, to ensure a high level of RNA integrity, 2µg of RNA was electrophoreased on an agarose gel and stained with ethidium bromide. Only samples which displayed two discreet bands corresponding to predominant ribosomal RNAs at ~5kb (28S) and ~2kb (18S) were used in subsequent

experiments. Samples meeting these standards of quality control were then immediately converted into more stable cDNA sequences and stored at -20ºC until being used for real time quantitative PCR (qPCR) gene expression analysis experiments.

2.12 RT-qPCR

To generate complementary DNA (cDNA) sequences from RNA samples, an initial reaction mixture was prepared by adding 3µg of RNA (tissue samples) or 1 µg of RNA (ventricular cells), 1µl of 10mM dNTPs (Invitrogen), 250ng random primers (Invitrogen) and RNAse-free H_2O (Ambion) to a total of 12µl. This mixture was then heated to 65ºC for 5 minutes. Subsequently, 4µl 5X Superscript II first strand buffer (Invitrogen), 1µl of 0.1M Dithiothreitol (Invitrogen) and 1µl RNAse OUT (Invitrogen) was added to each reaction mixture, and samples were incubated at room temperature for two minutes. Following incubation, 100U of Superscript II reverse transcriptase enzyme (SSII-RT) (Invitrogen) was added to each reaction tube and mixed gently using a pipette tip. All tubes were then incubated at 25ºC for 10minutes, 42ºC for 50 minutes and then heat inactivated at 70ºC for 15 minutes.

The cDNA templates were amplified by real time quantitative polymerase chain reaction (qPCR) using the primers listed in Table 2.12.1 The primers for NPRA, NPRC and GAPDH were generated using the NCBI primer design tool (http://www.ncbi.nlm.nih.gov/tools/primer-blast/). For each of these primer pairs, the optimal annealing temperature was determined empirically by performing qPCR efficiency experiments. Briefly, PCR products were purified using an Axygen (Union City, California, USA) purification kit, by following the manufacturer's instructions. A

10X serial dilution series of purified product was then generated, and subjected to qPCR analysis as described below. From these experiments, the efficiency of each primer pair was calculated using previously described methods (Taylor et al., 2010). The annealing temperature that yielded a reaction efficiency between 90-110% was used for subsequent gene expression analyses. All other primer pairs were generated using the NIH qPCR primer data base (http://mouseprimerdepot.nci.nih.gov/). An annealing temperature of 60ºC was used for each of these primers pairs. Each reaction mixture consisted 1.0µl of cDNA product, 1.0 µl of the forward and reverse primers (2.5µM), 1.0µl of 5X EVOlution EvaGreen® qPCR mix (Montreal Biotech Inc., Quebec City, Canada) and 2.0µl RNAse/DNAse free H_2O (Ambion). All qPCR reactions were performed for 40 cycles: 15sec at 95ºC, 60 sec at 60ºC using an ECO thermocycler (Illumina, San Diego, California, USA). Following completion of the amplification cycles, melt curves were generated by an additional cycle using the following conditions: 15 sec at 95ºC, 15sec at 60 ºC and 15sec at 95 ºC. The melt curve was performed to confirm the amplification of a single primer product. Additionally, qPCR amplification products were resolved by electrophoresis on a 1.5% agarose gel to confirm expected amplicon sizes.

Gene expression was normalized to the control housekeeping gene glyceraldehyde 3-phosphate dehydrogenase (GAPDH) using the $\Delta\Delta C_T$ method (Livak and Schmittgen, 2001). The threshold of fluorescence (dRN) was set to 0.1 and was used to determine the threshold cycle (C_T) value. The C_T value specifically refers to the cycle number at which the amplification plot for a particular gene intersects the dRn threshold. In a typical experiment where the relative expression of two genes was compared, the following sequence of calculations was performed to determine the $2^{-\Delta\Delta CT}$ value for each

gene. **1-** First, the ΔC_T value for each gene was determined by subtracting the C_T value of the control gene (GAPDH) from the C_T value of the corresponding experimental gene. **2-** The average of all ΔC_T values was then calculated. **3-** The average ΔC_T value obtained in step 2 was then subtracted from the ΔC_T values for each individual gene obtained in step 1 to yield the $\Delta\Delta C_T$ values. **4-** The $2^{-\Delta\Delta CT}$ was then calculated for each gene. **5-** Finally, the relative expression of each gene was determined by dividing the $2^{-\Delta\Delta CT}$ obtained for each gene by the $2^{-\Delta\Delta CT}$ of one selected gene. This maneuver enabled data to be expressed as the relative expression of each gene compared to the one selected gene, which was set to a value of 1.0.

2.13 Ca^{2+} Imaging using Fluo-8

The effects of nifedipine on intracellular Ca^{2+} (designated as $[Ca^{2+}]_i$) were monitored using the Screen Quest™ Fluo-8 NW Calcium assay (AAT Bioquest Inc. California, USA), according to the manufacturer's instructions. The Ca^{2+} indicator molecule Fluo-8 readily crosses the cell membrane due to the presence of non-polar acetoxymethyl (AM) esters. Once inside the cell, the lipophilic blocking groups are cleaved by non-selective esterases, resulting in a negatively charged molecule that remains inside cells. In response to Ca^{2+} binding, Fluo-8 undergoes a very large increase in fluorescence that can be detected at an emission wavelength of 514nm and used to monitor fluctuations in $[Ca^{2+}]_i$. Ventricles from E11.5 CD1 embryos were isolated, pooled and digested in 0.2% Type I collagenase (Worthington) for 30 minutes at 37ºC. Cell pellets were then obtained by centrifugation and neutralized with 10% DMEM as described earlier (Section 2.5). Cells diluted in 10% DMEM were seeded in fibronectin

coated wells of 96-well black wall/clear bottom plates (Greiner Bio-One, Catalogue # 655809) at a density of 25,000 cells/well. After 4 hours, media was changed and replaced with 1% DMEM containing various concentrations of nifedipine (1μM, 10μM or 100μM) or vehicle (DMSO) for 1 hour at 37ºC. After 1 hour cells were loaded with Fluo-8 dye loading solution (20μL of Fluo-8 NW stock solution into 10ml of 1X assay buffer consisting of: 9 ml Hanks' Buffer with 20mM HEPES and 1ml Pluronic F127 Plus) for 15 minutes at room temperature. The fluorescence intensity (corresponding to $[Ca^{2+}]_i$) was calculated at several time points after stimulation with 1μM isoproterenol (ISO, Sigma) based on the intensity of green pixels (representing Ca^{2+} sensitive Fluo-8 signal) via Colour-Subtractive Computer-Assisted Image Analysis software (Reindeer Graphics, Asheville, NC, USA) as previously described (Gaspard and Pasumarthi, 2008).

2.14 Protein Extraction and SDS-*PAGE* Electrophoresis

Ventricles from various developmental stages were isolated, pooled and homogenized in 1ml Tumor Lysis Buffer (1% NP40, 5mM EDTA, 150mM NaCl, 50mM Tris/HCl pH8.0, 1μl PMSF and 1μl Aprotinin). Each sample was then sonicated (Sonic Dismembrator, model 100; Thermo Fisher Scientific) three times at a setting of 3.5 and placed on ice for 15 minutes. Detergent soluble cytosolic fractions and detergent insoluble membrane fractions were separated by high speed centrifugation at 13,300 rpm for 15 minutes at 4°C. Equal volumes of protein extract, containing 40μg of protein, were denatured in Laemmli buffer [62.5 mM Tris-HCl pH 6.8, 0.5ml β-mercaptoethanol, 25% v/v glycerol, 2% w/v sodium dodecyl sulfate (SDS), 0.02% w/v bromophenol blue, and ddH_2O)]. Samples were then boiled at 95ºC for 3 minutes and stored at -80ºC. The

concentrations of all protein extracts were estimated against a BSA standard curve generated using Bradford Assay. The principle of the Bradford method is based on a shift in the absorbance maximum of Coomassie Blue (Pierce, Rockford, Illinois, USA) from 465 mm to 595 mm when bound to protein which results in color shift from brown to blue which can be measured using a spectrophotometer.

A total of 40µg of protein was separated on 12.5% or 16.5% SDS-polyacrylamide gels (0.375 M Tris/HCl pH 8.8, 0.08% w/v SDS, 12.5% w/v acrylamide, 0.2% v/v ammonium persulphate (APS), 40µl TEMED using a 1x Tris-glycine migration buffer (25mM Tris base, 190 mM glycine and 0.1% SDS at 8.3 pH) at 100 volts in a Mini-PROTEAN 3 gel electrophoresis unit (Bio-Rad, Mississauga, Ontario, Canada). Separated proteins were transferred from the gel to a nitrocellulose membrane (GE Healthcare Life Sciences), by applying a constant current of 100 volts for one hour (Transfer buffer: 25mM Tris base, 190 mM glycine and 20% methanol at pH 8.3). For detecting 3kD ANP peptide, transfer was performed using Tris-tricine buffer (Bio-Rad). Following the transfer, nitrocellulose membranes were stained with napthol blue (1% w/v napthol blue black, 45% v/v methanol, 45% v/v water, 10% v/v acetic acid) for 2 minutes to enable protein visualization and determine protein loading. Nitrocellulose membranes were then rinsed in ddH_20 and air dried prior to use for Western blot analyses.

2.15 Western Blot Analysis

To detect a protein of interest, the nitrocellulose membrane was first incubated with two changes of fresh blocking buffer (5% w/v powdered milk and 3% w/v BSA in PBS with 0.1% w/v Tween) for 30 minutes each. Next, membranes were incubated for 1

hour with primary antibodies diluted in blocking buffer. Primary antibodies used for Western blot analyses: rabbit polyclonal NPRA (1:200) (Santa Cruz, Catalogue # sc-25485), NPRC (1:200) (Santa Cruz, Catalogue # sc-25487), ANP (1:200) (Chemicon International, Billerica, Massachusetts, USA, Catalogue # CBL66).

Primary antibodies were removed and membranes were washed three times in PBS containing 0.1% Tween (0.1% PBST) for 15 minutes each with rocking and then incubated for 1 hour with secondary antibodies diluted in blocking buffer. Secondary antibodies used: goat-anti-rabbit (1:2000) (Bio-Rad, Catalogue #172-1019) or goat-anti-mouse (1:5000) (Bio-Rad, Catalogue #170-6516) antibodies conjugated to horse radish peroxidase. After removal of secondary antibodies, membranes were washed three times in PBST for 15 minutes each with rocking. Protein bands were detected by enhanced chemiluminescence method using ECL Plus Western Blotting Detection System (GE Healthcare Life Sciences) according to manufacturer's instruction.

2.16 Enzyme Linked Immunosorbant Assay (ELISA)

Tissue lysates from ventricles of either E11.5 or neonatal hearts were generated as described earlier (Section 2.14). Clear 96- well microtiter plates (Nunc, Catalogue # 167008) were coated with tissue lysate samples in 100µl per well of carbonate buffer (pH 9.6) overnight at 4°C. The following day, liquid was discarded by inversion and each well was washed five times with PBST. Each well was then blocked with 200µl of blocking buffer (5% BSA in PBST) at 37°C for 1 hour. Blocking buffer was then discarded and the wells were rinsed once with PBST before incubating with primary mouse monoclonal anti-ANP antibodies (8ng) (Chemicon, Catalogue # CBL66) diluted

in 100µl ELISA diluent (1% BSA in PBST) for 2 hours at room temperature. Primary antibodies were then removed and wells were washed five times for three minutes each with PBST. Secondary goat-anti-mouse antibodies (1:5000)(Bio-Rad Catalogue # 170-1019) conjugated to horse radish peroxidase diluted in 100µl of ELISA diluent were then added to each well for 2 hours at room temperature. Secondary antibodies were discarded and each well was washed five times for three minutes each with PBST. An aliquot of Ultra TMB-ELISA substrate (Pierce) was wrapped in foil to decrease exposure to light and equilibrated at room temperature. A volume of 100µl of Ultra TMB-ELISA substrate was added to each well and allowed to incubate at room temperature for ~20 minutes. The reaction was stopped by adding 100µl of 2M sulphuric acid to each well. The absorbance was then measured immediately at 450nm using a BMG POLARstar Omega plate reader (BMG Labtech, Ortenberg, Germany). The concentration of ANP was deduced by extrapolating absorbance readings from a standard curve generated using synthetic ANP (Bachem, Catalogue #H-2100.0500) and covered range of 40-0.3125ng.

2.17 Second Messenger Assays: cGMP and cAMP

Ventricles from E11.5 CD1 embryos were isolated, pooled and digested in 0.2% Type I collagenase (Worthington) for 30 minutes at 37ºC. Cell pellets were then obtained by centrifugation and neutralized with 10% DMEM as described earlier (Section 2.5). To determine the level of cGMP in E11.5 cells, cGMP competitive immunoassays were performed using the two step protocol of the cGMP *htrf* assay kit (Cisbio, Bedford, Massachusetts, USA Catalogue # 62GM2PEB) according to the manufacturer's instructions. The principle of this assay was based on the competition between

endogenous cGMP and a d2-dye labelled cGMP analogue (d2-cGMP) for binding sites on anti-cGMP monoclonal antibodies labelled with Cryptate (mAb-Cryptate). The specific signal which occurred due to the energy transfer between the d2-cGMP and mAb-Cryptate was inversely proportional to the concentration of endogenous cGMP contained within the experimental sample.

The two step protocol for the cGMP competitive immunoassay, consisting of a stimulation step and a detection step was performed as follows: **Step 1-Stimulation:** A volume of 5µl of cells (64,000 cells) in 10% DMEM was added to the experimental wells of white 384-well low volume plates (Greiner Bio-One Catalogue # 784075). Additionally, 5 µl of dilution buffer consisting of drug compounds of interest, diluted in 10% DMEM, was added to each experimental well to achieve a final volume of 10µl/well. The broad substrate phosphodiesterase inhibitor 3-isobutyl-1-methylxanthine (IBMX; Sigma) was also included in the dilution buffer at a concentration of 500µM in order to prevent cGMP degradation. The plate was then sealed and incubated at room temperature for 30 minutes. **Step 2- Detection:** A volume of 5µl d2-cGMP diluted in lysis buffer was added to each experimental well. Importantly, d2-cGMP was omitted from negative control wells in order to determine non-specific signal. A volume of 5µl mAb-Cryptate was added to each experimental well to achieve a total volume of 20µl/well. The plate was then sealed and stored at room temperature for one hour before being read on a POLARstar Omega plate reader (BMG Labtech). The d2-cGMP fluorophore was excited at a wavelength of 337nm and emission was detected at 665nm and 620nm. The calculation of the fluorescence ratio (665nm/620nm) was performed to minimize the photophysical interference which may have occurred due to medium

conditions such as the presence of serum. Results were calculated using the 665nm/620nm ratio and expressed as Delta F values using the following data reduction steps: **1-** First the 665nm/620nm ratio for each well was multiplied by 10^4, and the average values from replicate wells were calculated. **2-** The Delta F values were calculated by subtracting the negative control 665/620 ratio value from the sample 665/620 ratio value, dividing that by the negative control 665/620 ratio and multiplying by 100. A cGMP standard curve was generated by plotting the Delta F values obtained from standards with known cGMP concentrations and covered an average range of 0.49-500nM (final concentration of cGMP/well). The cGMP concentrations in experimental samples were deduced by extrapolating the respective Delta F values from the standard curve.

To determine the level of cAMP in E11.5 cells, cAMP competitive immunoassays were performed using the two step protocol of the cAMP dynamic 2 *htrf* assay kit (Cisbio, Catalogue # 62AM4PEB) according to the manufacturer's instructions. The principle and the two-step protocol of the cAMP competitive immunoassays were identical to those described above for the cGMP assay, with one important exception: **Step 1** (stimulation), 4,000 cells were added to each well (diluted in 5µl of 10% DMEM). The cAMP standard curve was generated by plotting the Delta F values obtained from multiple standards of known cAMP concentrations and covered an average range of 0.17-712nM (final concentration of cAMP/well).

2.18 Immunohistochemistry

2.18.1 Preparation and Processing of Paraffin Embedded Specimens

Embryos from E11.5 stage were harvested and placed in 10% neutral buffered formalin (10% NBF; Sigma) solution overnight at room temperature. For embryos harvested from later developmental stages (E14.5 and E16.5) the heads were removed and then embryos were immersed in 10% NBF for 2-4 days. The 10% NBF was then discarded and specimens were dehydrated with increasing concentrations of EtOH (70%, 95%, 100%) and cleared with xylenes in a ASP300 tissue auto-processor (Leica). Specimens were then infiltrated with liquid paraffin (Tissue Prep, Thermo Fisher Scientific) held at the melting point (56-57ºC) for 1 hour, embedded in paraffin using embedding rings and cooled at 4ºC to solidify. Thin, 10µm tissue sections were cut using a Shandon AS 325 microtome, (Thermo Fisher Scientific) transferred to a 45ºC water bath and then collected on Superfrost® Plus slides (Thermo Fischer Scientific). Slides were allowed to air dry in a 37ºC incubator overnight and then stored at room until further processing.

Slides processed for immunohistochemistry were cleared using two washes of xylenes (15 minutes each), and then rehydrated with two changes of decreasing concentrations of ethanol (100%, 95%, 70%, 50%, ddH_20) for two minutes each. An antigen retrieval step was performed by boiling the samples in antigen retrieval buffer (10mM Sodium citrate di-hydrate, 0.05% v/v, pH 6.0 and ddH_2O,) two times for thirty seconds each. For immunofluorescence, slides were then placed in a humid chamber and covered in blocking buffer solution (10% goat serum, 1% BSA) for one hour at room temperature. After 1 hour, blocking buffer was tipped off and primary antibodies diluted in blocking buffer were added overnight at 4ºC. For these experiments, the following

primary antibody dilutions were used: rabbit polyclonal ANP (1:100) (Santa Cruz, Catalogue # sc-20158) and mouse monoclonal phosphohistone- H3 (1:100) (PH3; Cell Signaling, Catalogue # 9701). Slides were then rinsed three times for five minutes each with PBS and incubated with secondary goat anti-mouse antibodies, conjugated to Alexa Fluor 555 (1:200) (Invitrogen) and goat anti-rabbit antibodies conjugated to Alexa Fluor 488 dye (1:200) (Invitrogen) for one hour. After washing with PBS three times for five minutes each, cell nuclei were counterstained by immersing slides in a solution of 1µg/ml Hoechst 33258 (Sigma) in PBS. Slides were then rinsed with PBS and mounted with 0.1% propyl gallate solution. Tissue sections were examined using a Leica DM2500 fluorescence microscope and images were captured using a Leica DFC 500 digital acquisition system.

2.18.2 Preparation and Processing of Frozen Specimens

Embryos from E11.5 stage were harvested and placed in a cryoprotectant 30% sucrose solution overnight at 4ºC with rocking. The following day, embryos were embedded in OCT medium (Sakura Finetek, Torrance, California, USA) using plastic embedding rings and frozen at -80ºC. Thin, 10µm tissue sections were cut using a CM3050 S cryostat (Leica) and collected on Superfrost® Plus slides (Fisher Scientific). Slides processed for DAB (3, 3' Diaminobenzidine) staining were fixed with ice cold methanol for 15 minutes at 4°C, rinsed with PBS and then permeabilized in 0.1% Triton X-100 for 5 minutes. Each slide was then placed in a humid chamber and covered with blocking buffer solution for one hour at room temperature. After 1 hour, blocking buffer was tipped off and primary antibodies diluted in blocking buffer were added at the

following concentrations: rabbit polyclonal NPRA (1:50) (Santa Cruz, Catalogue # sc-25485) and rabbit polyclonal NPRC (1:50) (Santa Cruz, Catalogue # sc-25487) for 1 hour at room temperature in a humid chamber and subsequently at 4ºC overnight. The following day, primary antibodies were tipped off and slides were rinsed with PBS three times for five minutes each before being incubated with secondary goat-anti-rabbit antibodies (Bio-Rad, Catalogue #172-1019) conjugated to horse radish peroxidase for one 1hour at room temperature. After extensive rinsing, a single SIGMA*FAST*^{TM} DAB tablet (Sigma) was dissolved in 15ml ultrapure H_2O by vortexing, and the resulting DAB solution was applied to tissue sections. The subsequent chromogenic reaction was monitored by light microscopy at low power to assess the degree of color development. Reactions were allowed to proceed for ~5-10 minutes, and were stopped by tipping off DAB solution and rinsing slides extensively with PBS. Slides were mounted with 0.1% propyl gallate solution, examined by light microscopy using a Leica DM2500 microscope and images were captured using a Leica DFC 500 digital acquisition system.

2.19 Cell Transplantation and Nifedipine Treatments

Ventricles from E11.5 NCRL embryos were isolated, pooled and digested in 0.2% Type I collagenase (Worthington) for 30 minutes at 37ºC. Cell pellets were then obtained by centrifugation and neutralized with 10% DMEM as described earlier (Section 2.5) and re-suspended to a concentration of 60,000 cells/µl in sterile PBS. Adult (~12 weeks) male C57Bl/6 mice were anesthetized by 1.25g of 2,2,2-tribromethanol (Sigma) dissolved in 1.25ml of Amyl Alcohol A730-1 (Fisher Scientific) added drop wise into 50ml of ddH_2O (13µl of 2.5% tribromoethanol solution per gram body weight). To maintain anesthesia

mice were administered 2.5% isoflurane using an animal ventilator (100-cycles/minute and 0.3cc volume). Using thoracotomy, the trachea was exposed, intubated and connected to an animal volume-controlled ventilator (Harvard Apparatus Small Animal Ventilator Model 687, Holliston, Massachusetts, USA). The heart was then exposed via sternotomy with the use of small retractors. For each experiment, 3 X 10^5 cells suspended in 5µl of PBS were injected directly into the left ventricle of the heart using a 28 gauge insulin ½ cc syringe. The incisions were then closed with interrupted 4 – 0 sutures, and the endotracheal tube was gently retracted after voluntary respiration resumed. Analgesics, Buprenorphine (0.03-0.05mg/kg body weight, IP) and Ketoprofen (2mg/kg body weight, administered via SC route) were given prior to surgery and once every 12 hours for the duration of the experimental protocol.

Adult C57Bl/6 male mice were injected once daily with a dose of 5mg/kg (average mass of 25g per mouse was assumed) of nifedipine (Sigma) or an equal volume of 10% Captisol (Captisol, La Jolla, California, USA) vehicle solution (sterile H_2O, 10% w/v Captisol). A total volume of 150µl of nifedipine or vehicle was delivered via the subcutaneous delivery route on the day of the cell transplantation surgery and once daily for two subsequent days. On the third day post-surgery, animals were sacrificed and processed for quantification of graft sizes as described below (Section 2.20).

2.20 Quantification of Graft Sizes

To determine the graft size obtained following intracardiac injection of E11.5 NCRL ventricular cells, adult mice were sacrificed 3 days post-cell injection by cervical dislocation, hearts were rapidly excised and placed in Flow Fix (recipe described in

Section 2.7) for 3 days at 4 ºC with rocking. Heart sections (25µm) were then cut using a motorized advanced vibroslice (MA752 Campden Instruments Ltd., Lafayette, Indiana, USA) in a PBS tissue bath and placed in X-Gal solution overnight at 37 ºC to elicit a blue chromogenic signal from the transplanted NCRL cells. The quantification of intracardiac grafts within 25µM tissue sections was performed via Colour-Subtractive Computer-Assisted Image Analysis as previously described (Gaspard and Pasumarthi, 2008). Areas occupied with blue pixels, representing the NCRL cardiac cell graft, were assessed from photomicrographs using image processing software developed by Reindeer Graphics (Asheville, North Carolina, USA). The surface area of the graft was calculated based on the area occupied by blue pixels. The approximate total volume of the graft for each heart was then calculated by multiplying the surface area of each section by 25µm. After quantification, tissue sections containing transplanted NCRL cells were placed in a cryoprotectant 30% sucrose solution overnight at 4ºC with rocking. The following day, tissue sections were stacked and placed in OCT medium using embedding rings and frozen at -80ºC until further processing for Hematoxylin & Eosin staining described in the following section (Section 2.21).

2.21 Hematoxylin & Eosin (H&E) Staining on Adult Heart Sections

Adult heart tissue sections (25µm) that were stacked in OCT were cut into smaller (10µm) sections using a Leica CM3050 S Cryostat and sections were collected on Superfrost® Plus slides (Fisher Scientific). Heart sections processed for H&E staining were immersed in instant hematoxylin solution (Thermo Electron Corporation, Pittsburg, Pennsylvania, USA) for 2 minutes and then rinsed under running water. Slides were then

immersed in a solution consisting of 0.25% HCl, washed under running water, and then immersed in bluing agent (0.05% lithium carbonate). Slides were then rinsed under running water and immersed in the following solutions for 30 seconds each: 95% ethanol, 95% ethanol, 100% ethanol and xylenes. Finally, slides were mounted with Cytoseal-60 (Richard-Allan Scientific, Kalamazoo, Michigan, USA), allowed to air dry and then examined by light microscopy using a Leica DM2500 microscope.

2.22 Electrocardiograms (ECG)

Prior to ECG recordings, mice were anesthetized by inhalation of 2.5% isoflurane using an animal ventilator (100-cycles/minute and 0.3cc volume). The ECG signal was obtained from using a bipolar 3-electrode 3-lead system. For this purpose, electrodes (AD Instruments, Inc. 2205 Executive Circle, Colorado Springs, USA) were gently placed under the skin in the left and right regions of the pectoral muscles of mice and under the skin of the left hind limb. ECG signals were recorded using Bio AMP and Power Lab 8/30 hardware and analyzed via Lab Chart 7 v.7.3.7 software provided by AD Instruments. ECGs were recorded at a sampling rate of 1 kHz using the Lab Chart software. Recordings were performed for a minimum of 2 minutes at baseline, and for a minimum of 20 minutes after dobutamine (Sigma) injections (1.5µg/g). At least 10 beats were averaged to determine the heart rate (beats per minute), RR, PR, QT, QRS, and P duration. Body temperature of all mice was maintained at 37ºC by placing the mouse on a small animal heating plate (Physitemp, Instruments Inc. Clifton, New Jersey, USA, Model # TCAT-2LV) and body temperature was continuously monitored using a rectal probe.

2.23 Statistical Analyses

Data are presented as mean ± standard error of the mean (SEM). Between groups comparisons were analyzed by ANOVA and Tukey multiple comparisons post hoc test. A two-tailed unpaired t-test was used to compare between two groups only. Significance for all analyses was assigned at $p<0.05$. For each experiment, the number of experiments/replicates is indicated in the corresponding figure legend.

Primer Name	Primer Sequence (5'→3')	Expected band sizes (bp)	
Nkx2.5-S	GCCCTGTCCCTCGGATTTCACACC		
Nkx2.5-AS	ACGCACTCACTTTAATGGGAAGAG	583	264
Cre-S	GATGACTCTGGTCAGAGATACCTG		
Rosa 1	AAAGTCGCTCTGAGTTGTTAT		
Rosa 2	GCGAAGAGTTTGTCCTCAACC	320	650
Rosa 3	GGAGCGGGAGAAATGGATATG		
Npr1-S	GCATGGTTCAGCTCTAAGAC		
Npr1-AS	CTAACCCTGTGAACTGTAAGC	500	339
Neo-AS	CCTTCAGTTATCTACATCTGC		
Cx40-S	CTCCAATTAACTCCTTGTGAGCC		
Cx40-AS	AGGCTGAATGGTATCGCACC	450	380
Neo-AS	CTTGCCGAATATCATGGTGG		
ANF-LacZ F	ATCCTTTGCGAATACGCCCACGCG	310	N/A
ANF-LacZ R	GCTGGTCACTTCGATGGTTTGCCC		

Table 2.3.1: List of primers used for genotyping and expected band sizes.

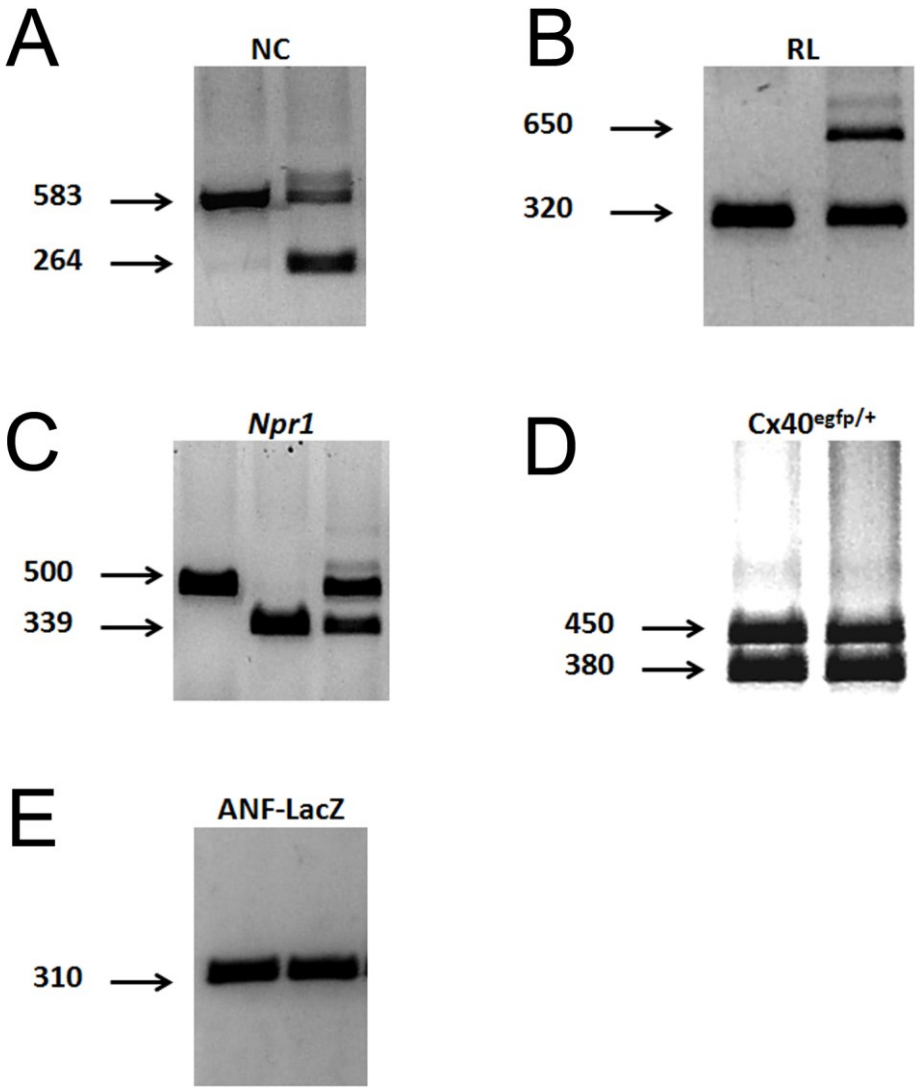

Figure 2.3.1: Expected band sizes from genotyping of various mouse strains. A) Nkx2.5-Cre (NC). **B)** Rosa-LacZ (RL). **C)** NPRA knockout (*Npr1*gene). **D)** $Cx40^{egfp/+}$. **E)** ANF-LacZ.

Table 2.12.1: List of primers used for real time quantitative PCR and expected amplicon sizes.

Primer Name	Primer Sequence (5'→3')	Expected Amplicon Sizes (bp)
GAPDH-F	TCGTCCCGTAGACAAAATGG	132
GAPDH-R	TTGAGGTCAATGAAGGGGTC	
$Ca_v1.1$-F	TCCTAATCGTCATCGGCAGC	94
$Ca_v1.1$-R	CCTCCACCCAGGCAATACAG	
$Ca_v1.2$-F	AGCAAGAACCACTGCGGAT	106
$Ca_v1.2$-R	GAAGAAATGCAGCAACAGCC	
$Ca_v1.3$-F	CATCCCATTCCCTGAAGATG	99
$Ca_v1.3$-R	TTCAGAAATGTCTCCACTGTAAAAA	
$Ca_v3.1$-F	TCCTGGTCAATACCCTCAGC	97
$Ca_v3.1$-R	AGGCTGGTGAAGACGATGTT	
$Ca_v3.2$-F	CCGAGGAGGCGATACTGG	130
$Ca_v3.2$-R	CTCGGTCATGGTGGCAGA	
Cyclin D1-F	CTCCTCTCCAAAATGCCAG	112
Cyclin D1-R	GGGTGGGTTGGAAATGAACT	
Cyclin D2-F	CAGCAGGATGATGAAGTGAACACA	168
Cyclin D2-R	GGATCCGGCGTTATGCTGCTCTT	
CDK4-F	TGCCAGAGATGGAGGAGTCT	109
CDK4-R	TTGTGCAGGTAGGAGTGCTG	
Cyclin E-F	TGTGAAAAGCGAGGATAGCA	139
Cyclin E-R	GATTTTCCGAGGCTGAATG	
Cyclin B1-F	TGTGTGAACCAGAGGTGGAA	114
Cyclin B1-R	GGCTTGGAGAGGGATTATCA	
p21-F	GAAACGCTTTCTGAGTTCGG	144
p21-R	GGGTCCTTTGAACTGGCTTC	
p27-F	GTGGACCAAATGCCTGACTC	126
p27-R	TTCTTCTGTTCTGTTGGCCC	

Primer Name	Primer Sequence (5'→3')	Expected Amplicon Sizes (bp)
GATA4-F	CTGGAAGACACCCCAATCTC	100
GATA4-R	CCATCTCGCCTCCAGAGT	
Hand2-F	CGGAGATCAAGAAGACCGAC	96
Hand2-R	TGGTTTTCTTGTCGTTGCTG	
MEF2C-F	TGGAGAGATGAAGTGAAGCG	93
MEF2C-R	GCACAGCTCAGTTCCCAAAT	
Tbx5-F	TGGTTGGAGGTGACTTTGTG	101
Tbx5-R	GGCAGTGATGACCTGGAGTT	
ANP-F	GGACTAGGCTGCAACAGCTTCCG	119
ANP-R	CCAAGCTGCGTGACACACCAC	
NPRA-F	CCGATACTGCCTCTTTGGAG	116
NPRA-R	CATCGAACTCTTCCAGCACA	
NPRC-F	ACAGCTCTCCTTGCAAATCATCAGG	184
NPRC-R	CGC AGC TCT CGA TGC TTC CCG	
Cx40-F	CAGAGCCTGAAGAAGCCAAC	137
Cx40-R	GACTGTGGAGTGCTTGTGGA	
HCN4-F	CCTCCTGCGCCTCTTGAGGCTTT	119
HCN4-R	TGCCAATGAGGTTCACGATGCGT	

CHAPTER 3: THE EFFECTS OF CALCIUM CHANNEL BLOCKADE ON PROLIFERATION AND DIFFERENTIATION OF CARDIAC PROGENITOR CELLS

3.1 Background and Hypothesis

Globally, cardiovascular diseases remain the number one cause of mortality (World Health Organization Statistics, www.who.int). Owing to a very low capacity of post-natal cardiomyocytes to divide (Pasumarthi and Field, 2002), cardiomyocytes lost to disease or injury are replaced by fibrotic scar tissue rather than new viable cardiomyocytes. While the presence of several endogenous cardiac stem/progenitor cells have been documented in the adult heart (Hierlihy et al., 2002; Beltrami et al., 2003; Oh et al., 2003) , they appear to be inadequate to respond to the massive cell loss associated with many forms of cardiovascular disease. Currently, pharmacological therapies and surgical interventions can slow the progression of heart disease, but cannot replace the lost cardiomyocytes. To this end, donor cell transplantation is emerging as a favorable strategy to restore heart function by replenishing the diseased heart with new functional cardiomyocytes (McMullen and Pasumarthi, 2007).

The discovery of functional coupling between transplanted fetal cardiomyocytes and host myocardium was a significant step towards the use of cell based therapies for myocardial repair (Rubart et al., 2003; Roell et al., 2007; Shiba et al., 2012). One of the major hurdles remaining in the cell transplantation field is the ability of transplanted cells to form larger graft sizes (Laflamme and Murry, 2005). A hallmark feature of embryonic cardiac progenitor cells (CPCs) is a high intrinsic capacity for proliferation which could in principle translate into larger graft sizes. Furthermore, CPCs have the

ability to differentiate into mature cardiomyocyte lineages (McMullen et al., 2009) and therefore have the potential to couple functionally with host myocardium. Based on these features, we believe that CPCs represent a promising candidate cell type for use in cell based therapies for myocardial repair. Previously, our group described the existence of CPCs in the embryonic heart at the post-chamber formation stage of E11.5 (Zhang and Pasumarthi, 2007; McMullen et al., 2009). We have also demonstrated that E11.5 cells containing a significantly higher proportion of CPCs can repopulate diseased hearts at a higher efficiency compared to E14.5 cells (unpublished data, manuscript in preparation). Currently, it is unclear whether existing cardiovascular drugs would have detrimental or protective effects on CPC transplantation.

Previously, it was shown that embryos exposed to the dihydropyridine (DHP) Ca^{2+} channel antagonist nifedipine displayed cardiac morphological abnormalities and altered expression of cardiac genes (Porter et al., 2003). Currently, our understanding of the molecular mechanisms underlying impaired cardiogenesis in response to Ca^{2+} channel blockade remains incomplete. **Thus, we tested the hypothesis that Ca^{2+} channel blockade by nifedipine disrupts the normal program of proliferation and differentiation of E11.5 CPCs and cardiomyocytes.** As a corollary, we also tested the hypothesis that systemic administration of nifedipine would have a detrimental effect on graft size formation following transplantation of E11.5 cells (mixed population of CPCs and cardiomyocytes)

3.2 Specific Aims

1. Determine the effects of nifedipine on proliferation of E11.5 CPCs and cardiomyocytes *in vitro*.

2. Investigate the effects of nifedipine on myofibrillogenesis of E11.5 cardiomyocytes.

3. Determine the effects of systemic administration of nifedipine on graft size formation following transplantation of E11.5 cardiac cells.

3.3 Results

3.3.1 Conditional Activation of β-galactosidase in Embryonic Cardiac Cells using Nkx2.5-Cre and Rosa LacZ Double Transgenic Mouse Model

The primary aim of this research study was to investigate the effects of Ca^{2+} channel inhibition on CPC and cardiomyocyte populations in the E11.5 heart. To distinguish cardiac cells from non-cardiomyogenic cell types found in the embryonic heart, we employed a double transgenic mouse model system which genetically labels all cells derived from the initial Nkx2.5 expressing cell lineage. The Nkx2.5-Cre transgenic strain (designated NC) was engineered to have an internal ribosomal entry sequence (IRES) and Cre-recombinase (Cre) coding sequence inserted into the 3' untranslated region of the Nkx2.5 gene (Stanley et al., 2002). Cre, a recombinase protein from the bacteriophage P1, mediates site specific recombination between specific DNA sequences known as LoxP sites, resulting in removal of intervening DNA sequences.

The ROSA- *Lac Z* reporter strain (designated RL) was engineered to have a transcriptional terminator stop cassette proximal to the β-galactosidase (*LacZ*) coding sequence (Soriano, 1999). The stop cassette harbors a neomycin selection gene plus

triple polyadenylation sites, and is flanked by LoxP sites. Upon translation of Nkx2.5 in the initial heart cell population of the double transgenic mice (designated NCRL), the Cre- recombinase gene was co-translated. The resulting Cre-protein excised the floxed stop cassette from ROSA-*Lac Z* transgene, allowing the expression of the *Lac Z* reporter, and detection of $Nkx2.5^{+}$ cell lineages thereafter (Figure 3.3.1A-C). Homozygous NC and RL mouse lines were routinely crossed to generate E11.5 embryos heterozygous for both transgenes. To confirm the double transgenic genotype of embryos used for experimental purposes, the atria were carefully dissected from each heart, and incubated in X-Gal (chromogenic β-gal substrate) solution in order to visualize the insoluble blue reaction product (Figure 3.3.1D). In preliminary studies, non-transgenic atria were shown to be negative in response to X-gal staining (data not shown).

3.3.2 Voltage Sensitive L-type and T-type Ca^{2+} Channels are Expressed in the Embryonic Ventricles

Dihydropyridine (DHP) Ca^{2+} channel antagonists potently inhibit voltage gated L-type Ca^{2+} channels (IC_{50}< 1μM)(Katzung, 2009) while at higher concentrations they can inhibit both L-Type and T-type Ca^{2+} channels (IC_{50} 10-100μM)(Perez-Reyes et al., 2009). To gain insight into the specific complement of voltage sensitive Ca^{2+} channels expressed in the murine embryonic ventricles, we determined the relative abundance of mRNA for several L-type Ca^{2+} channel isoforms ($Ca_v1.1$, $Ca_v1.2$ and $Ca_v1.3$) as well as T-type Ca^{2+} channel isoforms ($Ca_v3.1$ and $Ca_v3.2$) by real time quantitative polymerase chain reaction (qPCR) at E11.5 and also at later developmental/post-natal stages. In preliminary experiments, it was determined that glyceraldehyde 3-phosphate

dehydrogenase (GAPDH) expression levels remained unchanged across all developmental and postnatal stages examined, and was therefore used as an internal control gene to normalize data by correcting for variations in quantities of cDNA used as template (Figure 3.3.2A&B). At the E11.5 stage, the L-type Ca^{2+} channels $Ca_v1.2$ and $Ca_v1.3$ were the predominant Ca^{2+} channel isoforms expressed at the mRNA level (Figure 3.3.3A). At this stage, both T-type Ca^{2+} channel isoforms ($Ca_v3.1$ and $Ca_v3.2$) were also expressed, albeit at lower levels compared to the L-Type Ca^{2+} channels (Figure 3.3.3A).

To monitor fluctuations in Ca^{2+} channel expression in the ventricles throughout cardiac development, the relative abundance of each L-type and T-type Ca^{2+} channel isoform was also determined at later embryonic and postnatal stages (E14.5, E16.5, Neonatal and Adult). Results from these developmental analyses, which are presented in Figure 3.3.4A-E, revealed several notable trends: **1)** the relative expression of $Ca_v1.3$ and $Ca_v3.2$ were highest at E11.5 and progressively declined at later developmental stages (Figure 3.3.4C&E). **2)** Relative expression of $Ca_v1.2$ remained relatively constant across all developmental and postnatal stages (Figure 3.3.4B). **3)** Expression of $Ca_v1.1$was barely detectable during the entire embryonic and neonatal period but then increased ~300 fold at the Adult stage (Figure 3.3.4A). **4)** Expression of $Ca_v3.1$ progressively increased during the developmental and perinatal period before dropping precipitously at the Adult stage (Figure 3.3.4D). A side-by-side comparison of the relative expression levels of each L-type and T-type Ca^{2+} channel isoform at E11.5, E14.5, E16.5, Neonatal and Adult stages also provides a more clear indication of the predominant Ca^{2+} channel isoforms expressed at each individual stage (Figure 3.3.4F).

3.3.3 Characterization of Ca^{2+} Influx in Isoproterenol Stimulated Cells Treated with Nifedipine

Based on the knowledge that nifedipine can inhibit L-type and T-type Ca^{2+} channels with either high or low potency respectively, we examined the effects of various concentrations of nifedipine on intracellular Ca^{2+} (denoted as $[Ca^{2+}]_i$) fluctuations in the embryonic ventricular cell population. Acutely isolated E11.5 ventricular cells were plated in 96- well clear bottom plates and incubated with various doses of nifedipine (1μM, 10μM or 100μM) or vehicle (DMSO) for 1 hour. The $[Ca^{2+}]_i$ levels were then monitored in randomly selected fields at baseline and in response to isoproterenol (ISO) stimulation using the Ca^{2+} sensitive indicator Fluo-8 AM. The Acetoxymethyl (AM) esters that are attached to Fluo-8 molecules are non-polar groups that readily cross the cell membrane and then get rapidly hydrolyzed by intracellular esterases to generate charged groups that are retained within the cell. Upon binding to Ca^{2+}, Fluo-8 undergoes a >200 fold increase in fluorescence intensity which can be detected as emitted fluorescence at a wavelength of 514nm and used to monitor fluctuations in $[Ca^{2+}]_i$ levels. In cultures pre-incubated with vehicle for 1 hour, stimulation with ISO (1μM) resulted in $[Ca^{2+}]_i$ oscillations that were readily observable in a significant proportion of the total cell population from each field examined. By contrast, in cultures pre-incubated for 1 hour with either 1μM or 10μM nifedipine, $[Ca^{2+}]_i$ oscillations were observably smaller in amplitude and could only be detected in a relatively small proportion of the total cell population. Finally, in cultures pre-incubated with 100μM nifedipine for 1 hour, $[Ca^{2+}]_i$ oscillations were barely detectable and were present in only a very small proportion of the total cell population.

To quantify these observations, the average change in fluorescence intensity (corresponding to $[Ca^{2+}]_i$) that occurred in response to stimulation with ISO was calculated from randomly selected fields using Colour-Subtractive Computer-Assisted Image Analysis software as previously described (Gaspard and Pasumarthi, 2008). For these experiments, the baseline fluorescence intensity was set to a value of 1.0 and data are expressed as fold change at 1, 3 and 5 minute time points following ISO stimulation. In cultures pre-incubated with vehicle for 1 hour, ISO induced a significant increase in $[Ca^{2+}]_i$ compared to baseline at 3 and 5 minute time points (**3 minutes:** 5.4 ± 0.7 fold vs. baseline, **5 minutes:** 5.6 ± 0.6 fold vs. baseline) (Figure 3.3.5B&F). In cultures pre-incubated with 1μM nifedipine, an increase in $[Ca^{2+}]_i$ was observed at the 5 minute time point and this value did not differ in magnitude compared to control (5.9 ± 0.7 fold vs. baseline) (Figure 3.3.5C&F). By contrast, pre-incubation with 10μM nifedipine blunted the increase in $[Ca^{2+}]_i$ at 5 minutes compared to both control and 1μM values (2.4 ± 0.3 fold vs. baseline) (Figure 3.3.5D&F). Pre-incubation with 100μM nifedipine essentially abolished any ISO stimulated increase in $[Ca^{2+}]_i$ (1.1 ± 0.1 fold vs. baseline) (Figure 3.3.5E&F). These results, together with Ca^{2+} channel gene expression data (Figure 3.3.3), support the idea that Ca^{2+} channels with variable sensitivities to DHP Ca^{2+} channel antagonists exist in the ventricular myocardium at E11.5, and could be members of both the L-type and T-type families of voltage gated Ca^{2+} channels.

3.3.4 Nifedipine Causes a Decrease in DNA Synthesis in Cardiac Progenitor Cells and Cardiomyocyte Populations

Intracellular Ca^{2+} signalling cascades are well known regulators of cell proliferation in numerous cell types. Thus, we investigated the effects of Ca^{2+} channel blockade on proliferation kinetics of primary cultured E11.5 ventricular cells. The concentrations of 10μM and 100μM were selected for these analyses with the intention of either inhibiting L-type Ca^{2+} channels only (10μM) or both L-type and T-type Ca^{2+} channels (100μM). For these experiments, double transgenic embryos (NCRL) with genetically labelled $Nkx2.5^{+}$ lineage (express β-gal) were used to identify cardiac cells in culture, while immunolabelling for the differentiation marker sarcomeric myosin (MF20 antibodies) was used to confirm the identities of cardiomyocytes (Figure 3.3.6A-D). Using this model system, cells positive for β-Gal, but not MF20 ($\beta\text{-Gal}^{+}$/ $MF20^{-}$) were considered to be CPCs since previously we demonstrated that $Nkx2.5^{+}/MF20^{-}$ cells differentiate into $MF20^{+}$ expressing cardiomyocytes *in vitro* (McMullen et al., 2009). Conversely, cells positive for both β-Gal and MF20 ($\beta\text{-Gal}^{+}$/ $MF20^{+}$) were considered to be cardiomyocytes. Finally, cells that were negative for both β-Gal and MF20 ($\beta\text{-Gal}^{-}$/ $MF20^{-}$) were classified as non-cardiomyogenic cells.

Following a 16 hour incubation period with either vehicle or nifedipine (10μM or 100μM), rates of proliferation were determined using a tritiated [^{3}H]-thymidine incorporation assay. The principle of this assay is based on uptake of the radiolabelled thymidine analogue, [^{3}H]-thymidine, by cells undergoing *de novo* DNA synthesis during the S-phase of the cell cycle. Following autoradiographic processing, incorporation of [^{3}H]-thymidine into cells in the S-phase can be readily detected by the presence of

distinct silver grains in the nucleus (Figure 3.3.7). The percentage of cells in the S-phase out of the defined cell population was referred to as the labelling index (LI).

In vehicle treated control cultures, the CPC population had an average LI of 42.7 ± 4.2 %) which was significantly higher compared to the LI observed in the cardiomyocyte population (14.0 ± 3.4%) and was consistent with the inverse relationship that is known to exist between proliferation and differentiation during cardiogenesis (Figure 3.3.8A&B). Treatment with 10μM nifedipine was associated with a significant reduction in the LI of the CPC population (25.6 ± 3.9%), but did not have any effect on the LI of cardiomyocytes (11.9 ± 2.2%) (Figure 3.3.8A&B). By contrast, treatment with 100μM nifedipine drastically reduced proliferation in both the CPC (8.07 ± 4.1%) and cardiomyocyte (1.7± 0.3%) cell populations (Figure 3.3.8A&B). Furthermore, it was demonstrated that nifedipine treatment was associated with a dose dependent reduction in DNA synthesis of the non-cardiomyogenic cell population (β-gal$^-$/MF20$^-$) that was quantitatively similar to that observed in the CPC population (Figure 3.3.8C).

Based on the observation that 10μM nifedipine was associated with reduced proliferation of CPCs but not cardiomyocytes, we speculated that L-type Ca^{2+} current may play a more prominent role in regulating proliferation in CPCs. To gain insight into this issue, E11.5 NCRL primary cultures were generated and co-immunolabelled with MF20 and $Ca_v1.2$ L-type Ca^{2+} channel specific antibodies. Slides were also incubated overnight in X-gal in order to confirm the identities of cardiomyogenic cells. Interestingly, results from these experiments demonstrated that $Ca_v1.2$ immunoreactivity was strong in the nucleus/perinuclear region of the CPCs and cardiomyocytes, while

labelling of the plasma membrane tended to be more prominent in CPCs compared to cardiomyocytes (Figure 3.3.9).

3.3.5 Ca^{2+} Channel Blockade with Nifedipine is Associated with Gene Expression Changes in Cell Cycle Regulating Genes

To gain insight into potential molecular mechanisms underlying the effects of Ca^{2+} channel blockade on CPC and cardiomyocyte proliferation, we examined the effects of nifedipine on the expression of several positive and negative cell cycle regulating genes. Primary cultured E11.5 ventricular cells were incubated with either vehicle or nifedipine (10μM or 100μM) for 16 hours and subsequently analyzed for changes in expression of the positive cell cycle regulators Cyclin D1, Cyclin D2, CDK4, Cyclin E and Cyclin B1 as well cell cycle inhibitors p21 and p27. Using vehicle (DMSO) treated cultures as a point of reference (i.e. expression=1.0), results from these analyses, (Figure 3.3.10, and summarized in Table 3.3.1), demonstrated that treatment with either 10μM or 100μM nifedipine was associated with a significant reduction in expression in Cyclin B1 compared to control (**10μM**: 0.7 ± 0.06 and **100μM**: 0.7 ± 0.02), while other positive cell cycle genes remained unchanged. Additionally, 100μM nifedipine, but not 10μM, was associated with a ~ 2 fold increase in expression of the cell cycle inhibitor p27 (1.9 ± 0.2) but had no effect on expression of p21.

Thus far, work from Chapter 3 has demonstrated the nifedipine mediated Ca^{2+} channel blockade was associated with reduced rates of proliferation of CPCs and cardiomyocytes isolated from the E11.5 ventricles. Furthermore, the higher potency of nifedipine on inhibition of CPC versus cardiomyocyte proliferation highlights the

possibility that different Ca^{2+} channel isoforms with varying sensitivities to DHP antagonists may differentially regulate proliferation kinetics in these two distinct cell populations. Because intracellular Ca^{2+} signalling cascades have also been implicated as critical regulators of cardiomyocyte differentiation, we next sought to characterize the effects of nifedipine on myofibrillogenesis.

3.3.6 Ca^{2+} Channel Blockade is Associated with High Levels of Sarcomeric Disorganization in Embryonic Cardiomyocytes

To determine the effects of Ca^{2+} blockade on cardiomyocyte differentiation, we characterized the effects of nifedipine on the integrity of the contractile apparatus of E11.5 cardiomyocytes (β-gal^{+}/$MF20^{+}$) based on immunolabelling with antibodies against sarcomeric myosin (MF20). In control cultures incubated with vehicle (DMSO) for 16 hours, the vast majority of $MF20^{+}$ cardiomyocytes displayed organized muscle fiber bundles and a stellate morphology, which is characteristic of embryonic cardiomyocytes (Figure 3.3.11A). By contrast, in cultures treated with 10μM or 100μM nifedipine, cardiomyocytes generally appeared smaller in size and displayed poorly formed sarcomeric structures that were highly disorganized and/or misshaped (Figure 3.3.11B&C). To quantitatively measure of the impact of nifedipine on cardiomyocyte differentiation, the average cell size of cardiomyocytes from each treatment group was determined by measuring cell surface areas using Colour-Subtractive Computer-Assisted Image Analysis software (Gaspard and Pasumarthi, 2008). Results from these analyses demonstrated that the average surface area of cardiomyocytes from control cultures was ~2500 μm^2 (Figure 3.3.11D). Compared to control, significant reductions in

cardiomyocyte surface area were observed in response to either 10μM (~1000μm^2) or 100μM (~400μm^2) nifedipine (Figure 3.3.11D).

To determine whether nifedipine treatment was associated with altered differentiation kinetics, the relative abundance of CPCs (β-Gal$^+$/ MF20$^-$), cardiomyocytes (β-Gal$^+$/ MF20$^+$) and non-cardiomyogenic (β-Gal$^-$/ MF20$^-$) was quantified from control and nifedipine treated cultures. In control cultures, the cell population was composed of 49.3 ± 3.5% cardiomyocytes 40.1 ± 4.2% CPCs, and 11.1 ± 4.4% of non-cardiomyogenic cells (Figure 3.3.12). While the relative distribution of each cell type did not change in response to 10μM nifedipine treatment, a significant increase in relative proportion of cardiomyocytes (63.4 ± 1.8%) and a trend toward a decrease in CPCs (28.8 ± 1.4%) was observed in response to 100μM nifedipine (proportion of non-cardiomyogenic cell population did not change; 8.9 ± 1.2%).

To investigate potential molecular mechanisms underlying impaired myofibrillogenesis, we examined whether nifedipine had any effect on expression of a panel of transcription factors required for proper cardiogenesis including GATA4, Hand2, MEF2c and Tbx5. Compared to DMSO controls (Expression=1.0), it was determined that 100μM, but not 10μM nifedipine was associated with a modest but significant reduction of Tbx5 expression (0.7 ± 0.08), while GATA4, Hand2 and MEF2c levels remained unchanged (Figure 3.3.13A-D). Previously, it was demonstrated that translocation of MEF2c to the nucleus was critical for proper myofibrillogenesis and occurred via a Ca^{2+} dependent processes (Lynch et al., 2005). Based on this knowledge, we investigated the subcellular localization of MEF2c in E11.5 cardiomyocytes treated with either DMSO or 100μM nifedipine. In control cultures, intense MEF2c labelling

was readily observed in the nucleus, along with lower levels in the cytoplasmic compartment detected as small punctae (Figure 3.3.14A-D). By stark contrast, in cardiomyocytes from 100μM treated cultures, immunoreactive MEF2c was very faint in the nucleus, and mostly confined to the cytoplasm as small punctae (Figure 3.3.14E-H). As a readout of whether this mislocalization of MEF2c in the cytoplasm was associated with altered transcriptional activity, we quantified the expression of a known MEF2c target gene ANP (*Nppa*), in response to 100μM nifedipine. Compared to DMSO treated cultures (expression=1.0), a significant reduction in ANP gene expression (0.7±0.06) was measured in cultures treated with 100μM nifedipine (Figure 3.3.15).

3.3.7 Nifedipine has Detrimental Effects on Graft Size Formation Following Injection of E11.5 Ventricular Cells into Recipient Hearts

The *in vitro* data presented thus far in Chapter 3 have provided evidence that pharmacological Ca^{2+} channel blockade with the DHP Ca^{2+} channel antagonist nifedipine disrupts the normal program of proliferation and differentiation of E11.5 CPCs and cardiomyocytes. Based on this knowledge, we further hypothesized that the detrimental effects of nifedipine seen *in vitro* would translate into smaller graft size formation *in vivo* following cell transplantation. To test this hypothesis, approximately $3x10^5$ ventricular cells, acutely isolated from E11.5 double transgenic (NCRL) embryos, were transplanted via direct intracardiac injection into the left ventricles of healthy C57Bl/6 mice. Recipient mice subsequently received daily doses of either nifedipine (5mg/kg) or an equal volume of vehicle (10% captisol) for 3 days beginning on the day of the transplantation surgery. On the third day post-surgery, animals were sacrificed and

processed for quantification of graft sizes. Briefly, excised hearts were fixed, sliced into ~25μm sections, and then incubated in X-gal solution in order to visualize transplanted NCRL cells within the host tissue (blue reaction product). Areas occupied by blue pixels, corresponding to transplanted cells, were then quantified to estimate the total graft volume from each recipient heart using Colour-Subtractive Computer Assisted Image Analysis software (Gaspard and Pasumarthi, 2008).

In recipient mice receiving once daily doses of vehicle for 3 days, distinct regions of transplanted E11.5 cells were visible and tended to be spread out over relatively large surface areas (Figure 3.3.16A&B). By contrast, in mice receiving daily injection of nifedipine (5mg/kg dissolved in 10% captisol), engrafted regions tended to be smaller (Figure 3.3.16C&D). Quantification of the graft volume from recipient hearts confirmed that the average graft volume from vehicle treated recipients (0.045 ± 0.01 mm^3) was in fact significantly larger compared to the nifedipine treated group (0.0033 ± 0.001 mm^3) (Figure 3.3.16E).

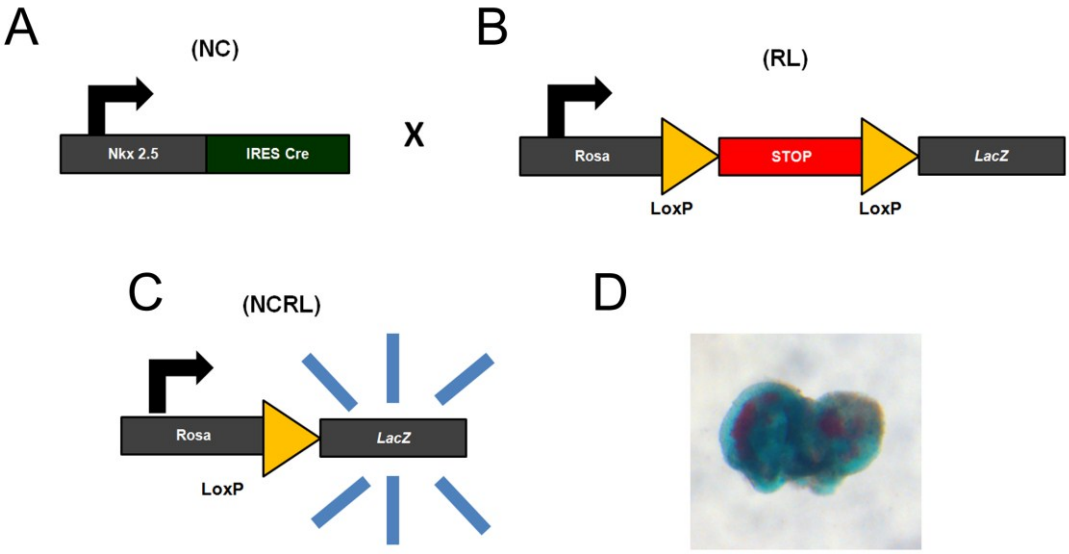

Figure 3.3.1: Conditional activation of the *LacZ* reporter gene genetically labels the Nkx2.5^{+} cell lineage. A) Schematic representation of Nkx2.5-Cre transgene (NC), engineered to have an internal ribosomal entry sequence (IRES) and Cre-recombinase (Cre) coding sequence inserted into the 3' untranslated region of the Nkx2.5 gene. **B)** Schematic representation of Rosa-*LacZ* (RL) reporter strain, engineered to have a transcriptional terminator stop cassette proximal to the β-galactosidase (*LacZ*) coding sequence which is flanked by LoxP sites. **C)** In double transgenic (NCRL) embryos, translation of Nkx2.5 in the initial heart cell population resulted in the co-translation of the Cre- recombinase gene. The resulting Cre-protein excised the floxed stop cassette from ROSA-*Lac Z* transgene, allowing the expression of the *Lac Z* reporter, and detection of Nkx2.5^{+} cell lineages thereafter. **D)** Confirmation of the double transgenic genotype of embryos was accomplished by incubating atria from each heart in X-Gal solution in order to visualize the insoluble blue reaction product.

A

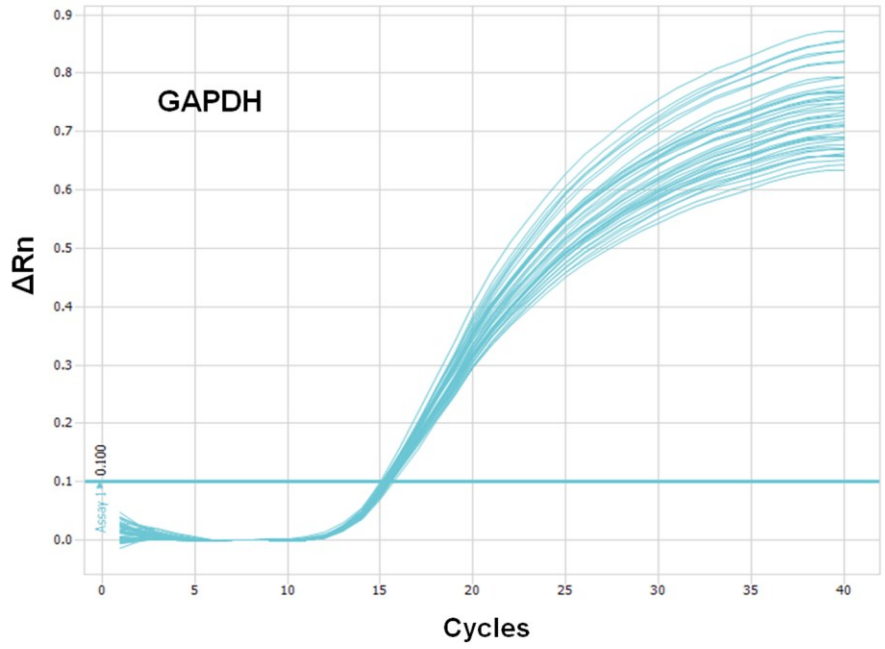

B

Dev. Stage	C_T ± SEM
E11.5	15.3 ± 0.06
E14.5	15.4 ± 0.03
E16.5	15.4 ± 0.1
Neonatal	15.7 ± 0.2
Adult	15.8 ± 0.2

Figure 3.3.2: Validation of GAPDH as internal control gene. A) Amplification plot of GAPDH shows all samples crossed the threshold (ΔRn=0.1) at approximately the same cycle number (average $C_T = 15.5 \pm 0.08$). **B)** Tabular summary of the average GAPDH C_T values obtained from multiple samples at each developmental stage. Because GAPDH was shown not to vary significantly between developmental and post-natal stages, it was used as a reference gene in subsequent experiments to normalize data by correcting for variations in quantities of cDNA used as template. N=5-6 independent RNA extractions/developmental stage, analyzed in duplicate for each extraction. One way ANOVA with Tukey post hoc test.

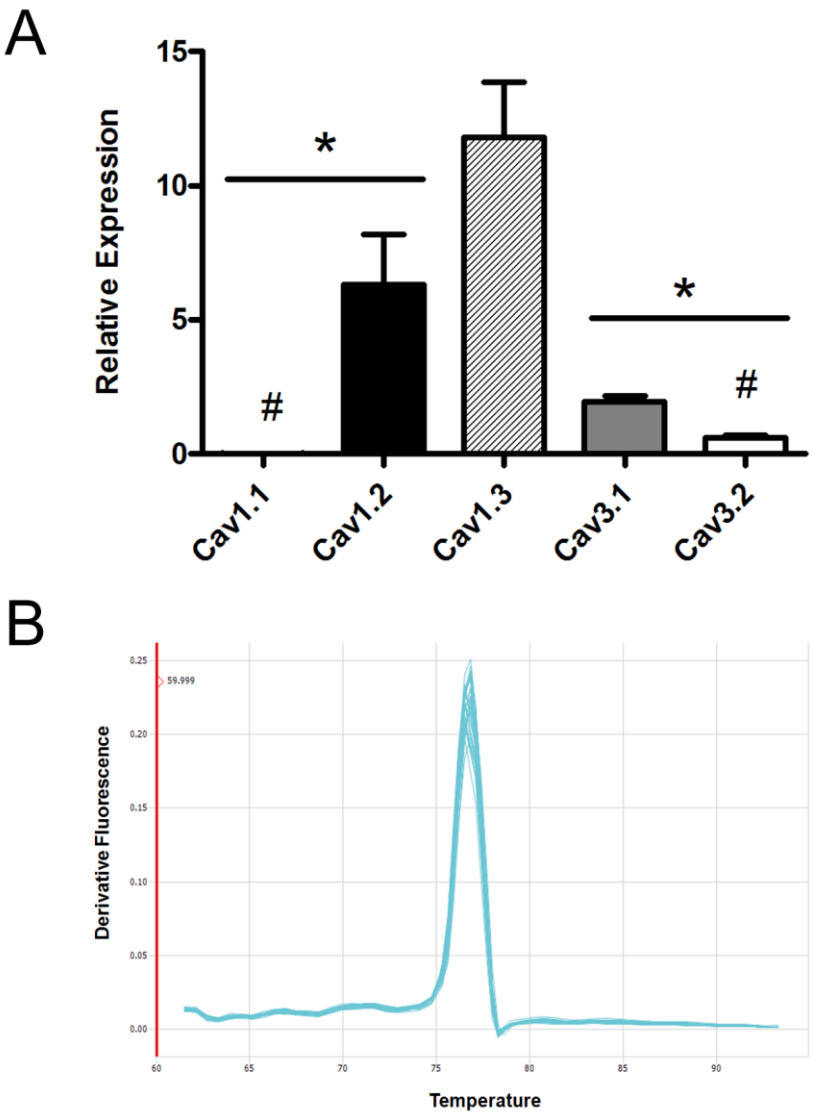

Figure 3.3.3: L-type and T-type Ca^{2+} channel expression in E11.5 ventricles. A) The relative expression levels of L-type Ca^{2+} channel isoforms ($Ca_v1.1$, $Ca_v1.2$ and $Ca_v1.3$) and T-type Ca^{2+} channel isoforms ($Ca_v3.1$ and $Ca_v3.2$) were measured in cardiac ventricles at E11.5 by real time quantitative PCR (all samples normalized to GAPDH). At this stage of development, the L-type Ca^{2+} channels $Ca_v1.2$ and $Ca_v1.3$ were the predominant Ca^{2+} channel isoforms expressed. The T-type Ca^{2+} channels $Ca_v3.1$ and $Ca_v3.2$ were also expressed, albeit at lower levels. Expression of $Ca_v1.1$ was virtually undetectable. **B)** Representative melt curve used to confirm the amplification of a single PCR product (example provided is $Ca_v1.3$). N=3-4 independent RNA extractions/developmental stage, analyzed in duplicate for each extraction. Each bar represents mean ± SEM. *$p < 0.05$ vs. $Ca_v1.3$; # $p < 0.05$ vs. $Ca_v1.2$, One-way ANOVA with Tukey post hoc test.

Figure 3.3.4: Developmental profiles of L-type and T-type Ca^{2+} channel isoforms. The relative expression of each Ca^{2+} channel isoform was determined in relation to the E11.5 stage (E11.5 expression=1.0). **A)** Expression of $Ca_v1.1$ was barely detectable throughout development and increased significantly at the adult stage. **B)** Relative expression of $Ca_v1.2$ did not vary significantly between any stages examined. **C)** Expression of $Ca_v1.3$ was highest at early developmental stages (E11.5 and E14.5) and then declined significantly later in development (E16.5-Adult). **D)** Expression of $Ca_v3.1$ showed a progressive increase during development and then dropped precipitously at the Adult stage. **E)** Expression of $Ca_v3.2$ was highest at E11.5 and then progressively declined at later developmental stages. **F)** Side-by-side comparison of the relative expression levels of each L-type and T-type Ca^{2+} channel isoform at E11.5, E14.5, E16.5, Neonatal and Adult stage (statistics not shown for **F**). N=3-4 independent RNA extractions/developmental stage, analyzed in duplicate for each extraction. Each bar represents mean ± SEM. Statistical differences are indicated under the appropriate graph for **A-E**. One-way ANOVA with Tukey post hoc test.

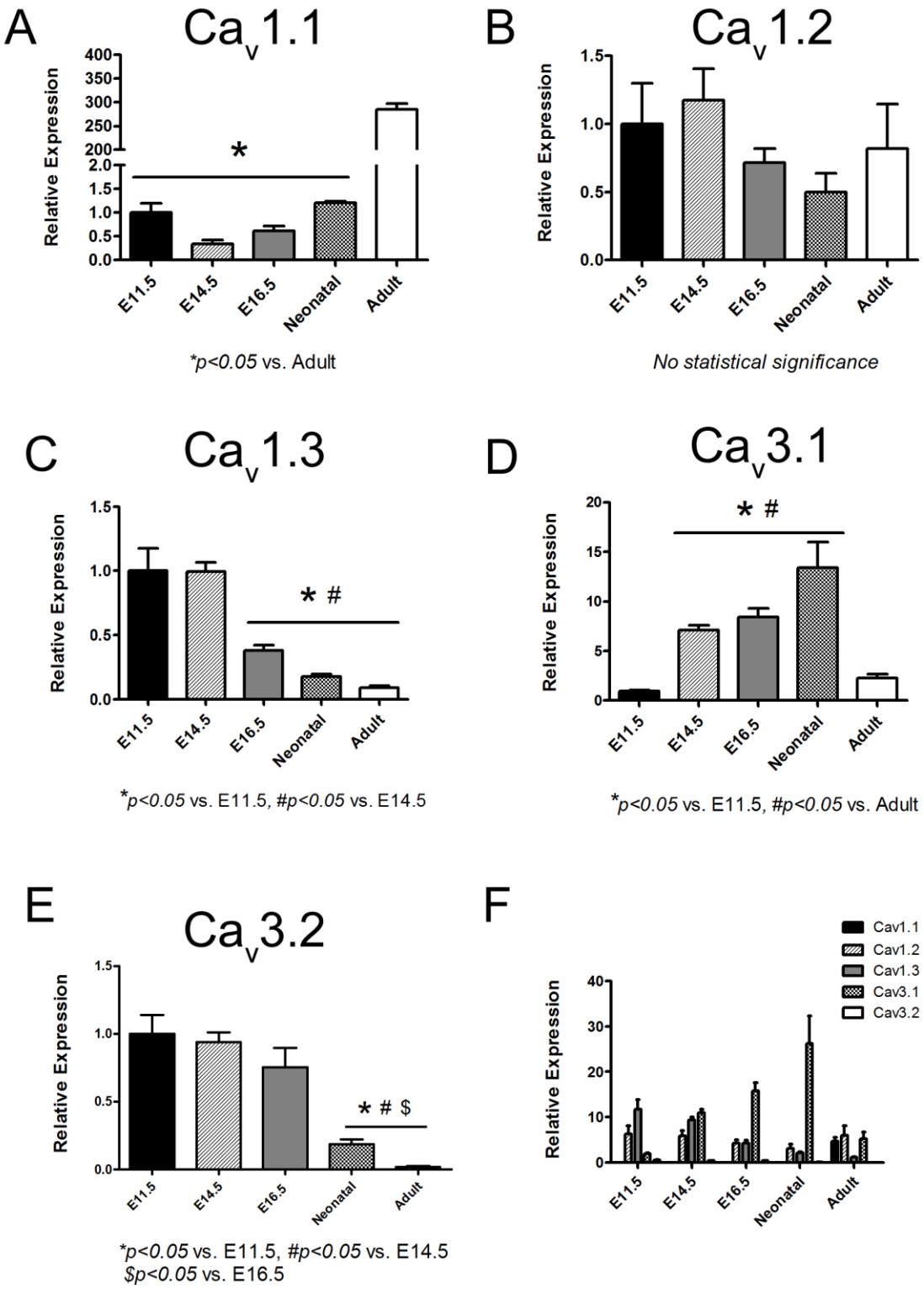
A
Ca$_v$1.1
Relative Expression
400
350
300
250
200
2.0
1.5
1.0
0.5
0.0
*
E11.5
E14.5
E16.5
Neonatal
Adult
*p<0.05 vs. Adult
B
Ca$_v$1.2
Relative Expression
1.5
1.0
0.5
0.0
E11.5
E14.5
E16.5
Neonatal
Adult
No statistical significance
C
Ca$_v$1.3
Relative Expression
1.5
1.0
0.5
0.0
* #
E11.5
E14.5
E16.5
Neonatal
Adult
*p<0.05 vs. E11.5, #p<0.05 vs. E14.5
D
Ca$_v$3.1
Relative Expression
20
15
10
5
0
* #
E11.5
E14.5
E16.5
Neonatal
Adult
*p<0.05 vs. E11.5, #p<0.05 vs. Adult
E
Ca$_v$3.2
Relative Expression
1.5
1.0
0.5
0.0
* # $
E11.5
E14.5
E16.5
Neonatal
Adult
*p<0.05 vs. E11.5, #p<0.05 vs. E14.5
$p<0.05 vs. E16.5
F
Cav1.1
Cav1.2
Cav1.3
Cav3.1
Cav3.2
Relative Expression
40
30
20
10
0
E11.5
E14.5
E16.5
Neonatal
Adult

Figure 3.3.5: The effects of Ca^{2+} channel blockade on isoproterenol induced fluctuations in intracellular Ca^{2+}. Acutely isolated E11.5 ventricular cells were incubated with various doses of nifedipine (1μM, 10μM or 100μM) or vehicle (DMSO) for 1 hour. The average change in fluorescence intensity (corresponding to intracellular Ca^{2+} levels) was then monitored in randomly selected fields at baseline and in response to isoproterenol (ISO; 1μM) stimulation using the Ca^{2+} sensitive indicator Fluo-8 AM. **A)** Representative micrograph of baseline fluorescence levels at time 0 (Fluorescence intensity =1.0). **B-E)** Representative micrographs taken 5 minutes post-ISO stimulation from cultures incubated with DMSO **(B)**, 1μM nifedipine **(C)**, 10μM nifedipine **(D)** or 100μM nifedipine **(E)**. **F)** Quantification of changes in fluorescence intensity that occurred in response to stimulation with ISO at 1, 3 and 5 minute time points. N=9 (3 independent experiments, 3 random fields/experiment). Data represent mean ± SEM **$p<0.05$* vs. DMSO and 1μM, *#$p<0.05$* vs. 1μM, 10μM and 100μM. One-way ANOVA with Tukey post hoc test. Scale bar=100μM.

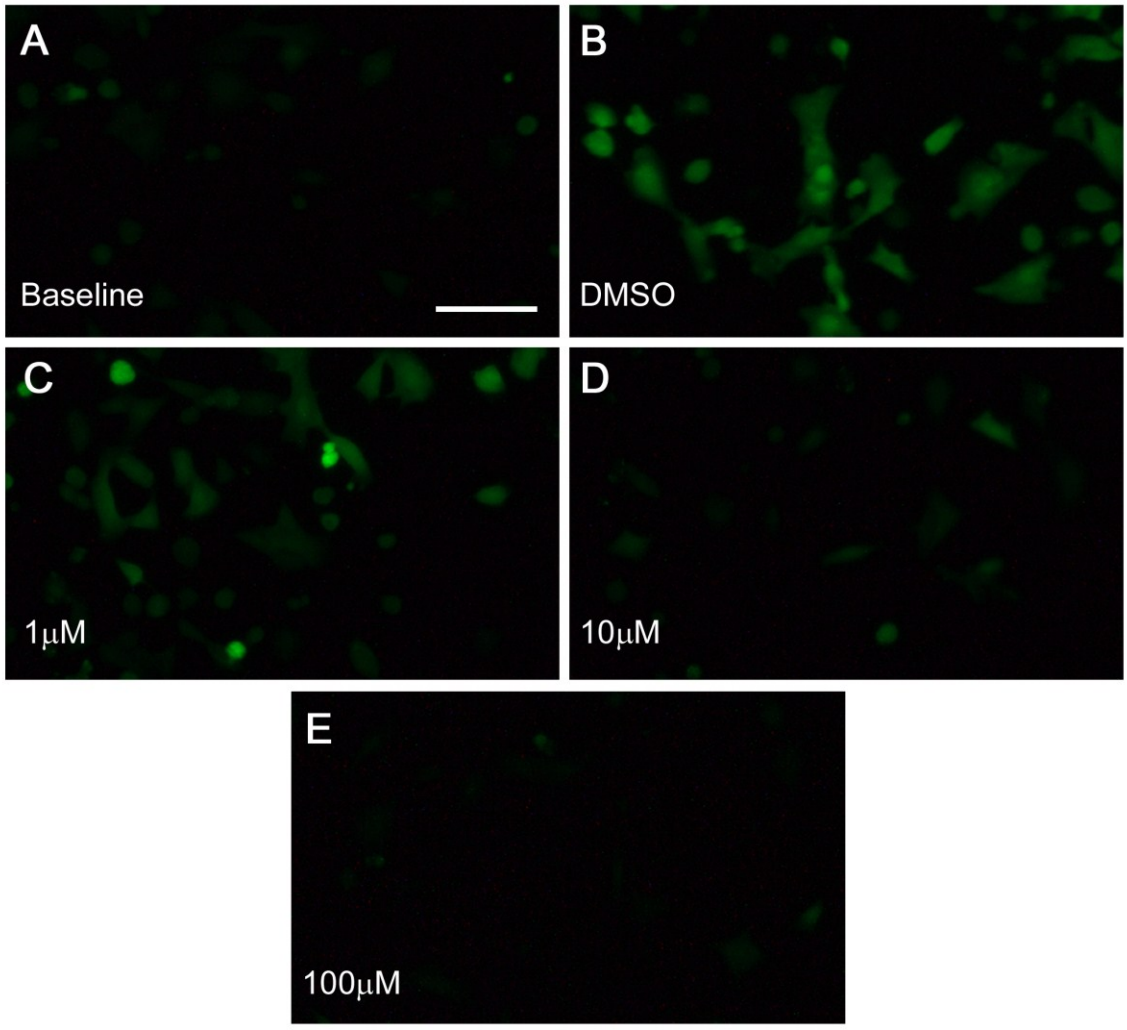
A
Baseline
B
DMSO
C
1μM
D
10μM
E
100μM
F
Relative fluorescence intensity (vs. baseline)
Time (min)
DMSO
1μm
10μm
100μm
#
*
*

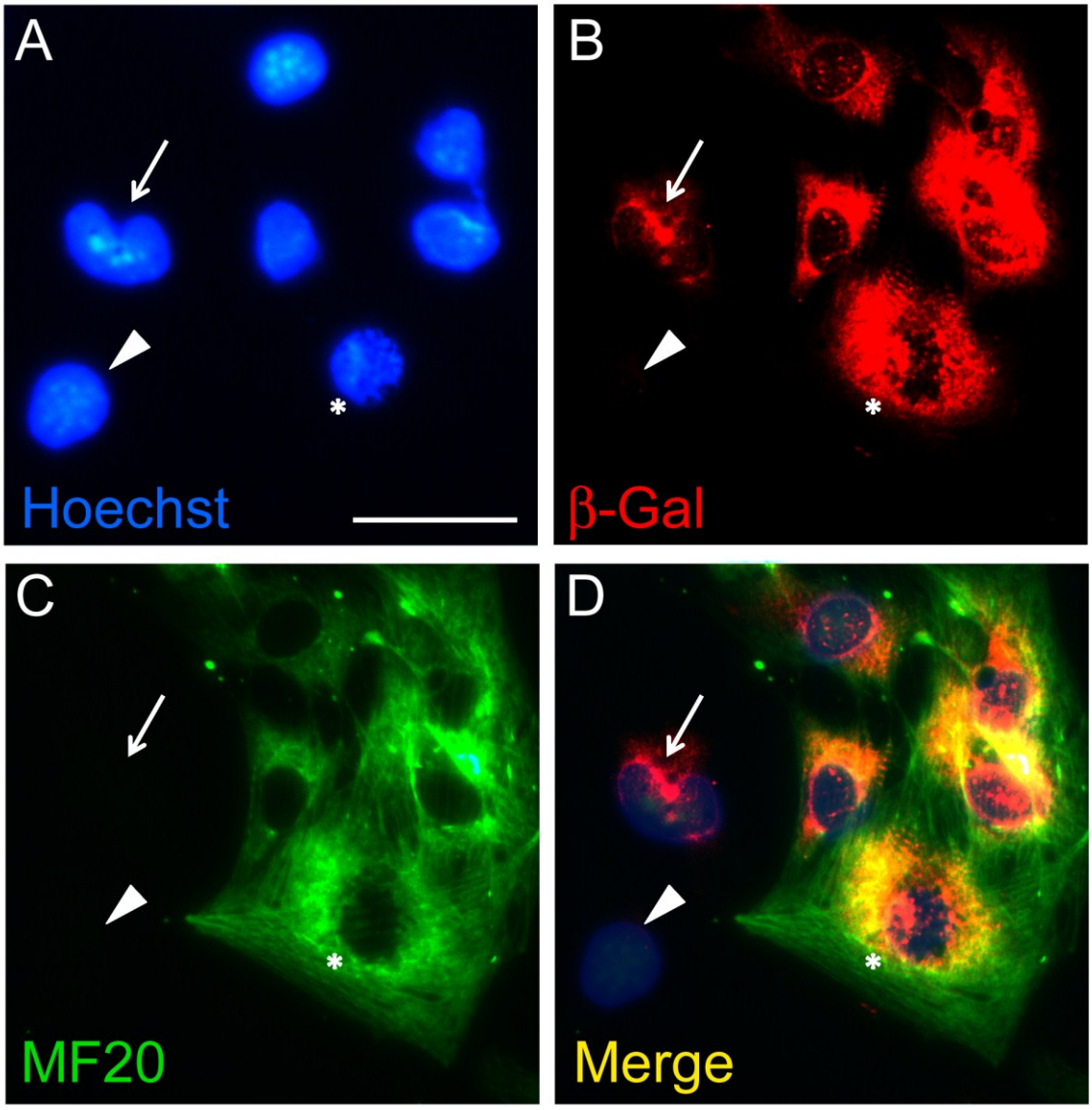

Figure 3.3.6: Identification of E11.5 cardiac progenitor cells and cardiomyocytes in culture. Double transgenic embryos (NCRL) with genetically labelled Nkx2.5^{+} lineage (express β-gal) were used to identify cardiac subpopulations in E11.5 primary ventricular cell cultures. **A-D)** The same field of cells stained with Hoechst nuclear stain **(A)**, β-galactosidase antibodies (β-Gal)**(B)**, sarcomeric myosin antibodies (MF20)**(C)** and merged images **(D).** Cells positive for β-Gal, but not MF20 (β-Gal^{+}/ MF20^{-}) were classified as cardiac progenitor cells (arrow), while cells positive for both β-Gal and MF20 (β-Gal^{+}/ MF20^{+}) were considered to be cardiomyocytes (asterisk). Cells that were negative for both β-Gal and MF20 (β-Gal^{-}/ MF20^{-}) were classified as non-cardiomyogenic cells (arrow head). Scale bar=25µm.

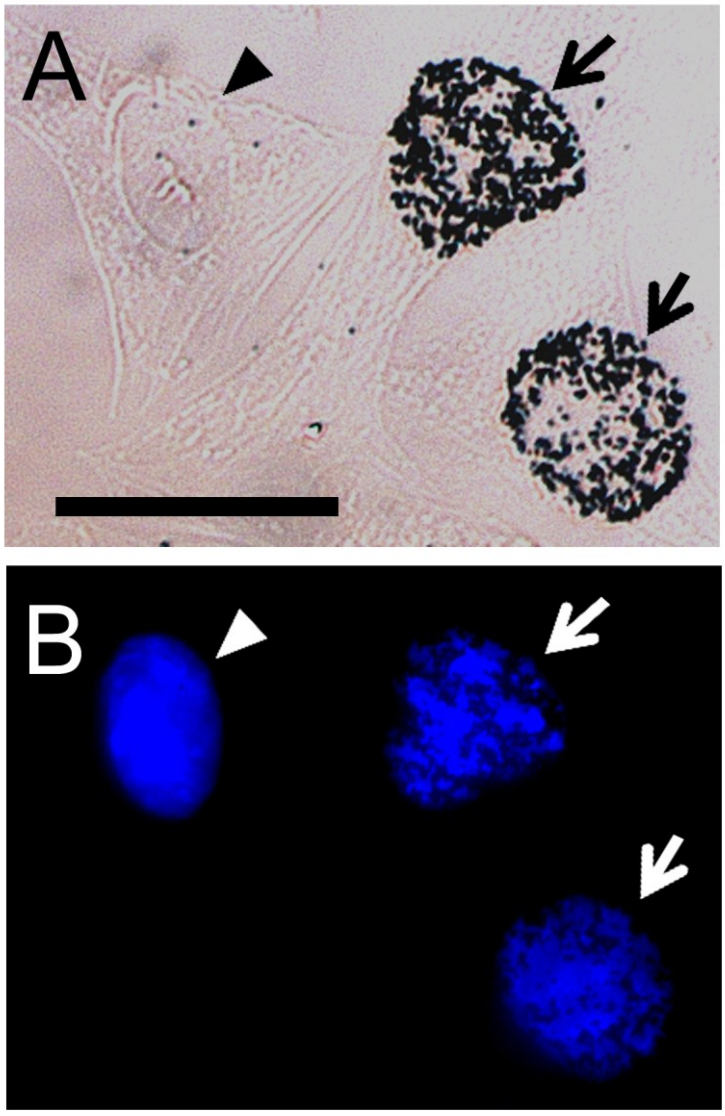

Figure 3.3.7: Visualization of cells in the S-phase of the cell cycle using a tritiated [^{3}H]- thymidine incorporation assay. Following autoradiographic processing, incorporation of [^{3}H]-thymidine into cells in the S-phase could be readily detected by the presence of distinct silver grains in the nucleus. **A)** Bright field image of three cells, two of which are synthesizing new DNA(arrows), and one that is not (arrowhead). **B)** Hoechst nuclear staining of the same three cells. Scale bar= 25µm.

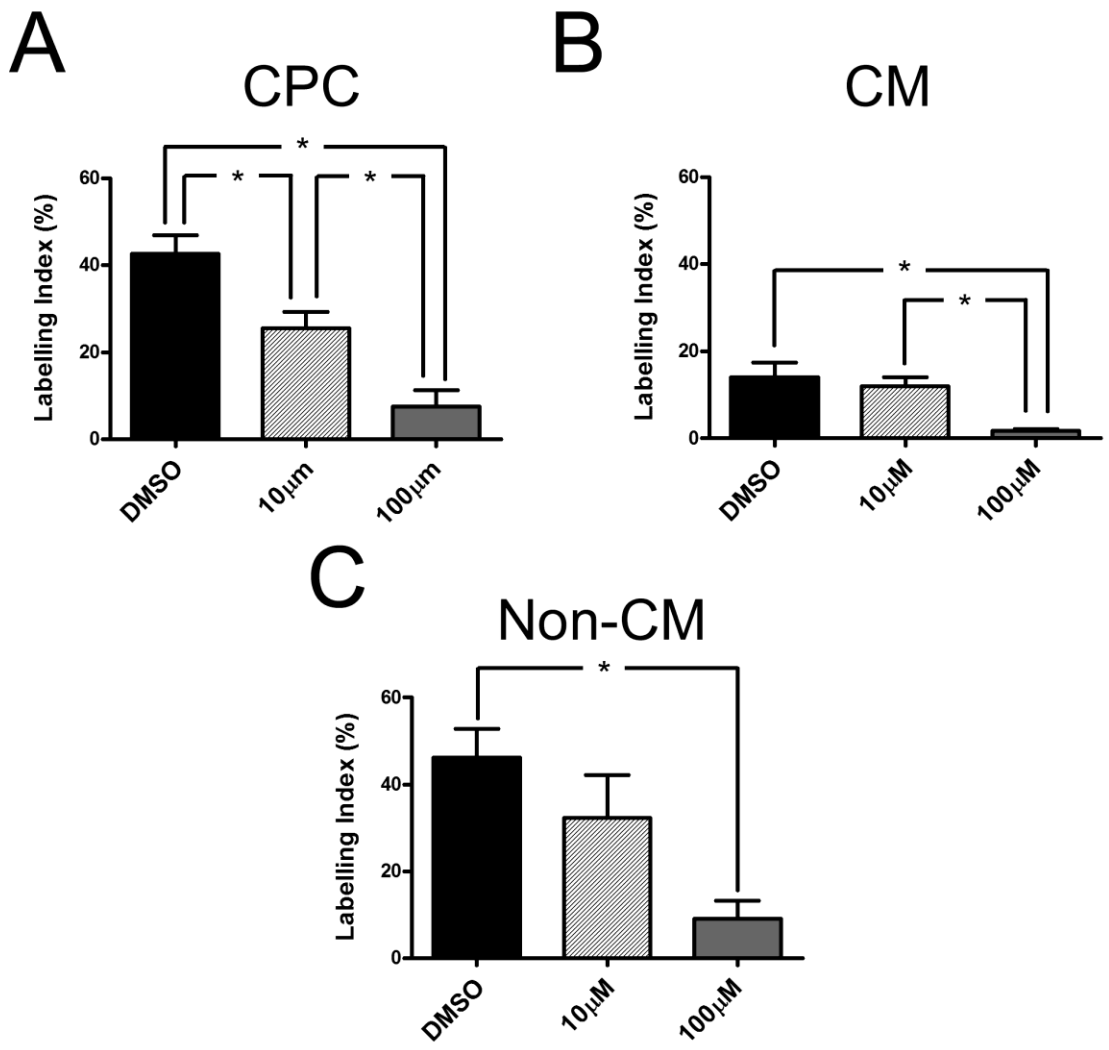

Figure 3.3.8: The effects of Ca^{2+} channel blockade on proliferation of E11.5 cardiac cell populations. Using a [^{3}H] - thymidine incorporation assay, the labelling index (LI; percentage of cells in the S-phase out of the defined cell population) was determined for subpopulations of E11.5 ventricular cells. **A)** In the cardiac progenitor cell (CPC) population (β-gal$^+$/MF20$^-$), a progressive decrease in LI was observed in response to either 10μM or 100μM nifedipine. **B)** In the cardiomyocyte (CM) population (β-gal$^+$/MF20$^+$) LI was unchanged in response to 10μM nifedipine, but was dramatically reduced in response to 100μM nifedipine. **C)** The LI of the non-cardiomyogenic (Non-CM) cell population (β-gal$^-$/MF20$^-$) was also significantly reduced in response to 100μM nifedipine. N=3-4 experiments/treatment group, ~400 cells counted/experiment. Each bar represents mean ± SEM. *$p<0.05$, One-way ANOVA with Tukey post hoc test.

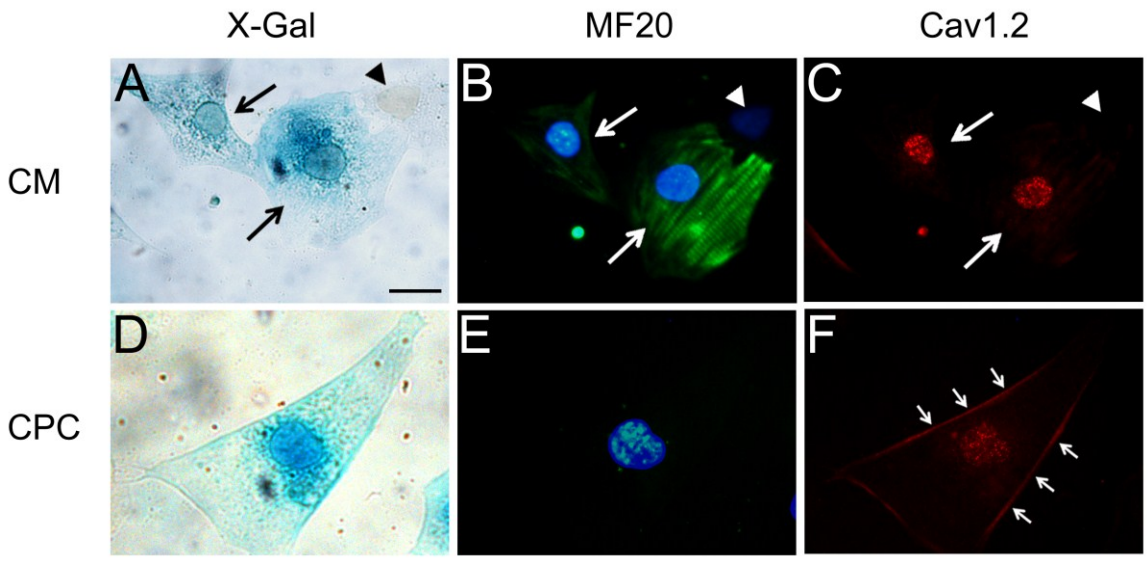

3.3.9: Immunolabelling of $Ca_v1.2$ L-type Ca^{2+} channels in E11.5 cardiac progenitor cells and cardiomyocytes. Double transgenic embryos (NCRL) with genetically labelled $Nkx2.5^+$ lineage (express β-gal) were used to identify cardiac subpopulations in E11.5 primary ventricular cell cultures by the presence of blue chromogenic signal following overnight incubation in X-gal solution **(A&D).** Immunolabelling with antibodies against sarcomeric myosin (MF20; green) was used to confirm the identities of cardiomyocytes (CM). The top panel **(A-C)** shows two cardiomyocytes ($X\text{-}gal^+/MF20^+$; indicated by arrows) with strong $Ca_v1.2$ (red) immunoreactivity in the nucleus/perinuclear area, but not around the plasma membrane. A non-cardiomyogenic cell in the same field ($X\text{-}gal^-/MF20^-$; indicated by arrowhead) did not show immunoreactivity in either the nucleus or around the plasma membrane. The bottom panel **(D-F)** shows a single cardiac progenitor cell (CPC) ($X\text{-}gal^+/MF20^-$) with strong immunoreactivity in the nucleus and around the plasma membrane (small arrows). Scale bar=10μm.

Gene	10μM	100μM
CYCLIN D1	↔	↔
CYCLIN D2	↔	↔
CYCLIN E	↔	↔
CYCLIN B1	↓	↓
CDK4	↔	↔
P27	↔	↑
P21	↔	↔

Table 3.3.1: Summary of the effects of Ca^{2+} channel blockade on expression of cell cycle regulating genes. Compared to vehicle (DMSO) treated control cultures (expression=1.0), treatment of E11.5 ventricular cell cultures with 10μM or 100μM nifedipine was associated with a significant reduction in expression of the positive cell cycle regulator Cyclin B1 (**10μM**: 0.7 ± 0.06 and **100μM**: 0.7 ± 0.02). Moreover, 100μM nifedipine (but not 10μM) was associated with a significant increase in the expression of the cell cycle inhibitor p27 (1.9 ± 0.2). N=3-5 experiments/treatment group. ↓= significant decrease, ↑= significant increase, ↔ = no change. Statistical significance assigned at $p<0.05$, One-way ANOVA with Tukey post hoc test.

Figure 3.3.10: Graphical summary of the effects of Ca^{2+} channel blockade on expression of cell cycle regulating genes. Compared to vehicle treated control cultures (expression=1.0), treatment of E11.5 ventricular cell cultures with 10μM or 100μM nifedipine was associated with a significant reduction in expression of the positive cell cycle regulator Cyclin B1 (**10μM**: 0.7 ± 0.06 and **100μM**: 0.7 ± 0.02). Moreover, 100μM nifedipine (but not 10μM) was associated with a significant increase in the expression of the cell cycle inhibitor p27 (1.9 ± 0.2). N=3-5 experiments/treatment group, analyzed in duplicate for each experiment. Each bar represents mean ± SEM. Meaning of each symbol is indicated under the appropriate graph. One-way ANOVA with Tukey post hoc test.

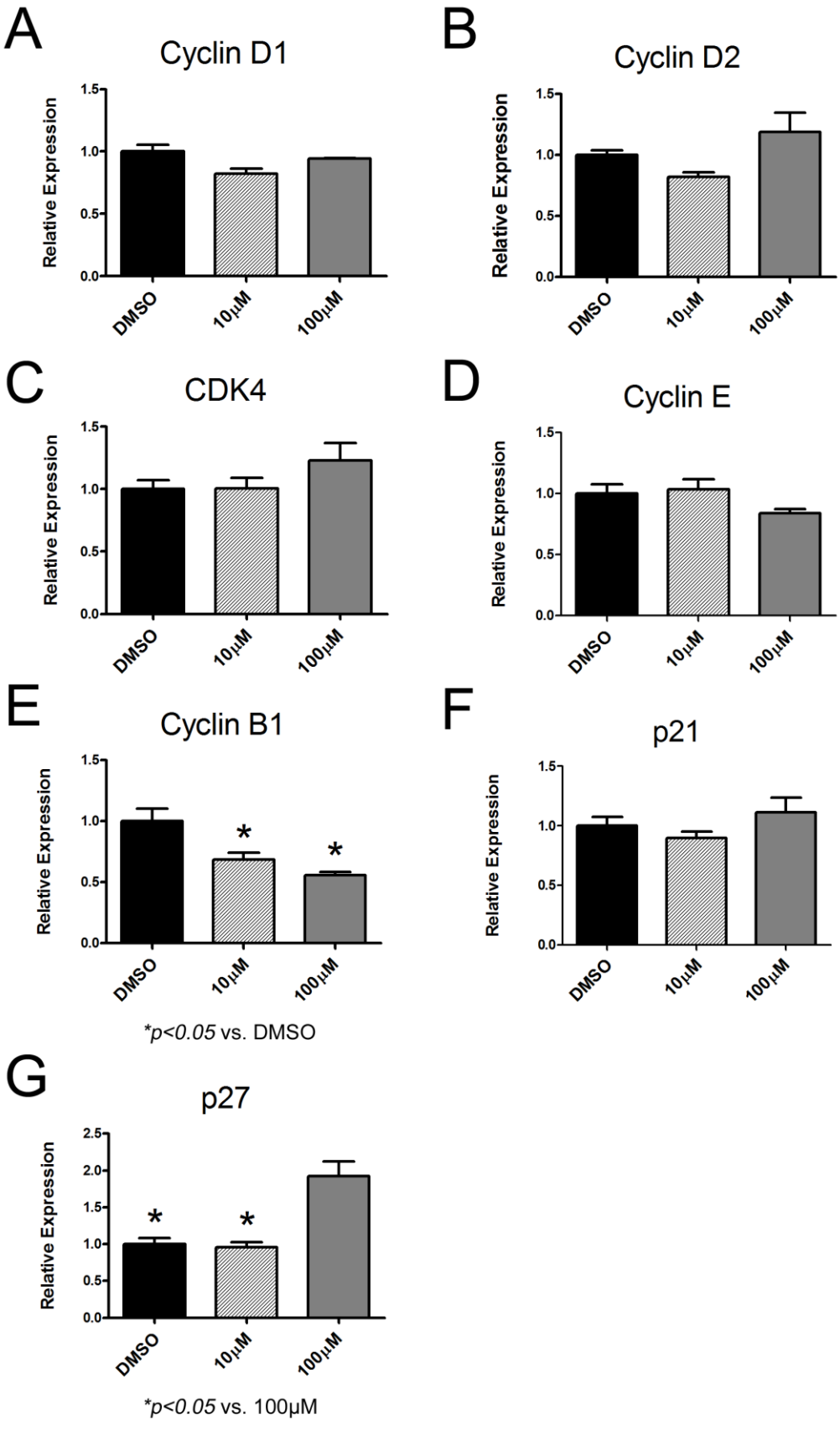
A
Cyclin D1
Relative Expression
1.5
1.0
0.5
0.0
DMSO
10μM
100μM
B
Cyclin D2
Relative Expression
1.5
1.0
0.5
0.0
DMSO
10μM
100μM
C
CDK4
Relative Expression
1.5
1.0
0.5
0.0
DMSO
10μM
100μM
D
Cyclin E
Relative Expression
1.5
1.0
0.5
0.0
DMSO
10μM
100μM
E
Cyclin B1
Relative Expression
1.5
1.0
0.5
0.0
*
*
DMSO
10μM
100μM
*p<0.05 vs. DMSO
F
p21
Relative Expression
1.5
1.0
0.5
0.0
DMSO
10μM
100μM
G
p27
Relative Expression
2.5
2.0
1.5
1.0
0.5
0.0
*
*
DMSO
10μM
100μM
*p<0.05 vs. 100μM

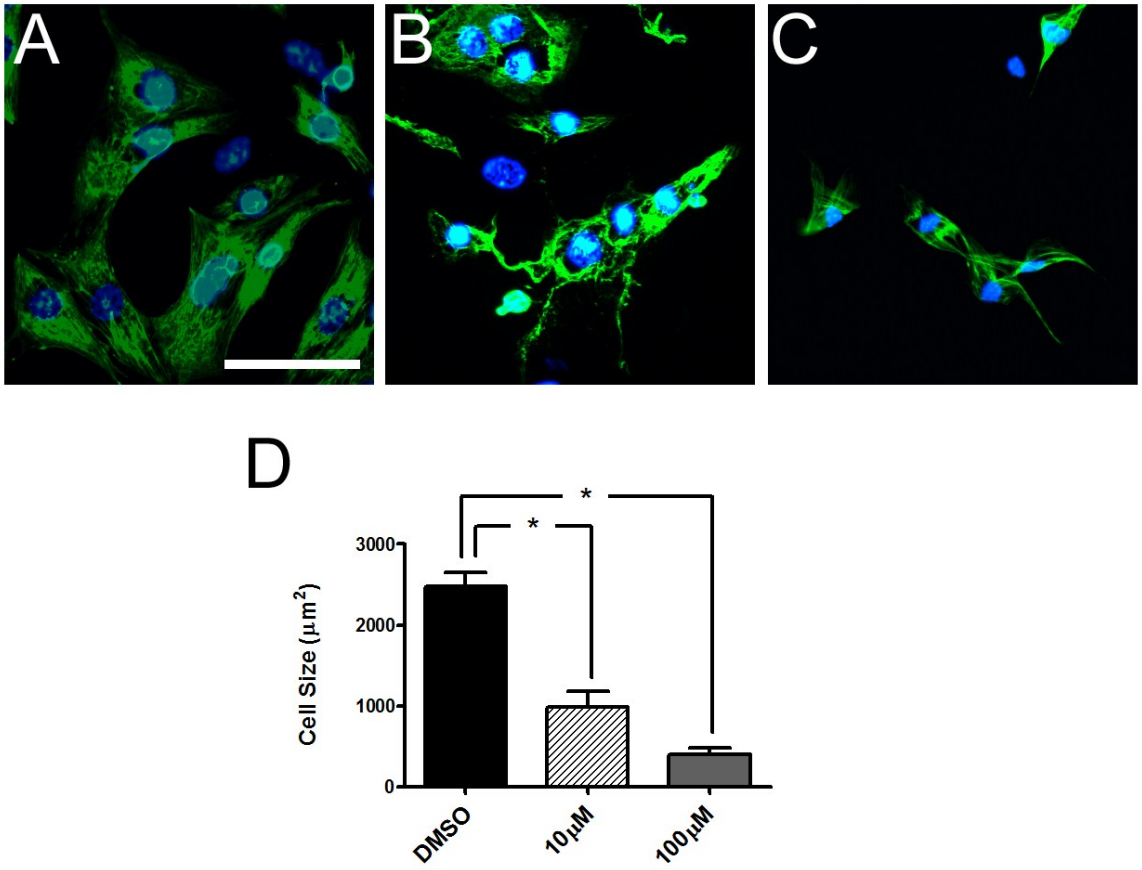

Figure 3.3.11: The effects of Ca^{2+} channel blockade on sarcomeric organization of E11.5 cardiomyocytes. **A)** In vehicle (DMSO) treated control cultures, the vast majority of $MF20^{+}$ cardiomyocytes displayed organized muscle fiber bundles and a stellate morphology, which is characteristic of embryonic cardiomyocytes. **B&C)** In cultures treated with either 10µM **(B)** or 100µM **(C)** nifedipine**,** cardiomyocytes generally appeared smaller in size and displayed poorly formed sarcomeric structures that were highly disorganized and/or misshaped compared to cardiomyocytes from control cultures. **D)** Quantification of cardiomyocyte size (surface area) confirmed that nifedipine treatment was associated with a significant reduction in cell size. N=3 independent experiments/treatment group, ~50 cells measured/experiment. Each bar represents mean ± SEM. *$p<0.05$, One-way ANOVA with Tukey post hoc test. Scale bar=25µM.

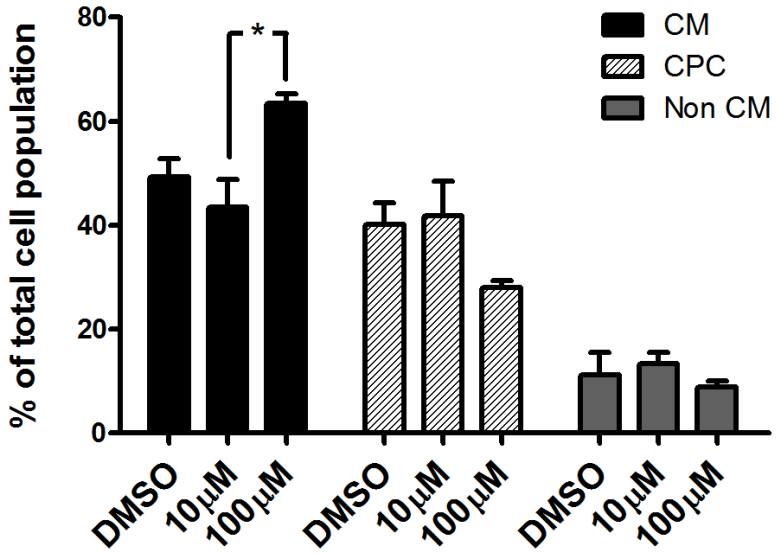

Figure 3.3.12: The effects of Ca^{2+} channel blockade on the relative distribution of E11.5 cardiac cell populations. In vehicle (DMSO) treated control cultures, the relative distribution of cardiomyocytes (CM), cardiac progenitor cells (CPC) and non-cardiomyogenic cells (Non CM) was determined to be 49.3 ± 3.5%(CM), 40.1 ± 4.2% (CPC), and 11.1 ± 4.4 % (Non CM). A significant increase in relative proportion of cardiomyocytes (63.4 ± 1.8%) and a trend toward a decrease in CPCs (28.8 ± 1.4%) was observed in response to 100μM nifedipine, while the non-cardiomyogenic cell population remained relatively constant across all treatments. N=3-4 experiments/treatment group, ~400 cells counted/experiment. Each bar represents mean ± SEM. *$p<0.05$, One-way ANOVA with Tukey post hoc test.

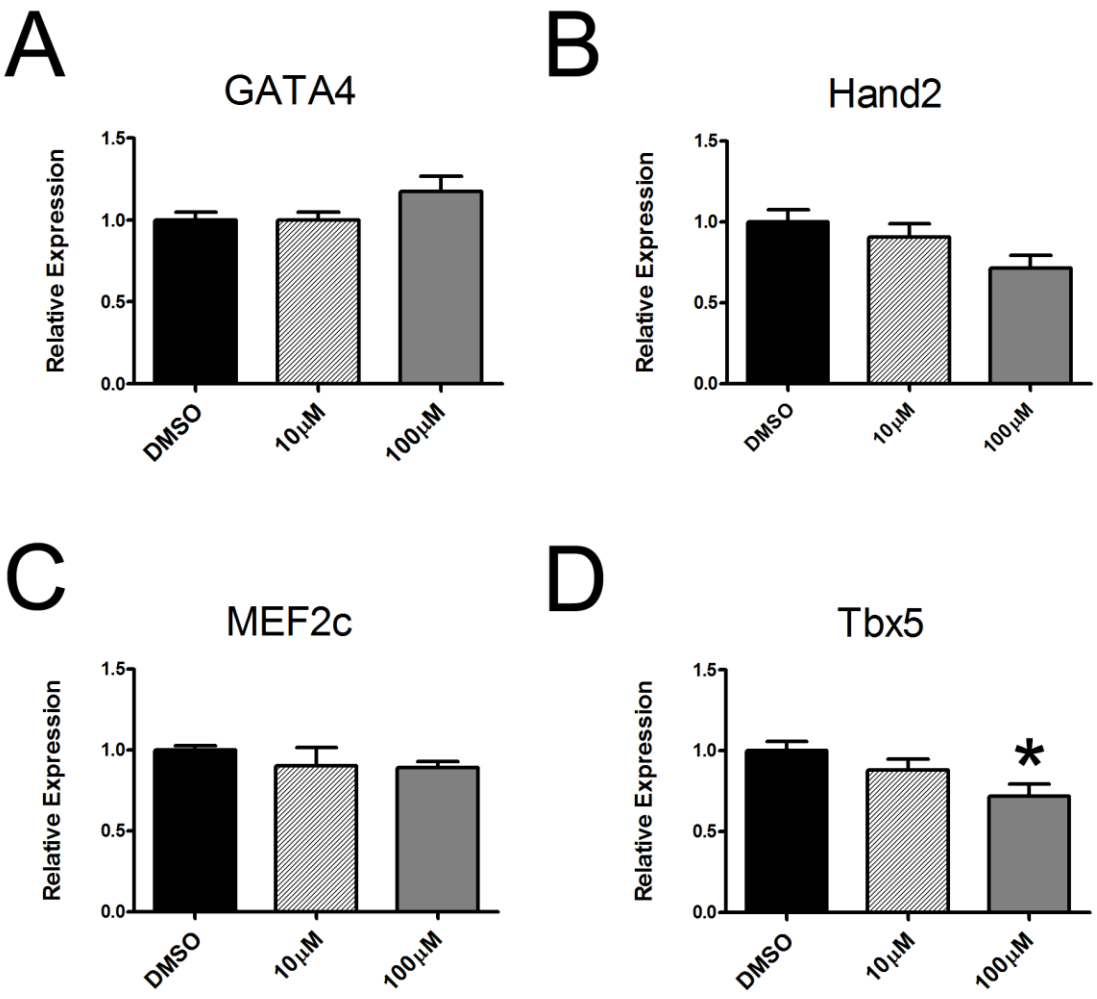

Figure 3.3.13: Graphical summary of the effects of Ca^{2+} channel blockade on expression of differentiation marker genes. Compared to vehicle (DMSO) treated control cultures (expression=1.0), treatment of E11.5 ventricular cell cultures with 100μM nifedipine was associated with a significant reduction in expression of Tbx5 (0.7 ± 0.08), while expression of all other genes tested remained unchanged in response to either 10μM or 100μM nifedipine. N=3-5 experiments/treatment group, analyzed in duplicate for each experiment. Each bar represents mean ± SEM. *$p<0.05$ vs. DMSO, One-way ANOVA with Tukey post hoc test.

Figure 3.3.14: Subcellular localization of MEF2c in response to Ca^{2+} channel blockade. E11.5 ventricular cell cultures were incubated with either DMSO or 100μM nifedipine for 16 hours, and then immunolabelled with MEF2c (red) as well as MF20 (green) antibodies to identify cardiomyocytes. **Panel A-D)** In cardiomyocytes from control cultures, MEF2c labelling was very strong in the nucleus (thick arrows), and also observed as small punctae in the cytoplasm (thin arrows). **Panel E-H)** By contrast, in cardiomyocytes from 100μM nifedipine treated cultures, immunoreactive MEF2c was very faint in the nucleus (thick arrows). In addition, some small punctae could be observed in the cytoplasmic compartment (thin arrows). Scale bars= 25μM.

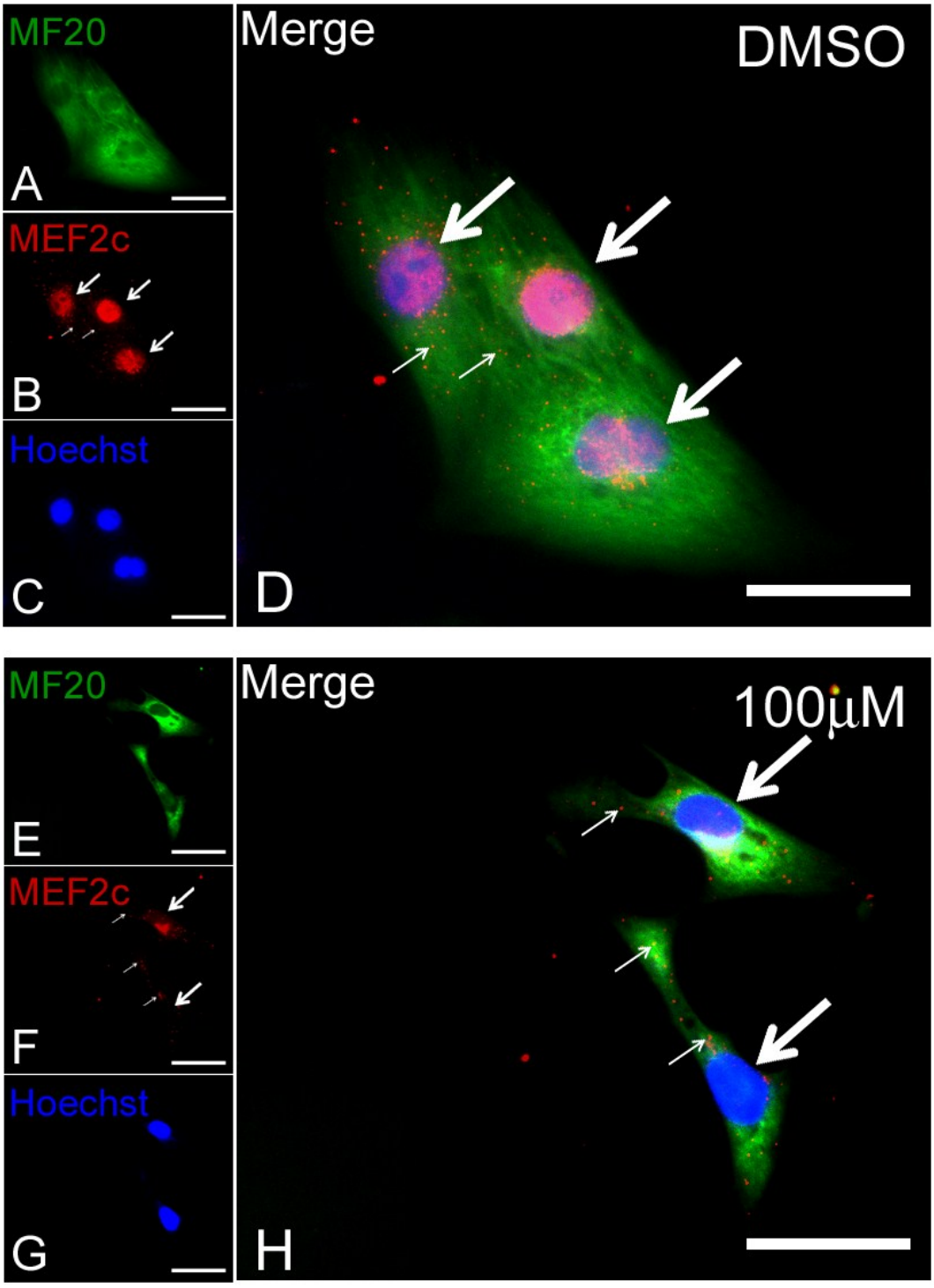
MF20
A
MEF2c
B
Hoechst
C
Merge
DMSO
D
MF20
E
MEF2c
F
Hoechst
G
Merge
100µM
H

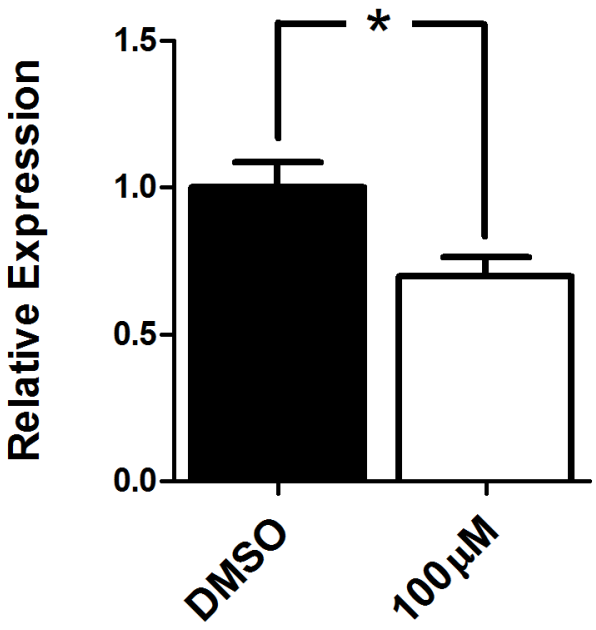

Figure 3.3.15: Effects of Ca^{2+} channel blockade on expression of atrial natriuretic peptide. Compared to DMSO treated control cultures (expression=1.0), a significant reduction in expression of ANP (0.7 ± 0.06) was observed in response to 100µM nifedipine. N=4-5 experiments/treatment group, analyzed in duplicate for each experiment. Each bar represents mean ± SEM. *$p<0.05$, two-tailed unpaired t-test.

Figure 3.3.16: The effects of nifedipine on graft size formation following injection of E11.5 ventricular cells into recipient hearts. Approximately $3x10^5$ ventricular cells, acutely isolated from E11.5 double transgenic (NCRL) embryos, were transplanted via direct intracardiac injection into the left ventricles of healthy recipient mice. Mice were divided into two groups which received either daily doses of nifedipine (5mg/kg) or an equal volume of vehicle (10% captisol) for 3 days. Subsequently, hearts were excised, sectioned and incubated in X-gal solution in order to visualize transplanted NCRL cells within the host tissue (blue; arrows). **A&B)** In vehicle treated animals, distinct regions of transplanted E11.5 cells were visible and tended to be spread out over relatively large surface areas (**A**=H&E and **B**=Brightfield). **C&D)** By contrast, in mice receiving daily injection of nifedipine, engrafted regions tended to be smaller (**C**=H&E and **D**=Brightfield). **E)** Quantification of the graft volumes confirmed that nifedipine was associated with a significant reduction in graft size. N=3 independent experiments/treatment group. Each bar represents mean ± SEM. **p<0.05*, two-tailed unpaired t-test.

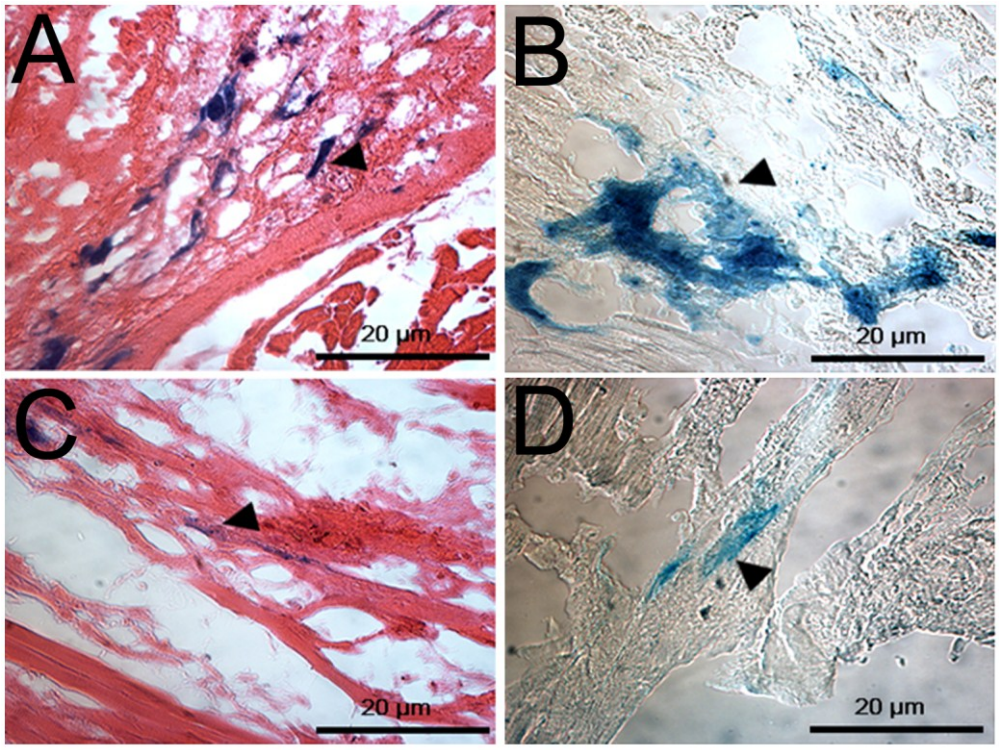
A
20 µm
B
20 µm
C
20 µm
D
20 µm

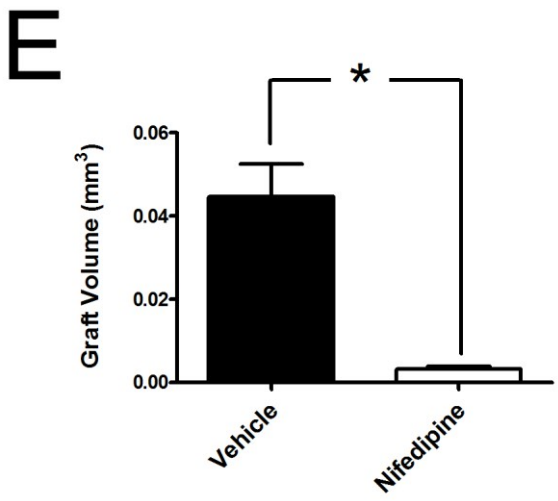
E
*
0.06
0.04
0.02
0.00
Graft Volume (mm3)
Vehicle
Nifedipine

CHAPTER 4: CHARACTERIZATION OF THE EFFECTS OF NATRIURETIC PEPTIDE SIGNALLING SYSTEMS ON PROLIFERATION OF CARDIAC PROGENITOR CELLS

4.1 Background and Hypothesis

It is well established that atrial natriuretic peptide (ANP) is synthesized and stored primarily in atrial cardiomyocytes of the post-natal heart, and gets released into the circulation as part of the heart's endocrine function to regulate body fluid homeostasis (Potter et al., 2006). In the ventricles of the adult heart, ANP expression is normally very low, but increases under pathological conditions and functions locally in an autocrine/paracrine fashion to antagonize hypertrophic cardiomyocyte growth (Chien et al., 1991; Kilic et al., 2007).

In the mammalian embryonic heart, ANP mRNA expression is first detectable in the primitive heart tube in cardiomyocytes destined to form both the atrial and ventricular chambers (Zeller et al., 1987). As development proceeds, however, ANP mRNA expression levels gradually decline in the ventricles but remain high in the atria. Based on the dynamic spatio-temporal expression of ANP in the ventricles during cardiogenesis, it has been speculated that ANP may be an important autocrine/paracrine regulator of cardiac cell growth in this compartment (Zeller et al., 1987; Cameron and Ellmers, 2003). Currently, however, specific gaps in our knowledge exist regarding whether ANP mRNA produced in the embryonic murine ventricles is also translated into biologically active protein that gets actively secreted into the extracellular environment. Furthermore, it remains uncertain whether ANP receptor mediated signalling systems are biologically intact in the embryonic ventricles.

Previous studies showed that ANP could either increase or decrease proliferation of embryonic/fetal cardiomyocytes from the avian or ovine heart respectively (Koide et al., 1996; O'Tierney et al., 2010). The effects of ANP on proliferation of either CPCs or cardiomyocytes from earlier developmental stages have not yet been explored. **Thus, we hypothesized that ANP is secreted by embryonic ventricular cells and acts as an autocrine/paracrine factor to regulate proliferation of CPCs and/or cardiomyocytes from the E11.5 heart.**

4.2 Specific Aims

1. Confirm the expression of ANP mRNA and protein in the murine ventricles at E11.5.

2. Determine whether ANP is actively secreted by primary cultured E11.5 ventricular cells.

3. Characterize the expression pattern and biological activity of ANP high affinity receptors (NPRA and NPRC) in ventricular cells at E11.5.

4.3 Results

4.3.1 ANP mRNA and Immunoreactive Protein are Expressed in the Ventricles at E11.5

The temporal pattern of ANP gene expression in mouse cardiac ventricles was determined by quantifying the relative abundance of mRNA transcripts at E11.5 and several other advanced developmental and post-natal stages by real time quantitative polymerase chain reaction (qPCR) (Figure 4.3.1A&B). Because expression levels of

GAPDH remained unchanged across all developmental and post-natal stages (Chapter 3, Figure 3.3.2), this gene was used to normalize data by correcting for variations in quantities of cDNA used as template. The highest level of ANP mRNA expression was observed at E11.5 and gradually declined at later developmental and post-natal stages (Figure 4.3.1A&B). Using E11.5 as a point of reference (i.e. expression=1.0), there was an approximately 2 fold decrease in ANP mRNA at E14.5 (0.51± 0.03 vs. E11.5). Gene expression did not vary significantly between E14.5, E16.5 and Neonatal (day 1) stages, but decreased significantly at Adult stages (~ 10 fold decrease from E11.5 to Adult stage).

To confirm that ANP mRNA was translated into immunoreactive protein, an enzyme linked immunosorbant assay (ELISA) was used to quantify ANP protein from ventricular tissue lysates at both E11.5 and neonatal stages. Consistent with mRNA expression data, the concentration of ANP protein in the ventricles at E11.5 was approximately 2 fold higher compared to the neonatal stage (**E11.5:** 4.3 ± 0.7ng ANP/µg of lysate vs. **Neonatal:** 2.3ng ± 0.5ng ANP/µg of lysate) (Figure 4.3.2).

4.3.2 Spatial Expression Pattern of Immunoreactive ANP in the Embryonic Heart at E11.5 and E14.5

To gain information on the spatial expression pattern of ANP in the murine embryonic heart, immunohistochemistry using ANP specific antibodies was performed on thin tissue sections from embryos at the midgestational stages of E11.5 and E14.5. At E11.5, the murine ventricles are composed of loosely packed trabeculated myocardium projecting into the lumen and a surrounding compact layer (Figure 4.3.3A&B). At the

E11.5 stage, we observed regions of strong immunoreactive ANP labelling in specific regions of the atria and also the trabeculae of the left ventricle (Figure 4.3.3B). ANP expression was also detectable, albeit at lower levels, in the trabecular myocardium of the right ventricle in some sections but was essentially absent from the developing compact myocardium of both ventricles (Figure 4.3.3B).

Between the stages of E11.5 and E14.5, the relative area occupied by the trabecular myocardium decreases, as the compact layer increases in thickness due to rapid cell proliferation in this compartment (Kirby, 2007). At E14.5, ANP expression remained restricted primarily to the trabecular myocardium of the left ventricle, and was essentially absent from the thickening compact zone of the myocardial free wall (Figure 4.3.4B). Collectively, analyses of temporal and spatial expression patterns of ANP in the developing mouse ventricles revealed that **1)** ANP mRNA and protein were expressed at higher levels in the ventricles at the E11.5 stage compared to later developmental and post-natal stages, and **2)** high levels of immunoreactive ANP expression were spatially restricted to the myocardial trabeculae at midgestational stages, which is consistent with expression patterns reported in the embryonic and fetal rat heart (Toshimori et al., 1987a).

4.3.3 Determination of ANP Secretion from Cultured E11.5 Ventricular Cells

To achieve an autocrine/paracrine effect, embryonic ventricular cells would be required to actively secrete ANP into their surrounding environment. To gain insight into this issue, ANP protein levels were measured by Western blot analyses in culture media samples collected from primary cultured E11.5 ventricular cells. Following a 24 hour

incubation period, conditioned media samples were separated by electrophoresis, transferred to a nitrocellulose membrane and probed using ANP specific antibodies. Results from these analyses revealed prominent immunoreactive bands at 34kD and 17kD as well as a band of weaker intensity at 3kD in conditioned media collected from ventricular cell cultures but not in control media samples that were not exposed to cells (Figure 4.3.5A). The 17kD band corresponds to the expected molecular weight of proANP, while the 3kD band corresponds to the proteolytically processed and biologically active form of ANP. The band seen at 34kD is presumably a dimer of 17kD proANP. To confirm whether the weak intensity of the 3kD ANP band was due to poor retention of smaller peptides on nitrocellulose after a long transfer period (1 hour used in initial experiments), we next performed transfer for a shorter, 17 minute period. Under these conditions, the 3kD band appeared to be more prominent in conditioned media samples collected from E11.5 cultures (Figure 4.3.5B). Thus, results from Western blot analyses provided evidence that ANP was actively secreted from E11.5 ventricular cells and also provided confirmation that proANP was cleaved into its biologically active form.

4.3.4 Natriuretic Peptide Receptor (NPR) Expression Patterns in the Embryonic Heart

An additional prerequisite condition for ANP to achieve an autocrine/paracrine effect would be expression of ANP high affinity receptors by either ANP secreting cells or those in close proximity. Quantitative analyses of mRNA transcripts for ANP high affinity receptors (NPRA and NPRC) revealed that both receptor subtypes were present at E11.5 and at later developmental stages and displayed differential expression patterns

(Figure 4.3.6A&B). Specifically, NPRA gene expression was lowest at E11.5 and increased significantly during the gestational period achieving a peak in expression levels at the Neonatal stage (**Neonatal** ~3 fold higher vs. **E11.5**). In contrast, NPRC gene expression was highest at E11.5 and decreased significantly by E16.5 and remained low at subsequent post-natal stages (**E11.5** expression was ~2 fold higher vs. **E16.5**). Side by side comparison of NPRA and NPRC expression at each developmental stage more clearly illustrates the receptor subtype switch that occurred from early to late developmental stages (Figure 4.3.7).

Western blot analyses were used to confirm the presence of NPRA and NPRC at the protein level at all developmental/post-natal stages using NPRA and NPRC specific antibodies (Figure 4.3.8A&B). Distinct bands were detected at 120kD and 66kD, corresponding to expected molecular weights of NPRA and NPRC respectively. The developmental changes in immunoreactive NPRA (Figure 4.3.8A) appeared to be consistent with gene expression data obtained by qPCR analysis (Figure 4.3.6A). Specifically, both of these analyses revealed an apparent increase in NPRA levels from E11.5 to E14.5 as well as a peak in expression at the neonatal stage. Also consistent with qPCR analyses of NPRC (Figure 4.3.6B), levels of immunoreactive protein appeared to higher at the gestational stages tested (E11.5, E14.5 and E16.5) compared to post-natal stages (Figure 4.3.8B). To gain insight into the spatial distribution patterns of NPR subtypes in the embryonic heart, immunohistochemical analyses (3, 3' Diaminobenzidine staining method) were performed on thin tissue sections obtained from E11.5 hearts using NPRA and NPRC specific antibodies (Figure 4.3.9A&B). Immunoreactive NPRA and NPRC were both broadly expressed in the ANP rich trabecular myocardium as well as

the ANP negative compact myocardium, with minimal expression observed in adjacent endocardial cushion tissue (Figure 4.3.9A&B).

4.3.5 Determination of the Effects of ANP on cGMP Production in E11.5 Ventricular Cells

Ligand binding of ANP to receptor guanylyl cyclases (NPRA and NPRB) has been shown to stimulate production of the second messenger molecule cGMP in various cell types including cardiomyocytes from near term fetal sheep (O'Tierney et al., 2010). To determine whether these signal transduction pathways were biologically intact at earlier developmental stages we determined the effects of ANP on cGMP production in acutely isolated E11.5 ventricular cells using a competitive immunoassay approach. The principle of this assay was based on the competition between endogenous cGMP and a cGMP analogue labelled with an energy donor molecule (d2-cGMP) for binding sites on anti-cGMP monoclonal antibodies labelled with Cryptate (mAb-Cryptate) (Figure 4.3.10). The specific signal that occurred due to the energy transfer between the d2-cGMP and mAb-Cryptate yielded a Delta F value that was inversely proportional to the concentration of endogenous cGMP. The obtained Delta F values could then be extrapolated from the cGMP standard curve (Figure 4.3.11) to deduce cGMP concentrations in each experimental sample.

To determine the optimal cell density for competition assays, a range of E11.5 ventricular cell densities were tested in the presence or absence of 1µg/ml ANP (Figure 4.3.12). Optimal cell density was selected based on the following criteria: **1)** basal level of cGMP production was within the linear range of the standard curve and **2**) a maximal

increase in signal amplitude between inactivated state (basal cGMP production), and activated condition (ANP stimulated cGMP production) was achieved. Using these selection criteria an optimal cell density of 64,000 cells per well was determined and used for all subsequent experiments (Figure 4.3.12).

To determine the effects of exogenous ANP treatment on cGMP production, E11.5 cells were stimulated with various concentrations of ANP (1, 10, 100, 1000 ng/ml). The level of cGMP measured under basal conditions was 19.1 ± 2.6 nM/ 64,000 cells (Figure 4.3.13). Due to considerable variability in basal levels of cGMP between independent experiments, basal levels from each experiment were set to a value of 1.0 and data represent fold change in cGMP concentration in response to different doses of ANP (Figure 4.3.13). At the two lowest concentrations of ANP tested (1ng/ml and 10ng/ml), there was no significant increase in cGMP observed compared to control (Figure 4.3.13). By contrast, 100ng/ml ANP was able to induce a significant, 1.4 fold increase in cGMP production (1.4 ± 0.09 vs. basal). A ten-fold higher dose of ANP (1000ng/ml) did not result in a further significant increase in cGMP production compared to 100ng/ml (**100ng/ml:** 1.4 ± 0.09 vs. **1000ng/ml:** 1.7 ± 0.2) (Figure 4.3.13).

4.3.6 Determination of the Effects of ANP on cAMP Production in E11.5 Ventricular Cells

While NPRC was initially believed to serve only as a clearance receptor (Maack et al., 1987), there is substantial evidence that this receptor couples to inhibitory (G_i) proteins to inhibit adenylyl cyclase and reduce cAMP production (Anand-Srivastava et al., 1986). Using a competitive immunoassay approach analogous to that described

above for cGMP, we examined the effects of exogenous ANP on cAMP production in E11.5 cells under basal conditions or in the presence of the non-selective β-adrenergic agonist, isoproterenol (ISO; 100nM).

Concentrations of cAMP for all experimental samples were extrapolated from a standard curve (Figure 4.3.14) generated using the same experimental procedure described for cGMP experiments. To determine the optimal cell density for cAMP experiments, a range of E11.5 ventricular cell densities were tested in the presence or absence of the direct activator of adenylyl cyclase, Forskolin (1μM) (Figure 4.3.15). A cell density of 4,000 cells/well was selected based the same two evaluation criteria described above for cGMP competition assays. Under basal conditions, the level of cAMP in E11.5 cells was 7.3 ± 1.6nM. Data in Figure 4.3.16 are expressed as fold change in cAMP concentrations compared to basal to normalize the baseline values obtained for individual experiments. Compared to baseline, ANP (1-100ng/ml) had no effect on levels of cAMP production (Figure 4.3.16). By contrast, stimulation with ISO (100nM) alone was able to induce a ~ 4 fold increase in cAMP levels compared to basal controls (**Basal:** 7.3 ± 1.6nM vs. **ISO:** 26.5± 9.1nM). When cells were co-treated with ISO (100nM) and ANP (100ng/ml), a modest reduction in cAMP production compared to ISO alone was observed but this result was variable between experiments and did not reach statistical significance (Figure 4.3.16).

Overall, based on collective data from cGMP and cAMP second messenger assays, we concluded that ANP mediated signal transduction pathways involving production of cGMP were biologically active in E11.5 ventricular cells. Conversely, our data could not provide substantial evidence that ANP signal transduction pathways

coupled to adenylyl cyclase activity were biologically intact under our experimental conditions. Furthermore, we concluded that ANP mediated guanylyl cyclase activity was via NPRA rather than NPRB based on previous *in vitro* data that showed ANP was able to elicit half-maximal production of cGMP via NPRA at a concentration of 3nM while 25μM ANP was required to achieve the same effect via NPRB (Schulz et al., 1989) (for our cGMP assays 100ng/ml was used and corresponds to ~30nM).

4.3.7 ANP High Expression Zones are Associated with a Low Mitotic Index in the E11.5 Ventricles

Thus far, work from Chapter 4 has provided evidence that the following prerequisites for ANP autocrine/paracrine signalling were met in the ventricles at the E11.5 developmental stage: **1)** ANP mRNA was translated into immunoreactive ANP protein, **2)** ANP was actively secreted into the extracellular compartment and **3)** ANP high affinity receptor subtypes (NPRA and NPRC) were expressed and coupled to signal transduction pathways involving guanylyl cyclase activity and production of cGMP. Based on these results, we proceeded to investigate the effects of ANP on proliferation of E11.5 cardiac progenitor cell (CPC) and cardiomyocyte populations.

As a first approximation toward determining whether regions of high ANP expression observed in the heart at E11.5 (See Figure 4.3.3) were associated with indices of proliferation that differed from regions of low ANP expression, thin tissue sections of the E11.5 heart were co-immunolabelled with antibodies against ANP and phosphohistone H3 (PH3). Phosphorylation of histone H3 occurs in the nucleus of cells in the mitosis phase of the cell cycle and is considered a reliable indicator of cell

proliferation (Hans and Dimitrov, 2001). In the ANP rich trabecular region of the left ventricle, there was an observably lower number of $PH3^+$ nuclei compared to the adjacent compact layer (Figure 4.3.17A). Similarly, in the right ventricle, $PH3^+$ nuclei appeared to be less abundant in the trabecular myocardium despite having lower levels of immunoreactive ANP (Figure 4.3.17B).

To determine the mitotic indices in the left and right ventricles, the percentage of $PH3^+$ nuclei out of the total number of nuclei was determined in regions of both high (designated ANP^+) and low ANP (designated ANP^-) expression that were defined based on immunolabelling with ANP specific antibodies. Results from these analyses confirmed that, in the left ventricle, the ANP^+ region had a significantly lower mitotic index compared to ANP^- regions (**ANP^+ :** 0.6 ± 0.07% vs. **ANP^-:** 1.5 ± 0.1%) (Figure 4.3.17C). Because it was difficult to reliably distinguish between ANP^+ and ANP^- regions in the right ventricle, the mitotic index was determined in the trabecular versus the compact myocardium. From these analyses, it was determined that the mitotic index was significantly lower in the trabecular myocardium compared to the surrounding compact layer (Figure 4.3.17D) (**Trabecular:** 0.8 ± 0.1% vs. **Compact:** 1.5 ± 0.06%).

4.3.8 Effects of Exogenous ANP on Proliferation of E11.5 Cardiac Progenitor Cells and Cardiomyocytes

Based on our data that showed ANP was able to stimulate guanylyl cyclase activity (Figure 4.3.13), we proceeded to investigate the effects of ANP on proliferation of E11.5 CPCs and cardiomyocytes in the presence or absence of the receptor guanylyl cyclase antagonist A71915. As an index of proliferation, primary cultured cells were

subjected to a [^{3}H] - thymidine incorporation assay following 24 hours of incubation with either ANP alone (1-100ng/ml) or co-treatment with ANP (100ng/ml) and A71915 (1μM, added 30 minutes prior to ANP). For these experiments, cultures were generated from ventricles of double transgenic (NCRL) embryos to enable distinction between CPCs and cardiomyocytes based on a combination of genetic labelling for Nkx2.5 and immunolabelling for the differentiation marker sarcomeric myosin as described earlier (See Chapter 3, Figure 3.3.6).

In vehicle (H_2O) treated control cultures, the CPC population had an average labelling index (LI; percentage of labelled nuclei/ total number of nuclei) of 53.8 ± 5.6%, which was significantly higher compared to the LI observed in the cardiomyocyte population (15.2 ± 3.2%) (Figure 4.3.18A&B). In parallel experiments, ANP (1-100ng/ml) was shown to cause a dose dependent decrease in proliferation of CPCs that reached statistical significance at the concentration of 100ng/ml (30.5 ± 0.5%) (Figure 4.3.18A) but had no effect on the cardiomyocyte population (Figure 4.3.18B). To investigate whether the decrease in proliferation observed in the CPC population could be mediated by the ANP/NPRA signalling axis, separate E11.5 cultures were pre-incubated with A71915 (1μM) for 30 minutes prior to addition of 100ng/ml ANP for an additional 24 hours. Results indicated that the reduction in proliferation associated with 100ng/ml ANP was abolished in response to pre-incubation with A71915 (49.9 ± 3.1%) in the CPC population (Figure 4.3.18A).

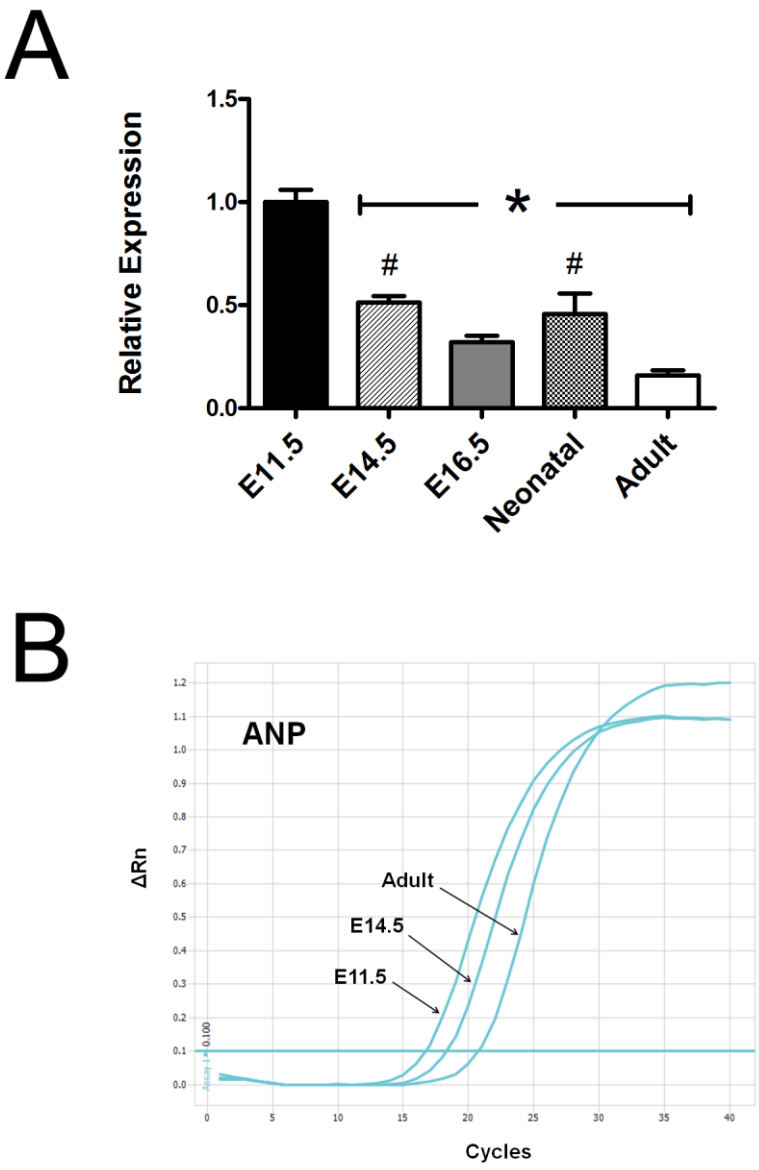

Figure 4.3.1: Developmental profile of ANP mRNA expression. A) The relative expression levels of ANP mRNA (normalized to GAPDH) were measured in cardiac ventricles at E11.5-Adult stages by real time quantitative PCR. The E11.5 stage served as the reference (i.e. expression=1.0) to which all other developmental stages were compared. Expression of ANP was highest at the E11.5 stage and showed a general trend toward lower expression levels at later developmental stages. **B)** Amplification plot from a representative qPCR experiment. The C_T value used to calculate the relative expression of each sample corresponded to the cycle number at which its amplification plot crossed the threshold of fluorescence (ΔRn=0.1), which is indicated by the horizontal blue line. N=5-6 independent RNA extractions/developmental stage analyzed in duplicate for each extraction. Each bar represents mean ± SEM. *$p < 0.05$ vs. E11.5; #$p < 0.05$ vs. Adult. One- way ANOVA with Tukey post hoc test.

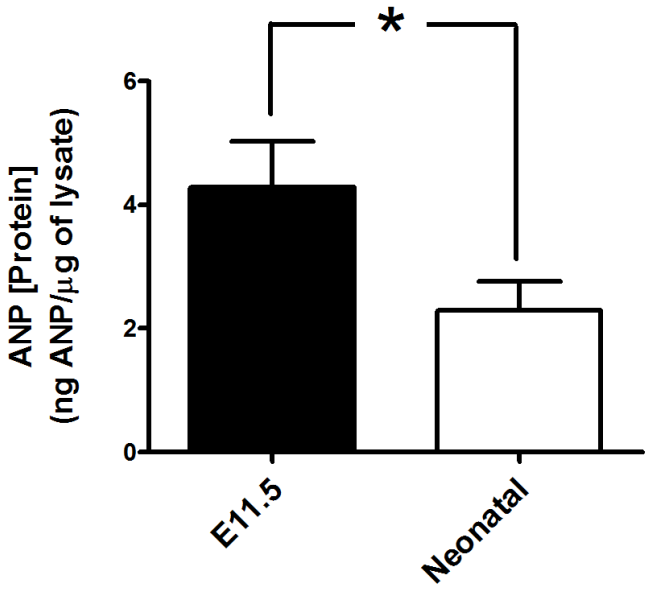

Figure 4.3.2: Quantification of ANP protein in E11.5 and neonatal ventricles. Ventricular tissue lysates from E11.5 and Neonatal stages were subjected to enzyme linked immunosorbant assay (ELISA). Results from these analyses revealed that ANP protein was significantly more abundant at E11.5 (4.3 ± 0.7ng of ANP/µg tissue lysate) compared to neonatal stages (2.3 ± 0.5ng of ANP/µg tissue lysate). N=4 (E11.5) and N=3 (Neonatal) independent experiments, 7 replicate wells/experiment. Each bar represents mean ± SEM. *$p < 0.05$, two-tailed unpaired t-test. Note: Data presented in this figure were generated in collaboration with honours student Kathleen McNeil and has appeared previously in her honours thesis.

4.3.3: Spatial expression pattern of immunoreactive ANP in the embryonic heart at E11.5. A) Coronal section (4-chamber view) of the E11.5 heart stained with Hoechst nuclear dye (blue) revealing the major anatomical features of the embryonic heart: The right atrium (RA), left atrium (LA), right ventricle, (RV), left ventricle (LV) and the forming interventricular septum (S). **B)** Overlay of Hoechst nuclear stain with ANP (green). Strong ANP immunolabelling was detected in the trabeculae of the left ventricle, which corresponds to the region indicated by the letter T. ANP immunoreactivity was also detected in luminal projections of the atrial chambers (arrows). In the trabeculae of the right ventricle, ANP was also detectable, albeit at lower levels compared to the left ventricle. ANP was generally excluded from the compact myocardium (corresponding to the region indicated by the letter C) of both the left and right ventricles. The inset, corresponding to the boxed area, more clearly demonstrates the strong labelling of ANP in the trabeculae (T), and its exclusion from the adjacent interventricular septum (S) and the compact myocardium (C).

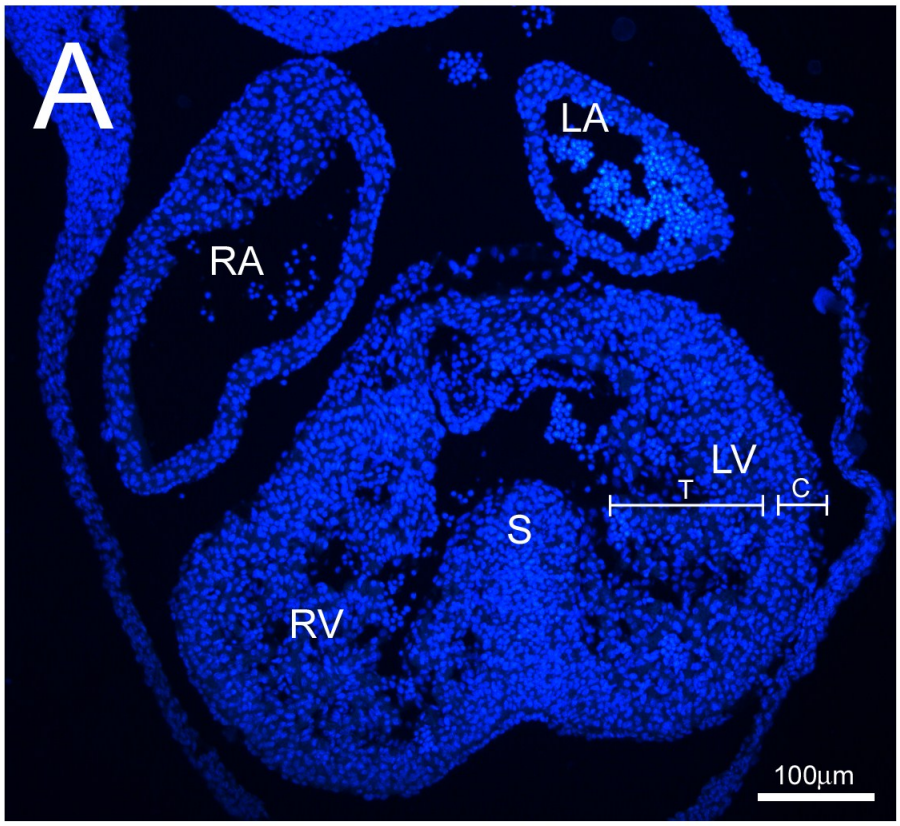
A
LA
RA
LV
T
C
S
RV
100µm

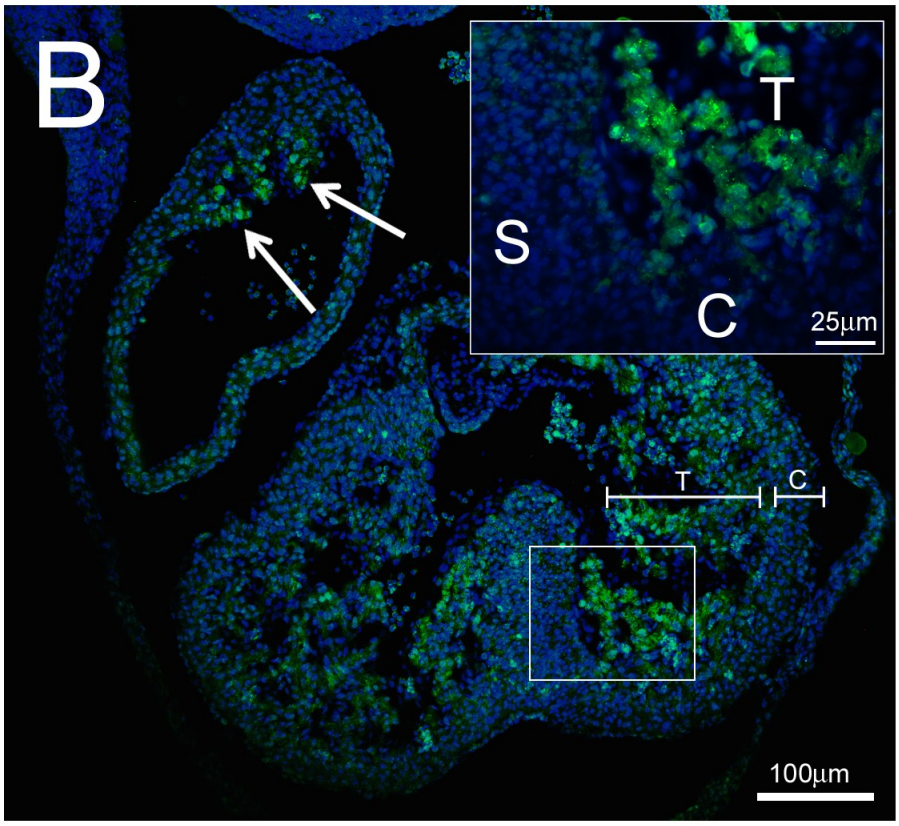
B
T
S
C
25µm
T
C
100µm

4.3.4: Spatial expression pattern of immunoreactive ANP in the left ventricle of the E14.5 heart. A) Sagittal section (2-chamber view) of the left ventricle of the E14.5 heart stained with Hoechst nuclear dye (blue) and showing the left atrium (LA) and the left ventricle (LV). **B)** Overlay of Hoechst nuclear stain with ANP (green). ANP labelling was strong in the trabeculae (region indicated by the letter T), but was generally absent from the thickening compact layer (region indicated by the letter C). The inset, corresponding to the boxed region, shows the strong labelling of ANP in the cells of the ventricular trabeculae.

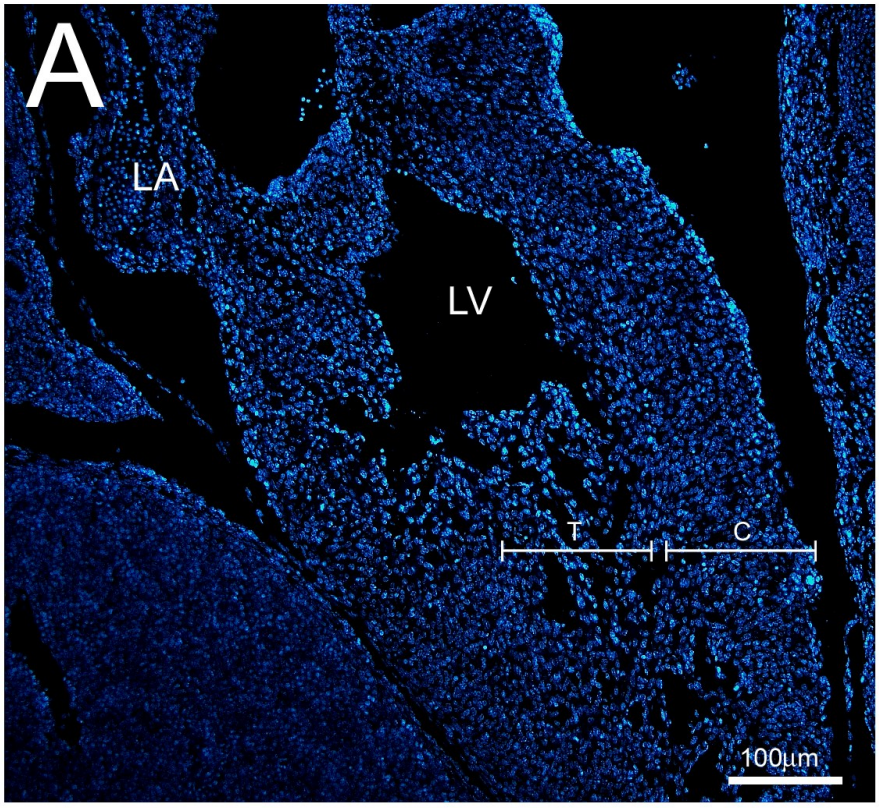
A
LA
LV
T
C
100µm

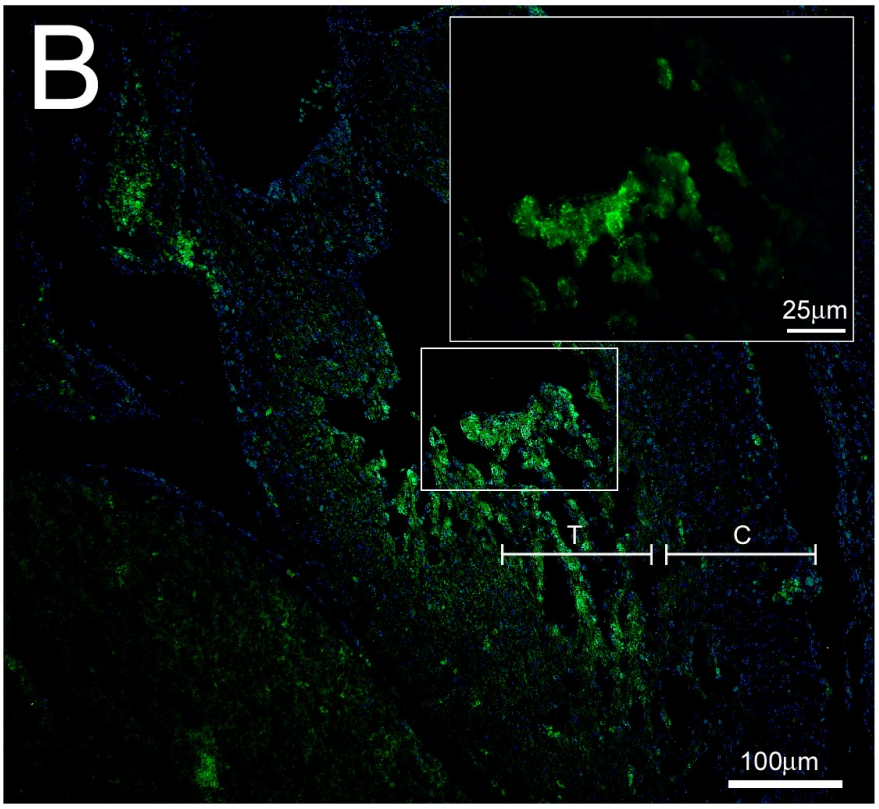
B
25µm
T
C
100µm

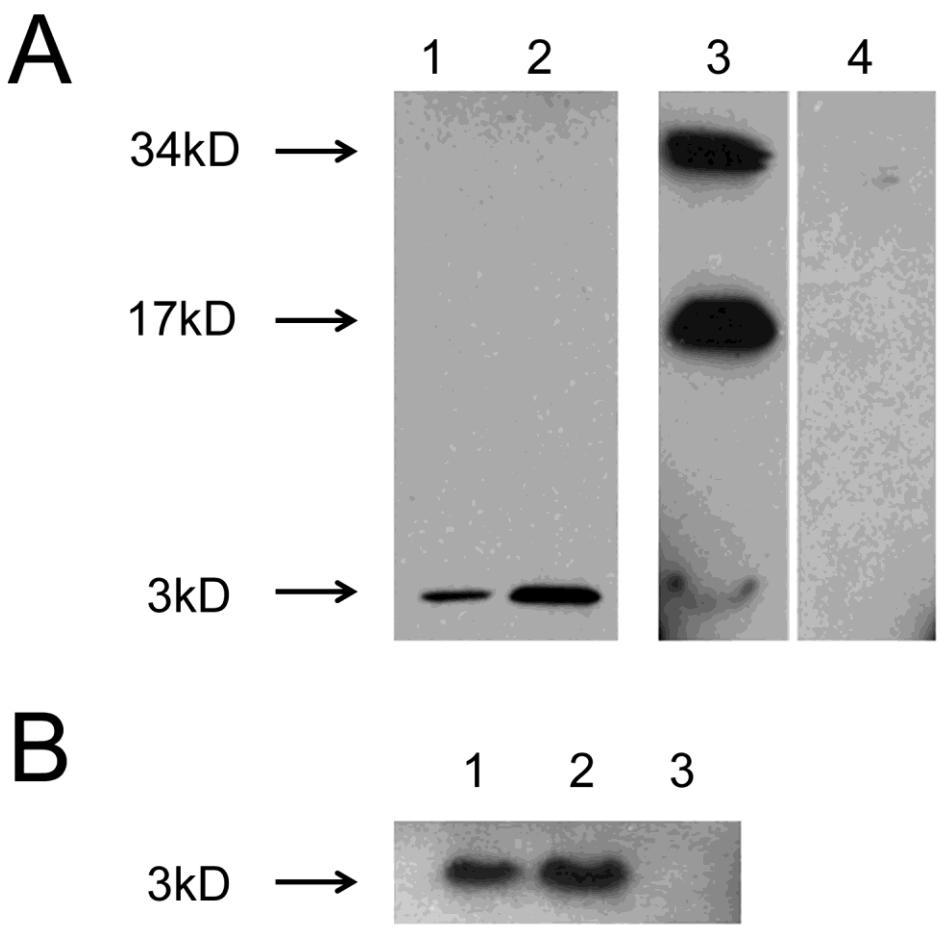

Figure 4.3.5: Detection of ANP in conditioned media samples from E11.5 ventricular cell cultures by Western blot analysis. A) Lane 1 and 2 are positive controls, where either 50ng (lane 1) or 100ng (lane 2) of synthetic ANP peptide were separated by electrophoresis on 16.5% SDS-polyacrylamide gels. Lane 3 corresponds to conditioned medium collected from a ventricular cell culture following a 24 hour period. Lane 4 is a negative control (DMEM with10% FBS; equal amount of protein). Immunoreactive bands were detected at 17kD, corresponding to proANP (1-126), as well as at 3kD, corresponding to the proteolytically processed/biologically active form of ANP (99-126). The band detected at 34kD is presumably a proANP dimer. **B)** In separate experiments, using shorter transfer time (17 minutes vs. 1 hour), more prominent immunoreactive bands could be detected at 3kD. Lane 1 and 2 correspond to conditioned media samples collected from E11.5 atrial and ventricular cell cultures respectively. Lane 3 corresponds to DMEM with 10% FBS. N=4 independent experiments.

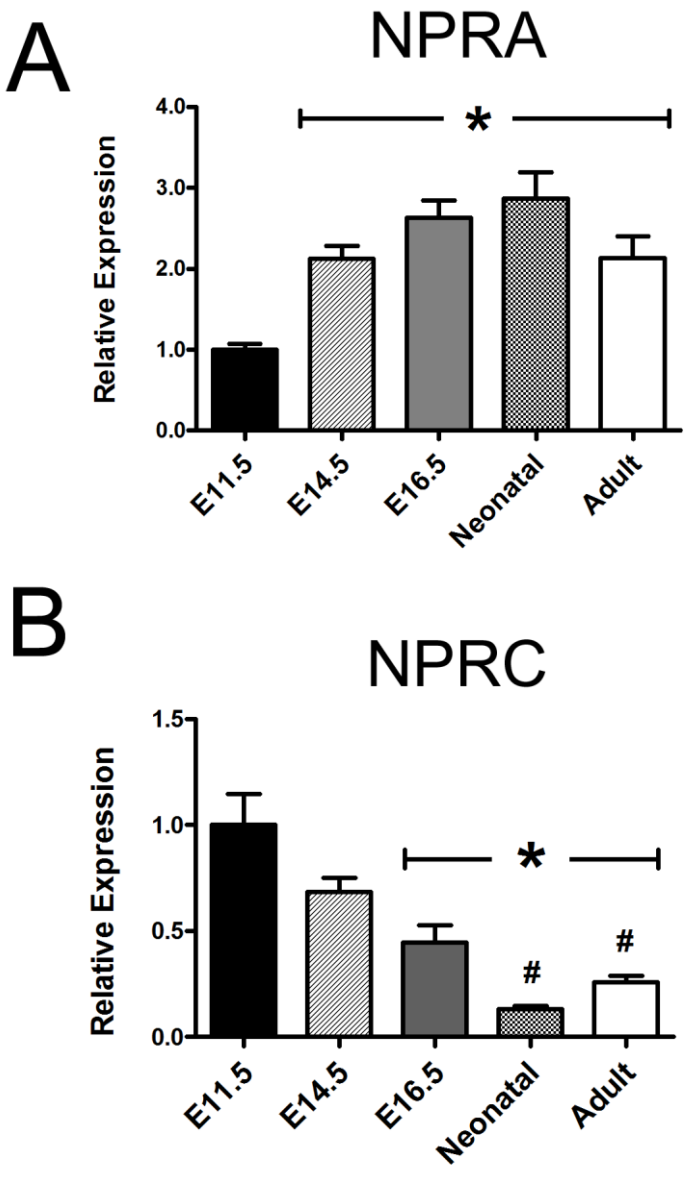

Figure 4.3.6: Developmental gene expression profiles of the ANP high affinity receptors NPRA and NPRC. The relative expression levels of NPRA and NPRC mRNA (normalized to GAPDH) were measured in cardiac ventricles at E11.5-Adult stages by real time quantitative PCR. For each gene, E11.5 served as the reference (i.e. Expression=1.0) to which all other developmental stages were compared. **A)** Expression levels of NPRA were lowest at E11.5 and increased significantly by E14.5. Expression levels of NPRA did not fluctuate significantly thereafter at E16.5, Neonatal or Adult stages. **B)** Expression levels of NPRC were highest at E11.5 and decreased significantly by E16.5. A further reduction in NPRC expression also occurred at Neonatal and Adult stages compared to E14.5. N=5-6 independent RNA extractions/developmental stage, analyzed in duplicate for each extraction. Each bar represents mean ± SEM. *$p < 0.05$ vs. E11.5; #$p < 0.05$ vs. E14.5, One- way ANOVA with Tukey post hoc test.

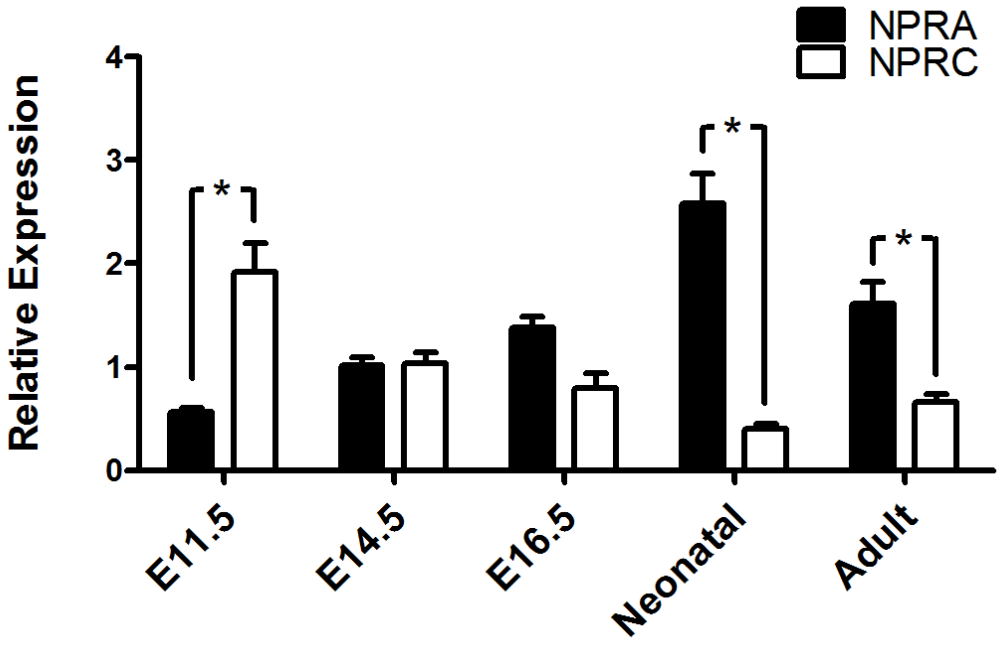

Figure 4.3.7: Direct comparison of NPRA versus NPRC gene expression in the ventricles throughout cardiac development. Side by side comparison of the relative expression of NPRA and NPRC from E11.5- Adult stages (same data presented in Figure 4.3.6) more clearly demonstrates the receptor subtype switch that occurred from early to late developmental stages. At E11.5, expression levels of NPRC were significantly higher compared to NPRA, while at E14.5 and E16.5 stages expression levels of NPRA and NPRC did not differ significantly from each other. At the Neonatal stage, NPRA expression levels increased significantly and remained elevated at the Adult stage. N=5-6 independent RNA extractions/developmental stage, analyzed in duplicate for each extraction. Each bar represents mean ± SEM. *$p < 0.05$, two-tailed unpaired t-test.

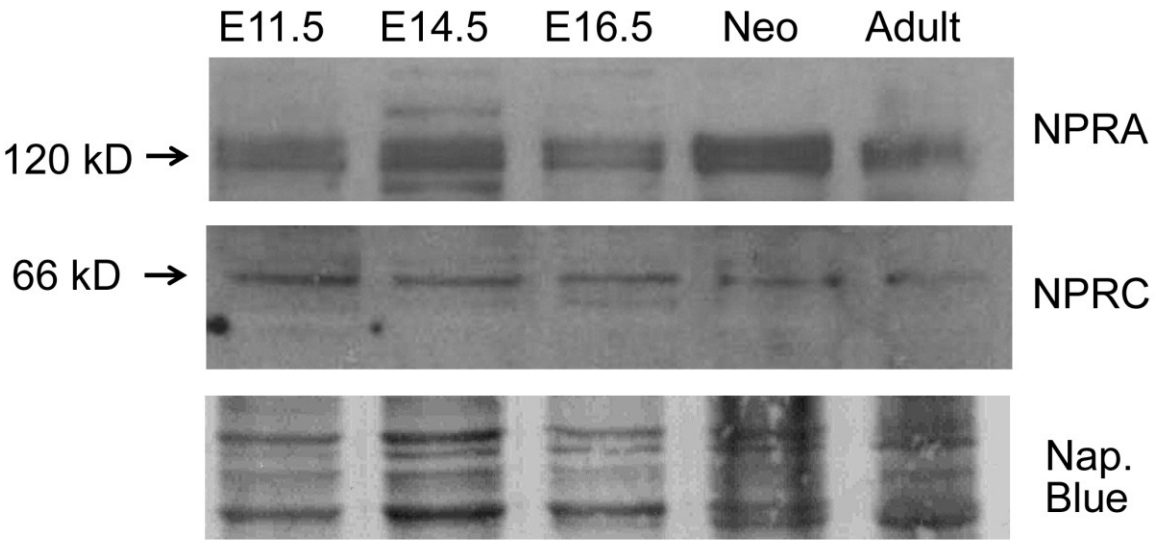

Figure 4.3.8: Western blot analyses of ventricular NPRA and NPRC protein at developmental and post-natal stages. Tissue lysates prepared from ventricles at E11.5-Adult stages were separated by electrophoresis on 12.5% SDS-polyacrylamide gels. Distinct bands were detected at 120kD and 66kD, corresponding to expected molecular weights of NPRA and NPRC respectively. An apparent increase in NPRA levels occurred from E11.5 to E14.5 and a peak in expression was detected at the Neonatal stage. Levels of NPRC were apparently higher at gestational stages (E11.5, E14.5 and E16.5) compared to post-natal stages (Neonatal and Adult). Blots were stained with Napthol blue (Nap. Blue) as a loading control. Blots presented are representative results obtained from Western blot experiments using tissue lysates from 2 independent protein extractions/developmental stage.

Figure 4.3.9: Spatial expression pattern of immunoreactive NPRA and NPRC in the embryonic heart at E11.5. Immunolabelling (3, 3' Diaminobenzidine; DAB staining method) of serial sections generated from E11.5 hearts revealed a broad expression pattern of both NPRA **(A)** and NPRC **(B)** that was strong in the trabecular (indicated by the letter T) and compact (indicated by the letter C) layers of the ventricles. **C)** Heart section subjected to DAB staining where primary antibodies were omitted. RA=right atrium, RV=right ventricle, LV=left ventricle, EC=endocardial cushion. Scale bar=100μm.

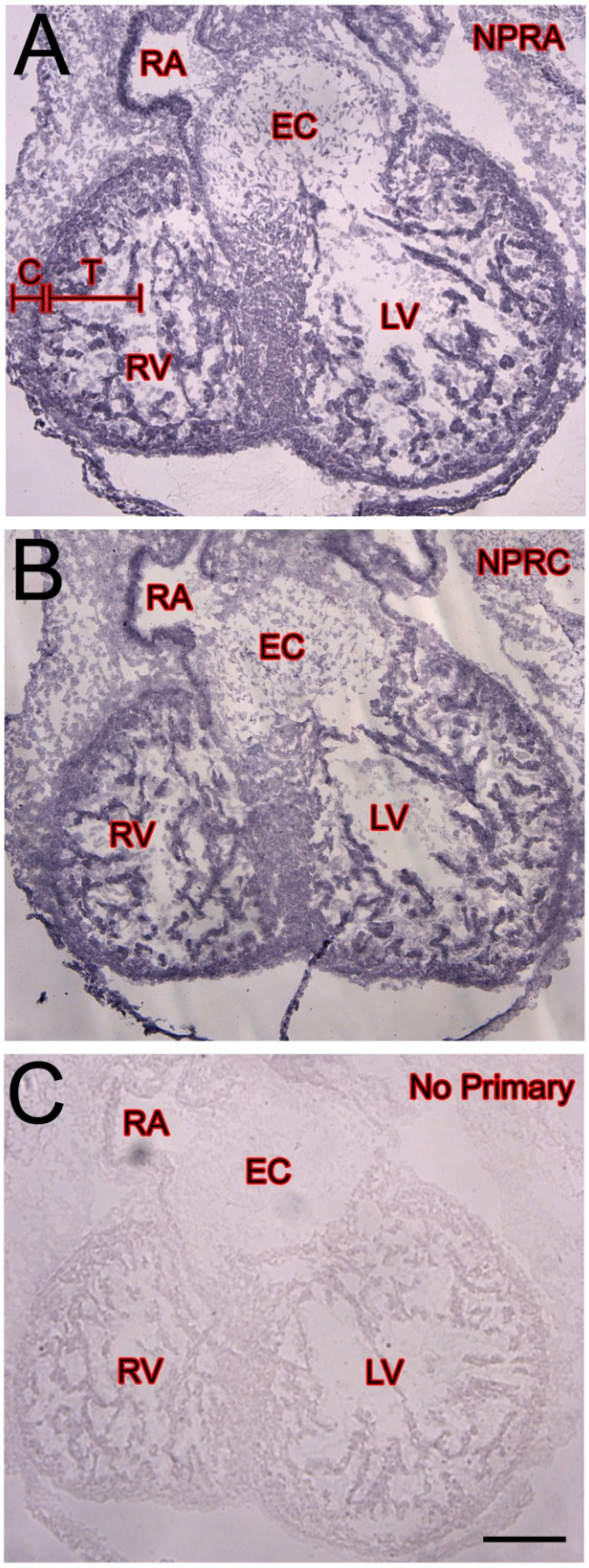
A
NPRA
RA
EC
C
T
LV
RV
B
NPRC
RA
EC
RV
LV
C
No Primary
RA
EC
RV
LV

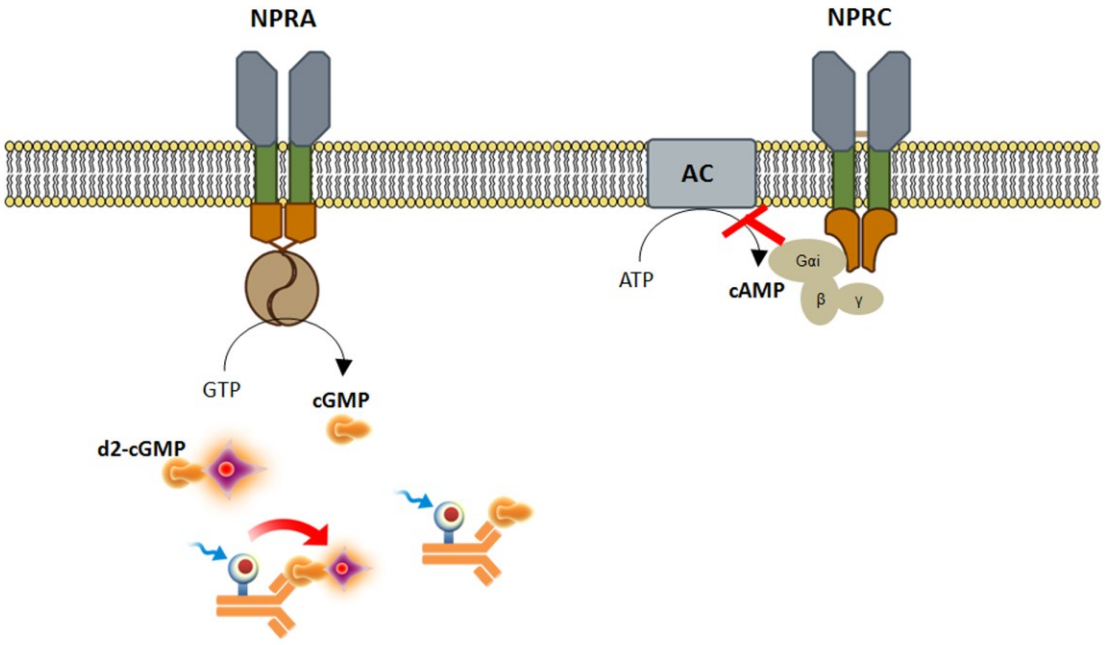

4.3.10: Schematic illustration of the principle of second messenger competitive immunoassays. Second messenger assays for detecting cGMP and cAMP relied on the same general principle. For simplicity, only the cGMP second messenger assay is described herein. In the first step of the assay, dispersed cells were incubated with ANP to stimulate production of cGMP. In the second step, competition was initiated between endogenous cGMP and a d2-dye labelled cGMP analogue for binding sites on anti-cGMP monoclonal antibodies labelled with the energy acceptor Cryptate. The specific signal (designated Delta F) which occurred due to the energy transfer between the d2-cGMP and Cryptate was inversely proportional to the concentration of endogenous cGMP contained within the experimental sample. Delta F values could then be extrapolated from a cGMP standard curve to deduce cGMP concentrations in each experimental sample.

A

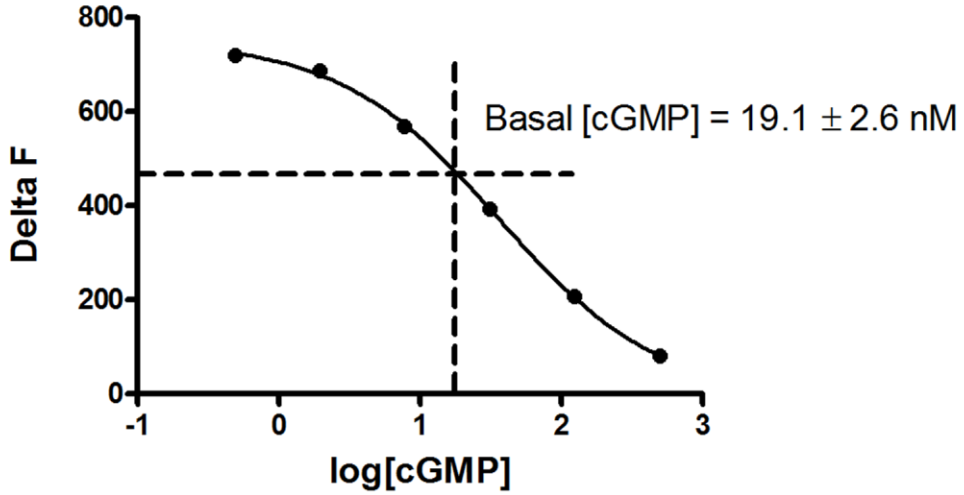

B

Final [cGMP] (nM)	Delta F
500.00	79
125.00	206
31.25	392
7.81	568
1.95	685
0.49	719

Figure 4.3.11: Generation of the cGMP standard curve. A) The cGMP standard curve was generated by plotting the Delta F values obtained from standards with known cGMP concentrations and covered an average range of 0.49-500nM (final concentration of cGMP/well). **B)** Table displaying the concentration of each of the provided standards as well as the corresponding Delta F values obtained experimentally. The dotted line represents the average basal level of cGMP measured from 64,000 E11.5 ventricular cells. Each point in **(A)** represents the mean of two independent experiments performed in duplicate wells.

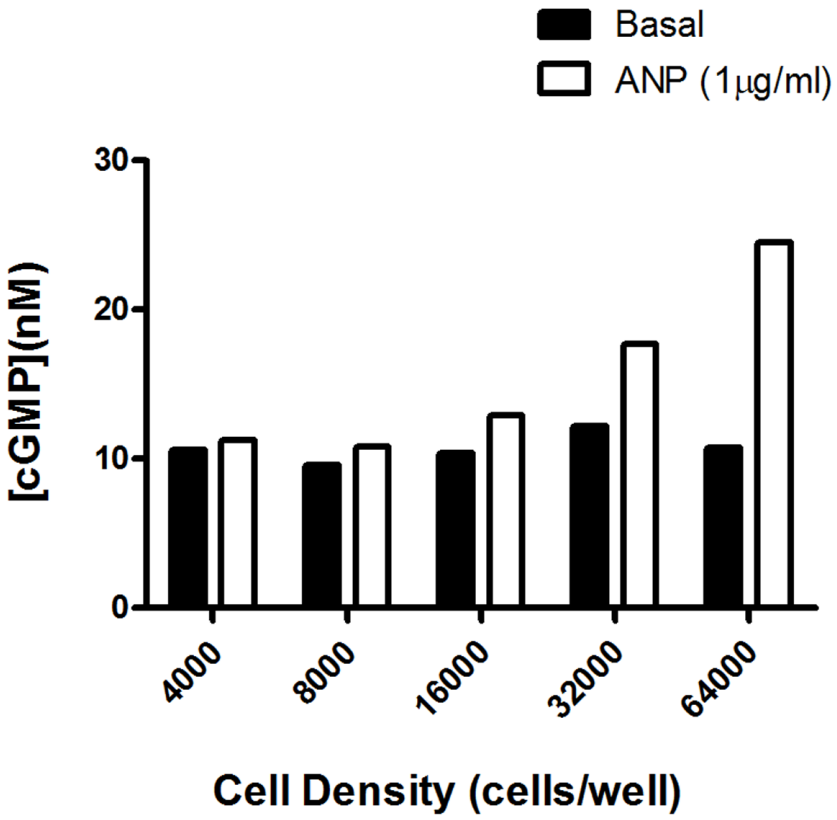

Figure 4.3.12: Cell density optimization for cGMP competitive immunoassays. To determine the optimal cell density for cGMP competitive immunoassays, a range of E11.5 ventricular cell densities were tested in the presence or absence of ANP (1μg/ml). Optimal cell density was selected based on the following criteria: **1)** basal level of cGMP production was within the linear range of the standard curve (See Figure 4.3.11) and **2**) a maximal increase in signal amplitude between inactivated state (basal cGMP production), and activated condition (ANP stimulated cGMP production) was achieved. Using these selection criteria an optimal cell density of 64,000 cells per well was determined and used for all subsequent experiments. Data are representative of N=2 independent experiments. Each data point is the average value obtained from duplicate wells.

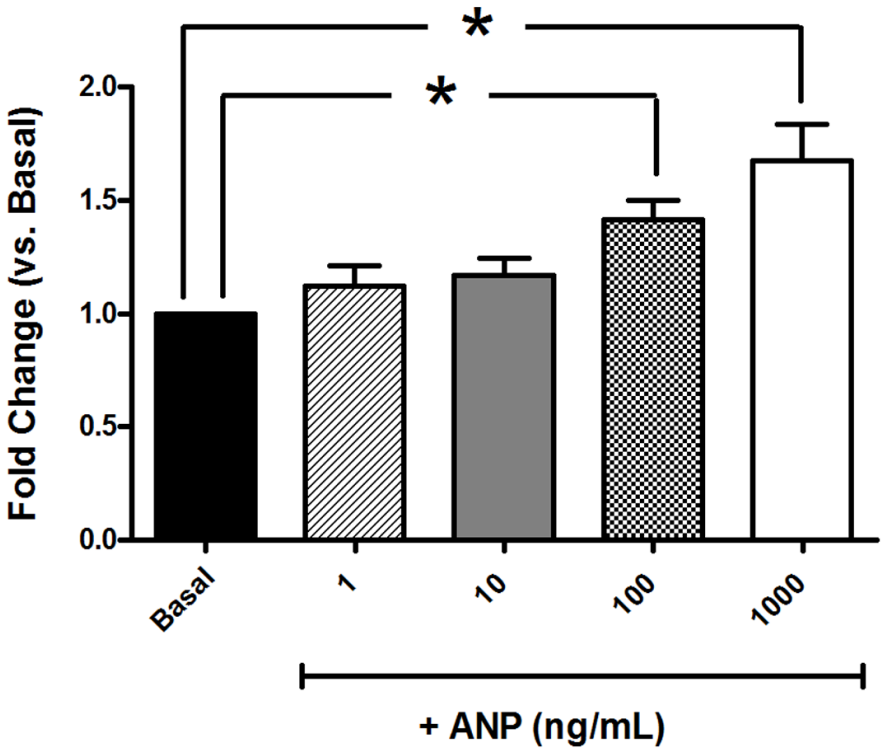

Figure 4.3.13: The effects of exogenous ANP on cGMP production in E11.5 ventricular cells. To determine the effects of exogenous ANP treatment on cGMP production, acutely isolated E11.5 cells were stimulated with various concentrations of ANP (1-1000ng/ml), and cGMP levels were measured using a competitive immunoassay (see Figure 4.3.10). The level of cGMP measured under basal conditions was 19.1 ± 2.6 nM/ 64,000 cells. Basal levels from each experiment were set to a value of 1.0 and data represent fold change in cGMP concentration in response to different doses of ANP. Stimulation with either 1ng/ml or 10ng/ml did not result in a significant increase in cGMP production compared to control. By contrast, 100ng/ml ANP was able to induce a significant 1.4 fold increase in cGMP production. N=5 independent experiments, performed in duplicate wells. Each bar represents mean ± SEM. *$p < 0.05$, One- way ANOVA with Tukey post hoc test.

A

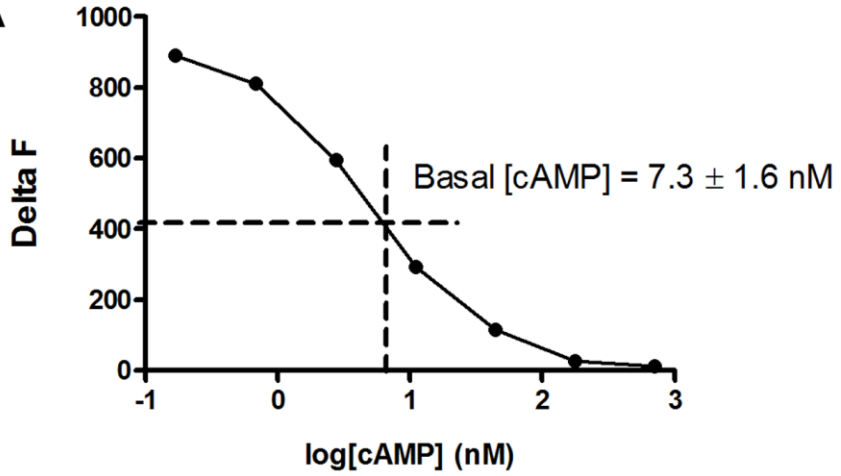

B

Final [cAMP] (nM)	Delta F
712	11
178	25
44.5	115
11.1	293
2.78	594
0.69	810
0.17	890

Figure 4.3.14: Generation of the cAMP standard curve. A) The cAMP standard curve was generated by plotting the Delta F values obtained from standards with known cAMP concentrations and covered an average range of 0.17-712 nM (final concentration of cAMP/well). **B)** Table displaying the concentration of each of the provided standards as well as the corresponding Delta F values obtained experimentally. The dotted line represents the average basal level of cAMP measured from 4,000 E11.5 ventricular cells. Each point in **(A)** represents the mean of two independent experiments performed in duplicate wells.

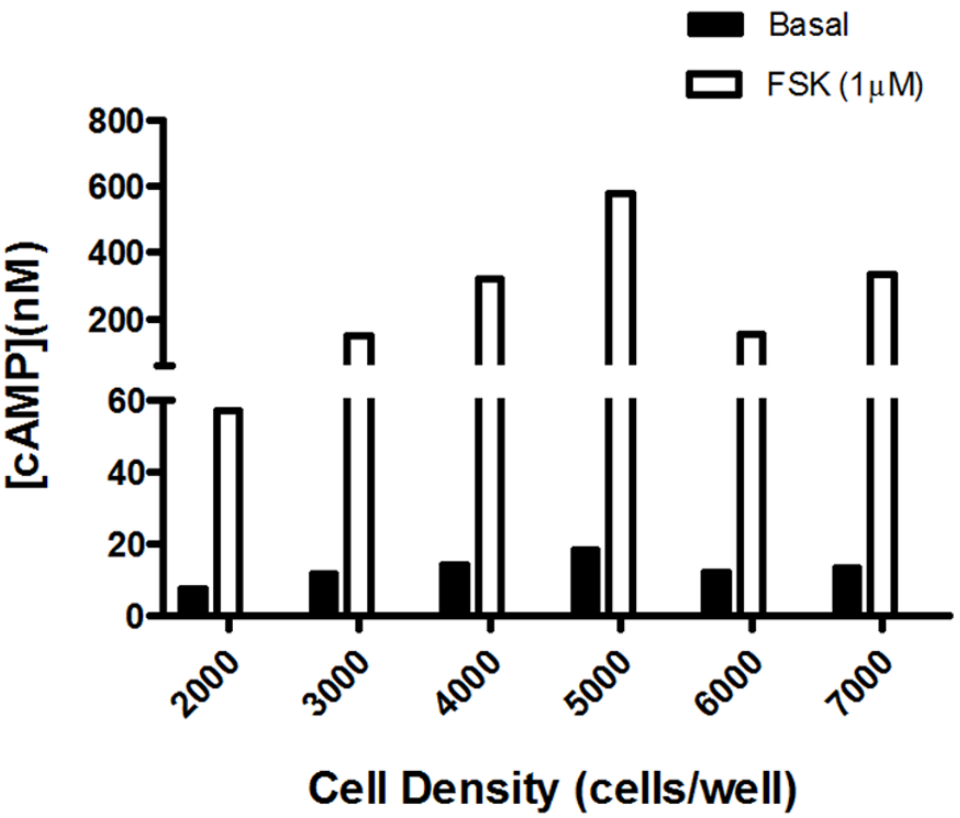

Figure 4.3.15: Cell density optimization for cAMP competitive immunoassays. To determine the optimal cell density for cAMP competitive immunoassays, a range of E11.5 ventricular cell densities were tested in the presence or absence of the direct adenylyl cyclase activator forskolin (FSK; 1μM). Optimal cell density was selected based on the following criteria: **1)** basal level of cAMP production was within the linear range of the standard curve (See Figure 4.3.14) and **2**) a maximal increase in signal amplitude between inactivated state (basal cAMP production), and activated condition (FSK stimulated cAMP production) was achieved. Using these selection criteria an optimal cell density of 4,000 cells per well was determined and used for all subsequent experiments. Data are representative of N=2 independent experiments. Each data point is the average value obtained from duplicate wells.

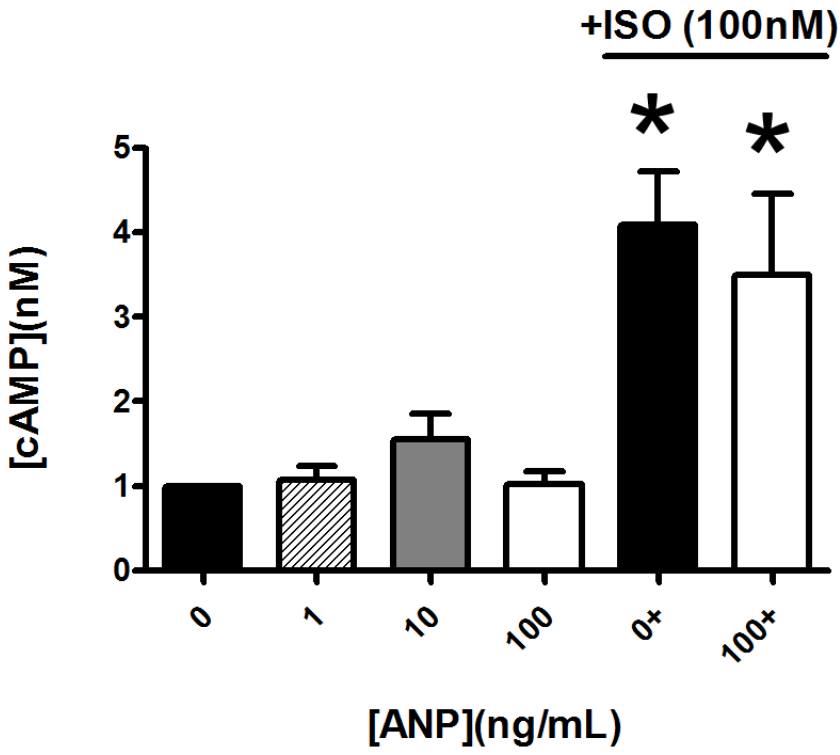

Figure 4.3.16: The effects of exogenous ANP on cAMP production in E11.5 ventricular cells. To determine the effects of exogenous ANP treatment on cAMP production, acutely isolated E11.5 cells were stimulated with various concentrations of ANP (1-100ng/ml), and cAMP levels were measured using a competitive immunoassay (see Figure 4.3.10). Under basal conditions, the level of cAMP in E11.5 cells was 7.3 ± 1.6nM. Basal levels (0ng/ml) from each experiment were set to a value of 1.0 and data represent fold change in cAMP concentration in response to different doses of ANP**.** Compared to basal, ANP (1-100ng/ml) had no effect on levels of cAMP production. By contrast, stimulation with ISO (100nM) alone was able to induce a ~ 4 fold increase in cAMP levels. When cells were co-treated with ISO (100nM) and ANP (100ng/ml), a modest reduction in cAMP production compared to ISO alone was observed but this result was not statistically significant. N=4 independent experiments, performed in duplicate wells. Each bar represents mean ± SEM. *$p < 0.05$ vs. basal, One way ANOVA with Tukey post hoc test.

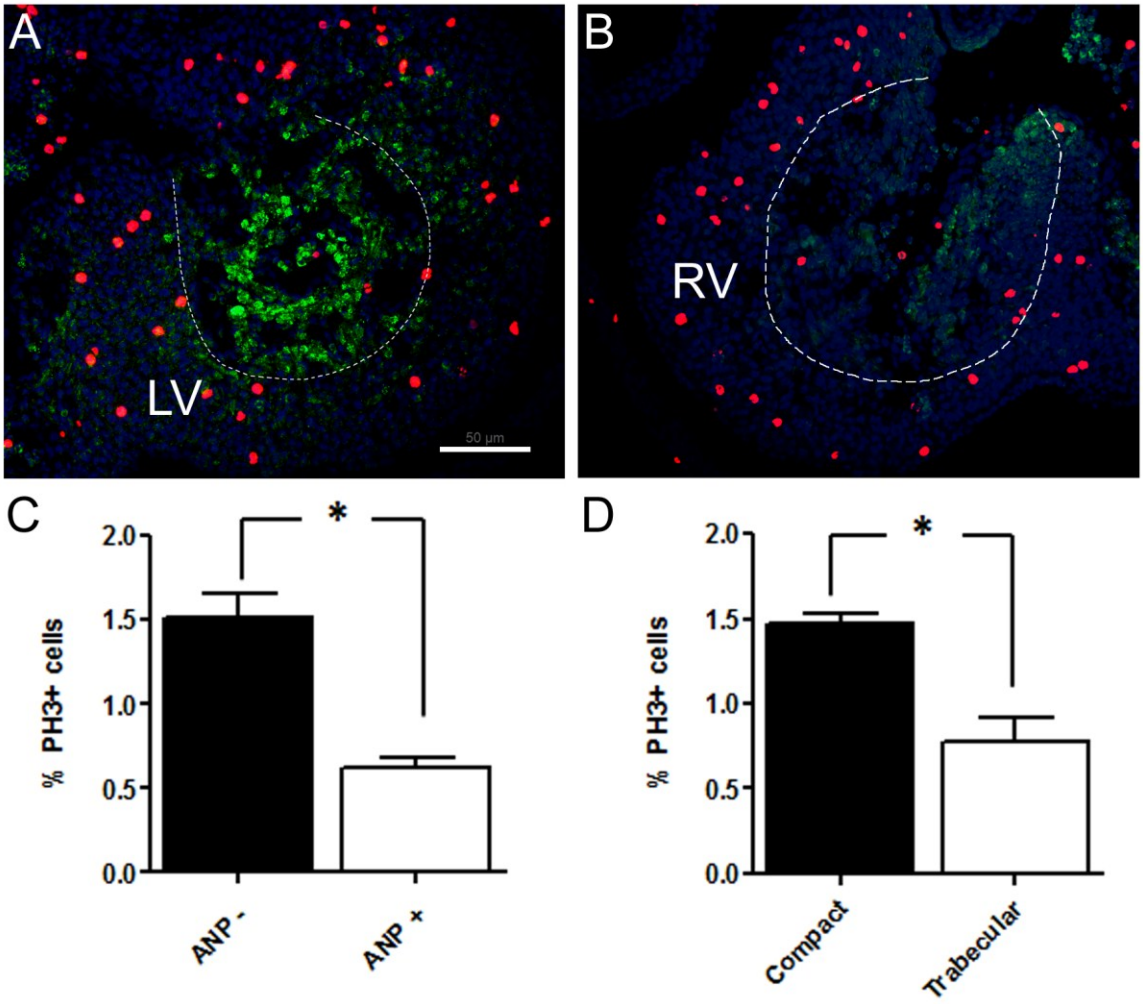

Figure 4.3.17: Determination of the mitotic index in regions of high and low immunoreactive ANP. A) Co-immunolabelling of E11.5 ventricular sections with specific antibodies against ANP (green) and the mitotic marker PH3 (red) revealed an observably lower number of $PH3^+$ nuclei in the ANP^+ trabecular myocardium (delineated by the dashed line) of the left ventricle (LV) compared to the ANP^- compact layer. **B)** In the right ventricle (RV), ANP^+ and ANP^- regions were difficult to discern, but an apparently lower number of $PH3^+$ nuclei were observed in the trabecular myocardium (delineated by the dashed line) compared to the compact layer. **C)** The mitotic index (percentage of $PH3^+$ nuclei/ total nuclei of the specified region) in the left ventricle was significantly lower in the ANP^+ vs. ANP^- regions. In the right ventricle, the trabecular myocardium displayed a lower mitotic index compared to the compact layer. N= 9 ventricular sections generated from 3 separate E11.5 embryos. Each bar represents mean ± SEM. $*p < 0.05$, two-tailed unpaired t-test. Scale bar= 50µm.

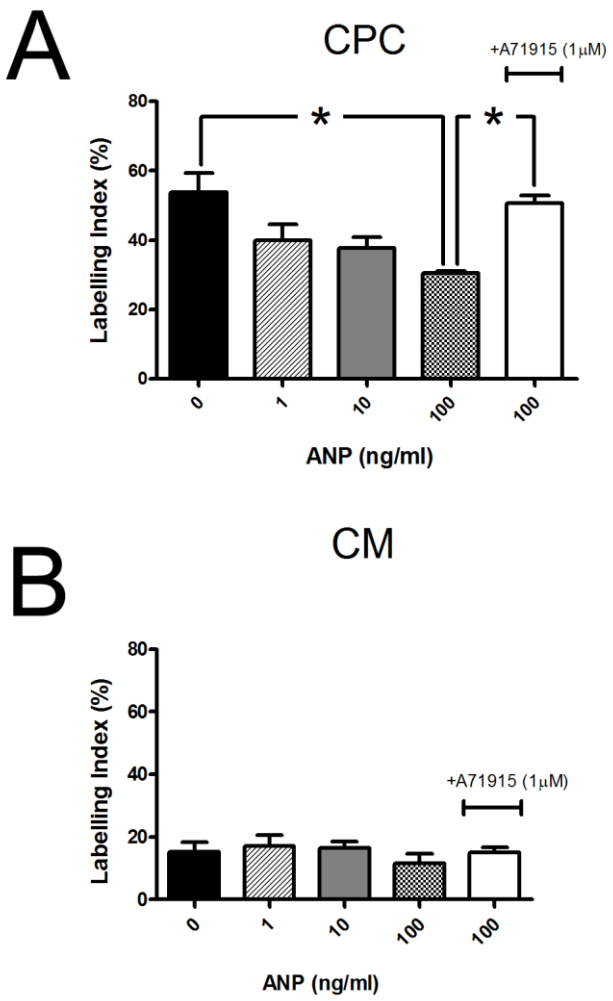

Figure 4.3.18: Effects of exogenous ANP on proliferation of E11.5 cardiac progenitor cells and cardiomyocytes. Using a [^{3}H] - thymidine incorporation assay, the labelling index (LI; percentage of cells in the S-phase out of the total number of cells in the defined cell population) was determined in the cardiac progenitor cell (CPC) and cardiomyocyte (CM) populations from E11.5 primary ventricular cell cultures. **A)** In the CPC population (β-gal$^+$/MF20$^-$), increasing concentrations of ANP were associated with a decline in LI compared to control cultures (0ng/ml) which reached statistical significance at the 100ng/ml concentration. In cultures pre-incubated with the NPRA/NPRB antagonist A71915, the reduction in proliferation associated with 100ng/ml ANP in the CPC population was abolished. **B)** In the cardiomyocyte population (β-gal$^+$/MF20$^+$) LI did not vary between control and any of the ANP concentrations tested. Pre-incubation with A71915 also had no effect on the cardiomyocyte population. N=3 independent experiments/treatment group, ~ 500 cells counted/experiment. Each bar represents mean ± SEM. *$p<0.05$, One-way ANOVA with Tukey post hoc test.

CHAPTER 5: INVESTIGATION OF ANP/NPRA SIGNALLING IN DEVELOPMENT OF THE VENTRICULAR CONDUCTION SYSTEM

5.1 Background and Hypothesis

Pioneering work using lineage tracing techniques in the developing chick heart demonstrated that working cardiomyocytes and conduction system cardiomyocytes are derived from a common pool of myogenic progenitor cells (Gourdie et al., 1995). Consistent with this discovery, our group tracked the differentiation of Nkx2.5^{+} CPCs isolated from E11.5 mouse ventricles *in vitro* and demonstrated that these cells were capable of forming both working cardiomyocytes and putative conduction system cardiomyocytes expressing lineage specific molecular markers (McMullen et al., 2009).

Several lines of evidence have been presented showing that cells within the ventricular trabeculae withdraw from the cell cycle and enter terminal differentiation pathways earlier than cells in the surrounding compact myocardium (Viragh and Challice, 1982; Gourdie et al., 1995; Sedmera et al., 2003). Furthermore, work in this thesis has demonstrated that the low mitotic index in the ventricular trabeculae is spatially associated with regions of high immunoreactive ANP in the left ventricle and that CPCs exposed to exogenous ANP undergo a reduction in cell cycle activity (Chapter 4 Figures 4.3.17 and 4.3.18) Based on this knowledge, we next asked the question as to whether this ANP mediated reduction in CPC proliferation could be coupled to preferential differentiation toward the cardiac conduction system (CCS) lineage. Previously, the secreted endothelial/endocardial proteins endothelin-1(ET-1) and neuregulin-1(NRG-1) were identified as paracrine factors involved in specification of the

ventricular CCS of chick and mouse (Gourdie et al., 1998; Rentschler et al., 2002; Patel and Kos, 2005). **Thus, we hypothesized that ANP is a secreted factor involved in specification and/or differentiation of ventricular cardiac conduction system cardiomyocytes.**

5.2 Specific Aims

1. Determine whether ANP receptor mediated signalling has any effect on conduction system gene expression.

2. Characterize ventricular conduction system development in mice lacking NPRA.

3. Assess conduction system function in adult mice lacking NPRA.

5.3 Results

5.3.1 Fluorescence Visualization of ANP Positive Cells by Monitoring β-Galactosidase Activity Controlled by ANP Promoter

The ANF-LacZ (designated here as ANP-LacZ) transgenic mouse model was generated by inserting a *LacZ* reporter gene under the transcriptional control of the ANP promoter into the genome (Habets et al., 2002). Chromogenic or fluorogenic β-galactosidase (β-gal) substrates can then be used to monitor ANP promoter activity. The fluorogenic β-gal substrate, fluorescein di β-D- galactopyranoside (FDG) has been used in conjunction with fluorescence-activated cell sorting (FACS) as a highly sensitive fluorescence-based assay of β-gal activity (Nolan et al., 1988). This assay relies on sequential hydrolysis of non-fluorescent FDG by β-gal first to fluorescein

monogalactosidase (FMG), and then to the highly fluorescent fluorescein (Rotman et al., 1963).

To determine the level of fluorescent signal associated with FDG, whole ventricles from ANP-LacZ$^+$ and ANP-LacZ$^-$ embryos from the same litter were incubated in FDG solution and subsequently examined by fluorescence microscopy (Figure 5.3.1A&B). The genotype of each embryo was determined by incubating the atria for 30 minutes in X-gal solution (chromogenic β-gal substrate) (data not shown). In the ANP-LacZ$^+$ ventricles, a strong green fluorescent signal could be detected after a 15 minute incubation period with FDG (Figure 5.3.1A). By contrast, after 15 minutes, ANP-LacZ$^-$ hearts had only faint background signal when examined at the same exposure as ANP-LacZ$^+$ hearts (Figure 5.3.1B).

5.3.2 Determination of Conduction System Marker Gene Expression in the ANP Expressing Cell Population

To determine whether expression of conduction system genes were enriched in the ANP$^+$ cell population of the E11.5 heart, the ANP-LacZ mouse model was employed to isolate ANP$^+$ from ANP$^-$ cells by FACS. Total RNA was then extracted from these two distinct cell populations, converted to cDNA sequences and analyzed for conduction system marker gene expression by qPCR. The atria from each E11.5 heart was also dissected and placed in X-gal for 30 minutes to confirm β-gal activity in ANP-LacZ$^+$ hearts. Only the ventricles corresponding X-gal$^+$ atria were used for FACS.

For each experiment, a control cell population (ANF-LacZ$^+$ cells, not incubated with FDG) was used to set the autofluorescence compensation level (Figure 5.3.2A&B).

In these control experiments, a single peak was observed corresponding to the level of background fluorescence, and this data was used to set the threshold fluorescence value for sorting experimental (FDG stained) cell populations into ANP^+ and ANP^- groups. FACS analysis of FDG stained cells revealed a single peak that was shifted to the right compared to unstained controls indicating β-gal mediated hydrolysis of FDG to fluorescein had occurred (Figure 5.3.2D). Sorted cells were separated into two sub-populations based on high or low fluorescence and designated as either **1)** ANP high expression (designated ANP^+) or **2)** ANP low expression (designated ANP^-).

Analysis of the conduction system marker genes Cx40 and HCN4 revealed that the ANP^+ cell population had a 3.7 fold higher expression of Cx40 and a 2.8 fold higher expression of HCN4 compared to the ANP^- population (Figure 5.3.3A&B). In parallel experiments, to confirm the presence of Cx40 protein in ANP^+ cells, ANP-LacZ primary cultures were incubated with X-gal and subsequently immunolabelled with Cx40 antibodies (Figure 5.3.4). In addition, these cells were also immunolabelled with MF20 antibodies against sarcomeric myosin to specifically identify cardiomyocytes. Consistent with FACS data, it was discovered that the majority of cardiomyocytes expressing ANP ($X\text{-}gal^+/MF20^+$) had clearly visible Cx40 labelling along the margins between adjacent cells (Figure 5.3.4). By contrast, Cx40 labelling was rarely observed in $X\text{-}gal^-$ cells (Figure 5.3.4).

5.3.3 Effects of Exogenous ANP Treatment on Conduction System Marker Gene Expression

To determine whether the observed co-expression of ANP with conduction system marker genes could be due to direct inductive effects of ANP, E11.5 ventricular cultures were incubated with ANP (100ng/ml) for 24 hours and subsequently analyzed for fluctuations in expression of Cx40 and HCN4 mRNA compared to vehicle (H_20) treated controls (expression=1.0) by qPCR analyses. This concentration of ANP was selected based on the anti-proliferative effects of 100ng/ml on E11.5 CPCs demonstrated previously (Chapter 4, Figure 4.3.18). Compared to vehicle treated controls, ANP was not associated with any significant difference in the gene expression levels of either Cx40 or HCN4 (Figure 5.3.5A&B).

Thus far, data presented in Chapter 5 have demonstrated that expression of the conduction system marker genes Cx40 and HCN4 were enriched in the ANP^+ population, **2)** immunoreactive Cx40 is present in individual ANP^+ cardiomyocytes and **3)** ANP did not have a direct inductive effect on expression of either Cx40 or HCN4 under our specific experimental conditions.

5.3.4 Expression of Proliferation and Conduction System Marker Genes in Ventricles of E14.5 Embryos Lacking NPRA

As an alternative approach to assessing the specific involvement of ANP/NPRA signalling system in development of the ventricular conduction system, we employed a previously established knockout mouse model in which the *Npr1* gene encoding NPRA was globally disrupted to generate a non-functional allele (Oliver et al., 1997).

Previously, it was reported that NPRA null ($NPRA^{-/-}$) offspring were observed at a lower than expected Mendelian frequency beginning at E16.5 (Scott et al., 2009). Similarly, in our hands, genotyping of offspring from heterozygous ($NPRA^{+/-}$) breeding pairs revealed a significantly lower than expected proportion of $NPRA^{-/-}$ animals (35.3% $NPRA^{+/+}$; 57.4% $NPRA^{+/-}$, 7.3% NPRA $^{-/-}$) at the time of weaning (~3 weeks) (Figure 5.3.6A), thus indicating a penetrance of ~70% mortality of $NPRA^{-/-}$ animals from our colony. Currently, it remains unknown whether increased mortality associated with germ-line ablation of the *Npr1* gene is associated with altered proliferation/differentiation kinetics during cardiogenesis. To gain insight into this issue, we compared expression levels of a panel of cell cycle genes and conduction system lineage marker genes from ventricles of $NPRA^{+/+}$, $NPRA^{+/-}$ and $NPRA^{-/-}$ E14.5 embryos. This developmental stage was selected for these analyses based on the following rationale: **1)** due to relatively small litter sizes obtained from heterozygous crosses, it was technically challenging to acquire a sufficient number of ventricles from each genotype at earlier developmental stages such as E11.5. **2)** By E14.5 the ventricular conduction system has undergone structural and functional maturation and overall proliferation rates in the E14.5 myocardium are significantly lower compared to E11.5 (Soonpaa et al., 1996). Thus, altered expression of proliferation/differentiation markers at this stage would likely be reflective of abnormal cardiac development.

Genotyping of E14.5 embryos used for gene expression analyses revealed that at E14.5, survival of $NPRA^{-/-}$ did not deviate from expected frequencies (21.4% $NPRA^{+/+}$; 51.8% $NPRA^{+/-}$, 26.8% NPRA $^{-/-}$) (Figure 5.3.6B). Quantitative analyses of gene expression of selected cell cycle genes (by qPCR) did not reveal any significant

differences between the three genotypes ($NPRA^{+/+}$, $NPRA^{+/-}$ and $NPRA^{-/-}$) (Figure 5.3.7A-D). Intriguingly, however, compared to $NPRA^{+/+}$ (expression=1.0), trends toward reduced expression of conduction system markers Cx40 and HCN4 were observed in $NPRA^{+/-}$ and $NPRA^{-/-}$ ventricles and appeared to be dependent on *Npr1* gene dosage (Figure 5.3.8A&B). Furthermore, ANP mRNA was significantly upregulated ~2.5 fold in $NPRA^{-/-}$ ventricles compared to ventricles from either $NPRA^{+/+}$ or $NPRA^{+/-}$ embryos (Figure 5.3.9).

5.3.5 Visualization of Ventricular Conduction System Development using the $Cx40^{egfp}$ Knockin Mouse Model

Investigations into the effects of particular genetic or environmental factors on CCS development has been greatly enhanced by the development of mouse models harboring reporter transgenes expressed specifically in either components or the entire conduction system. In the embryonic heart, Cx40 expression is expressed in the trabecular network (putative ventricular conduction system) and is gradually restricted to the Purkinje fibers of the mature heart while being excluded from surrounding working cardiomyocytes (Miquerol et al., 2004; Miquerol et al., 2010). Thus, the $Cx40^{egfp}$ mouse model, in which the vital enhanced green fluorescent protein (EGFP) is expressed under the control of the Cx40 gene (Miquerol et al., 2004), is particularly useful for studying the development of the ventricular conduction system. Recently, we have established a colony of $Cx40^{egfp}$ mice and confirmed previously reported EGFP expression patterns in E11.5 embryos and neonatal pups (Miquerol et al., 2004). Specifically, histological analyses of E11.5 embryos revealed strong EGFP signal in the atrial chambers as well as

the trabecular myocardium of the left ventricle and to a lesser extent in the trabeculae of the right ventricle (Figure 5.3.10A). Additionally, EGFP signal was detected in vascular endothelial cells.

Hearts from neonatal day 1 (ND1), pups examined by whole mount microscopy revealed strong EGFP signal in both atrial chambers and the coronary vasculature (Figure 5.3.10B). In the ventricles, EGFP signal could be detected from the exterior surface in regions corresponding to the underlying ventricular chambers but remained absent from the ventricular septum (Figure 5.3.10B). Incisions along the ventricular free wall were made to enable better visualization of the inner septal surface as well as the inner free wall of each ventricle (Figure 5.3.10C). Using this method, a broad network of $EGFP^{+}$ fiber-like bundles were observed extending in a parallel fashion from the base of left ventricular septum that corresponded to the left bundle branch (LBB) (Figure 5.3.10C). As the LBB extended toward the apex of the left ventricle, it gave rise to an extensive network of overlapping Purkinje fibers that formed a honeycomb like pattern within the ventricular free wall (Figure 5.3.10C). Examination of the right ventricle of ND1 pups revealed that the right bundle branch was composed of only a single fiber bundle that branched into a Purkinje fiber network that was not as extensive as that observed in the left ventricle (data not shown).

5.3.6 Using the $Cx40^{egfp}$ Model to Characterize Ventricular Cardiac Conduction System Development in Mice Lacking NPRA

Previously, it was shown that mice haploinsufficient for the cardiac transcription factor Nkx2.5 displayed a hypoplastic Purkinje fiber network which was visualized using

the Cx40 EGFP expression pattern (Jay et al., 2004; Meysen et al., 2007). Furthermore, electrocardiogram (ECG) analyses of $Cx40^{egfp/+}$/$Nkx2.5^{+/-}$ mice revealed electrophysiological abnormalities, including a prolonged QRS interval, that were consistent with Purkinje fiber abnormalities (Jay et al., 2004). Recently, we initiated breeding schemes between homozygous $Cx40^{egfp/egfp}$ mice with $NPRA^{+/-}$ mice to generate compound $Cx40^{egfp/+}$/ $NPRA^{x/x}$ offspring. Subsequent crosses between these F1 progeny were generated in an effort to obtain F2 embryos/pups harboring a single copy of Cx40 EGFP and a variable copy number of the NPRA gene. Thus far, E11.5 timed pregnant females have yielded $Cx40^{egfp/+}$ embryos that were also NPRA wildtype ($NPRA^{+/+}$) or heterozygous ($NPRA^{+/-}$), but not homozygous ($NPRA^{-/-}$). Histological analyses of these embryos revealed that the EGFP expression patterns did not appear to be different between $NPRA^{+/+}$ and $NPRA^{+/-}$ hearts (as seen in Figure 5.3.10A).

Similar to the situation at E11.5, breeding schemes have thus far failed to yield any $Cx40^{egfp/+}$/ $NPRA^{-/-}$ pups (15 pups, from 2 litters). However, preliminary comparisons of EGFP expression patterns between $Cx40^{egfp/+}$/ $NPRA^{+/+}$ and $Cx40^{egfp/+}$/ $NPRA^{+/-}$ new born pups appeared to reveal some potentially significant differences. In the ventricles of $Cx40^{egfp/+}$ /$NPRA^{+/+}$ hearts, the LBB was readily observed and was continuous with an extensively arborized Purkinje fiber network as described above (Figure 5.3.10C). Intriguingly, in 1 out of the 6 $Cx40^{egfp/+}$/ $NPRA^{+/-}$ pups examined, the individual fibers of the LBB appeared thinner and the overall network along the septal wall appeared far less dense compared to $Cx40^{egfp/+}$/ $NPRA^{+/+}$ littermates (Figure 5.3.11B). In some regions, there also appeared to be only minimal continuity between the LBB and the Purkinje fiber network (Figure 5.3.11B). Moreover, the extensive

honeycomb pattern of the Purkinje fiber network observed in $Cx40^{egfp/+}$/ $NPRA^{+/+}$ ventricles appeared to be far less extensive in the ventricles of this $Cx40^{egfp/+}$ /$NPRA^{+/-}$ pup (Figure 5.3.11B).

5.3.7 Electrocardiogram (ECG) Analyses of Mice Lacking NPRA

Initial generation and characterization of *Npr1*$^{-/-}$ mice revealed that these animals displayed cardiac hypertrophy and fibrosis as well as impaired hemodynamic parameters assessed by echocardiography (Oliver et al., 1997). To extend these observations, we performed electrocardiographic (ECG) analyses on surviving $NPRA^{-/-}$ mice as well as $NPRA^{+/-}$ and $NPRA^{+/+}$ littermates at 3-5 months of age to gain insight into whether *Npr1* ablation was associated with overt rhythm abnormalities. Salient features of a typical ECG recording include a P-wave that corresponds to depolarization of the atrial chambers, followed by a QRS complex corresponding to depolarization of the ventricles. In $NPRA^{+/+}$ and $NPRA^{+/-}$ mice the P-wave was always readily observable, while the P-wave of $NPRA^{-/-}$ mice tended to be smaller in amplitude and more difficult to detect (Figure 5.3.12). Compared to either $NPRA^{+/+}$ or $NPRA^{+/-}$ mice, the QRS amplitude tended to be greater and prolonged in $NPRA^{-/-}$ mice, while heart rate did not differ between any genotypes (Figure 5.3.12). In addition, prolonged P-R interval was observed in 1 out of 3 $NPRA^{+/-}$ mice (Figure 5.3.12C), but did not reach statistical significance. No indications of arrhythmic beats were observed in ECG recordings from any of the genotypes under baseline conditions. To determine whether arrhythmic activity could be triggered by sympathetic activation, ECG recordings were also captured following injection of dobutamine (1.5μg/g; injected IP)(Wiesmann et al., 2001).

Following administration of dobutamine, there was a predictable increase in heart rate from mice with each genotype (Figure 5.3.13). In addition, evidence of isolated periods of irregular electrical activity (e.g. abnormal/skipped beats) following injection of dobutamine was observed at low frequency (incidence of ~3 events per mouse per 20 minute recording) in $NPRA^{-/-}$ and $NPRA^{+/-}$ but not in $NPRA^{+/+}$ mice (Figure 5.3.14).

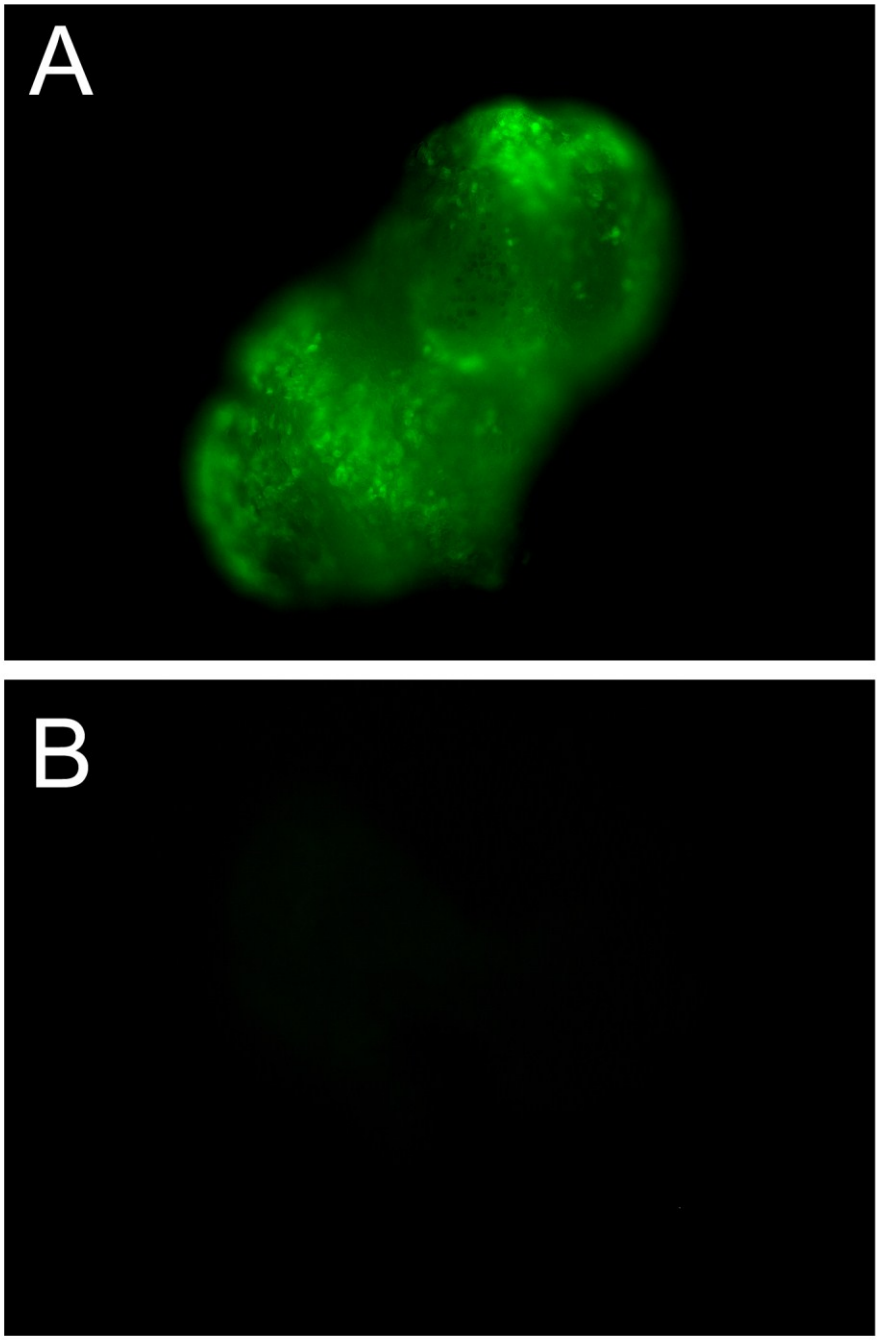

Figure 5.3.1: Visualization of ANP-LacZ expression by fluorescent β-galactosidase substrate fluorescein di β-D- galactopyranoside (FDG). Whole ventricles from either ANP-LacZ^{+} **(A)** or ANP-LacZ^{-} **(B)** hearts were incubated in FDG for 15 minutes, and then imaged by fluorescence microscopy. In ANP-LacZ^{+} hearts, the green fluorescent signal was readily detectable and was not uniform throughout the entire heart. In ANP-LacZ^{-} hearts, there was only a faint signal observed.

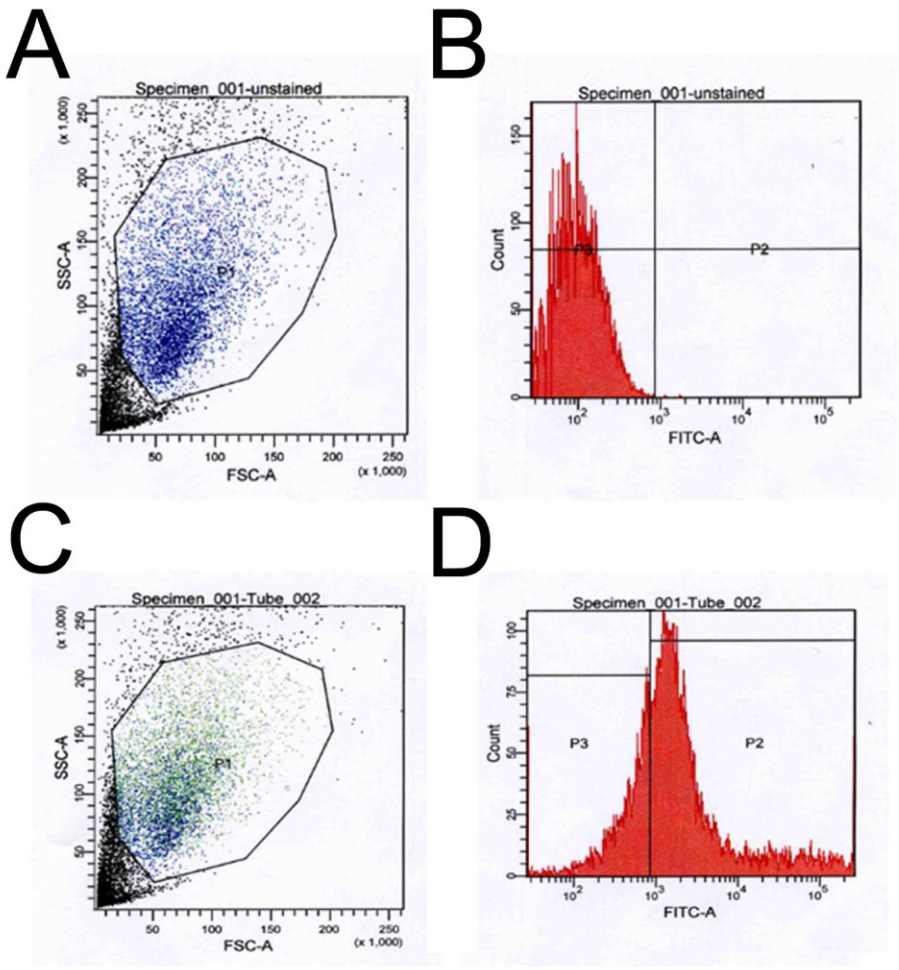

Figure 5.3.2: Representative Fluorescence Activated Cell Sorting (FACS) experiment using E11.5 ventricular cells from ANP-LacZ^{+} embryos. The top panel **(A&B)** corresponds to a representative control experiment in which cells from E11.5 ANP-LacZ^{+} ventricles were not treated with fluorescein di β-D- galactopyranoside (FDG) prior to FACS. The bottom panel **(C&D)** corresponds to a parallel experiment in which cells from E11.5 ANP-LacZ^{+} ventricles were incubated with (FDG). For control experiments, each dot in the outlined area seen in **(A)** corresponds to a single viable cell. The fluorescence intensity for each cell event is shown in **(B)** and corresponds to the background fluorescence. In FDG treated cells, there was a rightward shift in the overall fluorescence intensity of the cell population **(D).** A threshold fluorescence level was set based on the control experiments (vertical black line), and each individual cell was sorted based on whether fluorescence intensity was higher or lower than the threshold fluorescence value. The cell population with high fluorescence was designated as ANP^{+}, while the population with low fluorescence was designated as ANP^{-}.

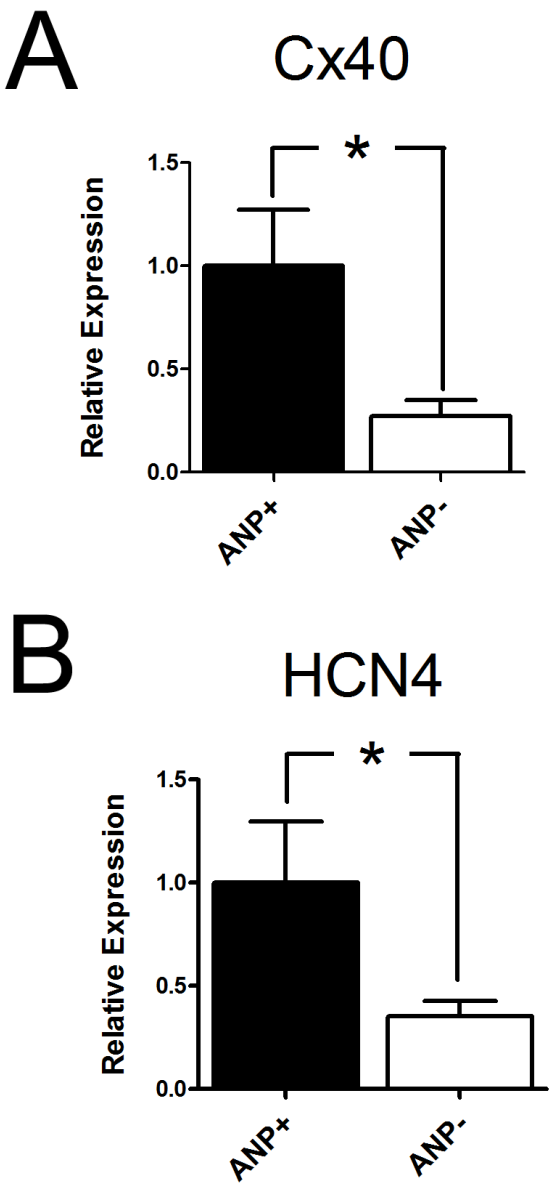

Figure 5.3.3: Gene expression analysis of ANP$^+$ and ANP$^-$ cell populations obtained from fluorescence activated cell sorting (FACS) of E11.5 ventricular cells. E11.5 ANP-LacZ ventricular cells were dispersed and incubated in FDG to identify cells expressing β-galactosidase (indicative of ANP promoter activity), and separated by FACS into populations of high ANP expression (designated ANP$^+$) and low ANP expression (designated ANP$^-$). The relative expression levels of Cx40 and HCN4 (normalized to GAPDH) were measured in ANP$^+$ and ANP$^-$ cells by real time quantitative PCR. Gene expression in the ANP$^+$ population served as the reference (i.e. expression=1.0). In the ANP$^+$ population there were significantly higher levels of expression of conduction system marker genes Cx40 **(A)** and HCN4 **(B)** compared to the ANP$^-$ cell population. N=4 independent experiments, analyzed in duplicate for each experiment. Each bar represents mean ± SEM. *$p < 0.05$, two-tailed unpaired t-test.

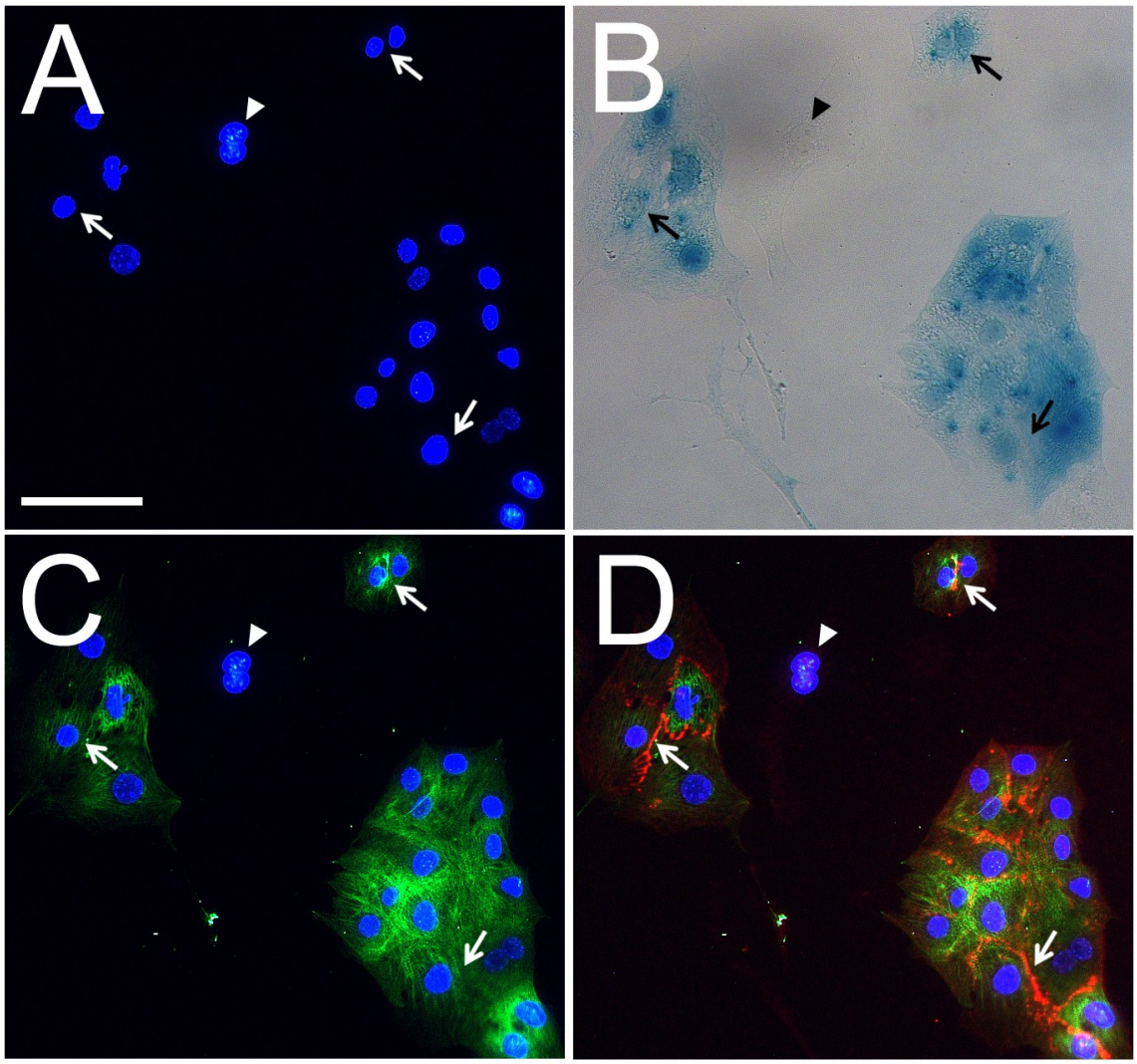

Figure 5.3.4: Expression of Cx40 protein in E11.5 ANP-LacZ^{+} cells. ANP-LacZ transgenic embryos were used to confirm expression of Cx40 in ANP^{+} cells (identified based on presence of blue chromogenic signal under brightfield microscopy). **A)** Field of cells labelled with Hoechst nuclear stain. **B)** Same field of cells imaged by brightfield to reveal the presence of ANP^{+} (blue) and ANP^{-} cells. **C)** Antibodies against sarcomeric myosin (green) were used to confirm the identity of cardiomyocytes. **D)** Overlayed image shows prominent Cx40 punctate labelling along the margins of ANP^{+} cardiomyocyte clusters (arrows). Conversely, Cx40 labelling was not observed in ANP^{-} cells (arrowhead). Scale bar= 25µm.

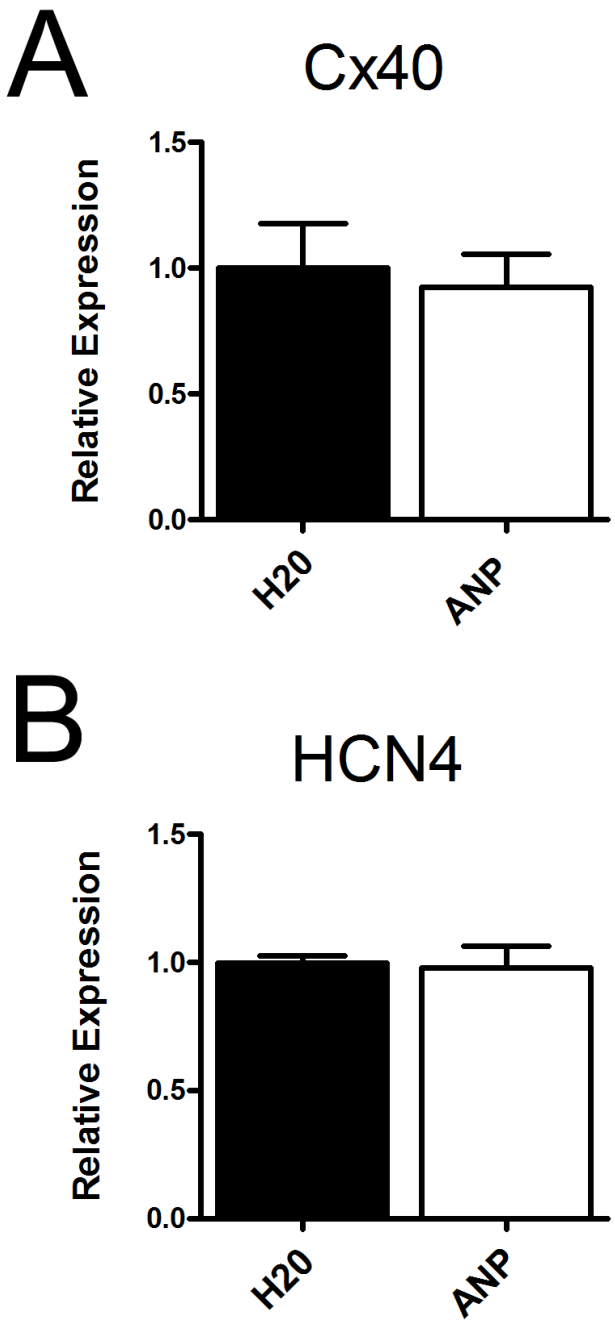

Figure 5.3.5: Effects of exogenous ANP on expression of conduction system marker genes Cx40 and HCN4. Compared to vehicle (H_2O) treated controls (Expression=1.0), the level of Cx40 **(A)** and HCN4 **(B)** gene expression did not vary significantly in response to exogenous ANP (100ng/ml), measured by qPCR. N=4 independent experiments/treatment group, analyzed in duplicate for each experiment. Each bar represents mean ± SEM. two-tailed unpaired t-test.

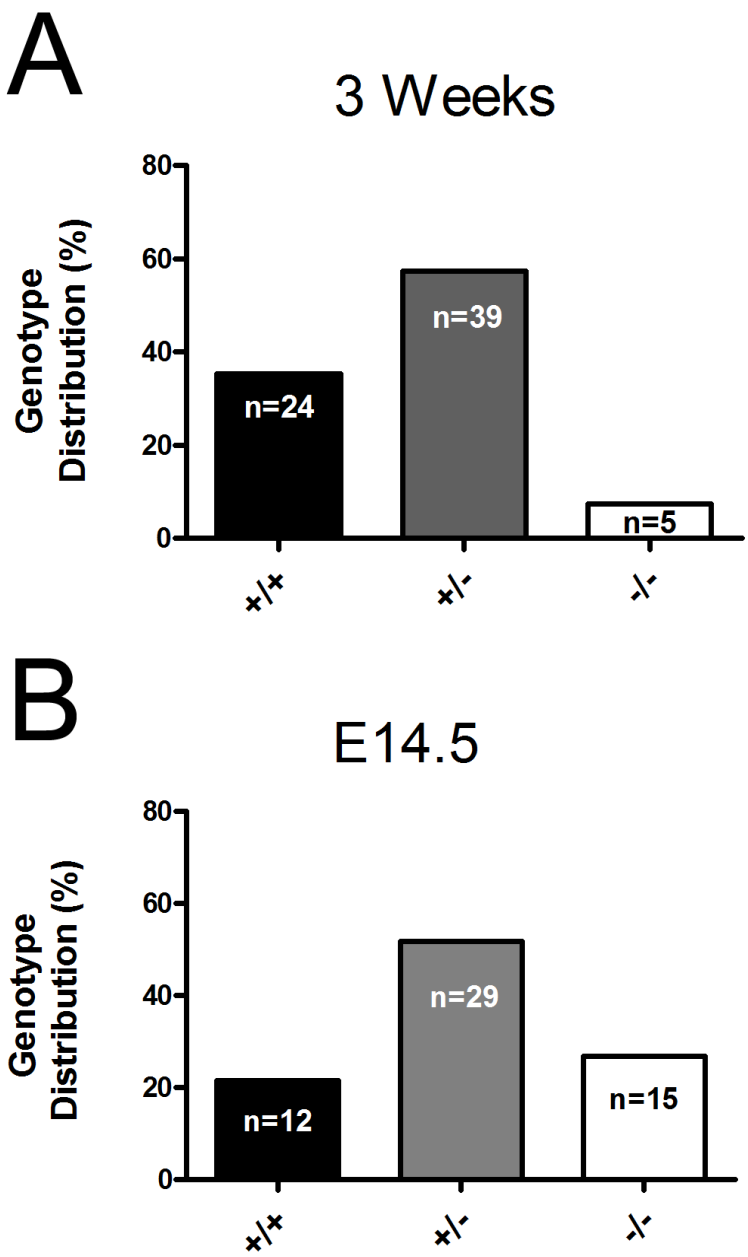

Figure 5.3.6: Genotype distribution resulting from NPRA$^{+/-}$ crosses at three weeks of age and E14.5. A) The relative genotype distribution of offspring resulting from heterozygous (NPRA$^{+/-}$ X NPRA$^{+/-}$) crosses revealed that only 7.3% of viable offspring harboured the NPRA$^{-/-}$genotype at 3 weeks of age (expected Mendelian frequency=25%). **B)** By contrast, 26.8% of E14.5 embryos resulting from heterozygous crosses had the NPRA$^{-/-}$ genotype. The numbers in each bar represent the total number of mice/embryos with each genotype.

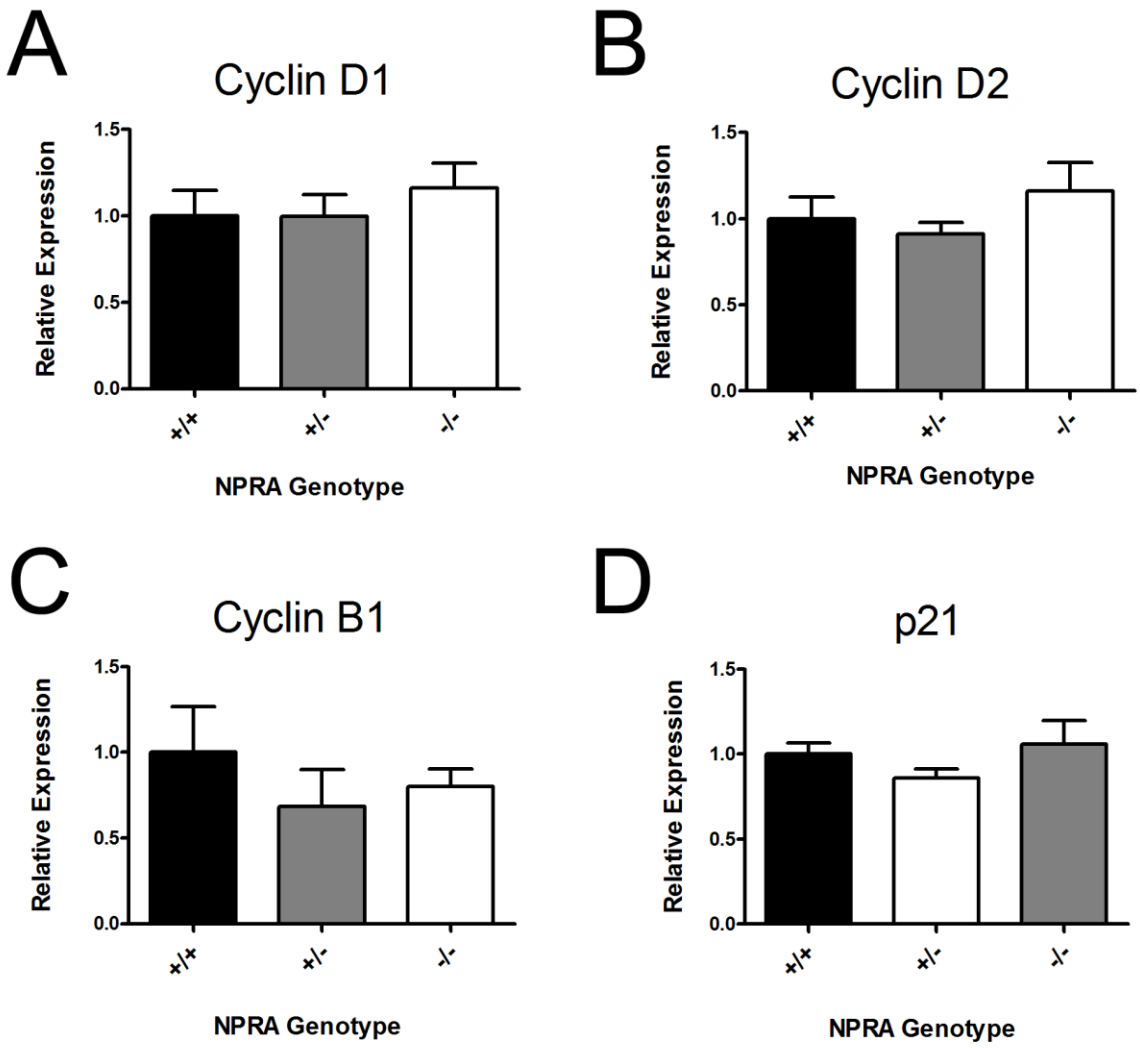

Figure 5.3.7: Graphical summary of the effects of NPRA ablation on expression levels of cell cycle regulating genes in E14.5 ventricles. Compared to the ventricles of wildtype embryos ($NPRA^{+/+}$; expression=1.0), there were no changes in the gene expression levels of either the positive cell cycle regulators Cyclin D1 **(A),** Cyclin D2 **(B)** and Cyclin B1 **(C)** or the cell cycle inhibitor p21 **(D)** associated with $NPRA^{+/-}$ or $NPRA^{-/-}$ genotype (analyzed by qPCR). N=3 independent RNA extractions /genotype, each extraction analyzed in duplicate. Each bar represents mean ± SEM. One-way ANOVA with Tukey post hoc test.

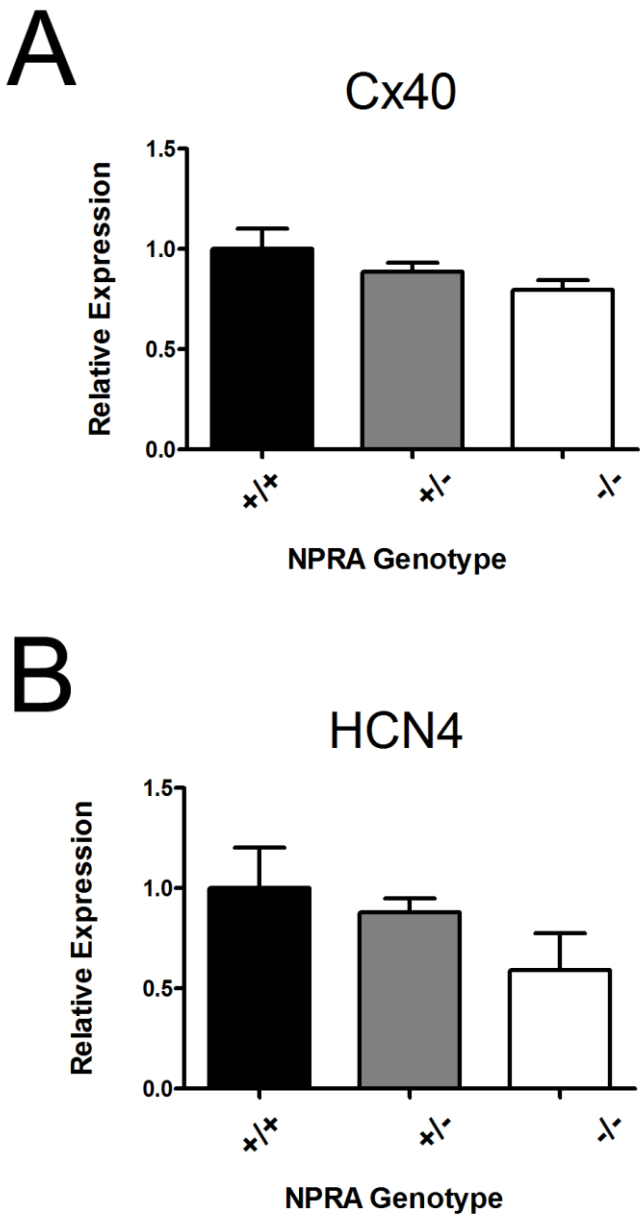

Figure 5.3.8: Expression of conduction system marker genes Cx40 and HCN4 in ventricles of E14.5 embryos lacking NPRA. Compared to the ventricles of wildtype embryos ($NPRA^{+/+}$; expression=1.0), trends toward reduced expression of conduction system markers Cx40 **(A)** and HCN4 **(B)** were observed in $NPRA^{+/-}$ and $NPRA^{-/-}$ ventricles and appeared to be dependent on *Npr1* gene dosage, but did not reach statistical significance (analyzed by qPCR). N=3 independent RNA extractions /genotype, each extraction analyzed in duplicate. Each bar represents mean ± SEM. One-way ANOVA with Tukey post hoc test.

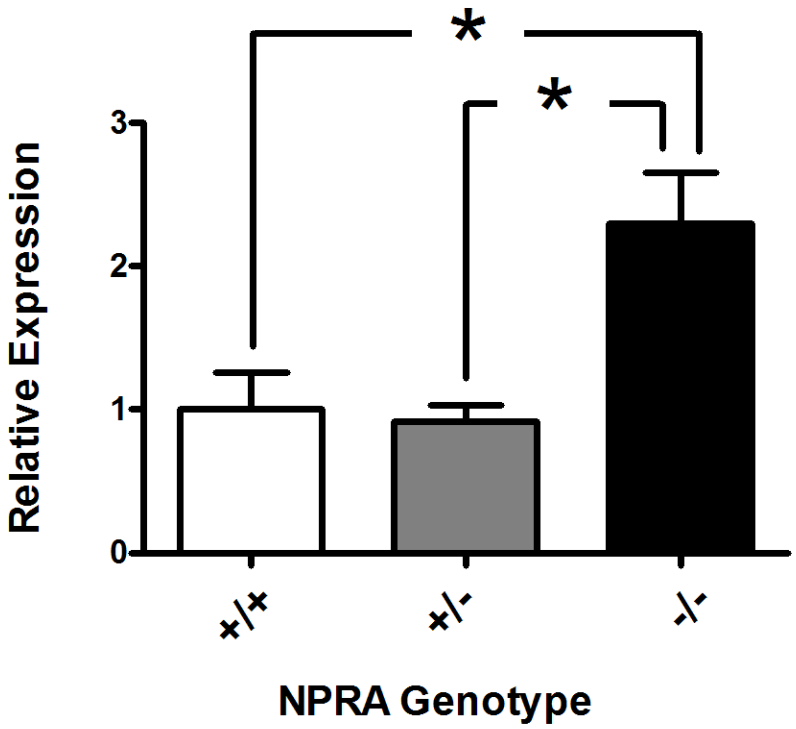

Figure 5.3.9: Expression of ANP in ventricles of E14.5 embryos lacking NPRA. Compared to wildtype ($NPRA^{+/+}$; expression=1.0), a significant (~ 2.5 fold) increase in expression of ANP mRNA was observed in ventricles of $NPRA^{-/-}$ embryos, but not in $NPRA^{+/-}$ ventricles (analyzed by qPCR). N=3 independent RNA extractions /genotype, each extraction analyzed in duplicate. Each bar represents mean ± SEM. *$p<0.05$, One-way ANOVA with Tukey post hoc test.

Figure 5.3.10: Visualization of ventricular conduction system development using the Cx40^{egfp} Knockin mouse model. **A)** Coronal section of E11.5 Cx40$^{egfp/+}$ heart revealed strong EGFP signal (corresponding to Cx40 expression) in the trabeculae (arrow) of the left ventricle (LV), while signal in the compact layer (arrowhead) was less prominent. In the right ventricle (RV), overall EGFP signal was less intense compared to the left ventricle, but displayed a similar spatial expression pattern with the strongest signal being detected in the trabecular myocardium. Strong EGFP signal was also detected in the atrial myocardium (right atrium; RA is displayed in this micrograph). **B)** Whole mount examination of a neonatal day 1 Cx40$^{egfp/+}$ pup revealed strong EGFP signal in both atrial chambers (RA) and (LA) and the coronary vasculature of the ventricles (arrow). In the left and right ventricles (LV and RV), EGFP signal could be detected from the exterior surface in regions corresponding to the underlying ventricular chambers but remained absent from the ventricular septum (S). **C)** An incision was made along the left ventricular free wall, and the each side was pulled back to expose the inner septal surface (delineated by the hashed line) as well as the inner surface of the left ventricular free wall (LVW). Using this method, a broad network of EGFP^{+} fiber-like bundles was observed extending in a parallel fashion from the base of left ventricular septum that corresponded to the left bundle branch (LBB). As the left bundle branch extended toward the apex of the left ventricle, it gave rise to an extensive network of overlapping Purkinje fibers (PF) that formed a honeycomb like pattern within the ventricular free wall. The inset, corresponding to the boxed region, more clearly demonstrates the honeycomb pattern (arrows). Scale bar=100μM.

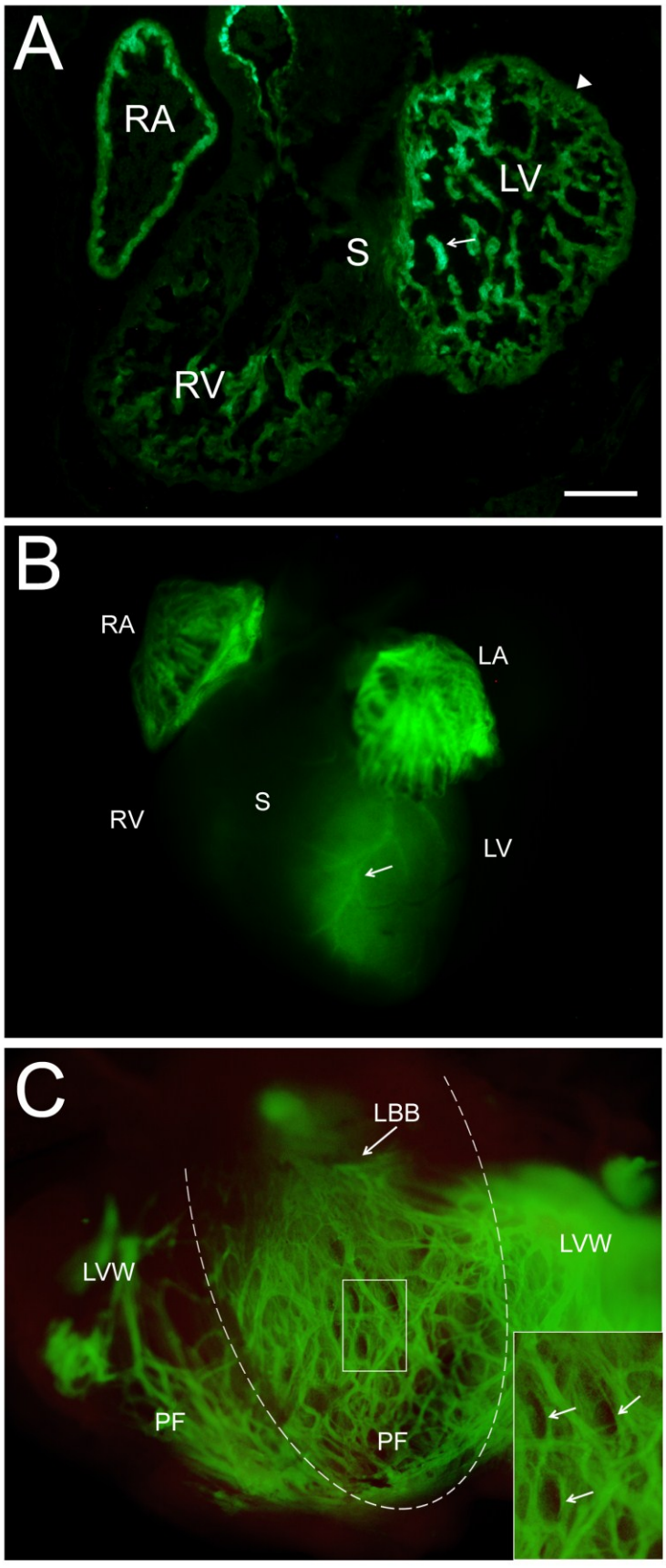
A
RA
LV
S
RV
B
RA
LA
S
RV
LV
C
LBB
LVW
LVW
PF
PF

Figure 5.3.11: Morphological characterization of conduction system development in mice lacking NPRA using the $Cx40^{egfp}$ model. **A)** In the left ventricles of neonatal day 1 pups with $Cx40^{egfp/+}$ /$NPRA^{+/+}$ genotype, the left bundle branch (LBB) was readily observable and was continuous with an extensively arborized Purkinje fiber (PF) network (described in greater detail in Figure 5.3.10). The inset, showing the boxed area, displays the typical honeycomb pattern that occured as a result of extensively overlapping Purkinje fibers. **B)** In the left ventricle of 1 out of 6 $Cx40^{egfp/+}$ /$NPRA^{+/-}$ pups examined thus far, an abnormal, hypoplastic Purkinje fiber network was observed. In some regions, there appeared to be only minimal continuity between the LBB and the Purkinje network within the left ventricular free wall (LVW) (arrows). Moreover, the extensive honeycomb pattern of the Purkinje fiber network observed in $Cx40^{egfp/+}$/ $NPRA^{+/+}$ ventricles appeared to be far less extensive in the ventricles of this $Cx40^{egfp/+}$ /$NPRA^{+/-}$ pup. The inset, showing the boxed area, shows a higher magnification of the thin strand extending from the LBB to the PF network in the LVW.

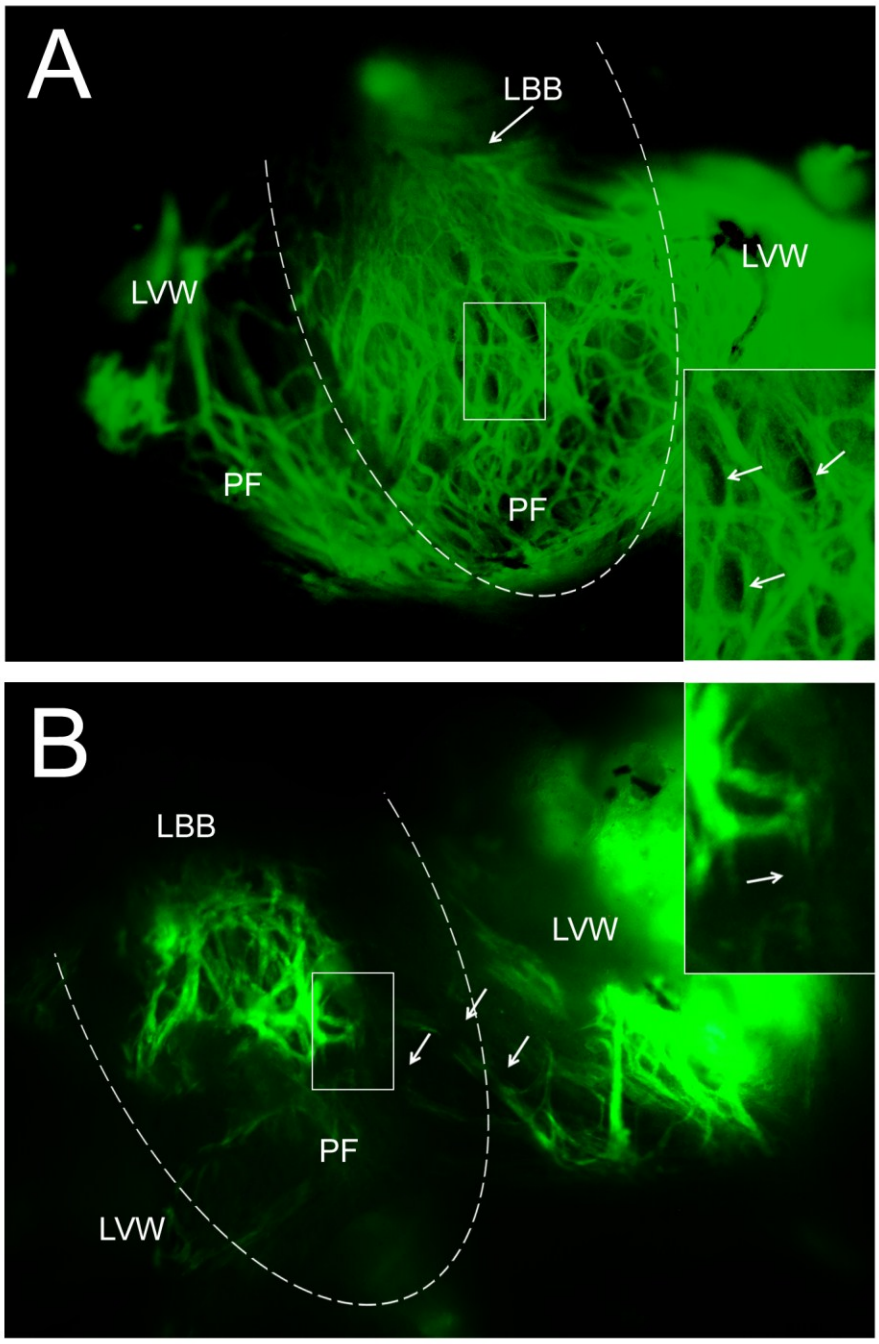
A
LBB
LVW
LVW
PF
PF
B
LBB
LVW
PF
LVW

Figure 5.3.12: Electrocardiographic analyses of mice lacking NPRA. A) Representative electrocardiogram (ECG) recording from a wildtype ($NPRA^{+/+}$) adult male mouse (~4 months old). **B-D)** Averaging views of ECGs measured from $NPRA^{+/+}$, $NPRA^{+/-}$ and $NPRA^{-/-}$ adult male mice were generated by taking the average values from 10 beats. In $NPRA^{+/+}$ **(B)** and $NPRA^{+/-}$ **(C)** mice , the P-wave was always readily observable, while in $NPRA^{-/-}$ mice **(D)** the P-wave tended to be smaller in amplitude and more difficult to detect. **E-G)** Compared to either $NPRA^{+/+}$ or $NPRA^{+/-}$ mice, the QRS interval was prolonged in $NPRA^{-/-}$ mice **(E)**, while the heart rate did not vary between genotypes **(F)**. In addition, prolonged P-R interval was observed in 1 out of 3 $NPRA^{+/-}$ mice, but did not reach statistical significance. A summary of heart rate (BPM; beats per minute) and QRS data is summarized in **(G)**. N=5 $NPRA^{+/+}$, 3 $NPRA^{+/-}$ and 3 $NPRA^{-/-}$ mice. Each bar represents mean ± SEM. *$p < 0.05$, One-way ANOVA with Tukey post hoc test.

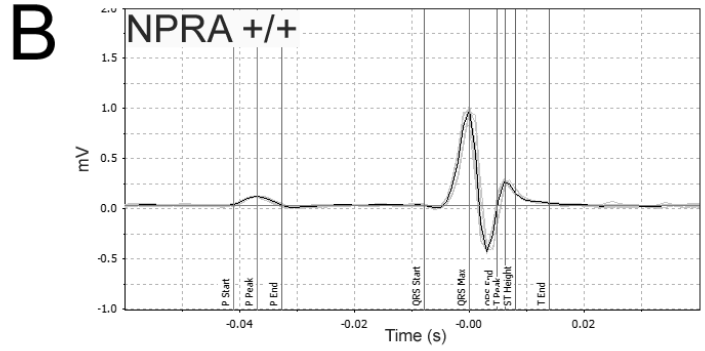

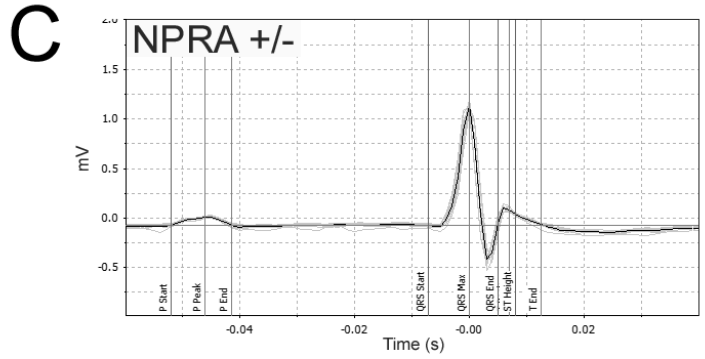

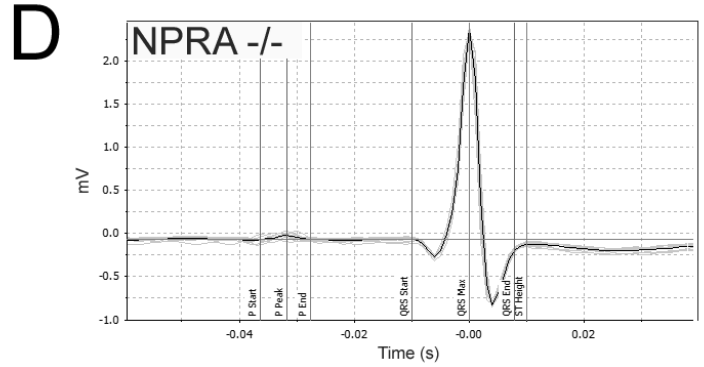

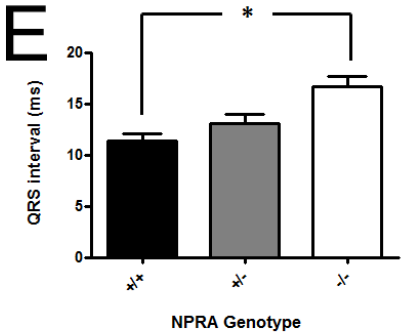

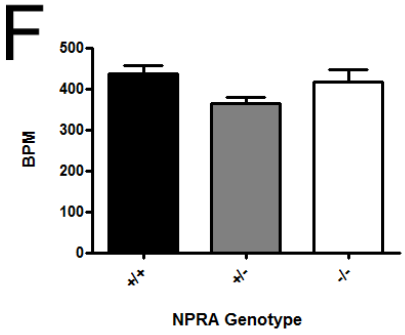

G

	+/+	+/-	-/-
HR	461 ± 20.4	356 ± 17.1	414 ± 29.5
QRS	11.2 ± 0.7	12.9 ± 0.9	16.9 ± 1.0

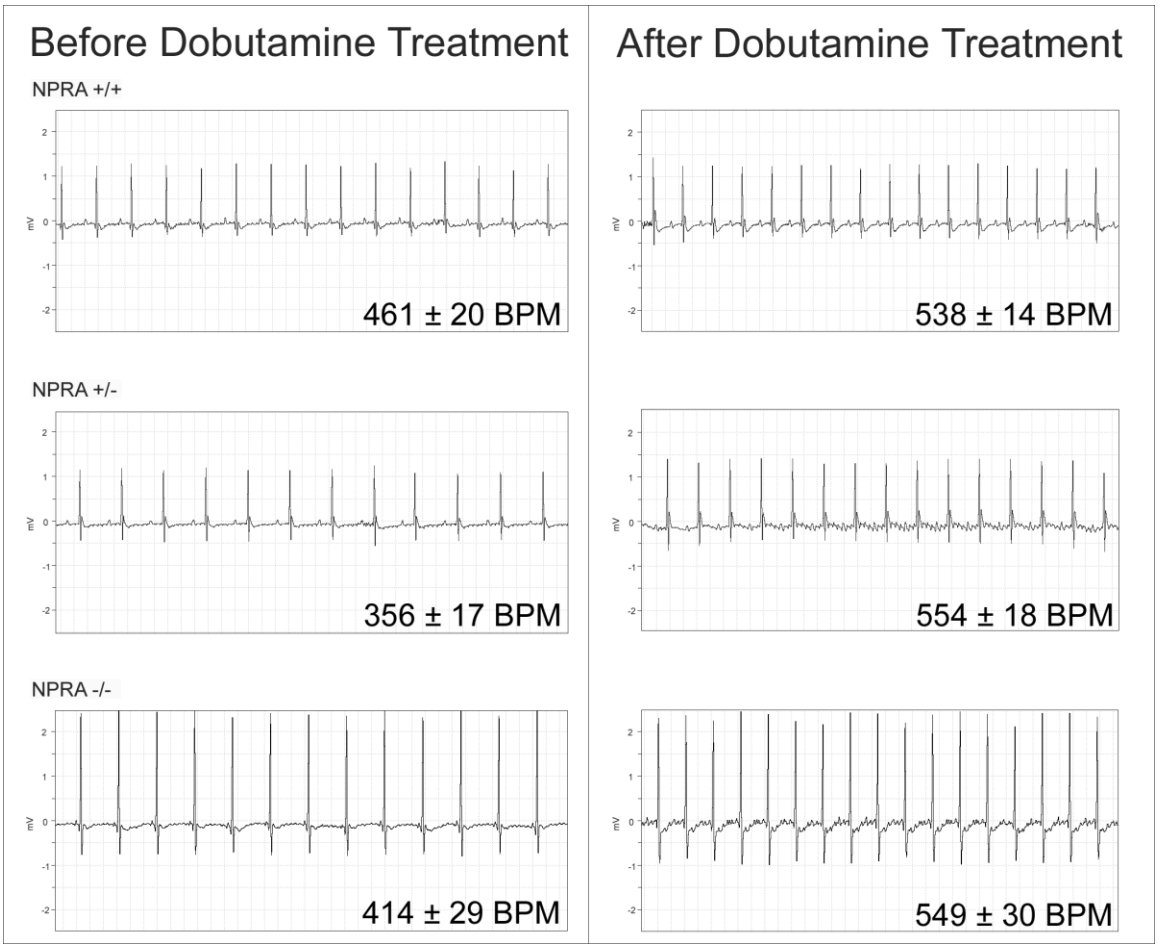

Figure 5.3.13: Electrocardiographic analyses of mice lacking NPRA following administration of dobutamine. Following administration of dobutamine (1.5µg/g) to adult (3-5 month old) male mice, there was a predictable increase in heart rate in mice with each genotype ($NPRA^{+/+}$, $NPRA^{+/-}$ and $NPRA^{-/-}$). The average heart rate before and after dobutamine injection are listed under each ECG recording. The data presented are single representative traces from a total of N=5 $NPRA^{+/+}$, 3 $NPRA^{+/-}$ and 3 $NPRA^{-/-}$ mice.

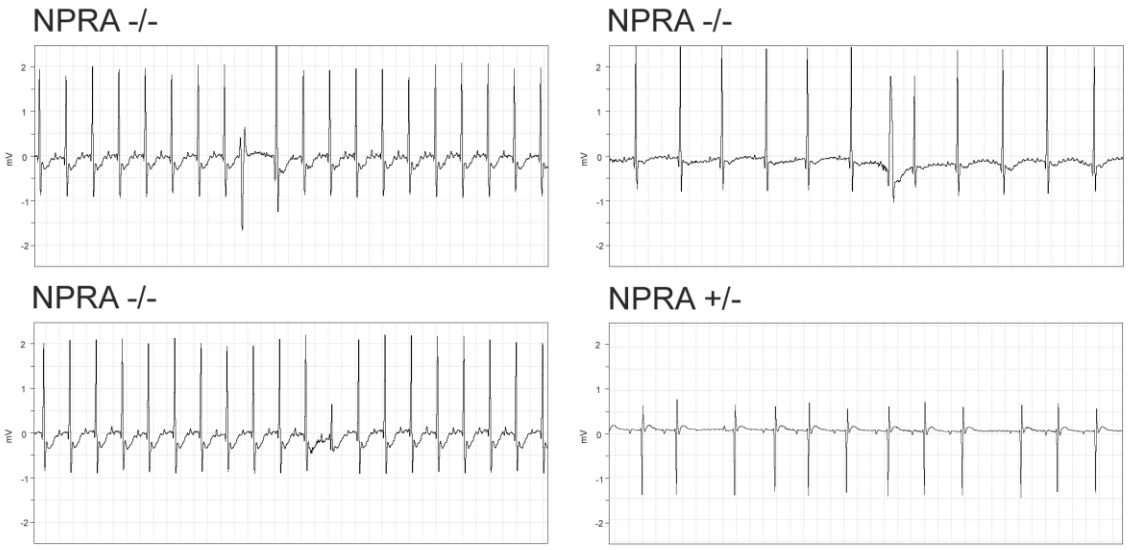

Figure 5.3.14: Evidence of irregular electrical activity triggered by sympathetic activation in mice lacking NPRA. Electrocardiogram (ECG) analyses were recorded from adult (3-5 months old) male mice lacking NPRA to determine if sympathetic activation via injection of dobutamine (1.5µg/g) could trigger any arrhythmic activity. Following administration of dobutamine, there was evidence of isolated periods of irregular electrical activity in $NPRA^{+/-}$ and $NPRA^{-/-}$ mice manifested as abnormal/skipped QRS complexes, which occurred at an incidence of ~3 events per mouse per 20 minute recording. The data presented are representative traces from a total of N=5 $NPRA^{+/+}$, 3 $NPRA^{+/-}$ and 3 $NPRA^{-/-}$ mice.

CHAPTER 6: DISCUSSION

6.1 Summary of Results

The overall aim of my doctoral thesis work was to characterize how specific factors regulate the proliferation and differentiation of cardiac progenitor cells (CPCs) and cardiomyocytes derived from the mouse embryonic ventricles at the developmental stage of E11.5. In particular, our interest in deciphering the molecular features of CPCs and the factors regulating their ability to divide and differentiate was driven by the potential that CPCs hold for use in future cell based therapies for myocardial repair.

To date, there is very little information regarding the beneficial or detrimental effects of cardiovascular drugs on cell transplantation therapies. Results presented in this thesis provided evidence that exposure to nifedipine, a member of the dihydropyridine class of Ca^{2+} channel blockers, was associated with reduced cell cycle activity of CPCs and impaired assembly of the contractile apparatus *in vitro*. Furthermore, following transplantation of E11.5 cells (containing CPCs); a reduction in graft size was observed in the ventricles of mice receiving daily doses of nifedipine compared to untreated animals.

Our efforts to characterize CPC proliferation and differentiation were also strongly motivated by the desire to provide novel insight into cellular mechanisms underlying proper heart formation. Despite knowledge of the dynamic expression pattern of ANP in the ventricles during the developmental period, a specific role for this hormone/paracrine factor in cardiogenesis has yet to be described. Results presented in this thesis provided evidence that ANP, via guanylyl cyclase linked receptor signalling pathways, caused a reduction in proliferation of E11.5 CPCs, suggesting that altered

proliferation kinetics during the developmental period could be a contributing factor to specific forms of congenital heart disease associated with dysregulated expression of ANP.

6.2 The Effects of Ca^{2+} Channel Blockade on Proliferation and Differentiation of Cardiac Progenitor Cells

6.2.1 Context

In Canada, there are an estimated 70,000 heart attacks every year which equates to one heart attack every 7 minutes (Heart and Stroke, www.heartandstroke.ca). Furthermore, an estimated 500,000 Canadians are currently living with heart failure and 50,000 new cases are diagnosed each year (Ross et al., 2006). Despite significant improvements in pharmacological therapies and biomedical technologies, the prognosis for heart failure patients remains grim with a five year age-adjusted mortality rate of 45% (Ross et al., 2006). For the most severe forms of cardiac dysfunction, heart transplantation remains the only effective therapy which can significantly improve longevity and quality of life (Copeland et al., 2004; Kasirajan et al., 2012). However, the number of eligible patients has persistently exceeded the number of available donor hearts (McManus et al., 1993; Heim et al., 2013) thus necessitating the development of innovative new therapies which are more broadly accessible. To this end, donor cell transplantation has emerged as a promising strategy to improve heart function by replenishing the damaged myocardium with new cardiomyocytes (Zhang and Pasumarthi, 2008).

While there is no consensus on the most suitable cell type, CPCs possess several features which make them an attractive candidate including (i) cardiomyogenic potential (ii) high rates of proliferation and (iii) low risk of tumor formation. According to Canadian clinical care guidelines, most patients who could benefit from cell transplantation therapy would be taking multiple cardiovascular drugs (McKelvie et al., 2013), thus highlighting the need to characterize potential interactions between drugs and transplanted cells. With this in mind, one of the primary aims of this thesis was to determine the effects of the DHP Ca^{2+} channel antagonist nifedipine on proliferation and differentiation of E11.5 CPCs *in vitro* and also assess the impact of systemic administration of nifedipine on graft size formation following transplantation of E11.5 ventricular cells (containing CPCs) into adult recipient mice.

6.2.2 Embryonic and Post-Natal Cardiac Progenitor Cells

The heart is formed from mesodermal progenitor cells located in the bi-lateral cardiogenic fields in the regions of the anterior lateral plate mesoderm (Kirby, 2007). During the process of cardiac development, it is generally believed that these progenitor cells rapidly proliferate and simultaneously differentiate toward mature cardiovascular lineages including working cardiomyocytes, cardiac conduction system myocytes as well as vascular, endocardial and epicardial cell types (Buckingham et al., 2005). Consistent with this notion, it was demonstrated that a sub-population of differentiating ES cells expressing the primitive streak marker *brachyury* and the vascular endothelial growth factor receptor 2 (VEGFR2, Flk-1) could give rise to cell lineages expressing endothelial, vascular smooth muscle and cardiomyocyte markers (Kattman et al., 2006). Similarly,

molecular analyses of cells isolated from the anterior region of the neural plate and head fold stage embryos were shown to express cardiac, endothelial and vascular smooth muscle associated genes following expansion in culture (Kattman et al., 2006), providing evidence that multipotent cardiovascular progenitor cells also exist *in vivo* at early stages of cardiac development. At the later developmental stage of E9.5, isolation of $Nkx2.5^+$ populations revealed that a sub-population of $Nkx2.5^+$ progenitor cells were also positive for the stem cell factor receptor, c-kit (Wu et al., 2006). Interestingly, these $Nkx2.5^+/c\text{-}kit^+$ cells were shown to be capable of differentiating toward the cardiomyocyte and vascular smooth muscle cell lineages, but did not express endothelial cell markers, indicating an early separation of the endothelial and myogenic lineages.

Previous work from our laboratory demonstrated that at E11.5, the myocardial layer of the murine ventricles was composed of approximately 40% undifferentiated $Nkx2.5^+$ CPCs and 60% cardiomyocytes expressing sarcomeric proteins (Zhang and Pasumarthi, 2007). In addition, lineage tracing studies revealed that E11.5 $Nkx2.5^+$ CPCs retained the potential to differentiate toward both working cardiomyocytes and putative conduction system cardiomyocytes (McMullen et al., 2009). Analyses at later developmental stages revealed a decline in the percentage of $Nkx2.5^+$ CPCs, which were shown to represent only 7% of the myocardial cell population in the E18.5 myocardium, likely due to the progressive differentiation toward mature myocardial lineages. Despite substantial evidence of undifferentiated cardiac stem/progenitor cells in the adult myocardium (Hierlihy et al., 2002; Beltrami et al., 2003; Oh et al., 2003; Martin et al., 2004), it remains uncertain whether these cell populations are remnants from the embryonic heart or represent mesodermal progenitors which migrate to the heart from

other compartments such as the bone marrow. Intriguingly, distinct, non-overlapping populations of adult progenitor/stem cell types appear to exist based on unique molecular signatures of internal and external cell surface markers including c-kit (Beltrami et al., 2003), stem cell antigen 1 (Sca-1)(Oh et al., 2003) and the ATP-binding cassette transporter (Abcg2) (Martin et al., 2004), which raises further questions about the embryonic/post-natal origin of these cell populations.

Regardless of their origin, common features of both embryonic and post-natal cardiac progenitors appear to be high proliferative capacity and the ability to differentiate toward mature cardiovascular lineages, making them attractive candidate cell types for myocardial repair. Consistent with this idea, recent Phase I clinical trials using autologous c-kit^{+} adult cardiac stem cells (CSC) (Bolli et al., 2011) and cardiosphere derived stem cells (Makkar et al., 2012) demonstrated reduced infarct size in patients suffering from ischemic heart disease or myocardial infarction. However, the mechanism responsible for autologous stem cell mediated myocardial repair remains unclear.

Results from this thesis, provided evidence that interactions between the pharmacological drug nifedipine and transplanted CPCs of embryonic origin had detrimental effects on grafting efficiency. These results raise the possibility that similar effects would be observed following transplantation of CSCs or other transplanted cell types and thus highlights the need for a more rigorous examination of the interactions between a broader spectrum of commonly used pharmacological drugs and transplanted cell types.

6.2.3 Intracellular Ca^{2+} Homeostasis and Cell Proliferation

In the adult heart, Ca^{2+} is a versatile second messenger that is most recognized for its essential role in cardiomyocyte contraction via the EC coupling mechanism (Bers, 2002). More recently, however, the role of Ca^{2+} in signal transduction via "excitation-transcription" coupling mechanisms has gained more attention and is recognized for its importance in regulating the hypertrophic response in pathological settings (Anderson, 2000; Maier and Bers, 2002). Among the Ca^{2+} activated proteins, Calmodulin (CaM) and Ca^{2+}/CaM dependent protein kinases (CaMK) as well as the phosphatase Calcineurin (CaN) figure prominently. For example, the transcription factors MEF2c and GATA4, which are involved in the hypertrophic process, have been shown to be activated by signalling cascades involving CaMK (Passier et al., 2000) and CaN (Molkentin et al., 1998) respectively.

Many of the same Ca^{2+} binding proteins and Ca^{2+} sensitive transcription factors (e.g. MEF2c and GATA4) involved in hypertrophic signalling in the adult myocardium are also critically involved in the cardiogenic process by orchestrating the cardiac specific gene expression program (Puceat and Jaconi, 2005). Accordingly, disruption of intracellular Ca^{2+} homeostasis would be expected to disrupt the normal program of proliferation and differentiation of embryonic CPCs and cardiomyocytes. Indeed, Porter and colleagues (2003) documented abnormal cardiac morphology following exposure of whole embryos (E7.5-E8.5) to the DHP Ca^{2+} channel antagonist nifedipine. Similarly, exposure of early chick embryos to the non-DHP Ca^{2+} channel blocker diltiazem was associated with impaired cardiomyogenesis in posterior regions of the heart fields which contain a significant number of undifferentiated CPCs (Linask and Linask, 2010). At the

cellular level, however, less is known about the effects of Ca^{2+} channel blockade on proliferation and differentiation kinetics of embryonic CPCs and cardiomyocytes. To address this issue work in this thesis examined the effects of nifedipine on primary cultured CPCs and cardiomyocytes from the E11.5 murine ventricles.

Using a tritiated-[^{3}H] thymidine incorporation assay as an index of proliferation (LI), we observed that 10μM nifedipine was associated with a significant reduction in proliferation of E11.5 CPCs, but had no effect on cardiomyocytes. By contrast, 100μM nifedipine essentially abolished proliferation in both the CPC and cardiomyocyte populations. Based on these results, we speculated that E11.5 CPCs and cardiomyocytes may express different complements of voltage gated Ca^{2+} channels with varying sensitivities to DHP antagonists and that Ca^{2+} currents through these channels are linked to the cell cycle machinery. Consistent with this view, L-type Ca^{2+} channels, which are potently inhibited by DHPs (IC_{50}< 1μM) (Katzung, 2009), were expressed in the E11.5 ventricular myocardium along with T-type Ca^{2+} channels, which are less potently inhibited by DHPs (IC_{50} 10-100μM) (Kumar et al., 2002; Shcheglovitov et al., 2005; Perez-Reyes et al., 2009). Thus, it is possible that proliferation mechanisms in CPCs may rely more on Ca^{2+} influx via L-Type Ca^{2+} channels, while in cardiomyocytes; proliferation may be more dependent on T-type Ca^{2+} current. Further support for this idea comes from our observation that $Ca_v1.2$ immunolabelling was more prominent in the plasma membranes of CPCs versus cardiomyocytes at the E11.5 stage. While we did not perform immunolabelling using T-type Ca^{2+} channel antibodies, information from such experiments could provide additional insight into the relative contribution of

different voltage gated Ca^{2+} channels in regulating proliferation in cell subpopulations in the embryonic heart.

6.2.4 Potential Mechanisms of L-Type versus T-type Ca^{2+} Channels in Regulating Proliferation

In various cell types, from both cardiovascular and non-cardiovascular origins, there is substantial evidence that T-type Ca^{2+} channels are critically involved in regulating proliferation, while L-type Ca^{2+} channels play a more minor role in this regard (Li et al., 2005; Panner and Wurster, 2006; Oguri et al., 2010). For example, in neonatal rat ventricular cardiomyocytes, inhibition of T-type Ca^{2+} channels using either 50μM $NiCl_2$, or 1μM mibefradil was associated with a reduction in glucose stimulated cell cycle activity, while 10μM nifedipine had no effect (Li et al., 2005). Similarly, mibefradil (T-type Ca^{2+} channel blocker) but not 10μM diltiazem (non-DHP L-type Ca^{2+} channel antagonist) was able to effectively inhibit cell proliferation of serum stimulated pulmonary artery smooth muscle cells (Rodman et al., 2005). Together, these reports highlight the specific involvement of T-type Ca^{2+} currents in regulating myocyte proliferation and are consistent with the view that T-type Ca^{2+} current may also be involved in regulating proliferation of E11.5 cardiomyocytes. It should be noted, however, that a limitation to dissecting the cellular effects of T-type Ca^{2+} currents is the lack of specific T-type Ca^{2+} channel antagonists (Lory et al., 2006). Because of this limitation, several studies have confirmed the specific involvement of T-type Ca^{2+} channels in regulating proliferation by also using the siRNA approach to interfere with expression of specific T-type Ca^{2+} channel isoforms (e.g. $Ca_v3.1$ and/or $Ca_v3.2$)

(Li et al., 2005; Oguri et al., 2010). Future work aimed at carrying out similar experiments in primary cultured E11.5 ventricular cell cultures would certainly be useful to confirm the specific involvement of T-type Ca^{2+} channels in modulating proliferation of CPCs and cardiomyocyte subpopulations.

While pharmacological and siRNA approaches targeting T-type Ca^{2+} channels have been shown to modulate cell proliferation, the underlying signalling mechanisms remain poorly defined. The family of Cyclins, along with their catalytically active partners (Cyclin dependent kinases; CDK) are important regulators of cardiac cell proliferation during the embryonic period (Brooks et al., 1997; Hotchkiss et al., 2012). In various cell types, the activity and/or expression of Cyclins and CDKs has also been shown to be dependent on Ca^{2+} sensitive upstream regulators including CaM (Kahl and Means, 2003; Koledova and Khalil, 2006) and phosphorylated extracellular signal-regulated kinases (ERK) (Shukla et al., 2005; Schultz et al., 2006). For example, depletion of intracellular Ca^{2+} levels in vascular smooth muscle cells was associated with reduced translocation of ERK to the nucleus, decreased expression of Cyclin D1 and delayed progression into the S-phase of the cell cycle (Shukla et al., 2005). Conversely, depletion of intracellular Ca^{2+} stores was shown to increase the expression of CDK inhibitors (p21 and p27) and reduce expression of several Cyclins including Cyclin D1 in cultured C6 glioma cells (Chen et al., 1999). Results presented in this thesis demonstrated that nifedipine was associated with a reduction in expression of Cyclin B1 and also an increase in the expression of the CDK inhibitor p27 and thus implicate similar signalling systems in the regulation of embryonic cardiac cell populations. In an effort to determine the specific upstream effectors which regulate expression of cell cycle

genes in E11.5 ventricular cells, our group has generated preliminary data showing that Ca^{2+} channel blockade using 100μM (but not 10μM) nifedipine was associated with a drastic reduction in total phospho-ERK levels by Western blot analysis (data not shown). Future work aimed at examining the subcellular localization of specific proteins (e.g. CaM, CaMKII, phospho-ERK, Cyclins and CDKs) in CPCs and cardiomyocytes using the NCRL approach could provide valuable insight into the molecular mechanisms underlying proliferative control of embryonic CPCs and cardiomyocytes.

6.2.5 The Effects of Nifedipine on the Assembly of the Contractile Apparatus

Several of the same Ca^{2+} signalling cascades involved in regulating cell proliferation appear to be critical for proper assembly of sarcomeric units into the contractile apparatus of cardiomyocytes (Puceat and Jaconi, 2005). For example, in neonatal rat ventricular myocytes, depletion of intracellular Ca^{2+} using the chelator BAPTA/AM or pharmacological inhibition of myosin light chain kinase (MLCK), which is a Ca^{2+}/CaM dependent enzyme (Sweeney et al., 1993), resulted in impaired sarcomeric organization (Aoki et al., 2000). Similarly, impaired myofibrillogenesis was observed in ES-cell derived cardiomyocytes by using either the BAPTA/AM approach or by pharmacological inhibition of CaMK (Li et al., 2002). Interestingly, in both of these studies, myofibrillogenesis could be rescued by restoring cytosolic Ca^{2+} using Ca^{2+} ionophores. Consistent with these observations, work in this thesis demonstrated that pharmacological blockade of Ca^{2+} influx using nifedipine was associated with impaired myofibrillogenesis of E11.5 cardiomyocytes which was evaluated based on a reduction in cardiomyocyte size and overt disorganization of the contractile apparatus.

It is noteworthy that in our experiments, a similar degree of sarcomeric disorganization was observed in response to either 10μM or 100μM nifedipine. Thus, while 10μM nifedipine was not sufficient to reduce cell cycle activity of E11.5 cardiomyocytes (based on [^{3}H]-thymidine experiments), this concentration was able to disrupt myofibrillogenesis, thus suggesting that distinct Ca^{2+} pools may be involved in regulating these two processes. Interestingly, differentiation of cultured murine neuronal stem/progenitor cells was impaired following exposure to 5μM nifedipine (D'Ascenzo et al., 2006), implicating L-type Ca^{2+} current in regulating transcriptional networks involved in the differentiation process in these cells and raising the possibility that similar mechanisms exist in embryonic cardiomyocytes. If L-type and T-type Ca^{2+} channels do in fact have distinct regulatory roles in modulating proliferation and differentiation of embryonic cardiac cells, this is likely achieved by the specific spatial distribution of each Ca^{2+} channel isoform in the plasma membrane as well as the subcellular localization of specific Ca^{2+} binding proteins and enzymes.

To investigate potential molecular mechanisms underlying impaired E11.5 cardiomyocyte differentiation, we examined the effects of nifedipine on expression of a panel of cardiogenic transcription factors GATA4, Hand2, MEF2c and Tbx5 (Song et al., 2012). While a modest, but significant, reduction in expression of Tbx5 was observed in response to 100μM nifedipine, expression of GATA4, MEF2c and Hand2 remained unchanged. Aside from gene expression levels, the subcellular localization of transcription factors is a key determinant of their transcriptional activity. Previously, it was shown that disruption of intracellular Ca^{2+} homeostasis in embryonic cardiomyocytes was associated with mislocalization of MEF2c in the cytoplasm and a reduction in

expression of MEF2c target genes including MLC2v (Lynch et al., 2005). Consistent with these findings, our data showed that in response to 100μM nifedipine, MEF2c was absent in the nucleus and was confined to the cytoplasm as small punctae. Moreover, we also observed a decrease in the expression of the gene encoding ANP (*Nppa*), which is a known transcriptional target of MEF2 transcription factors (Morin et al., 2000), further supporting the view that mislocalized MEF2c in the cytoplasm contributes to impaired myofibrillogenesis in E11.5 cardiomyocytes in response to Ca^{2+} channel blockade.

The concentrations of nifedipine (10μM and 100μM) used for experiments in this thesis were initially selected based on the report by Porter and colleagues (2003) which demonstrated that these concentrations of nifedipine (but not 1μM) were capable of eliciting a reduction in cardiac Ca^{2+} transients in cultured mouse embryos. It should be noted, however, that these concentrations are considerably higher than reported plasma concentrations of various formulations of nifedipine. Specifically, in a study comparing the pharmacokinetics of a once daily Gastro-Intestinal Therapeutic System (GITS) formulation of nifedipine to standard capsules or prolonged action tablets, the peak plasma concentration for each formulation was: (capsule: 196 ng/ml, prolonged action tablet: 85.5 ng/ml and GITS: 30.5 ng/ml) (Toal, 2004). However, it is also important to note that the reported plasma concentrations of nifedipine with all of these formulations could be achieved only after administering single or multiple doses ranging from 10-60 mg per individual. The concentrations used in our cell culture experiments corresponded to either 3,463ng/ml (10μM) or 34,630ng/ml (100μM) of nifedipine. Importantly, however, ~98% of nifedipine is bound to serum proteins under both *in vivo* and *in vitro* conditions (Rumiantsev et al., 1989) and thus biologically unavailable at its site of

pharmacological action (Meijer and Van der Sluijs, 1987). Therefore, in our *in vitro* culture system where cells were grown in medium containing 10% FBS, it is likely that only a small fraction of the total drug added to the medium remained unbound from serum proteins and therefore may in fact be reflective of clinically relevant drug concentrations.

6.2.6 The Effects of Systemic Administration of Nifedipine on Cell Transplantation

One of the defining features of CPCs that makes them an attractive candidate to be used in transplantation therapies is their high rate of proliferation which could ultimately translate into larger graft size formation. This concept of graft expansion due to proliferation *in vivo* was exemplified previously when grafts formed following transplantation of ES-cell derived cardiomyocytes underwent a 7-fold increase in size over a 4 week period (Laflamme et al., 2005). This dramatic increase in graft size was attributed to proliferation of transplanted cells based on their expression of cell cycle markers (Laflamme et al., 2005). Work from our laboratory has also demonstrated that transplantation of E11.5 cells containing a significantly higher proportion of CPCs can repopulate diseased hearts at a higher efficiency compared to E14.5 cells (unpublished data, manuscript in preparation), which could be due to higher proliferative activity of CPCs compared to cardiomyocytes.

Currently, there is scant information on the beneficial or detrimental effects of pharmacological compounds on the efficiency of cell transplantation therapies. This information, however, is directly relevant to the field of regenerative medicine since most patients who could benefit from cell transplantation therapy would most likely be taking

multiple drugs based on recommended Canadian and international guidelines for managing chronic cardiovascular diseases (Hunt, 2005; McKelvie et al., 2013; McMurray et al., 2013). In an effort to initiate investigations into this important issue, work from this thesis examined the effects of nifedipine on graft size formation following transplantation of E11.5 ventricular cells. Nifedipine was selected for these experiments primarily based on the findings of Porter and colleagues (2003), which demonstrated that nifedipine mediated Ca^{2+} channel blockade was associated with impaired cardiogenesis and altered cardiac gene expression in whole mouse embryos exposed to this drug. In addition, nifedipine was selected based on the much higher binding affinity of dihydropyridines for Ca^{2+} channels in the open and inactivated states which are achieved more frequently at depolarized membrane potentials (Hockerman et al., 1997; Katzung, 2009). Because embryonic cardiomyocytes display relatively high resting membrane potentials compared to mature cardiomyocytes (Sperelakis and Shigenobu, 1972; He et al., 2003), nifedipine was expected to inhibit Ca^{2+} influx into E11.5 cardiomyocytes with relatively high potency. On the other hand, the membrane potential of CPCs remains poorly defined and therefore the relative potency of DHP and other classes of Ca^{2+} channel blockers in these cells remains uncertain.

Given the reduction in proliferation of CPCs and cardiomyocytes observed in response to nifedipine treatment *in vitro*, we hypothesized that systemic administration of nifedipine would translate into smaller graft sizes following cell transplantation due to reduced proliferation *in vivo*. Indeed, results from transplantation experiments indicated that total graft volume occupied by transplanted NCRL cells was significantly reduced in nifedipine treated animals compared to vehicle treated controls. These results provided

strong evidence that interactions between transplanted cells and systemically administered drugs could interfere with the effectiveness of cell based therapies. While we have not yet examined whether this effect is due to reduced cell cycle activity of transplanted NCRL cells *in vivo*, future work dedicated to assessing the proliferation kinetics of transplanted cells based on either expression of cell cycle markers such as PH3 or a tritiated thymidine labelling approach could be used to gain valuable insight into this important issue. Additionally, while we speculated that reduced graft size was attributed to decreased proliferation, a limitation to our approach is the inability to definitively rule out the possibility that reduced engraftment into host myocardium was also a contributing factor.

It should also be noted that while DHP Ca^{2+} channel blocking drugs are commonly used to manage hypertension (Chobanian et al., 2003; Katzung, 2009), they are generally not prescribed to patients suffering from heart failure (McKelvie et al., 2013; McMurray et al., 2013). Conversely, among the most commonly prescribed pharmacological drugs for MI and heart failure patients are β-adrenergic receptor antagonists, angiotensin converting enzyme (ACE) inhibitors, angiotensin receptor blockers and diuretics (McKelvie et al., 2013). Conceivably, some of these drugs could have mechanisms of action that are common with nifedipine via modulation of intracellular Ca^{2+} levels in embryonic cardiomyocytes and/or CPCs. For example, stimulation of β-adrenergic receptors has been shown to enhance L-type Ca^{2+} current in murine embryonic ventricular cardiomyocytes as early as E9.5 and this effect could be reversed by the β-adrenergic receptor antagonist propranolol (Liu et al., 1999). In addition, Ang II has been shown to increase intracellular Ca^{2+} in neonatal ventricular

cardiomyocytes (Touyz et al., 1996), adult ventricular cardiomyocytes (Kilic et al., 2007) and ES- cell derived cardiomyocytes (Sedan et al., 2010). Thus, future studies aimed at characterizing the effects of various pharmacological compounds from these clinically relevant drug classes on proliferation and differentiation of embryonic cardiomyocytes and CPCs should be useful in predicting potentially detrimental or beneficial effects of these drugs on cell transplantation therapies.

From a practical standpoint, our approach of cell transplantation into recipient animals would not be feasible to analyze the effects of a large number of drugs alone and in combination on cell transplantation/graft size formation. Based on knowledge of such limitations, generation of engineered heart tissue (EHT) consisting of neonatal rat cardiomyocytes seeded onto collagen scaffolds were developed as a model system to efficiently evaluate numerous test cell populations and experimental conditions on cardiac cell transplantation (Song et al., 2010). Interestingly, using this approach, ES-cell derived CPCs were shown to mature and integrate into EHT and enhance the amplitude of tissue contraction (Song et al., 2010). Future work aimed at introducing pharmacological compounds into the microenvironment of the engineered tissue would certainly provide valuable insight into beneficial or detrimental interactions between a multitude of cardiovascular drugs and transplanted CPCs.

6.3 Characterization of ANP Receptor Signalling Systems in the Ventricles at E11.5 stage

6.3.1 Context

Heart development is a remarkable process, whereby the tubular heart undergoes complex morphogenetic changes to transform from a simple muscle covered tube to a specialized four-chambered pump. Congenital heart defects (CHDs), which occur as a result of abnormal cardiac development, are widespread in the human population, occurring in ~1% of live births (Hoffman, 1995; Bruneau, 2008). Owing to the limited capacity for post-natal cardiomyocytes to divide (Pasumarthi and Field, 2002), perturbations to the normal program of cardiac cell proliferation during development could have deleterious consequences on heart formation and function.

The expression of ANP in the embryonic heart is initiated in the primitive heart tube at early gestational stages and serves as a reliable marker of the differentiating atrial and ventricular myocardium (Christoffels et al., 2000). Importantly, genetic mutation of several key cardiac transcription factors that are known to regulate ANP gene expression have been associated with impaired cardiac development in experimental animal models of disease as well as in human patients with CHDs (Lin et al., 1997; Schott et al., 1998; Bruneau et al., 2001; Garg et al., 2003). Moreover, a dysregulated spatial expression pattern of ANP has been documented in a murine model of Holt-Oram Syndrome (Bruneau et al., 2001), which is caused by mutation of Tbx5 and is associated with defective septation and conduction system defects (Mori and Bruneau, 2004). A specific role for ANP in cardiac development, however, has yet to be described.

To extend previous observations of ANP mRNA expression in the trabecular myocardium of the midgestational murine ventricles (Zeller et al., 1987), work in this thesis confirmed the presence of immunoreactive ANP in this compartment at the E11.5 stage. Classical electron microscopy studies (Viragh and Challice, 1982) and more recent label dilution/cell birth dating approaches have provided strong evidence that cardiac cells in the ventricular trabeculae exit the cell cycle relatively early, enter mitotic quiescence and concomitantly differentiate into conduction system cardiomyocytes (Gourdie et al., 1998; Sedmera et al., 2003). Furthermore, electrical activation mapping of the embryonic heart has demonstrated that the trabecular myocardium serves as the preferential conduction route before establishment of the mature ventricular conduction system (i.e. bundle branches and Purkinje network) (Rentschler et al., 2001; Sankova et al., 2012).

Based on this knowledge, we speculated that high levels of ANP synthesis within the trabecular myocardium could be coupled to activation of NPR signalling systems in this compartment which serve to modulate cell proliferation and differentiation in an autocrine/paracrine manner. To achieve an autocrine/paracrine effect, ANP synthesized within the trabecular myocardium would also need to be secreted, processed to its biologically active form and have access to biologically intact NPRs. Currently, however, very little is known about whether these mechanisms are in place in the ventricles of the early four chambered heart. Thus, one of the primary aims of this thesis was to fill these specific gaps in our knowledge in an effort to provide novel insight into the role of ANP receptor mediated signalling systems in the embryonic heart.

6.3.2 Components of ANP Mediated Signalling Systems are Present in the Embryonic Ventricles at E11.5 Stage

Extensive work with neonatal rat ventricular cardiomyocytes has demonstrated that ANP gets secreted from these cells in a constitutive manner as well as in response to stimuli such as endothelin-1 (ET-1) (Bloch et al., 1986; Irons et al., 1993). Less, however, is known about whether ANP is also secreted from ventricular cells at earlier developmental stages. In this thesis, we discovered that immunoreactive ANP was present in conditioned media samples collected from E11.5 ventricular cell cultures. Specifically, results from these experiments revealed distinct bands corresponding to proANP (17kD) and biologically active ANP (3kD) in conditioned media samples. These results suggested that proANP, synthesized by E11.5 ventricular cells, was also actively secreted into the extracellular compartment and proteolytically processed into its active form.

Alternatively, it is possible that ANP detected in conditioned media samples could have occurred due to ruptured plasma membranes of dead cells and subsequent non-specific degradation of proANP into its smaller 3kD form. While we cannot definitively rule out this mechanism, our experimental procedure was designed to minimize this possibility. Specifically, E11.5 ventricular cells were plated overnight and then the following day media was aspirated and adherent cells were washed thoroughly with PBS to remove all dead cells. Fresh media was then added to the cells and collected 24 hours later and subjected to Western blot analysis for detection of ANP. Therefore, we are confident that the 3kD form of ANP measured from conditioned media samples was the result of active ANP secretion coupled to specific proteolytic processing. This view is further supported by the fact that corin, the type II transmembrane protease which cleaves

proANP into its active 3kD form, was shown to be expressed in the embryonic heart as early as E9.5 (Yan et al., 1999). Even more intriguing is the fact that between E11.5-E13.5 stages, corin was shown to be most abundantly expressed in the trabecular myocardium (Yan et al., 1999), thus supporting the view that a high local concentration of processed, biologically active ANP could be achieved specifically in this compartment.

Specific binding of radiolabelled ANP has been detected in various tissues of fetal and neonatal rats, including the kidney, adrenal gland and brain (Hersey et al., 1989; Brown and Zuo, 1995). More recently, an extensive analysis of NPR gene expression patterns was carried out in the developing murine nervous system (E10.5-E14.5), revealing predominant expression of NPRB and NPRC but not NPRA subtypes in various regions of the central and peripheral nervous systems (DiCicco-Bloom et al., 2004). In the adult heart, it has also been shown that NPRA, NPRB and NPRC are all expressed in working ventricular cardiomyocytes (Lin et al., 1995). Expression profiles of NPR subtypes in the midgestational heart, however, have not yet been determined. To gain insight into this issue, we characterized the gene expression levels of ANP high affinity receptors (NPRA and NPRC) in the cardiac ventricles at various developmental and postnatal stages. From these analyses, it was shown that both NPRA and NPRC transcripts were present throughout development, and displayed a subtype switch such that NPRC expression was highest at earlier stages, while NPRA was predominant later in development. Furthermore, immunolabelling experiments using NPRA and NPRC antibodies revealed broad spatial expression patterns for both receptors in the compact as well as trabecular myocardium. Collectively, overlapping expression patterns of ANP,

corin (Yan et al., 1999) and NPR subtypes in the trabecular myocardium are consistent with the notion that ANP may play an autocrine/paracrine role in regulating cardiac cell proliferation and/or differentiation in this compartment.

6.3.3 Biological Activity of Natriuretic Peptide Receptors in E11.5 Ventricular Cells

Aside from its well characterized endocrine role in regulating fluid homeostasis, ANP has been shown to potently regulate growth and proliferation of various cell types via autocrine/paracrine mode of action (D'Souza et al., 2004). The initial speculation that ANP could act locally, near its site of synthesis was borne from observations that several tissues other than the atria produced ANP at levels that were likely too low to contribute significantly to any endocrine function (Gardner et al., 1986). Accordingly, ANP has been shown to either positively or negatively modulate cell proliferation via NPRA or NPRC mediated signalling pathways in numerous cell types of cardiovascular or non-cardiovascular origin (Koide et al., 1996; Pandey et al., 2000; O'Tierney et al., 2010).

Activation of NPR signalling by ANP could either increase cGMP (NPRA/NPRB) or decrease cAMP (NPRC). In glial cells isolated from rat brain, ANP was shown to inhibit DNA synthesis in response to mitogenic stimuli via NPRC mediated reductions in the activity of mitogen activated protein kinases (MAPK) (Prins et al., 1996). By contrast, activation of NPRC using a receptor specific natriuretic peptide analogue was shown to stimulate proliferation of cultured murine Schwann cells (DiCicco-Bloom et al., 2004). Similar reports on the ability of ANP to stimulate or

inhibit proliferation via NPRA mediated signalling have also been reported in fetal/embryonic cardiomyocytes. Specifically, exogenous addition of human ANP on embryonic chick cardiomyocytes was shown to stimulate proliferation (Koide et al., 1996), while addition of rat ANP to fetal sheep cardiomyocytes was shown to inhibit proliferation by reducing Ang II stimulated activity of ERK, a member of the MAPK family (O'Tierney et al., 2010). Taken together, these studies indicate that the specific biological consequences of ANP are cell type specific and depend on the NPR subtypes that are expressed/biologically active. Moreover, it is noteworthy that heterologous systems (i.e. cells treated with ANP from different species) were employed in studies of cardiomyocyte proliferation which may have contributed to the different outcomes reported (see Chapter 1, Figure 1.5.2). Thus, in this thesis, we employed a homologous system (i.e. murine ANP on mouse primary cultures), to determine the effects of ANP on proliferation of E11.5 CPCs and cardiomyocytes.

To first gain insight into whether NPR signalling systems were biologically intact in ventricular cells at E11.5, we monitored fluctuations in the levels of the downstream second messengers cGMP and cAMP in response to ANP treatment. From these experiments, it was determined that ANP (100ng/ml) was able to elicit a significant increase in cGMP levels in acutely isolated E11.5 cells. Conversely, ANP treatment was not associated with any significant changes in cAMP levels under basal conditions, nor was it able to blunt the increase in cAMP associated with isoproterenol stimulation. Thus, from these analyses, we concluded that ANP guanylyl cyclase receptors were biologically active in E11.5 ventricular cells and thus proceeded to investigate whether

activation of these signalling systems could play any role in modulating cell proliferation in embryonic CPCs or cardiomyocytes.

6.3.4 Effects of Exogenous ANP on Proliferation of Cardiac Progenitor Cells

The plasma concentration of ANP has been shown to be ~5 times higher in the fetal compared to maternal circulation in sheep and in rats (Cheung et al., 1987; Wei et al., 1987). The actual plasma concentrations reported from these studies were 265pg/ml in fetal sheep (Cheung et al., 1987), while in rats levels were an order of magnitude higher at ~2700 pg/ml (Wei et al., 1987). Thus, in our second messenger assays, the concentration of ANP required to elicit a significant increase in cGMP production (100 ng/ml = 10^5 pg/ml) was approximately 40 times greater than circulating levels of ANP determined from fetal rat plasma. This fact raises some questions about the *in vivo* biological significance of receptor guanylyl cyclase activity in embryonic ventricular cells. However, we speculate that high levels of ANP synthesis and secretion specifically within the trabecular compartment of the ventricles could create a microenvironment with a high local ANP concentration which greatly exceeds that of the general circulation. Thus, we proceeded to test the effects of increasing concentrations of exogenous ANP (1-100ng/ml) on proliferation of E11.5 CPCs and cardiomyocytes. Results from these analyses revealed a progressive decrease in proliferation of CPCs with increasing concentrations of ANP, while proliferation rates in the cardiomyocyte population remained unchanged. Furthermore, the effects of ANP on CPC proliferation could be reversed by pre-incubation with an NPRA/NPRB antagonist, supporting the view that this decrease in proliferation was via receptor guanylyl cyclase activity.

To our knowledge, there is currently only one other report demonstrating an effect of ANP on proliferation of a cardiac precursor cell type (Stastna et al., 2010). Specifically, "cardiac stem cells" derived from adult rat ventricular tissue explants were shown to undergo ~30% reduction in proliferation following exposure to exogenous ANP (1µg/ml)(Stastna et al., 2010). Based on this discovery, the authors proposed that cellular cross talk in the form of secreted paracrine factors between cardiac stem cells and cardiomyocytes (which produce ANP) *in vivo* could have a significant impact on cell transplantation therapies using undifferentiated cell types (i.e. CPCs). One could also envision a similar situation of cellular crosstalk between undifferentiated CPCs and cardiomyocytes being of importance in the embryonic heart during cardiogenesis. In support of this view, we have confirmed the presence of CPCs and cardiomyocytes in close proximity to each other in the trabecular zone (ANP rich area) of the E11.5 ventricles by electron microscopy (unpublished data, not shown). Based on this knowledge, we propose that ANP secreted from cardiomyocytes in the trabeculae could serve as a paracrine signal for CPCs to exit the cell cycle, while CPCs in the compact zone would be less affected due the presence of an ANP concentration gradient within the embryonic ventricles. This view is further supported by the significantly lower mitotic activity (PH3 labelling index) that was observed in ANP rich trabecular zone versus the compact zone (low ANP) in the left ventricular myocardium at E11.5. Interestingly, the PH3 labelling index was also significantly lower in the trabecular zone of the right ventricle at E11.5 compared to the surrounding compact zone despite relatively low expression of ANP. One possible explanation for this result is that cells within the right ventricle have a much higher sensitivity to ANP compared to those in the left ventricle

which has been reported previously in fetal sheep cardiomyocytes (O'Tierney et al., 2010).

The fact that ANP stimulated cGMP production in acutely isolated E11.5 ventricular cells suggested that reduced cell cycle activity observed in CPCs could occur via receptor guanylyl cyclase activation. More specifically, because 100ng/ml (~30nM) is far below the concentration of ANP shown to elicit half-maximal cGMP production via NPRB (~25μM)(Schulz et al., 1989), we further propose that proliferation of E11.5 CPCs is controlled via NPRA mediated signalling pathways. Indeed, activation of NPRA in fetal sheep cardiomyocytes derived from the late gestational stage has been shown to decrease Ang II induced ERK activity as well as cell proliferation (O'Tierney et al., 2010). Future work aimed at identifying whether the ANP/NPRA signalling axis has any effect on ERK signalling pathways in CPCs/cardiomyocytes from earlier developmental stages would certainly provide valuable information pertaining to the precise molecular mechanisms regulating proliferation during the developmental period and are being actively pursued in our laboratory.

6.4 Investigation into the Potential Role of ANP Signalling in the Development of the Ventricular Cardiac Conduction System

6.4.1 Context

Lineage tracking analyses performed by our group and others have convincingly shown that working cardiomyocytes and cardiac conduction system cardiomyocytes are derived from a common pool of cardiomyogenic progenitor cells (Gourdie et al., 1995; Cheng et al., 1999; McMullen et al., 2009). Furthermore, an inverse relationship between

rates of cell proliferation and differentiation toward the ventricular conduction system lineage have been shown to occur in the developing chick and mouse heart (Gourdie et al., 1995; Sedmera et al., 2003). In Chapter 4 of this thesis, we provided evidence that exogenous ANP was associated with reduced rates of proliferation in undifferentiated CPCs that could be reversed by antagonizing receptor guanylyl cyclases. Furthermore, we showed that ANP rich regions of the trabecular myocardium were characterized by a lower index of proliferation compared to the adjacent compact layer. Since the trabeculae are known to house cellular progenitors of the ventricular conduction system (Fishman and Chien, 1997; Christoffels and Moorman, 2009), we speculated that reduced CPC proliferation mediated by ANP/NPRA signalling axis could be coupled to recruitment of these cells into the conduction system lineage.

Evidence that NPRA signalling systems play an important role in cardiac ontogeny have come from our observations, as well as those of other groups, that survival of mice lacking functional copies of the NPRA gene (*Npr1*$^{-/-}$) is significantly reduced (Knowles et al., 2001; Scott et al., 2009). Furthermore, it was reported that a high proportion of surviving NPRA$^{-/-}$ neonates displayed heart abnormalities including mesocardia or dextrocardia (Cameron and Ellmers, 2003). Currently, only scant information exists on the potential molecular mechanisms underlying increased rates of mortality and abnormal cardiac morphogenesis in NPRA$^{-/-}$ mice. To gain additional insight into this important issue, work in this thesis tested the hypothesis that the ANP/NPRA signalling axis plays a role in specification and/or differentiation of the ventricular cardiac conduction system.

6.4.2 Investigation into the Direct Inductive Effect of ANP on Expression of Ventricular Conduction System Markers

In the embryonic chick heart, the Purkinje fibers develop in close association with the developing coronary vasculature (Lu et al., 1993). This observation, led to the hypothesis that secreted factors from endothelial cells could provide instructive cues which guide undifferentiated cardiac precursor cells toward the conduction system cell lineage in a paracrine fashion (Gourdie et al., 1995). This hypothesis, was subsequently validated when the same group provided evidence that endothelin-1 (ET-1), a cytokine produced by endothelial cells could induce the expression of conduction system markers *in vitro* and *in vivo* (Gourdie et al., 1998; Takebayashi-Suzuki et al., 2000). A similar scenario has also been described in the developing mouse heart, where it was shown that the endocardial-derived growth factor neuregulin-1 (NRG-1) was capable of inducing ectopic expression of conduction system marker genes during a specific developmental time window between E8.5-E10.5 (Rentschler et al., 2002). Taken together, these paradigms set a strong precedent for the role of secreted protein factors in specifying the conduction system cell lineage in a paracrine fashion.

To gain insight into whether ANP could also serve as a paracrine factor involved in conduction system cell specification/differentiation, we analyzed the expression of the conduction system marker genes, Cx40 and HCN4 in E11.5 ANP^+ and ANP^- cell populations that were separated using the FACS technique. The selection of Cx40 as a conduction system marker gene was based on its expression in the ventricular conduction system primordium during development (i.e. trabecular myocardium), and its persistence in the bundle branches and Purkinje fibers in post-natal life (Miquerol et al., 2004; Sankova et al., 2012). Similarly, HCN4 is initially expressed at high levels in the

embryonic ventricles where most cardiomyocytes are spontaneously active (Schweizer et al., 2009), while in the mature mammalian heart HCN4 (and I_f current) is found in Purkinje fibers, but absent in working cardiomyocytes (Han et al., 2002; Miquerol et al., 2004). Moreover, HCN4 has recently been shown to be expressed in the first heart field precursor cells destined to form distinct components of the cardiac conduction system (Liang et al., 2013).

Results from our FACS analyses demonstrated that expression of both Cx40 and HCN4 were ~3 fold higher in the ANP^+ compared to the ANP^- cell population indicating an enrichment of conduction system markers in ANP^+ cells. In parallel cell culture experiments exogenous addition of ANP for a 24 hour time period was not associated with increased expression of either Cx40 or HCN4 suggesting that it may not have a direct inductive effect on conduction system gene expression. However, these results are inconclusive since additional experiments are warranted to monitor gene expression changes at earlier and later time points after ANP treatment. An alternative explanation could also be that the inductive effects of ANP are restricted to an earlier developmental time period as was seen by others with NRG-1 (Rentschler et al., 2002). With this possibility in mind, we have recently established a colony of $NPRA^{-/-}$ mice harboring the $Cx40^{egfp}$ transgene which will enable us to directly visualize the ventricular conduction system and characterize its development in hearts of mice lacking ANP/NPRA signalling system from the onset of cardiogenesis.

6.4.3 Characterization of Ventricular Conduction System Development in NPRA$^{-/-}$ Mice using the Cx40^{egfp} Mouse Model

Surviving adult mice lacking functional NPRA gene (*Npr1*) have elevated blood pressure and exhibit cardiac hypertrophy and interstitial fibrosis (Oliver et al., 1997). Observations of severe cardiac hypertrophy in NPRA$^{-/-}$ mice, which appeared to be disproportionate to the relatively mild elevation in blood pressure, led to speculation that ANP may also serve as an important regulator of cardiomyocyte growth. In support of this view, mice in which NPRA was selectively ablated in cardiomyocytes were shown to be normotensive, but still exhibited marked cardiac hypertrophy (Knowles et al., 2001). Subsequently, evidence that ANP inhibited cardiomyocyte growth in response to hypertrophic stimuli such as Ang II (Kilic et al., 2007; Li et al., 2009), firmly established its role as a regulator of cardiac growth in the adult heart and spurred investigations into the precise molecular underpinnings underlying this process (Tokudome et al., 2005; Ellmers et al., 2007; Kinoshita et al., 2010; Klaiber et al., 2010). Interestingly, reports demonstrating that hearts of NPRA$^{-/-}$ embryos are already enlarged at midgestation suggested that NPRA signalling also serves as an important regulator of cardiac growth during the developmental period (Ellmers et al., 2002; Scott et al., 2009). Currently, however, molecular mechanisms involved in NPRA mediated cardiac growth during cardiogenesis have remained largely unexplored.

A major conclusion drawn from the most extensive study of NPRA signalling during development thus far, was that the mechanisms by which natriuretic peptide signalling influences cardiac development are distinct from those which regulate pathological cardiac hypertrophy and fibrosis (Scott et al., 2009). This conclusion was drawn from the fact that no changes in hypertrophy related factors such as MEF2c,

GATA4 and SRF were detected in the ventricles from NPRA$^{-/-}$ embryos compared to wiltype controls at midgestation. In that study, the expression levels of cardiac conduction system marker genes were not examined. Thus, to extend these observations, we determined the expression of the conduction system marker genes Cx40 and HCN4 in ventricles from NPRA$^{-/-}$ embryos at midgestation (E14.5). Interestingly, a trend toward a decrease in the expression of both Cx40 and HCN4 was observed at this stage, and appeared to be related to the number of functional copies of *Npr1*. Following up on these results by increasing the number of experiments and also examining expression levels of other genes known to be important for specification, patterning and differentiation of the conduction system (e.g.Nkx2.5, Tbx5, Irx3 and others) (Hatcher and Basson, 2009), should provide valuable information pertaining to the potential role of NPRA signalling in the development of the ventricular conduction system.

The creation of transgenic mouse models which allow direct visualization of the cardiac conduction system have provided a valuable tool for studying the impact of genetic manipulations on conduction system development. Because Cx40 is expressed in both the primitive and mature components of the ventricular conduction system (Miquerol et al., 2004; Miquerol et al., 2010), the Cx40^{egfp} mouse model is particularly well suited for studying the development of this compartment. For example, the Cx40^{egfp} strain was previously used to demonstrate that haploinsufficiency of Nkx2.5 (Nkx2.5$^{+/-}$) was associated with overt hypoplasia of the fast conducting Purkinje network which was coupled to functional conduction system deficits including a prolonged QRS interval (Jay et al., 2004; Meysen et al., 2007).

Following similar lines of investigation used to study Nkx2.5$^{+/-}$ mice, we have initiated efforts to characterize the morphological and functional consequences of genetic ablation of NPRA using the Cx40^{egfp} mouse model. Preliminary results from these analyses have revealed that abnormal Purkinje fiber architecture and severe hypoplasia were observable with partial penetrance in NPRA$^{+/-}$ neonates but not in wildtype littermates (no viable compound Cx40^{egfp} /NPRA$^{-/-}$ pups generated thus far). In parallel experiments, electrocardiograms (ECG) revealed prolonged QRS interval in adult NPRA$^{-/-}$ mice (3-5 months) which is also similar to the situation observed in response to Nkx2.5 haploinsufficiency (Jay et al., 2004). Taken together, it is possible that the prolonged QRS interval may be a result of the hypocellular Purkinje fiber network, since each terminal Purkinje cell would be required to depolarize a larger region of working myocardium which is characterized by slower conduction velocity compared to Purkinje fibers. It should be noted, however, that an important limitation to our ECG analyses is that NPRA$^{-/-}$ mice display marked cardiac hypertrophy even at ~4 months of age (Oliver et al., 1997), and thus we cannot distinguish between the relative contributions of increased tissue mass versus aberrant conduction system activity to the observed prolongation of the QRS interval. Accordingly, future investigations aimed at characterizing the morphology of the ventricular conduction system in adult Cx40^{egfp}/NPRA$^{-/-}$ animals will be particularly useful in this regard and are being pursued in our laboratory.

An additional interesting discovery resulting from studies of Nkx2.5$^{+/-}$ mice was that working cardiomyocytes surrounding the EGFP^{+} Purkinje fibers showed a delay in withdrawal from the cell cycle (Meysen et al., 2007). Considering that the ANP gene

(*Nppa*) is a transcriptional target of Nkx2.5, and that ANP is a known regulator of cell proliferation, it is tempting to speculate that the ANP/NPRA system could function downstream of Nkx2.5 as a regulatory network involved in tightly controlling the balance between proliferation/differentiation that is essential for proper cardiogenesis.

6.4.4 Proposed Model for the Involvement of ANP/NPRA Signalling Axis in Ventricular Conduction System Development

The inductive effects of ET-1 and NRG-1 set a strong precedent for the role of paracrine signalling mechanisms in recruiting undifferentiated cells toward the conduction system lineage (Rentschler et al., 2002; Sedmera et al., 2008). In a situation analogous to the processing of proANP into the smaller biologically active ANP by the enzyme corin, the ET-1 precursor is proteolytically activated by the specific ET converting enzyme, ECE (Xu et al., 1994). In an elegant series of retroviral expression experiments in the embryonic chick heart, it was shown that co-expression of the ET-1 precursor (prepro-ET-1) and ECE resulted in robust ectopic expression of Purkinje fiber markers in the embryonic myocardium, while expression of prepro-ET-1 alone had no inductive effect (Takebayashi-Suzuki et al., 2000). A conclusion from this study was that sites of ET-1 biological activity *in vivo* are spatially defined by the expression pattern of ECE. Intriguingly, ECE expression has been shown to be enriched specifically in the trabecular myocardium of the murine heart at midgestation (Sedmera et al., 2008). Thus, enrichment of both ECE and corin in the region of the nascent murine ventricular conduction system seems to be well suited for creating high local concentrations of biologically active ligands (ET-1 and ANP) in that region and suggests that crosstalk

between intracellular signalling pathways mediated by their cognate receptors may be involved in conduction system specification/differentiation.

The growth/differentiation factor NRG-1 has also been implicated in conduction system specification based on its critical role in the elaboration of the trabecular network during cardiogenesis (Pentassuglia and Sawyer, 2009) and its ability to induce ectopic conduction system marker gene expression in ventricles of mouse embryos (Rentschler et al., 2002) and in cultured embryonic murine cardiomyocytes (Patel and Kos, 2005). Following secretion, NRG-1 diffuses through the extracellular matrix to activate the receptor tyrosine kinases (RTK) ErbB4 and ErbB2 (Mei and Xiong, 2008) which are expressed in the trabecular myocardium of the embryonic heart (Gassmann et al., 1995). Thus, based on the spatially overlapping expression of ANP signalling machinery with that of ET-1 and NRG-1 in the region of the developing ventricular conduction system, we propose a model in which these three distinct signalling systems function in a complex intracellular signalling network which is involved in conduction system development.

In support of this view, ANP was shown to blunt the stimulatory effects of ET-1 on MAPK/ERK2 activity in kidney mesangial cells (Pandey et al., 2000). Furthermore, these effects of ANP were abolished by treating cells with A71915 (NPRA/B antagonist). In adult cardiomyocytes, stimulatory effects of ET-1 on ERK were also shown to be abolished by RGS2 (regulator of G-protein signalling 2) (Snabaitis et al., 2005). Interestingly, RGS2, has been shown to function as negative regulator of Gq signalling proteins in the cardiovascular system and is specifically activated by cGMP dependent protein kinases (PKG) (Xie and Palmer, 2007). Work in this thesis has demonstrated that

stimulation of E11.5 ventricular cells with ANP was associated with an increase in cGMP production. Thus, it is possible that the ANP/NPRA signalling system converges with the ET-1 mediated signalling system to regulate ERK activity in the embryonic heart.

To our knowledge, specific crosstalk between NPRA and NRG-1 signalling pathways has not yet been documented. However, ANP has been shown to reduce ERK activity stimulated by the platelet derived growth factor (Pandey et al., 2000), which also signals via RTK mechanisms (Fantl et al., 1993). Given the role of ERK in promoting cell cycle activity (Chambard et al., 2007), we speculate that ANP signalling may serve as a brake to slow proliferation of undifferentiated cells by antagonizing proliferative signals from ET-1 and/or NRG-1. Future investigations into whether this reduction in proliferation is coupled to specification toward the conduction system lineage by direct modulation of the transcriptional machinery, and subsequently determining the molecular effectors that are involved in this process would certainly enhance our understanding of the signalling systems which govern the balance between proliferation and differentiation that is required for proper heart development.

6.5 Significance and Future Directions

6.5.1 The Effects of Ca^{2+} Channel Blockade and ANP Signalling on Cell Transplantation

Heart disease continues to be a major cause of morbidity and mortality in Canada (Ross et al., 2006). The inability of current pharmacological therapies and surgical interventions to replace myocardium lost to disease or injury has served as the driving

force behind the field of regenerative medicine. While ES cells hold the ultimate regenerative potential, teratoma formation following ES cell transplantation into host myocardium (Nussbaum et al., 2007) clearly indicated that the heart lacks the appropriate molecular cues required to guide these multipotent cells toward the myocardial cell fate. In an effort to minimize the risk of teratoma formation, several committed cell types were rigorously examined in experimental animal models to determine their potential for myocardial repair (McMullen and Pasumarthi, 2007). From these efforts, skeletal myoblasts and bone marrow stem cells (BMSC) advanced to human clinical trials due in part to the relative ease of obtaining these cells autologously from patient biopsies and the ability to expand these cells *in vitro* prior to transplantation. Unfortunately, skeletal myoblasts showed only modest improvements in cardiac performance and were associated with a high prevalence of dangerous arrhythmias (Menasche et al., 2003), most likely due to the inability of these cells to transdifferentiate into cardiomyocytes and couple functionally with the host myocardium. In some cases, clinical trials using BMSCs have reported improvements in cardiac performance in treated patients compared to controls (Assmus et al., 2002; Stamm et al., 2003). Conversely, more recent clinical trials have failed to demonstrate significant long term functional improvements associated with BMSC therapy (Janssens et al., 2006; Beitnes et al., 2009). Furthermore, the benefits associated with BMSCs are widely believed to occur as a result of favorable scar remodeling and/or improved angiogenesis possibly due to paracrine factors secreted from the transplanted cells but not via transdifferentiation into cardiomyocytes.

In stark contrast to skeletal myoblasts and BMSCs, transplanted fetal cardiomyocytes have been shown to integrate functionally with host myocardium

(Rubart et al., 2003) and suppress the induction of ventricular tachycardia in experimental models of cardiac injury (Roell et al., 2007). CPCs, which have the ability to differentiate into cardiomyocytes *in vitro* (McMullen et al., 2009), are also a highly proliferative cell type. Thus, we have hypothesized that following transplantation, CPCs could undergo several rounds of cell division leading to larger graft size formation and could simultaneously integrate molecular signals from the host myocardium required for differentiation toward appropriate cardiomyocyte lineages. Recent reports from clinical trials indicating that transplantation of cardiac stem cells isolated from the adult heart is safe and leads to functional improvements in ischemic heart disease and MI patients are also very encouraging (Bolli et al., 2011; Makkar et al., 2012).

Since virtually every candidate that could benefit from cell based therapies for myocardial repair would be taking some form of cardiovascular medication (McKelvie et al., 2013), a better understanding of the potential interactions between pharmacological drugs and transplanted cell types is imperative. One of the principle findings of this thesis was that the pharmacological Ca^{2+} channel blocker, nifedipine, was associated with reduced proliferation of E11.5 CPCs and impaired myofibrillogenesis *in vitro*. Furthermore, these *in vitro* effects translated into reduced graft size formation *in vivo* following transplantation of E11.5 cardiac cells (containing CPCs) into the host myocardium of mice receiving daily doses of nifedipine. These results have provided new knowledge to the cell transplantation field regarding drug/cell interactions and underscore the need for future studies aimed at examining a broader range of clinically relevant cardiovascular drugs. Future work in our laboratory will be aimed at quantifying the expression of cell cycle markers such as PH3 in the engrafted

myocardium to confirm whether the reduced graft sizes associated with nifedipine treatment are due to decreased proliferation of transplanted cells. In addition, future experiments will be dedicated to dissecting the specific contributions of L-type and T-type Ca^{2+} channels as well as the specific downstream Ca^{2+} sensitive proteins/enzymes (e.g. CaM, CaMK, CaN, ERK) involved in modulating CPC and cardiomyocyte proliferation/differentiation. This information would certainly provide valuable new insight into the precise molecular mechanisms regulating cardiac cell development and could be used to devise strategies to pharmacologically modulate cell proliferation/differentiation and thereby enhance graft size and/or viability.

Aside from exposure to pharmacological drugs, transplanted CPCs would also be exposed to a variety of endogenous hormones/signalling molecules in the host environment which could modulate cell proliferation and differentiation and thus influence the outcome of transplantation therapies. Because ANP expression is reinitiated in the ventricles in pathological settings (Chien et al., 1991), undifferentiated CPCs transplanted into the diseased myocardium would likely be exposed to relatively high concentrations of this hormone/paracrine factor. Given that work from this thesis has provided new evidence that ANP causes a reduction in CPC proliferation *in vitro*, it is possible that exposure of transplanted CPCs to high levels of ANP could also result in smaller graft sizes *in vivo* following cell transplantation. Consistent with our findings, it has been shown that cardiac stem cells isolated from the adult heart also underwent a reduction in proliferation in response to exogenous ANP treatment (Stastna et al., 2010). Thus, it appears that ANP mediated signal transduction pathways are important regulators of proliferation in both embryonic, as well as adult cardiac stem/progenitor cells. Given

that stimulation of E11.5 ventricular cells was associated with increased cGMP production, future work in our laboratory will be aimed at confirming whether cGMP sensitive signalling intermediates (e.g. PKG, PDEs, ERK) are responsible for mediating the antiproliferative effects of ANP in embryonic CPCs. Interestingly, treatment of human ES cell derived cardiomyocytes with a pro-survival cocktail was shown to improve engraftment and enhance global contractile function better than untreated cardiomyocytes following transplantation into the injured rat heart (Laflamme et al., 2007). One could envision that including a pharmacological inhibitor of NPRA into a pro-survival cocktail could also confer a proliferative advantage to CPCs prior to transplantation and thus lead to larger graft size formation and improved cardiac performance.

Work from this thesis also explored the possibility that ANP serves as an autocrine/paracrine factor involved in the specification of the cardiac conduction system lineage during cardiac ontogeny. Future work in our laboratory is aimed at more thoroughly examining whether ANP has a direct effect on lineage commitment toward the conduction system fate by examining expression of CCS markers in response to shorter/longer periods of exposure to exogenous ANP. Furthermore, ongoing efforts are focused on substantiating our preliminary findings of anatomical defects in the patterning/development of the ventricular Purkinje fiber network in a subset of mice lacking functional copies of the NPRA gene. Certainly, determining whether ANP is involved in lineage specification has potential implications in the cell transplantation field. First, given that ventricular ANP synthesis is significantly enhanced in the diseased myocardium (Chien et al., 1991), exposure of transplanted CPCs to high levels of ANP

could activate NPR signal transduction pathways which could induce ectopic pacemaker formation and in turn evoke dangerous cardiac arrhythmias. On the other hand, given the growing interest in the development of biological pacemakers (Rosen et al., 2011), exogenous ANP could be used in combination with other factors to facilitate the enrichment of pacemaker/conduction-like cell populations *in vitro,* which could in turn be used to treat patients with aberrant conduction system function resulting from cardiac disease or injury.

6.5.2 The Effects of Ca^{2+} Channel Blockade and ANP Signalling on Cardiac Development

While determining the effects of pharmacological drugs and endogenous factors on embryonic cardiac cell proliferation and differentiation provides clear benefits to the field of regenerative medicine, this information also provides new knowledge regarding the developmental biology of the heart. Due to the highly unpredictable effects of pharmacological drugs on the developing fetus, major ethical issues surround the inclusion of pregnant women in clinical trials for new drug therapies (Macklin, 2010). Intuitively, similar considerations also pose as a hurdle to evaluating the effects of medications commonly used to treat chronic illnesses (including those of the cardiovascular system) on cardiac development. Based on our *in vitro* data which showed that nifedipine was associated with altered proliferation and differentiation kinetics of embryonic CPCs and cardiomyocytes, it could be predicted that this drug would have detrimental effects on cardiac development during the embryonic period. Indeed, nifedipine is known to cross the placenta (Manninen and Juhakoski, 1991), and

there is experimental evidence that exposure to nifedipine is associated with abnormal mammalian heart development (Porter et al., 2003). Based on this information, the development of high throughput systems to evaluate the effects of pharmacological compounds on proliferation and differentiation of embryonic cardiac cells could have predictive value regarding the effects of drug compounds on cardiac development. This information could in turn be used to inform decisions on treatment programs for pregnant women based on careful evaluation of potential benefits and risks associated with the pharmacological therapy.

In the developing heart, the expression of ANP serves as a reliable marker of the differentiating chamber myocardium (Christoffels et al., 2000). Because the normal spatiotemporal expression pattern of ANP has been so well characterized during cardiac development, dysregulated ANP expression patterns have also become a useful marker for abnormal heart development. The first example of the utility of ANP as a readout for abnormal patterning of the heart came from analyses of the mouse model for Holt-Oram syndrome (Bruneau et al., 2001) which is caused by an autosomal dominant mutation in the transcription factor Tbx5 (Li et al., 1997). In humans and in mice, cardiac manifestations of Tbx5 mutations include variable septal defects and conduction system disturbances (Basson et al., 1994; Newbury-Ecob et al., 1996; Bruneau et al., 2001). Intriguingly, in mice haploinsufficient for Tbx5, ANP expression was shown to no longer be confined to the left ventricle of the embryonic heart, but instead was spread across the interventricular groove and into the right ventricle (Bruneau et al., 2001). Based on our discovery that ANP was associated with a reduction in the rate of CPC proliferation *in vitro*, it is tempting to speculate that septal defects associated with Holt- Oram syndrome

could be partly attributed to the anti-proliferative effects of ANP in the region of the developing septum, where it is normally not expressed. It should be noted, however, that no septal or valve defects were reported in mice in which the *Nppa* (ANP) gene had been either ablated (John et al., 1996) or overexpressed (Barbee et al., 1994) although structural defects were not rigorously examined in either of these studies. Similarly, no major structural defects have been reported in humans with genetic polymorphisms in the *Nppa* gene, although affected individuals showed increased risk of atrial fibrillation via unknown mechanisms (Hodgson-Zingman et al., 2008; Ren et al., 2010). Given that BNP is also expressed in the embryonic mammalian heart (Cameron et al., 1996) it is possible that this peptide could play a compensatory role in situations where normal expression patterns of ANP have been altered. Interestingly, however, disruption of the NPRA receptor which mediates the effects of both ANP and BNP has been associated with hypertension and marked cardiac hypertrophy in mice (Oliver et al., 1997) and humans (Nakayama et al., 2000), but no septal defects have been reported in either case. Thus, while work from this thesis has provided evidence that the ANP/NPRA signalling system modulates CPC proliferation, the potential *in vivo* consequences associated with altered proliferation kinetics due to disruption of this signalling system remain to be determined. The fact that conduction system deficits can also occur in the absence of overt cardiac structural defects, further underscores the importance of continuing our investigations into the effects of NPRA ablation on conduction system development using the $Cx40^{egfp}$ model. Results from these experiments could contribute new knowledge to the field of developmental biology regarding the signalling networks involved in proper cardiac development and could also be used to inform new and

improved strategies for diagnosis and treatment of several forms of congenital heart disease.

Overall, it is our hope that findings from this thesis work will provide meaningful insight into molecular mechanisms governing proliferation and differentiation of embryonic CPCs and that this information can be used to expedite the development of effective cell based therapies for myocardial repair and also improve our understanding of the developmental processes underlying proper cardiogenesis.

REFERENCES

Alsan BH, Schultheiss TM. 2002. Regulation of avian cardiogenesis by Fgf8 signaling. Development 129:1935-1943.

Anand-Srivastava MB, Srivastava AK, Cantin M. 1987. Pertussis toxin attenuates atrial natriuretic factor-mediated inhibition of adenylate cyclase. Involvement of inhibitory guanine nucleotide regulatory protein. J Biol Chem 262:4931-4934.

Anand-Srivastava MB, Thibault G, Sola C, Fon E, Ballak M, Charbonneau C, Haile-Meskel H, Garcia R, Genest J, Cantin M. 1989. Atrial natriuretic factor in Purkinje fibers of rabbit heart. Hypertension 13:789-798.

Anand-Srivastava MB, Vinay P, Genest J, Cantin M. 1986. Effect of atrial natriuretic factor on adenylate cyclase in various nephron segments. Am J Physiol 251:F417-423.

Anderson ME. 2000. Connections count : excitation-contraction meets excitation-transcription coupling. Circ Res 86:717-719.

Aoki H, Sadoshima J, Izumo S. 2000. Myosin light chain kinase mediates sarcomere organization during cardiac hypertrophy in vitro. Nat Med 6:183-188.

Argentin S, Ardati A, Tremblay S, Lihrmann I, Robitaille L, Drouin J, Nemer M. 1994. Developmental stage-specific regulation of atrial natriuretic factor gene transcription in cardiac cells. Mol Cell Biol 14:777-790.

Assmus B, Schachinger V, Teupe C, Britten M, Lehmann R, Dobert N, Grunwald F, Aicher A, Urbich C, Martin H, Hoelzer D, Dimmeler S, Zeiher AM. 2002. Transplantation of Progenitor Cells and Regeneration Enhancement in Acute Myocardial Infarction (TOPCARE-AMI). Circulation 106:3009-3017.

Barbee RW, Perry BD, Re RN, Murgo JP, Field LJ. 1994. Hemodynamics in transgenic mice with overexpression of atrial natriuretic factor. Circ Res 74:747-751.

Barnett P, van den Boogaard M, Christoffels V. 2012. Localized and temporal gene regulation in heart development. Curr Top Dev Biol 100:171-201.

Basson CT, Cowley GS, Solomon SD, Weissman B, Poznanski AK, Traill TA, Seidman JG, Seidman CE. 1994. The clinical and genetic spectrum of the Holt-Oram syndrome (heart-hand syndrome). N Engl J Med 330:885-891.

Beblo DA, Veenstra RD. 1997. Monovalent cation permeation through the connexin40 gap junction channel. Cs, Rb, K, Na, Li, TEA, TMA, TBA, and effects of anions Br, Cl, F, acetate, aspartate, glutamate, and NO3. J Gen Physiol 109:509-522.

Beitnes JO, Hopp E, Lunde K, Solheim S, Arnesen H, Brinchmann JE, Forfang K, Aakhus S. 2009. Long-term results after intracoronary injection of autologous mononuclear bone marrow cells in acute myocardial infarction: the ASTAMI randomised, controlled study. Heart 95:1983-1989.

Belaguli NS, Sepulveda JL, Nigam V, Charron F, Nemer M, Schwartz RJ. 2000. Cardiac tissue enriched factors serum response factor and GATA-4 are mutual coregulators. Mol Cell Biol 20:7550-7558.

Beltrami AP, Barlucchi L, Torella D, Baker M, Limana F, Chimenti S, Kasahara H, Rota M, Musso E, Urbanek K, Leri A, Kajstura J, Nadal-Ginard B, Anversa P. 2003. Adult cardiac stem cells are multipotent and support myocardial regeneration. Cell 114:763-776.

Bers DM. 2002. Cardiac excitation-contraction coupling. Nature 415:198-205.

Bloch KD, Seidman JG, Naftilan JD, Fallon JT, Seidman CE. 1986. Neonatal atria and ventricles secrete atrial natriuretic factor via tissue-specific secretory pathways. Cell 47:695-702.

Bolli R, Chugh AR, D'Amario D, Loughran JH, Stoddard MF, Ikram S, Beache GM, Wagner SG, Leri A, Hosoda T, Sanada F, Elmore JB, Goichberg P, Cappetta D, Solankhi NK, Fahsah I, Rokosh DG, Slaughter MS, Kajstura J, Anversa P. 2011. Cardiac stem cells in patients with ischaemic cardiomyopathy (SCIPIO): initial results of a randomised phase 1 trial. Lancet 378:1847-1857.

Brooks G, Poolman RA, McGill CJ, Li JM. 1997. Expression and activities of cyclins and cyclin-dependent kinases in developing rat ventricular myocytes. J Mol Cell Cardiol 29:2261-2271.

Brown J, Zuo Z. 1995. Natriuretic peptide receptors in the fetal rat. Am J Physiol 269:E253-268.

Bruneau BG. 2008. The developmental genetics of congenital heart disease. Nature 451:943-948.

Bruneau BG. 2011. Atrial natriuretic factor in the developing heart: a signpost for cardiac morphogenesis. Can J Physiol Pharmacol 89:533-537.

Bruneau BG, Nemer G, Schmitt JP, Charron F, Robitaille L, Caron S, Conner DA, Gessler M, Nemer M, Seidman CE, Seidman JG. 2001. A murine model of Holt-Oram syndrome defines roles of the T-box transcription factor Tbx5 in cardiogenesis and disease. Cell 106:709-721.

Buckingham M, Meilhac S, Zaffran S. 2005. Building the mammalian heart from two sources of myocardial cells. Nat Rev Genet 6:826-835.

Burgess TL, Kelly RB. 1987. Constitutive and regulated secretion of proteins. Annu Rev Cell Biol 3:243-293.

Cameron VA, Aitken GD, Ellmers LJ, Kennedy MA, Espiner EA. 1996. The sites of gene expression of atrial, brain, and C-type natriuretic peptides in mouse fetal development: temporal changes in embryos and placenta. Endocrinology 137:817-824.

Cameron VA, Ellmers LJ. 2003. Minireview: natriuretic peptides during development of the fetal heart and circulation. Endocrinology 144:2191-2194.

Cantin M, Thibault G, Haile-Meskel H, Ding J, Milne RW, Ballak M, Charbonneau C, Nemer M, Drouin J, Garcia R, et al. 1989. Atrial natriuretic factor in the impulse-conduction system of rat cardiac ventricles. Cell Tissue Res 256:309-325.

Cao L, Gardner DG. 1995. Natriuretic peptides inhibit DNA synthesis in cardiac fibroblasts. Hypertension 25:227-234.

Chambard JC, Lefloch R, Pouyssegur J, Lenormand P. 2007. ERK implication in cell cycle regulation. Biochim Biophys Acta 1773:1299-1310.

Chang MS, Lowe DG, Lewis M, Hellmiss R, Chen E, Goeddel DV. 1989. Differential activation by atrial and brain natriuretic peptides of two different receptor guanylate cyclases. Nature 341:68-72.

Chapman SC, Schubert FR, Schoenwolf GC, Lumsden A. 2003. Anterior identity is established in chick epiblast by hypoblast and anterior definitive endoderm. Development 130:5091-5101.

Chen YJ, Lin JK, Lin-Shiau SY. 1999. Proliferation arrest and induction of CDK inhibitors p21 and p27 by depleting the calcium store in cultured C6 glioma cells. Eur J Cell Biol 78:824-831.

Cheng G, Litchenberg WH, Cole GJ, Mikawa T, Thompson RP, Gourdie RG. 1999. Development of the cardiac conduction system involves recruitment within a multipotent cardiomyogenic lineage. Development 126:5041-5049.

Cheung CY, Gibbs DM, Brace RA. 1987. Atrial natriuretic factor in maternal and fetal sheep. Am J Physiol 252:E279-282.

Chien KR, Knowlton KU, Zhu H, Chien S. 1991. Regulation of cardiac gene expression during myocardial growth and hypertrophy: molecular studies of an adaptive physiologic response. Faseb J 5:3037-3046.

Chinkers M, Garbers DL, Chang MS, Lowe DG, Chin HM, Goeddel DV, Schulz S. 1989. A membrane form of guanylate cyclase is an atrial natriuretic peptide receptor. Nature 338:78-83.

Chinkers M, Wilson EM. 1992. Ligand-independent oligomerization of natriuretic peptide receptors. Identification of heteromeric receptors and a dominant negative mutant. J Biol Chem 267:18589-18597.

Chiu RC, Zibaitis A, Kao RL. 1995. Cellular cardiomyoplasty: myocardial regeneration with satellite cell implantation. Ann Thorac Surg 60:12-18.

Chobanian AV, Bakris GL, Black HR, Cushman WC, Green LA, Izzo JL, Jr., Jones DW, Materson BJ, Oparil S, Wright JT, Jr., Roccella EJ. 2003. Seventh report of the Joint National Committee on Prevention, Detection, Evaluation, and Treatment of High Blood Pressure. Hypertension 42:1206-1252.

Christoffels VM, Habets PE, Franco D, Campione M, de Jong F, Lamers WH, Bao ZZ, Palmer S, Biben C, Harvey RP, Moorman AF. 2000. Chamber formation and morphogenesis in the developing mammalian heart. Dev Biol 223:266-278.

Christoffels VM, Moorman AF. 2009. Development of the cardiac conduction system: why are some regions of the heart more arrhythmogenic than others? Circ Arrhythm Electrophysiol 2:195-207.

Church DJ, Braconi S, van der Bent V, Vallotton MB, Lang U. 1994a. Protein kinase C-dependent prostaglandin production mediates angiotensin II-induced atrial-natriuretic peptide release. Biochem J 298 (Pt 2):451-456.

Church DJ, van der Bent V, Vallotton MB, Capponi AM, Lang U. 1994b. Calcium influx in platelet activating factor-induced atrial natriuretic peptide release in rat cardiomyocytes. Am J Physiol 266:E403-409.

Clozel JP, Ertel EA, Ertel SI. 1997. Discovery and main pharmacological properties of mibefradil (Ro 40-5967), the first selective T-type calcium channel blocker. J Hypertens Suppl 15:S17-25.

Cohen NM, Lederer WJ. 1988. Changes in the calcium current of rat heart ventricular myocytes during development. J Physiol 406:115-146.

Colomer JM, Terasawa M, Means AR. 2004. Targeted expression of calmodulin increases ventricular cardiomyocyte proliferation and deoxyribonucleic acid synthesis during mouse development. Endocrinology 145:1356-1366.

Copeland JG, Smith RG, Arabia FA, Nolan PE, Sethi GK, Tsau PH, McClellan D, Slepian MJ. 2004. Cardiac replacement with a total artificial heart as a bridge to transplantation. N Engl J Med 351:859-867.

Crabtree GR. 2001. Calcium, calcineurin, and the control of transcription. J Biol Chem 276:2313-2316.

Cribbs LL, Martin BL, Schroder EA, Keller BB, Delisle BP, Satin J. 2001. Identification of the t-type calcium channel (Ca(v)3.1d) in developing mouse heart. Circ Res 88:403-407.

Dai YS, Cserjesi P, Markham BE, Molkentin JD. 2002. The transcription factors GATA4 and dHAND physically interact to synergistically activate cardiac gene expression through a p300-dependent mechanism. J Biol Chem 277:24390-24398.

D'Ascenzo M, Piacentini R, Casalbore P, Budoni M, Pallini R, Azzena GB, Grassi C. 2006. Role of L-type Ca2+ channels in neural stem/progenitor cell differentiation. Eur J Neurosci 23:935-944.

Davis DL, Edwards AV, Juraszek AL, Phelps A, Wessels A, Burch JB. 2001. A GATA-6 gene heart-region-specific enhancer provides a novel means to mark and probe a discrete component of the mouse cardiac conduction system. Mech Dev 108:105-119.

de Bold AJ, Borenstein HB, Veress AT, Sonnenberg H. 1981. A rapid and potent natriuretic response to intravenous injection of atrial myocardial extract in rats. Life Sci 28:89-94.

de Bold AJ, Flynn TG. 1983. Cardionatrin I - a novel heart peptide with potent diuretic and natriuretic properties. Life Sci 33:297-302.

De Young MB, Keller JC, Graham RM, Wildey GM. 1994. Brefeldin A defines distinct pathways for atrial natriuretic factor secretion in neonatal rat atrial and ventricular myocytes. Circ Res 74:33-40.

Delorme B, Dahl E, Jarry-Guichard T, Marics I, Briand JP, Willecke K, Gros D, Theveniau-Ruissy M. 1995. Developmental regulation of connexin 40 gene expression in mouse heart correlates with the differentiation of the conduction system. Dev Dyn 204:358-371.

DiCicco-Bloom E, Lelievre V, Zhou X, Rodriguez W, Tam J, Waschek JA. 2004. Embryonic expression and multifunctional actions of the natriuretic peptides and receptors in the developing nervous system. Dev Biol 271:161-175.

D'Souza SP, Davis M, Baxter GF. 2004. Autocrine and paracrine actions of natriuretic peptides in the heart. Pharmacol Ther 101:113-129.

Durocher D, Nemer M. 1998. Combinatorial interactions regulating cardiac transcription. Dev Genet 22:250-262.

Edwards BS, Zimmerman RS, Schwab TR, Heublein DM, Burnett JC, Jr. 1988. Atrial stretch, not pressure, is the principal determinant controlling the acute release of atrial natriuretic factor. Circ Res 62:191-195.

Ellmers LJ, Knowles JW, Kim HS, Smithies O, Maeda N, Cameron VA. 2002. Ventricular expression of natriuretic peptides in Npr1(-/-) mice with cardiac hypertrophy and fibrosis. Am J Physiol Heart Circ Physiol 283:H707-714.

Ellmers LJ, Scott NJ, Piuhola J, Maeda N, Smithies O, Frampton CM, Richards AM, Cameron VA. 2007. Npr1-regulated gene pathways contributing to cardiac hypertrophy and fibrosis. J Mol Endocrinol 38:245-257.

Ertel EA, Campbell KP, Harpold MM, Hofmann F, Mori Y, Perez-Reyes E, Schwartz A, Snutch TP, Tanabe T, Birnbaumer L, Tsien RW, Catterall WA. 2000. Nomenclature of voltage-gated calcium channels. Neuron 25:533-535.

Evans MJ, Kaufman MH. 1981. Establishment in culture of pluripotential cells from mouse embryos. Nature 292:154-156.

Evans SM, Yelon D, Conlon FL, Kirby ML. 2010. Myocardial lineage development. Circ Res 107:1428-1444.

Fabiato A. 1983. Calcium-induced release of calcium from the cardiac sarcoplasmic reticulum. Am J Physiol 245:C1-14.

Fantl WJ, Johnson DE, Williams LT. 1993. Signalling by receptor tyrosine kinases. Annu Rev Biochem 62:453-481.

Fawcett DW, McNutt NS. 1969. The ultrastructure of the cat myocardium. I. Ventricular papillary muscle. J Cell Biol 42:1-45.

Ferron L, Capuano V, Deroubaix E, Coulombe A, Renaud JF. 2002. Functional and molecular characterization of a T-type Ca(2+) channel during fetal and postnatal rat heart development. J Mol Cell Cardiol 34:533-546.

Fishman MC, Chien KR. 1997. Fashioning the vertebrate heart: earliest embryonic decisions. Development 124:2099-2117.

Flynn TG, Davies PL, Kennedy BP, de Bold ML, de Bold AJ. 1985. Alignment of rat cardionatrin sequences with the preprocardionatrin sequence from complementary DNA. Science 228:323-325.

Flynn TG, de Bold ML, de Bold AJ. 1983. The amino acid sequence of an atrial peptide with potent diuretic and natriuretic properties. Biochem Biophys Res Commun 117:859-865.

Focaccio A, Volpe M, Ambrosio G, Lembo G, Pannain S, Rubattu S, Enea I, Pignalosa S, Chiariello M. 1993. Angiotensin II directly stimulates release of atrial natriuretic factor in isolated rabbit hearts. Circulation 87:192-198.

Forssmann WG, Richter R, Meyer M. 1998. The endocrine heart and natriuretic peptides: histochemistry, cell biology, and functional aspects of the renal urodilatin system. Histochem Cell Biol 110:335-357.

Fuller F, Porter JG, Arfsten AE, Miller J, Schilling JW, Scarborough RM, Lewicki JA, Schenk DB. 1988. Atrial natriuretic peptide clearance receptor. Complete sequence and functional expression of cDNA clones. J Biol Chem 263:9395-9401.

Gardner DG, Deschepper CF, Ganong WF, Hane S, Fiddes J, Baxter JD, Lewicki J. 1986. Extra-atrial expression of the gene for atrial natriuretic factor. Proc Natl Acad Sci U S A 83:6697-6701.

Garg V, Kathiriya IS, Barnes R, Schluterman MK, King IN, Butler CA, Rothrock CR, Eapen RS, Hirayama-Yamada K, Joo K, Matsuoka R, Cohen JC, Srivastava D. 2003. GATA4 mutations cause human congenital heart defects and reveal an interaction with TBX5. Nature 424:443-447.

Gaspard GJ, Pasumarthi KB. 2008. Quantification of cardiac fibrosis by colour-subtractive computer-assisted image analysis. Clin Exp Pharmacol Physiol 35:679-686.

Gassmann M, Casagranda F, Orioli D, Simon H, Lai C, Klein R, Lemke G. 1995. Aberrant neural and cardiac development in mice lacking the ErbB4 neuregulin receptor. Nature 378:390-394.

Goetz SC, Conlon FL. 2007. Cardiac progenitors and the embryonic cell cycle. Cell Cycle 6:1974-1981.

Gomora JC, Enyeart JA, Enyeart JJ. 1999. Mibefradil potently blocks ATP-activated K(+) channels in adrenal cells. Mol Pharmacol 56:1192-1197.

Gourdie RG, Mima T, Thompson RP, Mikawa T. 1995. Terminal diversification of the myocyte lineage generates Purkinje fibers of the cardiac conduction system. Development 121:1423-1431.

Gourdie RG, Severs NJ, Green CR, Rothery S, Germroth P, Thompson RP. 1993. The spatial distribution and relative abundance of gap-junctional connexin40 and connexin43 correlate to functional properties of components of the cardiac atrioventricular conduction system. J Cell Sci 105 (Pt 4):985-991.

Gourdie RG, Wei Y, Kim D, Klatt SC, Mikawa T. 1998. Endothelin-induced conversion of embryonic heart muscle cells into impulse-conducting Purkinje fibers. Proc Natl Acad Sci U S A 95:6815-6818.

Goy MF, Oliver PM, Purdy KE, Knowles JW, Fox JE, Mohler PJ, Qian X, Smithies O, Maeda N. 2001. Evidence for a novel natriuretic peptide receptor that prefers brain natriuretic peptide over atrial natriuretic peptide. Biochem J 358:379-387.

Habets PE, Moorman AF, Clout DE, van Roon MA, Lingbeek M, van Lohuizen M, Campione M, Christoffels VM. 2002. Cooperative action of Tbx2 and Nkx2.5 inhibits ANF expression in the atrioventricular canal: implications for cardiac chamber formation. Genes Dev 16:1234-1246.

Hamet P, Tremblay J, Pang SC, Garcia R, Thibault G, Gutkowska J, Cantin M, Genest J. 1984. Effect of native and synthetic atrial natriuretic factor on cyclic GMP. Biochem Biophys Res Commun 123:515-527.

Han W, Bao W, Wang Z, Nattel S. 2002. Comparison of ion-channel subunit expression in canine cardiac Purkinje fibers and ventricular muscle. Circ Res 91:790-797.

Hans F, Dimitrov S. 2001. Histone H3 phosphorylation and cell division. Oncogene 20:3021-3027.

Harvey RP. 1996. NK-2 homeobox genes and heart development. Dev Biol 178:203-216.

Harvey RP. 2002. Patterning the vertebrate heart. Nat Rev Genet 3:544-556.

Hatcher CJ, Basson CT. 2009. Specification of the cardiac conduction system by transcription factors. Circ Res 105:620-630.

He JQ, Ma Y, Lee Y, Thomson JA, Kamp TJ. 2003. Human embryonic stem cells develop into multiple types of cardiac myocytes: action potential characterization. Circ Res 93:32-39.

Heim C, Nooh E, Kondruweit M, Weyand M, Tandler R. 2013. Single centre experience with prolonged waiting time on transplant list with "high-urgency" status. Thorac Cardiovasc Surg 61:251-254.

Hersey RM, Nazir MA, Whitney KD, Klein RM, Sale RD, Hinton DA, Weisz J, Gattone VH, 2nd. 1989. Atrial natriuretic peptide in heart and specific binding in organs from fetal and newborn rats. Cell Biochem Funct 7:35-41.

Hierlihy AM, Seale P, Lobe CG, Rudnicki MA, Megeney LA. 2002. The post-natal heart contains a myocardial stem cell population. FEBS Lett 530:239-243.

Hirano Y, Fozzard HA, January CT. 1989. Characteristics of L- and T-type Ca2+ currents in canine cardiac Purkinje cells. Am J Physiol 256:H1478-1492.

Hiroi Y, Kudoh S, Monzen K, Ikeda Y, Yazaki Y, Nagai R, Komuro I. 2001. Tbx5 associates with Nkx2-5 and synergistically promotes cardiomyocyte differentiation. Nat Genet 28:276-280.

Hockerman GH, Peterson BZ, Johnson BD, Catterall WA. 1997. Molecular determinants of drug binding and action on L-type calcium channels. Annu Rev Pharmacol Toxicol 37:361-396.

Hodgson-Zingman DM, Karst ML, Zingman LV, Heublein DM, Darbar D, Herron KJ, Ballew JD, de Andrade M, Burnett JC, Jr., Olson TM. 2008. Atrial natriuretic peptide frameshift mutation in familial atrial fibrillation. N Engl J Med 359:158-165.

Hoffman JI. 1995. Incidence of congenital heart disease: I. Postnatal incidence. Pediatr Cardiol 16:103-113.

Holtwick R, van Eickels M, Skryabin BV, Baba HA, Bubikat A, Begrow F, Schneider MD, Garbers DL, Kuhn M. 2003. Pressure-independent cardiac hypertrophy in mice with cardiomyocyte-restricted inactivation of the atrial natriuretic peptide receptor guanylyl cyclase-A. J Clin Invest 111:1399-1407.

Horio T, Nishikimi T, Yoshihara F, Matsuo H, Takishita S, Kangawa K. 2000. Inhibitory regulation of hypertrophy by endogenous atrial natriuretic peptide in cultured cardiac myocytes. Hypertension 35:19-24.

Horsthuis T, Houweling AC, Habets PE, de Lange FJ, el Azzouzi H, Clout DE, Moorman AF, Christoffels VM. 2008. Distinct regulation of developmental and heart disease-induced atrial natriuretic factor expression by two separate distal sequences. Circ Res 102:849-859.

Hotchkiss A, Robinson J, MacLean J, Feridooni T, Wafa K, Pasumarthi KB. 2012. Role of D-type cyclins in heart development and disease. Can J Physiol Pharmacol 90:1197-1207.

Houslay MD, Milligan G. 1997. Tailoring cAMP-signalling responses through isoform multiplicity. Trends Biochem Sci 22:217-224.

Hunt SA. 2005. ACC/AHA 2005 guideline update for the diagnosis and management of chronic heart failure in the adult: a report of the American College of Cardiology/American Heart Association Task Force on Practice Guidelines (Writing Committee to Update the 2001 Guidelines for the Evaluation and Management of Heart Failure). J Am Coll Cardiol 46:e1-82.

Inagami T, Misono KS, Fukumi H, Maki M, Tanaka I, Takayanagi R, Imada T, Grammer RT, Naruse M, Naruse K, et al. 1987. Structure and physiological actions of rat atrial natriuretic factor. Hypertension 10:I113-117.

Inoue K, Naruse K, Yamagami S, Mitani H, Suzuki N, Takei Y. 2003. Four functionally distinct C-type natriuretic peptides found in fish reveal evolutionary history of the natriuretic peptide system. Proc Natl Acad Sci U S A 100:10079-10084.

Irons CE, Sei CA, Glembotski CC. 1993. Regulated secretion of atrial natriuretic factor from cultured ventricular myocytes. Am J Physiol 264:H282-285.

Jamieson JD, Palade GE. 1964. Specific Granules in Atrial Muscle Cells. J Cell Biol 23:151-172.

Janssens S, Dubois C, Bogaert J, Theunissen K, Deroose C, Desmet W, Kalantzi M, Herbots L, Sinnaeve P, Dens J, Maertens J, Rademakers F, Dymarkowski S, Gheysens O, Van Cleemput J, Bormans G, Nuyts J, Belmans A, Mortelmans L, Boogaerts M, Van de Werf F. 2006. Autologous bone marrow-derived stem-cell transfer in patients with ST-segment elevation myocardial infarction: double-blind, randomised controlled trial. Lancet 367:113-121.

Jay PY, Harris BS, Maguire CT, Buerger A, Wakimoto H, Tanaka M, Kupershmidt S, Roden DM, Schultheiss TM, O'Brien TX, Gourdie RG, Berul CI, Izumo S. 2004. Nkx2-5 mutation causes anatomic hypoplasia of the cardiac conduction system. J Clin Invest 113:1130-1137.

John SW, Veress AT, Honrath U, Chong CK, Peng L, Smithies O, Sonnenberg H. 1996. Blood pressure and fluid-electrolyte balance in mice with reduced or absent ANP. Am J Physiol 271:R109-114.

Kahl CR, Means AR. 2003. Regulation of cell cycle progression by calcium/calmodulin-dependent pathways. Endocr Rev 24:719-736.

Kamino K, Hirota A, Fujii S. 1981. Localization of pacemaking activity in early embryonic heart monitored using voltage-sensitive dye. Nature 290:595-597.

Kangawa K, Matsuo H. 1984. Purification and complete amino acid sequence of alpha-human atrial natriuretic polypeptide (alpha-hANP). Biochem Biophys Res Commun 118:131-139.

Kasirajan V, Tang DG, Katlaps GJ, Shah KB. 2012. The total artificial heart for biventricular heart failure and beyond. Curr Opin Cardiol 27:301-307.

Kattman SJ, Huber TL, Keller GM. 2006. Multipotent flk-1+ cardiovascular progenitor cells give rise to the cardiomyocyte, endothelial, and vascular smooth muscle lineages. Dev Cell 11:723-732.

Katz AM. 2011. Physiology of the Heart, Fifth Edition. Philadelphia, PA: Lippincott William & Wilkins. 3-575 pp.

Katzung BG. 2009. Basic and Clinical Pharmacology. McGraw Hill. 1-1218 pp.

Kaupp UB, Seifert R. 2002. Cyclic nucleotide-gated ion channels. Physiol Rev 82:769-824.

Kilic A, Bubikat A, Gassner B, Baba HA, Kuhn M. 2007. Local actions of atrial natriuretic peptide counteract angiotensin II stimulated cardiac remodeling. Endocrinology 148:4162-4169.

Kim D. 1992. A mechanosensitive K+ channel in heart cells. Activation by arachidonic acid. J Gen Physiol 100:1021-1040.

Kim D. 1993. Novel cation-selective mechanosensitive ion channel in the atrial cell membrane. Circ Res 72:225-231.

Kinnunen P, Taskinen T, Jarvinen M, Ruskoaho H. 1991. Effect of phorbol ester on the release of atrial natriuretic peptide from the hypertrophied rat myocardium. Br J Pharmacol 102:453-461.

Kinoshita H, Kuwahara K, Nishida M, Jian Z, Rong X, Kiyonaka S, Kuwabara Y, Kurose H, Inoue R, Mori Y, Li Y, Nakagawa Y, Usami S, Fujiwara M, Yamada Y, Minami T, Ueshima K, Nakao K. 2010. Inhibition of TRPC6 channel activity contributes to the antihypertrophic effects of natriuretic peptides-guanylyl cyclase-A signaling in the heart. Circ Res 106:1849-1860.

Kirby ML. 2007. Cardiac Development. New York: Oxford University Press. 3-273 pp.

Kisch B. 1956. Electron microscopy of the atrium of the heart. I. Guinea pig. Exp Med Surg 14:99-112.

Klaiber M, Kruse M, Volker K, Schroter J, Feil R, Freichel M, Gerling A, Feil S, Dietrich A, Londono JE, Baba HA, Abramowitz J, Birnbaumer L, Penninger JM, Pongs O, Kuhn M. 2010. Novel insights into the mechanisms mediating the local antihypertrophic effects of cardiac atrial natriuretic peptide: role of cGMP-dependent protein kinase and RGS2. Basic Res Cardiol 105:583-595.

Klitzner TS, Friedman WF. 1989. A diminished role for the sarcoplasmic reticulum in newborn myocardial contraction: effects of ryanodine. Pediatr Res 26:98-101.

Klug MG, Soonpaa MH, Koh GY, Field LJ. 1996. Genetically selected cardiomyocytes from differentiating embronic stem cells form stable intracardiac grafts. J Clin Invest 98:216-224.

Knowles JW, Esposito G, Mao L, Hagaman JR, Fox JE, Smithies O, Rockman HA, Maeda N. 2001. Pressure-independent enhancement of cardiac hypertrophy in natriuretic peptide receptor A-deficient mice. J Clin Invest 107:975-984.

Koide M, Akins RE, Harayama H, Yasui K, Yokota M, Tuan RS. 1996. Atrial natriuretic peptide accelerates proliferation of chick embryonic cardiomyocytes in vitro. Differentiation 61:1-11.

Koledova VV, Khalil RA. 2006. Ca2+, calmodulin, and cyclins in vascular smooth muscle cell cycle. Circ Res 98:1240-1243.

Komuro I, Izumo S. 1993. Csx: a murine homeobox-containing gene specifically expressed in the developing heart. Proc Natl Acad Sci U S A 90:8145-8149.

Kumar PP, Stotz SC, Paramashivappa R, Beedle AM, Zamponi GW, Rao AS. 2002. Synthesis and evaluation of a new class of nifedipine analogs with T-type calcium channel blocking activity. Mol Pharmacol 61:649-658.

Kuno T, Andresen JW, Kamisaki Y, Waldman SA, Chang LY, Saheki S, Leitman DC, Nakane M, Murad F. 1986. Co-purification of an atrial natriuretic factor receptor and particulate guanylate cyclase from rat lung. J Biol Chem 261:5817-5823.

Kupershmidt S, Yang T, Anderson ME, Wessels A, Niswender KD, Magnuson MA, Roden DM. 1999. Replacement by homologous recombination of the minK gene with lacZ reveals restriction of minK expression to the mouse cardiac conduction system. Circ Res 84:146-152.

Laflamme MA, Chen KY, Naumova AV, Muskheli V, Fugate JA, Dupras SK, Reinecke H, Xu C, Hassanipour M, Police S, O'Sullivan C, Collins L, Chen Y, Minami E, Gill EA, Ueno S, Yuan C, Gold J, Murry CE. 2007. Cardiomyocytes derived from human embryonic stem cells in pro-survival factors enhance function of infarcted rat hearts. Nat Biotechnol 25:1015-1024.

Laflamme MA, Gold J, Xu C, Hassanipour M, Rosler E, Police S, Muskheli V, Murry CE. 2005. Formation of human myocardium in the rat heart from human embryonic stem cells. Am J Pathol 167:663-671.

Laflamme MA, Murry CE. 2005. Regenerating the heart. Nat Biotechnol 23:845-856.

Laine M, Arjamaa O, Vuolteenaho O, Ruskoaho H, Weckstrom M. 1994. Block of stretch-activated atrial natriuretic peptide secretion by gadolinium in isolated rat atrium. J Physiol 480 (Pt 3):553-561.

Lang RE, Tholken H, Ganten D, Luft FC, Ruskoaho H, Unger T. 1985. Atrial natriuretic factor--a circulating hormone stimulated by volume loading. Nature 314:264-266.

LaPointe MC, Deschepper CF, Wu JP, Gardner DG. 1990. Extracellular calcium regulates expression of the gene for atrial natriuretic factor. Hypertension 15:20-28.

Laragh JH. 1985. Atrial natriuretic hormone, the renin-aldosterone axis, and blood pressure-electrolyte homeostasis. N Engl J Med 313:1330-1340.

Laskowski A, Woodman OL, Cao AH, Drummond GR, Marshall T, Kaye DM, Ritchie RH. 2006. Antioxidant actions contribute to the antihypertrophic effects of atrial natriuretic peptide in neonatal rat cardiomyocytes. Cardiovasc Res 72:112-123.

Lew RA, Baertschi AJ. 1989. Endothelial cells stimulate ANF secretion from atrial myocytes in co-culture. Biochem Biophys Res Commun 163:701-709.

Li J, Puceat M, Perez-Terzic C, Mery A, Nakamura K, Michalak M, Krause KH, Jaconi ME. 2002. Calreticulin reveals a critical Ca(2+) checkpoint in cardiac myofibrillogenesis. J Cell Biol 158:103-113.

Li M, Zhang M, Huang L, Zhou J, Zhuang H, Taylor JT, Keyser BM, Whitehurst RM, Jr. 2005. T-type Ca2+ channels are involved in high glucose-induced rat neonatal cardiomyocyte proliferation. Pediatr Res 57:550-556.

Li QY, Newbury-Ecob RA, Terrett JA, Wilson DI, Curtis AR, Yi CH, Gebuhr T, Bullen PJ, Robson SC, Strachan T, Bonnet D, Lyonnet S, Young ID, Raeburn JA, Buckler AJ, Law DJ, Brook JD. 1997. Holt-Oram syndrome is caused by mutations in TBX5, a member of the Brachyury (T) gene family. Nat Genet 15:21-29.

Li Y, Saito Y, Kuwahara K, Rong X, Kishimoto I, Harada M, Adachi Y, Nakanishi M, Kinoshita H, Horiuchi M, Murray M, Nakao K. 2009. Guanylyl cyclase-A inhibits angiotensin II type 2 receptor-mediated pro-hypertrophic signaling in the heart. Endocrinology 150:3759-3765.

Liang X, Wang G, Lin L, Lowe J, Zhang Q, Bu L, Chen YH, Chen J, Sun Y, Evans SM. 2013. HCN4 Dynamically Marks the First Heart Field and Conduction System Precursors. Circ Res.

Light DB, Corbin JD, Stanton BA. 1990. Dual ion-channel regulation by cyclic GMP and cyclic GMP-dependent protein kinase. Nature 344:336-339.

Lin Q, Schwarz J, Bucana C, Olson EN. 1997. Control of mouse cardiac morphogenesis and myogenesis by transcription factor MEF2C. Science 276:1404-1407.

Lin X, Hanze J, Heese F, Sodmann R, Lang RE. 1995. Gene expression of natriuretic peptide receptors in myocardial cells. Circ Res 77:750-758.

Linask KL, Linask KK. 2010. Calcium channel blockade in embryonic cardiac progenitor cells disrupts normal cardiac cell differentiation. Stem Cells Dev 19:1959-1965.

Lincoln TM, Cornwell TL. 1993. Intracellular cyclic GMP receptor proteins. Faseb J 7:328-338.

Lipscombe D, Helton TD, Xu W. 2004. L-type calcium channels: the low down. J Neurophysiol 92:2633-2641.

Liu W, Yasui K, Arai A, Kamiya K, Cheng J, Kodama I, Toyama J. 1999. beta-adrenergic modulation of L-type Ca2+-channel currents in early-stage embryonic mouse heart. Am J Physiol 276:H608-613.

Liu W, Yasui K, Opthof T, Ishiki R, Lee JK, Kamiya K, Yokota M, Kodama I. 2002. Developmental changes of Ca(2+) handling in mouse ventricular cells from early embryo to adulthood. Life Sci 71:1279-1292.

Livak KJ, Schmittgen TD. 2001. Analysis of relative gene expression data using real-time quantitative PCR and the 2(-Delta Delta C(T)) Method. Methods 25:402-408.

Lopez MJ, Wong SK, Kishimoto I, Dubois S, Mach V, Friesen J, Garbers DL, Beuve A. 1995. Salt-resistant hypertension in mice lacking the guanylyl cyclase-A receptor for atrial natriuretic peptide. Nature 378:65-68.

Lory P, Bidaud I, Chemin J. 2006. T-type calcium channels in differentiation and proliferation. Cell Calcium 40:135-146.

Lowe DG. 1992. Human natriuretic peptide receptor-A guanylyl cyclase is self-associated prior to hormone binding. Biochemistry 31:10421-10425.

Lowe DG, Chang MS, Hellmiss R, Chen E, Singh S, Garbers DL, Goeddel DV. 1989. Human atrial natriuretic peptide receptor defines a new paradigm for second messenger signal transduction. Embo J 8:1377-1384.

Lu Y, James TN, Yamamoto S, Terasaki F. 1993. Cardiac conduction system in the chicken: gross anatomy plus light and electron microscopy. Anat Rec 236:493-510.

Lynch J, Guo L, Gelebart P, Chilibeck K, Xu J, Molkentin JD, Agellon LB, Michalak M. 2005. Calreticulin signals upstream of calcineurin and MEF2C in a critical Ca(2+)-dependent signaling cascade. J Cell Biol 170:37-47.

Lyons GE. 1994. In situ analysis of the cardiac muscle gene program during embryogenesis. Trends Cardiovasc Med 4:70-77.

Lyons GE, Schiaffino S, Sassoon D, Barton P, Buckingham M. 1990. Developmental regulation of myosin gene expression in mouse cardiac muscle. J Cell Biol 111:2427-2436.

Maack T, Suzuki M, Almeida FA, Nussenzveig D, Scarborough RM, McEnroe GA, Lewicki JA. 1987. Physiological role of silent receptors of atrial natriuretic factor. Science 238:675-678.

Macklin R. 2010. Enrolling pregnant women in biomedical research. Lancet 375:632-633.

Maier LS, Bers DM. 2002. Calcium, calmodulin, and calcium-calmodulin kinase II: heartbeat to heartbeat and beyond. J Mol Cell Cardiol 34:919-939.

Makkar RR, Smith RR, Cheng K, Malliaras K, Thomson LE, Berman D, Czer LS, Marban L, Mendizabal A, Johnston PV, Russell SD, Schuleri KH, Lardo AC, Gerstenblith G, Marban E. 2012. Intracoronary cardiosphere-derived cells for heart regeneration after myocardial infarction (CADUCEUS): a prospective, randomised phase 1 trial. Lancet 379:895-904.

Manninen AK, Juhakoski A. 1991. Nifedipine concentrations in maternal and umbilical serum, amniotic fluid, breast milk and urine of mothers and offspring. Int J Clin Pharmacol Res 11:231-236.

Martin CM, Meeson AP, Robertson SM, Hawke TJ, Richardson JA, Bates S, Goetsch SC, Gallardo TD, Garry DJ. 2004. Persistent expression of the ATP-binding cassette transporter, Abcg2, identifies cardiac SP cells in the developing and adult heart. Dev Biol 265:262-275.

Martin GR. 1981. Isolation of a pluripotent cell line from early mouse embryos cultured in medium conditioned by teratocarcinoma stem cells. Proc Natl Acad Sci U S A 78:7634-7638.

Martin-Puig S, Wang Z, Chien KR. 2008. Lives of a heart cell: tracing the origins of cardiac progenitors. Cell Stem Cell 2:320-331.

Matsukawa N, Grzesik WJ, Takahashi N, Pandey KN, Pang S, Yamauchi M, Smithies O. 1999. The natriuretic peptide clearance receptor locally modulates the physiological effects of the natriuretic peptide system. Proc Natl Acad Sci U S A 96:7403-7408.

McDonough PM, Stella SL, Glembotski CC. 1994. Involvement of cytoplasmic calcium and protein kinases in the regulation of atrial natriuretic factor secretion by contraction rate and endothelin. J Biol Chem 269:9466-9472.

McGrath MF, de Bold ML, de Bold AJ. 2005. The endocrine function of the heart. Trends Endocrinol Metab 16:469-477.

McKelvie RS, Moe GW, Ezekowitz JA, Heckman GA, Costigan J, Ducharme A, Estrella-Holder E, Giannetti N, Grzeslo A, Harkness K, Howlett JG, Kouz S, Leblanc K, Mann E, Nigam A, O'Meara E, Rajda M, Steinhart B, Swiggum E, Le VV, Zieroth S, Arnold JM, Ashton T, D'Astous M, Dorian P, Haddad H, Isaac DL, Leblanc MH, Liu P, Rao V, Ross HJ, Sussex B. 2013. The 2012 Canadian Cardiovascular Society heart failure management guidelines update: focus on acute and chronic heart failure. Can J Cardiol 29:168-181.

McKinsey TA, Zhang CL, Olson EN. 2002. MEF2: a calcium-dependent regulator of cell division, differentiation and death. Trends Biochem Sci 27:40-47.

McManus RP, O'Hair DP, Beitzinger JM, Schweiger J, Siegel R, Breen TJ, Olinger GN. 1993. Patients who die awaiting heart transplantation. J Heart Lung Transplant 12:159-171; discussion 172.

McMullen NM, Pasumarthi KB. 2007. Donor cell transplantation for myocardial disease: does it complement current pharmacological therapies? Can J Physiol Pharmacol 85:1-15.

McMullen NM, Zhang F, Hotchkiss A, Bretzner F, Wilson JM, Ma H, Wafa K, Brownstone RM, Pasumarthi KB. 2009. Functional characterization of cardiac progenitor cells and their derivatives in the embryonic heart post-chamber formation. Dev Dyn 238:2787-2799.

McMurray JJ, Adamopoulos S, Anker SD, Auricchio A, Bohm M, Dickstein K, Falk V, Filippatos G, Fonseca C, Gomez-Sanchez MA, Jaarsma T, Kober L, Lip GY, Maggioni AP, Parkhomenko A, Pieske BM, Popescu BA, Ronnevik PK, Rutten FH, Schwitter J, Seferovic P, Stepinska J, Trindade PT, Voors AA, Zannad F, Zeiher A, Bax JJ, Baumgartner H, Ceconi C, Dean V, Deaton C, Fagard R, Funck-Brentano C, Hasdai D, Hoes A, Kirchhof P, Knuuti J, Kolh P, McDonagh T, Moulin C, Reiner Z, Sechtem U, Sirnes PA, Tendera M, Torbicki A, Vahanian A, Windecker S, Bonet LA, Avraamides P, Ben Lamin HA, Brignole M, Coca A, Cowburn P, Dargie H, Elliott P, Flachskampf FA, Guida GF, Hardman S, Iung B, Merkely B, Mueller C, Nanas JN, Nielsen OW, Orn S, Parissis JT, Ponikowski P. 2013. ESC guidelines for the diagnosis and treatment of acute and chronic heart failure 2012: The Task Force for the Diagnosis and Treatment of Acute and Chronic Heart Failure 2012 of the European Society of Cardiology. Developed in collaboration with the Heart Failure Association (HFA) of the ESC. Eur J Heart Fail 14:803-869.

Mei L, Xiong WC. 2008. Neuregulin 1 in neural development, synaptic plasticity and schizophrenia. Nat Rev Neurosci 9:437-452.

Meijer DK, Van der Sluijs P. 1987. The influence of binding to albumin and alpha 1-acid glycoprotein on the clearance of drugs by the liver. Pharm Weekbl Sci 9:65-74.

Melo LG, Steinhelper ME, Pang SC, Tse Y, Ackermann U. 2000. ANP in regulation of arterial pressure and fluid-electrolyte balance: lessons from genetic mouse models. Physiol Genomics 3:45-58.

Menasche P, Hagege AA, Vilquin JT, Desnos M, Abergel E, Pouzet B, Bel A, Sarateanu S, Scorsin M, Schwartz K, Bruneval P, Benbunan M, Marolleau JP, Duboc D. 2003.

Autologous skeletal myoblast transplantation for severe postinfarction left ventricular dysfunction. J Am Coll Cardiol 41:1078-1083.

Meysen S, Marger L, Hewett KW, Jarry-Guichard T, Agarkova I, Chauvin JP, Perriard JC, Izumo S, Gourdie RG, Mangoni ME, Nargeot J, Gros D, Miquerol L. 2007. Nkx2.5 cell-autonomous gene function is required for the postnatal formation of the peripheral ventricular conduction system. Dev Biol 303:740-753.

Mikawa T, Hurtado R. 2007. Development of the cardiac conduction system. Semin Cell Dev Biol 18:90-100.

Miquerol L, Meysen S, Mangoni M, Bois P, van Rijen HV, Abran P, Jongsma H, Nargeot J, Gros D. 2004. Architectural and functional asymmetry of the His-Purkinje system of the murine heart. Cardiovasc Res 63:77-86.

Miquerol L, Moreno-Rascon N, Beyer S, Dupays L, Meilhac SM, Buckingham ME, Franco D, Kelly RG. 2010. Biphasic development of the mammalian ventricular conduction system. Circ Res 107:153-161.

Molkentin JD, Lin Q, Duncan SA, Olson EN. 1997. Requirement of the transcription factor GATA4 for heart tube formation and ventral morphogenesis. Genes Dev 11:1061-1072.

Molkentin JD, Lu JR, Antos CL, Markham B, Richardson J, Robbins J, Grant SR, Olson EN. 1998. A calcineurin-dependent transcriptional pathway for cardiac hypertrophy. Cell 93:215-228.

Moorman AF, Lamers WH. 1994. Molecular anatomy of the developing heart. Trends Cardiovasc Med 4:257-264.

Mori AD, Bruneau BG. 2004. TBX5 mutations and congenital heart disease: Holt-Oram syndrome revealed. Curr Opin Cardiol 19:211-215.

Morin S, Charron F, Robitaille L, Nemer M. 2000. GATA-dependent recruitment of MEF2 proteins to target promoters. Embo J 19:2046-2055.

Morin S, Pozzulo G, Robitaille L, Cross J, Nemer M. 2005. MEF2-dependent recruitment of the HAND1 transcription factor results in synergistic activation of target promoters. J Biol Chem 280:32272-32278.

Moskowitz IP, Kim JB, Moore ML, Wolf CM, Peterson MA, Shendure J, Nobrega MA, Yokota Y, Berul C, Izumo S, Seidman JG, Seidman CE. 2007. A molecular pathway including Id2, Tbx5, and Nkx2-5 required for cardiac conduction system development. Cell 129:1365-1376.

Murry CE, Keller G. 2008. Differentiation of embryonic stem cells to clinically relevant populations: lessons from embryonic development. Cell 132:661-680.

Murry CE, Wiseman RW, Schwartz SM, Hauschka SD. 1996. Skeletal myoblast transplantation for repair of myocardial necrosis. J Clin Invest 98:2512-2523.

Murthy KS, Makhlouf GM. 1999. Identification of the G protein-activating domain of the natriuretic peptide clearance receptor (NPR-C). J Biol Chem 274:17587-17592.

Myers DC, Fishman GI. 2003. Molecular and functional maturation of the murine cardiac conduction system. Trends Cardiovasc Med 13:289-295.

Nagase M, Katafuchi T, Hirose S, Fujita T. 1997. Tissue distribution and localization of natriuretic peptide receptor subtypes in stroke-prone spontaneously hypertensive rats. J Hypertens 15:1235-1243.

Nakayama T, Soma M, Takahashi Y, Rehemudula D, Kanmatsuse K, Furuya K. 2000. Functional deletion mutation of the 5'-flanking region of type A human natriuretic peptide receptor gene and its association with essential hypertension and left ventricular hypertrophy in the Japanese. Circ Res 86:841-845.

Nemer M, Lavigne JP, Drouin J, Thibault G, Gannon M, Antakly T. 1986. Expression of atrial natriuretic factor gene in heart ventricular tissue. Peptides 7:1147-1152.

Newbury-Ecob RA, Leanage R, Raeburn JA, Young ID. 1996. Holt-Oram syndrome: a clinical genetic study. J Med Genet 33:300-307.

Nguemo F, Fleischmann BK, Gupta MK, Saric T, Malan D, Liang H, Pfannkuche K, Bloch W, Schunkert H, Hescheler J, Reppel M. 2013. The L-type Ca2+ channels blocker nifedipine represses mesodermal fate determination in murine embryonic stem cells. PLoS One 8:e53407.

Nielsen MS, Nygaard Axelsen L, Sorgen PL, Verma V, Delmar M, Holstein-Rathlou NH. 2012. Gap junctions. Compr Physiol 2:1981-2035.

Niwa N, Yasui K, Opthof T, Takemura H, Shimizu A, Horiba M, Lee JK, Honjo H, Kamiya K, Kodama I. 2004. Cav3.2 subunit underlies the functional T-type Ca2+ channel in murine hearts during the embryonic period. Am J Physiol Heart Circ Physiol 286:H2257-2263.

Nolan GP, Fiering S, Nicolas JF, Herzenberg LA. 1988. Fluorescence-activated cell analysis and sorting of viable mammalian cells based on beta-D-galactosidase activity after transduction of Escherichia coli lacZ. Proc Natl Acad Sci U S A 85:2603-2607.

Nussbaum J, Minami E, Laflamme MA, Virag JA, Ware CB, Masino A, Muskheli V, Pabon L, Reinecke H, Murry CE. 2007. Transplantation of undifferentiated murine embryonic stem cells in the heart: teratoma formation and immune response. Faseb J 21:1345-1357.

Ogawa H, Qiu Y, Ogata CM, Misono KS. 2004. Crystal structure of hormone-bound atrial natriuretic peptide receptor extracellular domain: rotation mechanism for transmembrane signal transduction. J Biol Chem 279:28625-28631.

Oguri A, Tanaka T, Iida H, Meguro K, Takano H, Oonuma H, Nishimura S, Morita T, Yamasoba T, Nagai R, Nakajima T. 2010. Involvement of CaV3.1 T-type calcium channels in cell proliferation in mouse preadipocytes. Am J Physiol Cell Physiol 298:C1414-1423.

Oh H, Bradfute SB, Gallardo TD, Nakamura T, Gaussin V, Mishina Y, Pocius J, Michael LH, Behringer RR, Garry DJ, Entman ML, Schneider MD. 2003. Cardiac progenitor cells from adult myocardium: homing, differentiation, and fusion after infarction. Proc Natl Acad Sci U S A 100:12313-12318.

Oliver PM, Fox JE, Kim R, Rockman HA, Kim HS, Reddick RL, Pandey KN, Milgram SL, Smithies O, Maeda N. 1997. Hypertension, cardiac hypertrophy, and sudden death in mice lacking natriuretic peptide receptor A. Proc Natl Acad Sci U S A 94:14730-14735.

Olson EN, Srivastava D. 1996. Molecular pathways controlling heart development. Science 272:671-676.

Ono K, Iijima T. 2010. Cardiac T-type Ca(2+) channels in the heart. J Mol Cell Cardiol 48:65-70.

O'Tierney PF, Chattergoon NN, Louey S, Giraud GD, Thornburg KL. 2010. Atrial natriuretic peptide inhibits angiotensin II-stimulated proliferation in fetal cardiomyocytes. J Physiol 588:2879-2889.

Pagano M, Anand-Srivastava MB. 2001. Cytoplasmic domain of natriuretic peptide receptor C constitutes Gi activator sequences that inhibit adenylyl cyclase activity. J Biol Chem 276:22064-22070.

Pandey KN. 2005. Biology of natriuretic peptides and their receptors. Peptides 26:901-932.

Pandey KN, Nguyen HT, Li M, Boyle JW. 2000. Natriuretic peptide receptor-A negatively regulates mitogen-activated protein kinase and proliferation of mesangial cells: role of cGMP-dependent protein kinase. Biochem Biophys Res Commun 271:374-379.

Panner A, Wurster RD. 2006. T-type calcium channels and tumor proliferation. Cell Calcium 40:253-259.

Passier R, Zeng H, Frey N, Naya FJ, Nicol RL, McKinsey TA, Overbeek P, Richardson JA, Grant SR, Olson EN. 2000. CaM kinase signaling induces cardiac hypertrophy and activates the MEF2 transcription factor in vivo. J Clin Invest 105:1395-1406.

Pasumarthi KB, Field LJ. 2002. Cardiomyocyte cell cycle regulation. Circ Res 90:1044-1054.

Patel R, Kos L. 2005. Endothelin-1 and Neuregulin-1 convert embryonic cardiomyocytes into cells of the conduction system in the mouse. Dev Dyn 233:20-28.

Patten BM. 1949. Initiation and early changes in the character of the heart beat in vertebrate embryos. Physiol Rev 29:31-47.

Paul AK, Marala RB, Jaiswal RK, Sharma RK. 1987. Coexistence of guanylate cyclase and atrial natriuretic factor receptor in a 180-kD protein. Science 235:1224-1226.

Penner R, Neher E. 1988. The role of calcium in stimulus-secretion coupling in excitable and non-excitable cells. J Exp Biol 139:329-345.

Pentassuglia L, Sawyer DB. 2009. The role of Neuregulin-1beta/ErbB signaling in the heart. Exp Cell Res 315:627-637.

Perez-Reyes E. 2003. Molecular physiology of low-voltage-activated t-type calcium channels. Physiol Rev 83:117-161.

Perez-Reyes E, Van Deusen AL, Vitko I. 2009. Molecular pharmacology of human Cav3.2 T-type Ca2+ channels: block by antihypertensives, antiarrhythmics, and their analogs. J Pharmacol Exp Ther 328:621-627.

Perriard JC, Hirschy A, Ehler E. 2003. Dilated cardiomyopathy: a disease of the intercalated disc? Trends Cardiovasc Med 13:30-38.

Pikkarainen S, Tokola H, Kerkela R, Ruskoaho H. 2004. GATA transcription factors in the developing and adult heart. Cardiovasc Res 63:196-207.

Porter GA, Jr., Makuck RF, Rivkees SA. 2003. Intracellular calcium plays an essential role in cardiac development. Dev Dyn 227:280-290.

Potter LR, Abbey-Hosch S, Dickey DM. 2006. Natriuretic peptides, their receptors, and cyclic guanosine monophosphate-dependent signaling functions. Endocr Rev 27:47-72.

Prins BA, Weber MJ, Hu RM, Pedram A, Daniels M, Levin ER. 1996. Atrial natriuretic peptide inhibits mitogen-activated protein kinase through the clearance receptor. Potential role in the inhibition of astrocyte proliferation. J Biol Chem 271:14156-14162.

Puceat M, Jaconi M. 2005. Ca2+ signalling in cardiogenesis. Cell Calcium 38:383-389.

Qu Y, Boutjdir M. 2001. Gene expression of SERCA2a and L- and T-type Ca channels during human heart development. Pediatr Res 50:569-574.

Rana MS, Christoffels VM, Moorman AF. 2013. A molecular and genetic outline of cardiac morphogenesis. Acta Physiol (Oxf) 207:588-615.

Rebsamen MC, Church DJ, Morabito D, Vallotton MB, Lang U. 1997. Role of cAMP and calcium influx in endothelin-1-induced ANP release in rat cardiomyocytes. Am J Physiol 273:E922-931.

Reinecke H, Murry CE. 2002. Taking the death toll after cardiomyocyte grafting: a reminder of the importance of quantitative biology. J Mol Cell Cardiol 34:251-253.

Ren X, Xu C, Zhan C, Yang Y, Shi L, Wang F, Wang C, Xia Y, Yang B, Wu G, Wang P, Li X, Wang D, Xiong X, Liu J, Liu Y, Liu M, Tu X, Wang QK. 2010. Identification of NPPA variants associated with atrial fibrillation in a Chinese GeneID population. Clin Chim Acta 411:481-485.

Rentschler S, Vaidya DM, Tamaddon H, Degenhardt K, Sassoon D, Morley GE, Jalife J, Fishman GI. 2001. Visualization and functional characterization of the developing murine cardiac conduction system. Development 128:1785-1792.

Rentschler S, Zander J, Meyers K, France D, Levine R, Porter G, Rivkees SA, Morley GE, Fishman GI. 2002. Neuregulin-1 promotes formation of the murine cardiac conduction system. Proc Natl Acad Sci U S A 99:10464-10469.

Rodman DM, Reese K, Harral J, Fouty B, Wu S, West J, Hoedt-Miller M, Tada Y, Li KX, Cool C, Fagan K, Cribbs L. 2005. Low-voltage-activated (T-type) calcium channels control proliferation of human pulmonary artery myocytes. Circ Res 96:864-872.

Roell W, Lewalter T, Sasse P, Tallini YN, Choi BR, Breitbach M, Doran R, Becher UM, Hwang SM, Bostani T, von Maltzahn J, Hofmann A, Reining S, Eiberger B, Gabris B, Pfeifer A, Welz A, Willecke K, Salama G, Schrickel JW, Kotlikoff MI, Fleischmann BK. 2007. Engraftment of connexin 43-expressing cells prevents post-infarct arrhythmia. Nature 450:819-824.

Rose RA, Lomax AE, Kondo CS, Anand-Srivastava MB, Giles WR. 2004. Effects of C-type natriuretic peptide on ionic currents in mouse sinoatrial node: a role for the NPR-C receptor. Am J Physiol Heart Circ Physiol 286:H1970-1977.

Rosen MR, Robinson RB, Brink PR, Cohen IS. 2011. The road to biological pacing. Nat Rev Cardiol 8:656-666.

Rosenkranz AC, Woods RL, Dusting GJ, Ritchie RH. 2003. Antihypertrophic actions of the natriuretic peptides in adult rat cardiomyocytes: importance of cyclic GMP. Cardiovasc Res 57:515-522.

Rosenzweig A, Seidman CE. 1991. Atrial natriuretic factor and related peptide hormones. Annu Rev Biochem 60:229-255.

Ross H, Howlett J, Arnold JM, Liu P, O'Neill BJ, Brophy JM, Simpson CS, Sholdice MM, Knudtson M, Ross DB, Rottger J, Glasgow K. 2006. Treating the right patient at the right time: access to heart failure care. Can J Cardiol 22:749-754.

Rotman B, Zderic JA, Edelstein M. 1963. Fluorogenic substrates for beta-D-galactosidases and phosphatases derived from flurescein (3,6-dihydroxyfluoran) and its monomethylether. Proc Natl Acad Sci U S A 50:1-6.

Rubart M, Pasumarthi KB, Nakajima H, Soonpaa MH, Nakajima HO, Field LJ. 2003. Physiological coupling of donor and host cardiomyocytes after cellular transplantation. Circ Res 92:1217-1224.

Rumiantsev DO, Piotrovskii VK, Metelitsa VI, Slastnikova ID, Martsevich S, Kokurina EV. 1989. Serum binding of nifedipine and verapamil in patients with ischaemic heart disease on monotherapy. Br J Clin Pharmacol 28:357-361.

Ruskoaho H. 1992. Atrial natriuretic peptide: synthesis, release, and metabolism. Pharmacol Rev 44:479-602.

Salters CR, Jr., Bailey AL, Whayne TF, Jr. 2010. Current treatment of heart failure in the USA. Expert Rev Cardiovasc Ther 8:279-290.

Sankova B, Benes J, Jr., Krejci E, Dupays L, Theveniau-Ruissy M, Miquerol L, Sedmera D. 2012. The effect of connexin40 deficiency on ventricular conduction system function during development. Cardiovasc Res 95:469-479.

Sassoon DA, Garner I, Buckingham M. 1988. Transcripts of alpha-cardiac and alpha-skeletal actins are early markers for myogenesis in the mouse embryo. Development 104:155-164.

Schaub MC, Hefti MA, Harder BA, Eppenberger HM. 1997. Various hypertrophic stimuli induce distinct phenotypes in cardiomyocytes. J Mol Med (Berl) 75:901-920.

Schenk DB, Phelps MN, Porter JG, Fuller F, Cordell B, Lewicki JA. 1987. Purification and subunit composition of atrial natriuretic peptide receptor. Proc Natl Acad Sci U S A 84:1521-1525.

Schott JJ, Benson DW, Basson CT, Pease W, Silberbach GM, Moak JP, Maron BJ, Seidman CE, Seidman JG. 1998. Congenital heart disease caused by mutations in the transcription factor NKX2-5. Science 281:108-111.

Schultz K, Fanburg BL, Beasley D. 2006. Hypoxia and hypoxia-inducible factor-1alpha promote growth factor-induced proliferation of human vascular smooth muscle cells. Am J Physiol Heart Circ Physiol 290:H2528-2534.

Schulz S, Singh S, Bellet RA, Singh G, Tubb DJ, Chin H, Garbers DL. 1989. The primary structure of a plasma membrane guanylate cyclase demonstrates diversity within this new receptor family. Cell 58:1155-1162.

Schweizer PA, Yampolsky P, Malik R, Thomas D, Zehelein J, Katus HA, Koenen M. 2009. Transcription profiling of HCN-channel isotypes throughout mouse cardiac development. Basic Res Cardiol 104:621-629.

Scott NJ, Ellmers LJ, Lainchbury JG, Maeda N, Smithies O, Richards AM, Cameron VA. 2009. Influence of natriuretic peptide receptor-1 on survival and cardiac hypertrophy during development. Biochim Biophys Acta 1792:1175-1184.

Sedan O, Dolnikov K, Zeevi-Levin N, Fleishmann N, Spiegel I, Berdichevski S, Amit M, Itskovitz-Eldor J, Binah O. 2010. Human embryonic stem cell-derived cardiomyocytes can mobilize 1,4,5-inositol trisphosphate-operated [Ca2+]i stores: the functionality of angiotensin-II/endothelin-1 signaling pathways. Ann N Y Acad Sci 1188:68-77.

Sedmera D, Harris BS, Grant E, Zhang N, Jourdan J, Kurkova D, Gourdie RG. 2008. Cardiac expression patterns of endothelin-converting enzyme (ECE): implications for conduction system development. Dev Dyn 237:1746-1753.

Sedmera D, Reckova M, DeAlmeida A, Coppen SR, Kubalak SW, Gourdie RG, Thompson RP. 2003. Spatiotemporal pattern of commitment to slowed proliferation in the embryonic mouse heart indicates progressive differentiation of the cardiac conduction system. Anat Rec A Discov Mol Cell Evol Biol 274:773-777.

Sei CA, Glembotski CC. 1990. Calcium dependence of phenylephrine-, endothelin-, and potassium chloride-stimulated atrial natriuretic factor secretion from long term primary neonatal rat atrial cardiocytes. J Biol Chem 265:7166-7172.

Sharma GD, Nguyen HT, Antonov AS, Gerrity RG, von Geldern T, Pandey KN. 2002. Expression of atrial natriuretic peptide receptor-A antagonizes the mitogen-activated protein kinases (Erk2 and P38MAPK) in cultured human vascular smooth muscle cells. Mol Cell Biochem 233:165-173.

Shcheglovitov A, Zhelay T, Vitko Y, Osipenko V, Perez-Reyes E, Kostyuk P, Shuba Y. 2005. Contrasting the effects of nifedipine on subtypes of endogenous and recombinant T-type Ca2+ channels. Biochem Pharmacol 69:841-854.

Shiba Y, Fernandes S, Zhu WZ, Filice D, Muskheli V, Kim J, Palpant NJ, Gantz J, Moyes KW, Reinecke H, Van Biber B, Dardas T, Mignone JL, Izawa A, Hanna R, Viswanathan M, Gold JD, Kotlikoff MI, Sarvazyan N, Kay MW, Murry CE, Laflamme MA. 2012. Human ES-cell-derived cardiomyocytes electrically couple and suppress arrhythmias in injured hearts. Nature 489:322-325.

Shukla N, Rowe D, Hinton J, Angelini GD, Jeremy JY. 2005. Calcium and the replication of human vascular smooth muscle cells: studies on the activation and translocation of extracellular signal regulated kinase (ERK) and cyclin D1 expression. Eur J Pharmacol 509:21-30.

Singh S, Lowe DG, Thorpe DS, Rodriguez H, Kuang WJ, Dangott LJ, Chinkers M, Goeddel DV, Garbers DL. 1988. Membrane guanylate cyclase is a cell-surface receptor with homology to protein kinases. Nature 334:708-712.

Small EM, Krieg PA. 2003. Transgenic analysis of the atrialnatriuretic factor (ANF) promoter: Nkx2-5 and GATA-4 binding sites are required for atrial specific expression of ANF. Dev Biol 261:116-131.

Snabaitis AK, Muntendorf A, Wieland T, Avkiran M. 2005. Regulation of the extracellular signal-regulated kinase pathway in adult myocardium: differential roles of G(q/11), Gi and G(12/13) proteins in signalling by alpha1-adrenergic, endothelin-1 and thrombin-sensitive protease-activated receptors. Cell Signal 17:655-664.

Song H, Yoon C, Kattman SJ, Dengler J, Masse S, Thavaratnam T, Gewarges M, Nanthakumar K, Rubart M, Keller GM, Radisic M, Zandstra PW. 2010. Interrogating functional integration between injected pluripotent stem cell-derived cells and surrogate cardiac tissue. Proc Natl Acad Sci U S A 107:3329-3334.

Song K, Nam YJ, Luo X, Qi X, Tan W, Huang GN, Acharya A, Smith CL, Tallquist MD, Neilson EG, Hill JA, Bassel-Duby R, Olson EN. 2012. Heart repair by reprogramming non-myocytes with cardiac transcription factors. Nature 485:599-604.

Soonpaa MH, Kim KK, Pajak L, Franklin M, Field LJ. 1996. Cardiomyocyte DNA synthesis and binucleation during murine development. Am J Physiol 271:H2183-2189.

Soriano P. 1999. Generalized lacZ expression with the ROSA26 Cre reporter strain. Nat Genet 21:70-71.

Sperelakis N, Pappano AJ. 1983. Physiology and pharmacology of developing heart cells. Pharmacol Ther 22:1-39.

Sperelakis N, Shigenobu K. 1972. Changes in membrane properties of chick embryonic hearts during development. J Gen Physiol 60:430-453.

Squire JM. 1997. Architecture and function in the muscle sarcomere. Curr Opin Struct Biol 7:247-257.

Srivastava D, Olson EN. 2000. A genetic blueprint for cardiac development. Nature 407:221-226.

Stamm C, Westphal B, Kleine HD, Petzsch M, Kittner C, Klinge H, Schumichen C, Nienaber CA, Freund M, Steinhoff G. 2003. Autologous bone-marrow stem-cell transplantation for myocardial regeneration. Lancet 361:45-46.

Stanley EG, Biben C, Elefanty A, Barnett L, Koentgen F, Robb L, Harvey RP. 2002. Efficient Cre-mediated deletion in cardiac progenitor cells conferred by a 3'UTR-ires-Cre allele of the homeobox gene Nkx2-5. Int J Dev Biol 46:431-439.

Stastna M, Chimenti I, Marban E, Van Eyk JE. 2010. Identification and functionality of proteomes secreted by rat cardiac stem cells and neonatal cardiomyocytes. Proteomics 10:245-253.

Steinhelper ME, Cochrane KL, Field LJ. 1990. Hypotension in transgenic mice expressing atrial natriuretic factor fusion genes. Hypertension 16:301-307.

Stults JT, O'Connell KL, Garcia C, Wong S, Engel AM, Garbers DL, Lowe DG. 1994. The disulfide linkages and glycosylation sites of the human natriuretic peptide receptor-C homodimer. Biochemistry 33:11372-11381.

Sudoh T, Kangawa K, Minamino N, Matsuo H. 1988. A new natriuretic peptide in porcine brain. Nature 332:78-81.

Sudoh T, Minamino N, Kangawa K, Matsuo H. 1990. C-type natriuretic peptide (CNP): a new member of natriuretic peptide family identified in porcine brain. Biochem Biophys Res Commun 168:863-870.

Suga S, Nakao K, Hosoda K, Mukoyama M, Ogawa Y, Shirakami G, Arai H, Saito Y, Kambayashi Y, Inouye K, et al. 1992. Receptor selectivity of natriuretic peptide family, atrial natriuretic peptide, brain natriuretic peptide, and C-type natriuretic peptide. Endocrinology 130:229-239.

Sweeney HL, Bowman BF, Stull JT. 1993. Myosin light chain phosphorylation in vertebrate striated muscle: regulation and function. Am J Physiol 264:C1085-1095.

Takebayashi-Suzuki K, Yanagisawa M, Gourdie RG, Kanzawa N, Mikawa T. 2000. In vivo induction of cardiac Purkinje fiber differentiation by coexpression of preproendothelin-1 and endothelin converting enzyme-1. Development 127:3523-3532.

Tam PP, Parameswaran M, Kinder SJ, Weinberger RP. 1997. The allocation of epiblast cells to the embryonic heart and other mesodermal lineages: the role of ingression and tissue movement during gastrulation. Development 124:1631-1642.

Tanaka M, Chen Z, Bartunkova S, Yamasaki N, Izumo S. 1999. The cardiac homeobox gene Csx/Nkx2.5 lies genetically upstream of multiple genes essential for heart development. Development 126:1269-1280.

Taylor DA, Atkins BZ, Hungspreugs P, Jones TR, Reedy MC, Hutcheson KA, Glower DD, Kraus WE. 1998. Regenerating functional myocardium: improved performance after skeletal myoblast transplantation. Nat Med 4:929-933.

Taylor S, Wakem M, Dijkman G, Alsarraj M, Nguyen M. 2010. A practical approach to RT-qPCR-Publishing data that conform to the MIQE guidelines. Methods 50:S1-5.

Thattaliyath BD, Firulli BA, Firulli AB. 2002. The basic-helix-loop-helix transcription factor HAND2 directly regulates transcription of the atrial naturetic peptide gene. J Mol Cell Cardiol 34:1335-1344.

Thomson JA, Itskovitz-Eldor J, Shapiro SS, Waknitz MA, Swiergiel JJ, Marshall VS, Jones JM. 1998. Embryonic stem cell lines derived from human blastocysts. Science 282:1145-1147.

Toal CB. 2004. Formulation dependent pharmacokinetics--does the dosage form matter for nifedipine? J Cardiovasc Pharmacol 44:82-86.

Tokudome T, Horio T, Kishimoto I, Soeki T, Mori K, Kawano Y, Kohno M, Garbers DL, Nakao K, Kangawa K. 2005. Calcineurin-nuclear factor of activated T cells pathway-dependent cardiac remodeling in mice deficient in guanylyl cyclase A, a receptor for atrial and brain natriuretic peptides. Circulation 111:3095-3104.

Toshimori H, Toshimori K, Oura C, Matsuo H. 1987a. Immunohistochemical study of atrial natriuretic polypeptides in the embryonic, fetal and neonatal rat heart. Cell Tissue Res 248:627-633.

Toshimori H, Toshimori K, Oura C, Matsuo H. 1987b. Immunohistochemistry and immunocytochemistry of atrial natriuretic polypeptide in porcine heart. Histochemistry 86:595-601.

Touyz RM, Sventek P, Lariviere R, Thibault G, Fareh J, Reudelhuber T, Schiffrin EL. 1996. Cytosolic calcium changes induced by angiotensin II in neonatal rat atrial and ventricular cardiomyocytes are mediated via angiotensin II subtype 1 receptors. Hypertension 27:1090-1096.

Tripathi S, Pandey KN. 2012. Guanylyl cyclase/natriuretic peptide receptor-A signaling antagonizes the vascular endothelial growth factor-stimulated MAPKs and downstream effectors AP-1 and CREB in mouse mesangial cells. Mol Cell Biochem 368:47-59.

Viana F, Van den Bosch L, Missiaen L, Vandenberghe W, Droogmans G, Nilius B, Robberecht W. 1997. Mibefradil (Ro 40-5967) blocks multiple types of voltage-gated calcium channels in cultured rat spinal motoneurones. Cell Calcium 22:299-311.

Viragh S, Challice CE. 1977. The development of the conduction system in the mouse embryo heart. II. Histogenesis of the atrioventricular node and bundle. Dev Biol 56:397-411.

Viragh S, Challice CE. 1982. The development of the conduction system in the mouse embryo heart. Dev Biol 89:25-40.

Waldman SA, Rapoport RM, Murad F. 1984. Atrial natriuretic factor selectively activates particulate guanylate cyclase and elevates cyclic GMP in rat tissues. J Biol Chem 259:14332-14334.

Wei YF, Rodi CP, Day ML, Wiegand RC, Needleman LD, Cole BR, Needleman P. 1987. Developmental changes in the rat atriopeptin hormonal system. J Clin Invest 79:1325-1329.

Wiesmann F, Ruff J, Engelhardt S, Hein L, Dienesch C, Leupold A, Illinger R, Frydrychowicz A, Hiller KH, Rommel E, Haase A, Lohse MJ, Neubauer S. 2001. Dobutamine-stress magnetic resonance microimaging in mice : acute changes of cardiac geometry and function in normal and failing murine hearts. Circ Res 88:563-569.

Winquist RJ, Faison EP, Waldman SA, Schwartz K, Murad F, Rapoport RM. 1984. Atrial natriuretic factor elicits an endothelium-independent relaxation and activates particulate guanylate cyclase in vascular smooth muscle. Proc Natl Acad Sci U S A 81:7661-7664.

Wu SM, Fujiwara Y, Cibulsky SM, Clapham DE, Lien CL, Schultheiss TM, Orkin SH. 2006. Developmental origin of a bipotential myocardial and smooth muscle cell precursor in the mammalian heart. Cell 127:1137-1150.

Xie GX, Palmer PP. 2007. How regulators of G protein signaling achieve selective regulation. J Mol Biol 366:349-365.

Xu D, Emoto N, Giaid A, Slaughter C, Kaw S, deWit D, Yanagisawa M. 1994. ECE-1: a membrane-bound metalloprotease that catalyzes the proteolytic activation of big endothelin-1. Cell 78:473-485.

Yan W, Sheng N, Seto M, Morser J, Wu Q. 1999. Corin, a mosaic transmembrane serine protease encoded by a novel cDNA from human heart. J Biol Chem 274:14926-14935.

Yan W, Wu F, Morser J, Wu Q. 2000. Corin, a transmembrane cardiac serine protease, acts as a pro-atrial natriuretic peptide-converting enzyme. Proc Natl Acad Sci U S A 97:8525-8529.

Yang-Feng TL, Floyd-Smith G, Nemer M, Drouin J, Francke U. 1985. The pronatriodilatin gene is located on the distal short arm of human chromosome 1 and on mouse chromosome 4. Am J Hum Genet 37:1117-1128.

Zeller R, Bloch KD, Williams BS, Arceci RJ, Seidman CE. 1987. Localized expression of the atrial natriuretic factor gene during cardiac embryogenesis. Genes Dev 1:693-698.

Zhang F, Pasumarthi KB. 2007. Ultrastructural and immunocharacterization of undifferentiated myocardial cells in the developing mouse heart. J Cell Mol Med 11:552-560.

Zhang F, Pasumarthi KB. 2008. Embryonic stem cell transplantation: promise and progress in the treatment of heart disease. BioDrugs 22:361-374.

Zwi-Dantsis L, Gepstein L. 2012. Induced pluripotent stem cells for cardiac repair. Cell Mol Life Sci 69:3285-3299.